

Postcranial morphology of the South African middle Permian pareiasaurs from the Karoo Basin of South Africa

Marc J. Van den Brandt^{1*}, Julien Benoit¹, Fernando Abdala^{1,2} & Bruce S. Rubidge¹

¹Evolutionary Studies Institute and School of Geosciences, University of the Witwatersrand, Johannesburg, PO WITS 2050, South Africa

²Unidad Ejecutora Lillo, CONICET-Fundación Miguel Lillo, Miguel Lillo 251, Tucumán, Argentina

Received 24 August 2020. Accepted 15 February 2021

Pareiasaurs were relatively abundant and globally distributed herbivorous parareptiles of the middle to late Permian. The basal-most pareiasaurs, the Bradysauria, are restricted to the middle Permian of South Africa and went extinct at the end of the Guadalupian (Capitanian) at the top of the *Tapinocephalus* Assemblage Zone. Currently, three genera are recognized in this group: *Bradysaurus*, *Embrithosaurus* and *Nochelesaurus*, but their postcrania are poorly known, and consequently poorly understood. In this paper, our third contribution designed to improve understanding of the Bradysauria, we present a detailed comparative postcranial description and updated diagnoses for *Bradysaurus baini*, *Embrithosaurus schwarzi* and *Nochelesaurus alexanderi*. *Bradysaurus baini* has one postcranial autapomorphy: anterior dorsal osteoderms smooth and strongly convex, with an incipient central boss, and very light ornamentation. Three pelvic autapomorphies of *Embrithosaurus schwarzi* are confirmed: anterior portion of the iliac blades flat and vertical (not everted or upturned); iliac blades diverge anteriorly, oriented at 45–60° off the sagittal plane; and a very thick pelvic symphysis. For *Nochelesaurus alexanderi* we remove all three of the postcranial autapomorphies previously proposed. To the diagnoses of each species, we have added several new distinguishing postcranial features, within the local group of middle Permian pareiasaurs. The results reinforce our previous cranial studies concluding that three valid species of pareiasaurs are represented in the South African middle Permian.

Key words: Capitanian, Guadalupian, Pareiasauria, Parareptilia, *Tapinocephalus* Assemblage Zone.

Palaeontologia africana 2021. ©2021 Marc J. Van den Brandt, Julien Benoit, Fernando Abdala & Bruce S. Rubidge. This is an open-access article published under the Creative Commons Attribution 4.0 Unported License (CC BY4.0). To view a copy of the license, please visit <http://creativecommons.org/licenses/by/4.0/>. This license permits unrestricted use, distribution, and reproduction in any medium, provided the original author and source are credited. The article is permanently archived at: <http://wiredspace.wits.ac.za/handle/10539/31290>

INTRODUCTION

Pareiasaurs were a group of abundant armoured, herbivorous parareptiles with a worldwide distribution, which flourished in the middle to late Permian (Boonstra 1969; Lee 1993, 1994, 1997a,b). In the *Tapinocephalus* Assemblage Zone (AZ) of the Beaufort Group of the South African Karoo Supergroup pareiasaurs are relatively abundant, comprising approximately 25% of the total of the vertebrate fauna (Boonstra 1969; Day 2013; Nicolas 2007; Smith & Keyser 1995a; Van der Walt 2011).

South African pareiasaurs are distributed in two distinct stratigraphic ranges, where representatives of three different morphotypes occur. (1) In the middle Permian *Tapinocephalus* AZ (Boonstra 1932a; Day & Rubidge 2020; Lee 1997a; Smith & Keyser 1995a) only the large basal pareiasaurs *Bradysaurus*, *Embrithosaurus*, and *Nochelesaurus* are known with a restricted dermal armour comprising a narrow band of isolated osteoderms above the vertebral column (Boonstra 1934b; Canoville & Chinsamy 2017; Lee 1994, 1997a; Scheyer & Sander 2009; Watson 1914). These taxa become extinct at the top of the Abrahamskraal Formation of the Beaufort Group (Day 2013; Nicolas 2007) which has been correlated with the

end-Guadalupian extinction event (Day 2013; Day *et al.* 2015). (2) In the late Permian *Tropidostoma*, *Cistecephalus*, and *Daptocephalus* AZs (Kitching 1995; Smith 2020; Smith & Keyser 1995b,c; Viglietti *et al.* 2015; Viglietti 2020) are medium-to-large-sized pareiasaurs which have isolated osteoderms covering the entire body (e.g. *Pareiasaurus* and *Pareiasuchus*), and dwarf pareiasaurs with united osteoderms forming a carapace over the entire body (e.g. *Nanopareia*, *Anthodon*, and *Pumiliopareia*) (Boonstra 1934b; Canoville & Chinsamy 2017; Findlay 1970; Lee 1997a; Scheyer & Sander 2009; Watson 1914). Pareiasaurians become extinct at the Permo-Triassic boundary (Lee 1997a; Nicolas 2007; Van den Brandt *et al.* 2020).

The basal pareiasaurs appear abruptly in the fossil record in the middle Permian of South Africa, exhibiting all the characteristic pareiasaurian traits at their first occurrence (Boonstra 1934a; Houghton & Boonstra 1929; Seeley 1888, 1892; Watson 1914). It is unknown how far back the evolutionary history of pareiasaurs stretch. The basal-most pareiasaurian species are quite similar in morphology and little evidence of clear ancestor candidate taxa have been found (Boonstra 1932a). The clade achieved a high level of diversity and a worldwide distribution by the late Permian, before their ultimate demise at

*Author for correspondence. E-mail: marcvandenbrandt@gmail.com

the Permo-Triassic boundary. The oldest and also most basal middle Permian South African taxa are therefore crucial to understanding the origin and subsequent diversification of the group (Benton 2016; Jalil & Janvier 2005; Lee 1997a,b; Liu & Bever 2018; Tsuji 2010; Tsuji *et al.* 2013; Turner *et al.* 2015; Van den Brandt *et al.* 2020).

After a long history of taxonomic confusion and inflated numbers of taxa, four species of basal pareiasaurs from the *Tapinocephalus* AZ are currently recognized since the review of Lee (1994, 1997a): *Bradysaurus baini*, *B. seeleyi*, *Embrithosaurus schwarzi* and *Nochelesaurus alexanderi*. However, despite Lee's updated diagnoses, these pareiasaurs remain poorly understood and understudied.

Van den Brandt *et al.* (2020) produced an updated cranial description and diagnosis for *Embrithosaurus schwarzi*, and performed a phylogenetic analysis of the pareiasaurs, establishing the new clade Bradysauria which included all the genera from the *Tapinocephalus* AZ. A second contribution produced the first detailed cranial description and updated diagnosis for *Nochelesaurus alexanderi* (Van den Brandt *et al.* 2021). This third contribution aims to provide the first modern comparative postcranial analysis for the three genera of middle Permian South African pareiasaurs and represents the first modern treatment of the postcranial skeleton of representatives of this group. We expect our efforts to integrate cranial and postcranial details will enhance diagnoses and enable incorporation of more anatomical information in pareiasaurian phylogenetic studies, an endeavour that will be produced in a forthcoming contribution.

Brief history and current state of postcranial knowledge

Bradysaurus baini (Seeley 1892)

H.G. Seeley visited South Africa in 1889 and collected two relatively complete pareiasaur specimens that he described in detail (Seeley 1892), assigning the fragmentary specimen, NHMUK PV R 1970 (see institutional abbreviations below), to *Pareiasaurus bombidens* (Owen 1876) and the very complete NHMUK PV R 1971, to the new species *Pareiasaurus baini*. This historically important specimen is mounted on permanent display at the Natural History Museum in London (Fig. 2). Later, Watson (1914) elevated NHMUK PV R 1971 to a new genus, calling the species *Bradysaurus baini* as he considered *Pareiasaurus* to comprise specimens with an extensive covering of body osteoderms, a feature lacking in NHMUK PV R 1971.

Bradysaurus baini was retained by Haughton & Boonstra (1929) who provided a very brief cranial diagnosis. Boonstra (1934a), based only on skull features, greatly expanded the diagnosis of the species. Descriptions of the postcranium of *Bradysaurus baini* was included in the series of 'Pareiasaurian Studies' papers published by Haughton & Boonstra between 1929 and 1934 with each paper dedicated to a specific postcranial anatomical region. The postcrania of *Bradysaurus baini* has not been described in detail since that time.

Lee (1994, 1997a) produced accurate cranial illustrations for *Bradysaurus baini* and comparative illustrations of the

major postcranial elements. He recognized three cranial autapomorphies for *Bradysaurus baini* and noted a few postcranial differences between the taxon and the other middle Permian South African pareiasaurs.

Embrithosaurus schwarzi (Watson 1914)

Broom (1903) described the holotype of *Embrithosaurus schwarzi* (SAM-PK-8034) and mistakenly assigned it to *Pareiasaurus serridens* (see below). Noting the skull as crushed and with very few cranial sutures identifiable, Broom (1903) focused his description on the postcranium. Even so, the postcranial description is brief, as Broom noted that most of the new skeleton closely resembled that of the very complete and recently described *Pareiasaurus/Bradysaurus baini* (NHMUK PV R 1971) (Seeley 1892). Consequently, Broom provided very brief descriptions of the vertebrae, scapulocoracoids, cleithra, clavicles, interclavicle, humeri, tibia, fibula, and a large astragalocalcaneum. However, he did describe the radii, ulnae, femora, and the pelvis in more detail as he noticed several differences in these bones of *Embrithosaurus schwarzi* compared to those of *P. baini*. Rough drawings of most of the postcranial elements were produced by Broom (1903: plate XV, figs 1–24) including a full body restoration of the animal in a living posture (Broom 1903: plate XVI; here Fig. 1) which Broom (1913) used as a model of a complete *Pareiasaurus serridens*.

Noting several important differences between Broom's (1903) specimen and the holotype of *Pareiasaurus serridens* (NHMUK PV R 4063), Watson (1914) assigned Broom's specimen as the holotype of the new taxon *Embrithosaurus schwarzi* and provided a brief diagnosis. Since then, *Embrithosaurus schwarzi* has been considered valid by all subsequent taxonomic workers, but it remains poorly known with brief diagnoses based mostly on only cranial features (Boonstra 1934a, 1969; Haughton & Boonstra 1929; Kuhn 1969; Lee 1994, 1997a; Van den Brandt 2016). A detailed redescription of the cranium of *Embrithosaurus schwarzi* has recently been published (Van den Brandt *et al.* 2020).

Lee (1994, 1997a) proposed three pelvic autapomorphies for *Embrithosaurus schwarzi*. Most of these pelvic characters had been documented previously (e.g. Haughton & Boonstra 1930; Watson 1914). Lee provided a brief postcranial description of *Embrithosaurus*, and noted important postcranial differences between *Embrithosaurus* and the other co-occurring middle Permian South African pareiasaurs.

Nochelesaurus alexanderi (Haughton and Boonstra 1929)

In a short addendum at the end of a pareiasaurian cranial paper describing a weathered juvenile skull, Broom (1924: 507) briefly described and named the new species *Pareiasaurus strubeni* based on a lower jaw with 'considerably large' teeth. Haughton & Boonstra (1929) allocated Broom's (1924) large-toothed specimen to the new genus *Nochelesaurus*, as *N. strubeni*, and created the new species *N. alexanderi*. Their very brief cranial diagnosis was greatly expanded by Boonstra (1934a). Most of the postcranial elements, apart from the pelvis of

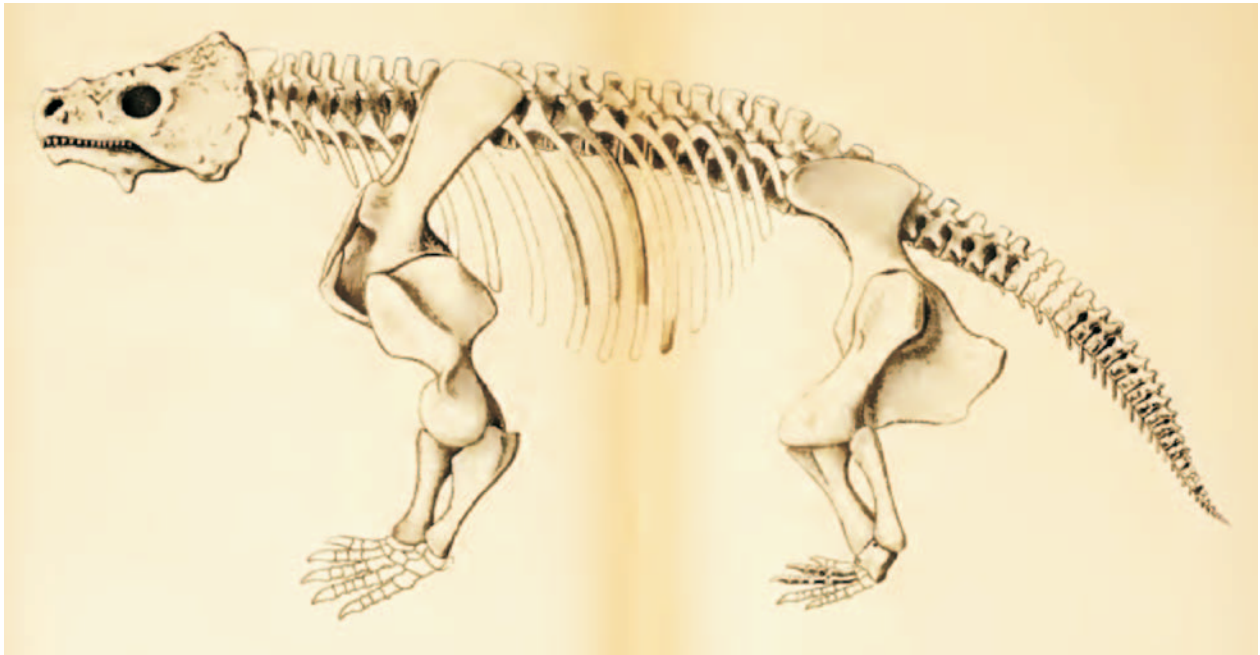


Figure 1. Full body reconstruction of the holotype of *Embrithosaurus schwarzi* (SAM-PK-8034) by Broom (1903). Most of the skeleton is shown as preserved (shaded elements). Unshaded elements (not preserved) include the manus, most of the pes (except for two digits), most of the ribs, a section of three anterior caudal vertebrae, and several posterior caudal vertebrae. Animal approximately 3 m long.

Nochelesaurus were first described in the ‘Pareiasaurian Studies’ series of papers produced by Haughton & Boonstra between 1929 and 1934.

Lee (1994, 1997a) declared *Nochelesaurus strubeni* as *nomina vana* noting that the holotype is based on indeterminate material in the Broom Collection of the American Museum of Natural History (New York). He also synonymized *Dolichopareia angusta* and *Brachypareia watsoni* with *Nochelesaurus alexanderi*, and produced a brief description of the postcranium, including three post-

cranial autapomorphies. The first detailed cranial description of *Nochelesaurus alexanderi* has recently been completed (Van den Brandt *et al.* 2021), but this species will not be completely understood until the postcranium is described in detail.

Aims of this paper

In this paper, we re-describe the postcranial elements of *Bradysaurus baini*, *Embrithosaurus schwarzi* and *Nochelesaurus alexanderi* using the holotypes and important, often



Figure 2. Photograph of the mounted holotype of *Bradysaurus baini* (NHMUK PV R 1971) on display in the ‘From the Beginning’ permanent exhibit, Natural History Museum, London. Animal approximately 3 m long.

historical, referred specimens. Particular emphasis is placed on comparing the distinguishing features of each genus and on postcranial features related to pareiasaurian phylogenetic characters.

MATERIALS AND METHODS

Comparative material

Comparative postcranial material of non middle Permian pareiasaur species, include the following: PIN 4546/18, holotype osteoderms of *Obirkovia gladiator*; PIN 2005/1532, articulated holotype skull and skeleton of *Scutosaurus karpinskii*; PIN 2005/1533, PIN 2005/1534, PIN 2005/1535, PIN 2005/1536, PIN 2005/1537, and PIN 2005/1578, articulated skulls and skeletons of *Scutosaurus karpinskii*; NHMUK PV R 4027, casts of ulnae of *Scutosaurus karpinskii*; BPI/I/548, skull and skeleton of an almost complete vertebral column with hundreds of weathered osteoderms, and parts of the shoulder and pelvic girdles of a specimen of *Anthodon serrarius*; SAM-PK-K10036, complete articulated skull and skeleton of a *Pareiasaurus serridens*.

Preparation and preservation

Bradysaurus baini NHMUK PV R 1971

The postcranium of the holotype of *Bradysaurus baini* was mechanically prepared at the Natural History Museum in London in 1891 (Seeley 1892). Seeley (1892) states that the right side of the animal was better preserved and in natural articulation, compared to the exposed, weathered, and somewhat scattered left side. For the current project, the specimen was dismounted from display and disassembled for study in 2019. The original preparation by R. Hall (Seeley 1892) is admirable and no additional postcranial preparation was needed for this study. The external bony surfaces are in excellent condition, generally better preserved than the postcranial elements of the holotypes of *Embrithosaurus schwarzi* and *Nochelesaurus alexanderi*. Most major elements on the right side are completely preserved, but on the left side large portions of most major elements are reconstructed in dark grey plaster, modelled and mirrored from the intact right elements.

Embrithosaurus schwarzi SAM-PK-8034

The skull and postcranium of the holotype of *Embrithosaurus schwarzi* had previously been mechanically prepared under the direction of Robert Broom in 1902 and 1903 at the Iziko South African Museum in Cape Town. For the current project, extensive additional postcranial preparation over nine months, using compressed air driven air scribes with a tungsten carbide tip, was undertaken by Pepson Mukanela and Marc Van den Brandt at the ESI, University of the Witwatersrand, Johannesburg, in 2017. Severe historical mechanical preparation has damaged the external surface of most postcranial elements with long scratches and chisel gauge marks. Weathering damage is also apparent. As a result, it is difficult to identify and describe fine surface details. It is also

challenging to distinguish bone from the matrix on this specimen.

Nochelesaurus alexanderi SAM-PK-6239

Additional postcranial preparation was performed on the holotype of *Nochelesaurus alexanderi* (SAM-PK-6239) using compressed air driven air scribes with a tungsten carbide tip, by Pepson Mukanela, Gilbert Mokgethoa and Charlton Dube (ESI) in 2018. As in the holotype of *Embrithosaurus schwarzi*, long scratches and chisel marks are present as a result of harsh historical preparation using hammers and chisels, making it difficult to identify fine surface features. Several postcranial elements were originally fragmented and reconstructed using dark grey plaster as a binder, such as the left humerus and right femur, each consisting of three or four large fragments held together. As is the case with the holotype of *Embrithosaurus schwarzi* it is sometimes challenging to distinguish bone from the matrix.

Key to interpretive drawings

Dotted lines represent missing sections. Light grey indicates sides of bones, bone breaks, matrix, plaster, or glue; black indicates deep cavities, foramen or fenestra. Note: we employ the methodology used by Benton (2016) of noting the relevant phylogenetic characters condition as each element is described.

SYSTEMATIC PALAEOLOGY

Reptilia Laurenti, 1768

Parareptilia Olson, 1947

Pareiasauria Seeley, 1888

Pareiasauridae Cope, 1896

Bradysauria Van den Brandt, Abdala and Rubidge, 2020

Bradysaurus Watson, 1914

Bradysaurus baini Seeley, 1892

Holotype

NHMUK PV R 1971 comprises a complete skull and separate lower jaw with very complete postcranial material including a complete shoulder girdle and pelvis, complete vertebral column, missing only the end of the caudal vertebrae. Right fore- and hind-limbs are complete. Left humerus, radius, ulna, femur, tibia, and fibula are partially preserved. Both astragalocalcanea are preserved. Only a few ribs are preserved.

Referred material

CGP/1/2268, large skull and articulated anterior half of the postcranium of *Bradysaurus baini*; CGP/1/2269, juvenile skull and articulated anterior third of the postcranium of *Bradysaurus baini*; NHMUK PV R 1970, snout and partial cranium of *Bradysaurus baini*, SAM-PK-5002, skull, lower jaw and postcranium of *Bradysaurus baini*; SAM-PK-3718, holotype of *Bradysaurus vanderbyli*, very large skull and lower jaw, most of the dorsal vertebral column, and partial pectoral and pelvic girdles of *Bradysaurus baini*; SAM-PK-5624, very complete, articulated, mounted *Bradysaurus baini* skull and skeleton on permanent display at the Iziko South African Museum, Cape Town (SAM).

Locality, stratigraphy and age

NHMUK PV R 1971 was collected on 12 August 1889 by Seeley, T. Bain, J.S. Marais, and S Marais from the farm De Bad in the Beaufort West district of the Western Cape Province (Seeley 1892). Day (2013) and Day *et al.* (2015) considered this locality to be high in the *Tapinocephalus* AZ, and assigned to the lower to mid Moordenaars Member of the Abrahamskraal Formation of the Beaufort Group.

Revised postcranial diagnosis

One postcranial autapomorphy: anterior dorsal osteoderms smooth and strongly convex, with an incipient central boss, and very light ornamentation (Turner *et al.* 2015, character 135).

Bradysaurus differs from co-occurring pareiasaurs in having: epicondyles of the humerus extend distally far beyond the radial and ulnar articulation surfaces, appearing forked (Turner *et al.* 2015, character 98); wider proximal and distal humerus; proximal internal trochanter of the femur high, wide and strongly curved, with a perpendicular edge; distal internal trochanter with a short anterior (preaxial) process/projection; second sacral rib is the largest sacral rib; from the 5th vertebrae backwards, the parapophysial and diapophysial processes fuse into a single vertical flange, creating a transverse process with a single lateral facet; posterior dorsal osteoderms with shallow circular central hollow and very light ornamentation.

Bradysaurus differs from *Embrithosaurus* in having: low and wide posteroventral process on the clavicle, lacking a distinct notch just medial to the process; humerus with deep intercondylar fossa; delto-pectoral crest large, robust, and 'heart-shaped', with a notch on the ventro-distal corner; short, crescent-shaped, insertion point for muscle attachment on the humeral shaft of the dorsal proximal humerus; presence of a distinct, vertical ridge on the medial radius; pelvis low and wide; posterior portion of the iliac blade vertical, oriented parallel to the sagittal plane, and with dorsal margins medially curved and convex a short distance; anterior portion of the iliac blades deeply concave laterally, upwardly bent (everted) 55°–60° (character 111) to present a large surface in dorsal view, strongly curved with the anterior process tip pointing 45° off the sagittal plane and extending out far laterally from the main body of the blade; iliac shaft oriented anterodorsally, more horizontally, 60° off the vertical plane (character 113); puboischiatic plate wide, long, dorsally and ventrally flat; pelvis symphysis dorsoventrally low and anteroposteriorly long (character 118); ventral keel on the puboischiatic plate low and narrow and extends obliquely at a shallow angle; median pubic process small, extending a short distance ventrally, with sharp square edges; major trochanter posterior projection short; small 40° angle between the lateral and medial facets of the proximal articulation surface of the tibia; distal tibia ventromedially expanded and wide; wide tibial shaft; caudal vertebrae with L-shaped lateral projections (character 85).

Bradysaurus differs from *Nochelesaurus* in having: short scapula blade, mid scapula blade anteroposteriorly wide,

distal scapula blade flared; preaxial and postaxial margins of distal scapula blade curved; medial process of scapula blade low and wide; proximal and distal expansions of the humerus twisted 60–80° apart and almost perpendicular; symmetrical distal and proximal radius; postaxial shaft of femur notable bulged/convex; lateral condyle of the femur extends distally moderately (20–45 mm) beyond the medial condyle; proximal and distal notches of the major trochanter of the femur.

Embrithosaurus Watson, 1914

Embrithosaurus schwarzi Watson, 1914

Holotype

SAM-PK-8034 comprises a distorted skull with the occluded lower jaw, vertebrae 1 to 27 with articulated osteoderms, two small articulated caudal vertebrae, partial left scapulocoracoid, cleithrum, left and right clavicle, and interclavicle, complete right humerus, partial left humerus, complete right radius, partial left radius, both ulnae complete, both femora complete, both tibia complete, right fibula, partial left fibula, complete pelvis, two digits of the forelimb and two digits of the hindlimb, several small unprepared fragments of vertebrae, ribs and phalanges, labelled as 'doubtful association' that have been excluded from the postcranial description.

Referred material

BP/1/7241, subadult specimen comprising a proximal left femur, a more complete right femur, and a few small fragments of ribs, vertebrae, and unidentified postcrania; CGP CBT 112, skull, occluded lower jaw and very complete skeleton of a very large specimen of *Embrithosaurus schwarzi*; FMNH UR 2443, partial lower jaw, partial left scapulocoracoid, left humerus, proximal end of articulated left radius and ulna, pelvis, right femur, a dorsal vertebra, and some fragments; FMNH UR 2486, left pelvis; SAM-PK-9116, distal left ulna, partial left femur, partial acetabulum, hindlimb in a plaster jacket, forelimb in a plaster jacket, portions of distal radii, ulnae, tibiae and fibulae, several large unidentified postcranial fragments.

Locality, stratigraphy and age

According to Broom, SAM-PK-8034 was collected by A.W. Rogers and E.H.L. Schwarz in 1902 on the farm Hoogeveld Lot A (Hoogeveld 270), in the Gouph region, near Knoflock's Fontein, Van der Byl's Kraal, Prince Albert district of the Western Cape Province (Broom 1903). Day (2013) and Day *et al.* (2015) consider this locality to be high in the *Tapinocephalus* AZ, in the stratigraphic interval of 2150–2250 m above the base of Abrahamskraal Formation, which is in the lower part of the Moordenaars Member.

Revised postcranial diagnosis

Three unambiguous pelvic postcranial autapomorphies (modified from Lee 1994, 1997a): 1) anterior portion of the iliac blades flat and vertical/dorsoventral (not everted or upturned) (Turner *et al.* 2015, character 111); 2) iliac blades diverge anteriorly, oriented 45–60° off the sagittal plane,

and; 3) pelvic symphysis very thick dorsoventrally (Turner *et al.* 2015, character 119).

Embrithosaurus differs from co-occurring pareiasaurs in: high and wide posteroventral process on the clavicle and presence of a deep notch medial to the posteroventral process in most specimens; humerus with shallow intercondylar fossa (character 103); delto-pectoral crest small, anteroposteriorly narrow, and with a long, shallow groove on the ventral surface; shaft of the dorsal proximal humerus lacking a short, curved muscular ridge; major trochanter projects far posteriorly (character 122); proximal internal trochanter high, narrow and gently curved, forming a s-shaped structure, with a perpendicular proximal edge; distal internal trochanter with an anterior process; large 60° angle between the medial and lateral facets of the proximal articulation surface of the tibia; narrow tibial shaft; distal tibia narrow and symmetrical; anterior and posterior osteoderms with distinct, rugose, irregular and tab-like (L- or E-shaped) central boss, and a thin and flat periphery with radial ridges (character 136).

Embrithosaurus differs from *Bradysaurus* in having: epicondyles of the humerus do not extend distally far beyond the radial and ulnar articulation surfaces; narrower proximal and distal humerus; pelvis high and narrow; iliac blades straight and laterally flat to very slightly shallowly concave; extreme anteroventral margin of the anterior process of the iliac blade is very slightly curved and bent upwards and laterally outwards; iliac shaft oriented anterodorsally, vertically directed, 30° off the vertical plane (character 113); puboischiatic plate narrow and short; with a strongly and evenly concavely curved (not flat) dorsal surface; pelvic symphysis anteroposteriorly short (character 118); keel on ventral puboischiatic plate high and wide, with with steep 50° oblique lateral sides; median pubic process large, tongue-shaped with rounded edges, extending far anteroventrally; parapophysial and diapophysial processes fuse into a single process, creating a single vertical lateral facet from the 6th vertebra backwards; first sacral rib is the largest; caudal vertebrae with straight lateral projections (character 85).

Embrithosaurus differs from *Nochelesaurus* in: short scapula blade, mid scapula blade anteroposteriorly wide, distal scapula blade flared; preaxial and postaxial margins of distal scapula blade curved; medial process of scapula blade low and wide; proximal and distal expansions of the humerus twisted 60–80° apart and almost perpendicular; symmetrical distal and proximal radius; postaxial shaft of femur notable bulged/convex; lateral condyle of the femur extends distally moderately (30–45 mm) beyond the medial condyle; proximal and distal notches of the major trochanter of the femur.

Nochelesaurus Haughton and Boonstra, 1929

Nochelesaurus alexanderi Haughton and Boonstra, 1929

Holotype

SAM-PK-6239 comprises the dorsal and right side of the skull and fragments of the right lower jaw, braincase and palate, a partial right scapulocoracoid, cleithrum and

clavicle, partial interclavicle, damaged left humerus, seven articulated osteoderms, complete right femur and tibia, fibula fragment, astragalocalcaneum, and several unnumbered unidentified fragments.

Referred material

FMNH UR 2436; a distal humerus, a complete radius, and the proximal end of another radius; FMNH UR 2480, twenty-one weathered and articulated vertebrae, a humerus, both tibia, one tarsal element, and some postcranial fragments; SAM-PK-6238 (holotype of *Dolichopareia angusta*, Haughton and Boonstra, 1929), a partial skull and lower jaw, partial shoulder girdle, both humeri, right radius and ulna, right fibula, second (axis) to 16th vertebrae, and rib fragments.

Locality, stratigraphy and age

SAM-PK-6239 was collected in 1923 from the farm Boesmanskop (Bushmans Kop 302), Beaufort West district of the Western Cape Province, and named after Dr Alexander du Toit, a noted South African geologist (Haughton & Boonstra 1929). Day (2013) and Day *et al.* (2015) consider this locality high in the *Tapinocephalus* AZ, restricted to the uppermost Karelskraal Member of the Abrahamskraal Formation.

Revised postcranial diagnosis

Nochelesaurus differs from co-occurring pareiasaurs in having: most specimens with a long and narrow scapula blade; mid scapula blade anteroposteriorly constricted and very narrow; distal scapula blade narrow with little anteroposterior flaring, preaxial and postaxial margins of distal scapula blade straight and only very slightly curved in most specimens, expanding gradually (character 88); medial process of scapula blade high; proximal and distal expansions of the humerus very flat, only 20–40° apart and almost on the same plane (character 92); tubercle sometimes present on the postaxial margin of the intercondylar fossa of the humerus; ventrolaterally expanded distal radius; postaxial shaft of femur straight (not notable bulged/convex); lateral condyle of the femur extends distally far (70 mm) beyond the medial condyle in most specimens; major trochanter posterior projection very short; absence of or very shallow proximal and distal notches of the major trochanter of the femur; proximal internal trochanter low and narrow, straight or very slightly curved, with an oblique proximal edge (character 125); distal internal trochanter without an anterior process; osteoderms with a wide central boss covering most of the scute, round or comprising five or six rugose, flattened, radial, tab-like processes, with a high and thick periphery.

Remarks

Concerning Lee's (1994, 1997a) three postcranial autapomorphies proposed for *Nochelesaurus alexanderi*: 1) the subscapular fossa is not located close to the anterior margin of the scapula blade and is removed as an autapomorphy; 2) the tubercle on the humerus is manifestly present in only one specimen of *Nochelesaurus*, and

it is removed as an autapomorphy and considered an individual variation within the genus, and 3) the flange on the dorsal femur that projects distally far beyond the postaxial tibial facet does not consist of an obvious flange, instead the distal extension of the lateral condyle of the femur is furthest in most specimens, but not all specimens of *Nochelesaurus*, and is therefore removed as an autapomorphy and considered individual variation within the genus.

Nochelesaurus differs from *Bradysaurus* in having: epicondyles of the humerus do not extend distally far beyond the radial and ulnar articulation surfaces in most specimens; narrower proximal and distal humerus; parapophysial and diapophysial processes fuse into a single process, creating a single vertical lateral facet from the 6th vertebrae backwards.

Nochelesaurus differs from *Embrithosaurus* in having: low and wide posteroventral process on the clavicle, and lacking a distinct notch just medial to the process; humerus with deep intercondylar fossa; delto-pectoral crest large, robust, and 'heart-shaped', with a notch on the ventro-distal corner; short, crescent-shaped, insertion point for muscle attachment on the humeral shaft of the dorsal proximal humerus; presence of a distinct, vertical ridge on the medial radius; small 40° angle between the lateral and medial facets of the proximal articulation surface of the tibia; distal tibia ventromedially expanded and wide; wide tibial shaft.

POSTCRANIAL DESCRIPTION

The description of *Bradysaurus baini* is based primarily on the holotype NHMUK PV R 1971 and referred specimens NHMUK PV R 1970 and SAM-PK-5002. *Embrithosaurus schwarzi* is based primarily on the holotype SAM-PK-8034 and referred specimen CGP CBT 112. *Nochelesaurus alexanderi* is based primarily on the holotype SAM-PK-6239 and referred specimen SAM-PK-6238 (holotype of *Dolichopareia angusta*). Additional referred specimens are noted in the text. The holotypes of *Bradysaurus baini* and *Nochelesaurus alexanderi* are large adult specimens of similar size, whereas the holotype of *Embrithosaurus schwarzi* is slightly smaller, with slightly more gracile elements and may be a late subadult.

Axial skeleton: vertebrae and ribs

We describe the vertebrae of these pareiasaurs in five distinct regions: the anterior cervicals (atlas and axis), the posterior cervicals, and the dorsals (anterior and posterior), sacral and caudal vertebrae. The holotype of *Embrithosaurus schwarzi* (SAM-PK-8034) preserves the atlas, axis, posterior cervicals, dorsals, sacrals, and six anterior caudal vertebrae, in good condition and additional preparation was performed for this project. Broom (1903) noted 20 presacral vertebrae in the holotype of *Embrithosaurus* but only 19 presacrals were recognized by Lee (1994, 1997a) and in this contribution. Lee (1994, 1997a) stated that the holotype of *Nochelesaurus alexanderi* (SAM-PK-6239) preserved six caudal vertebrae but despite a thorough search we were unable to find them. *Nochelesaurus alexanderi* specimen SAM-PK-6238 preserves the

axis, posterior cervicals (3rd to 5th vertebrae), and most of the dorsals (6th to 16th vertebrae), all very poorly preserved and over-prepared. The holotype of *Bradysaurus baini* (NHMUK PV R 1971) preserves an almost complete vertebral column, but the historical preparation was rough and superficial.

Atlas

In the holotype of *Embrithosaurus*, the atlas and axis are preserved in articulation (Figs 3, 4), whereas in *Bradysaurus baini* the atlas and axis are preserved separately and have been very crudely prepared (Fig. 5). In *Embrithosaurus*, the paired neural arches of the atlas (atlantal arches) are no longer present but were illustrated by Boonstra (1934c: 53, text-fig. 2, At.A; here Fig. 3) as curved, clasping bands covering the lateral aspects of the convexly bulged pleurocentrum, extending dorsally from just below the ventral border of the pleurocentrum to just above the neural canal. The holotype of *Bradysaurus baini* preserves a partial left atlantal arch as a large, long, curved bone, tightly articulated, and covering the posterolateral left side of the occipital condyle of the skull. It forms a concavely curved posterodorsal surface for the reception of the convexly bulged pleurocentrum of the anterior atlas. Also on the occipital condyle, posteroventrally, is a partial atlantal intercentrum. In the holotype of *Embrithosaurus* a very small, unpaired midline atlantal intercentrum (currently missing) was positioned ventrally between the atlas and axis (Boonstra 1934c: 53, text-fig. 2; here Fig. 3; Broom 1903).

In *Embrithosaurus* and *Bradysaurus* the anterior side of the pleurocentrum of the atlas is easily identifiable as a strongly convex dominant dome, with a raised central section for articulation with the posterior concavity of the occipital condyle of the skull. The posterior side of the

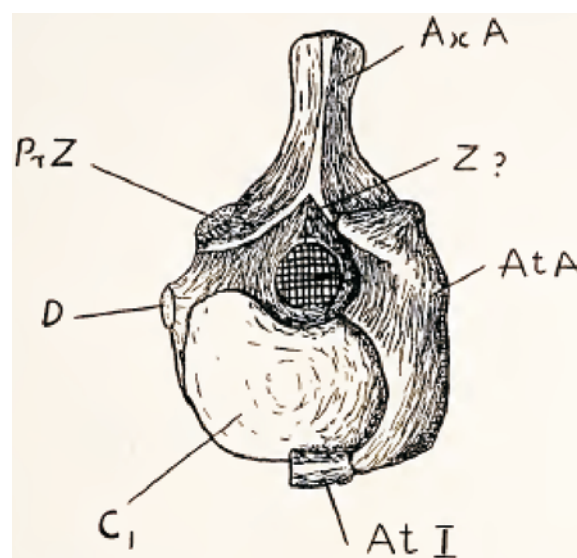


Figure 3. Anterior view of atlas and axis of *Embrithosaurus schwarzi* (SAM-PK-8034) taken from Boonstra (1934c: 53, text-fig. 2). Boonstra figured only the left half of the atlantal arch, At.A (omitting the right from the figure) and the left half of the unpaired atlantal intercentrum, At.I (omitting the right) from the sketch. At.A, atlantal arch; At.I, atlantal intercentrum; Ax.A, axial arch; C1, atlantal pleurocentrum (odontoid); D, diapophyses on atlantal and axial arch; Pr.Z, axial prezygapophysis; Z?, an undeveloped zygosphenes? Scale approximately 9 cm wide.

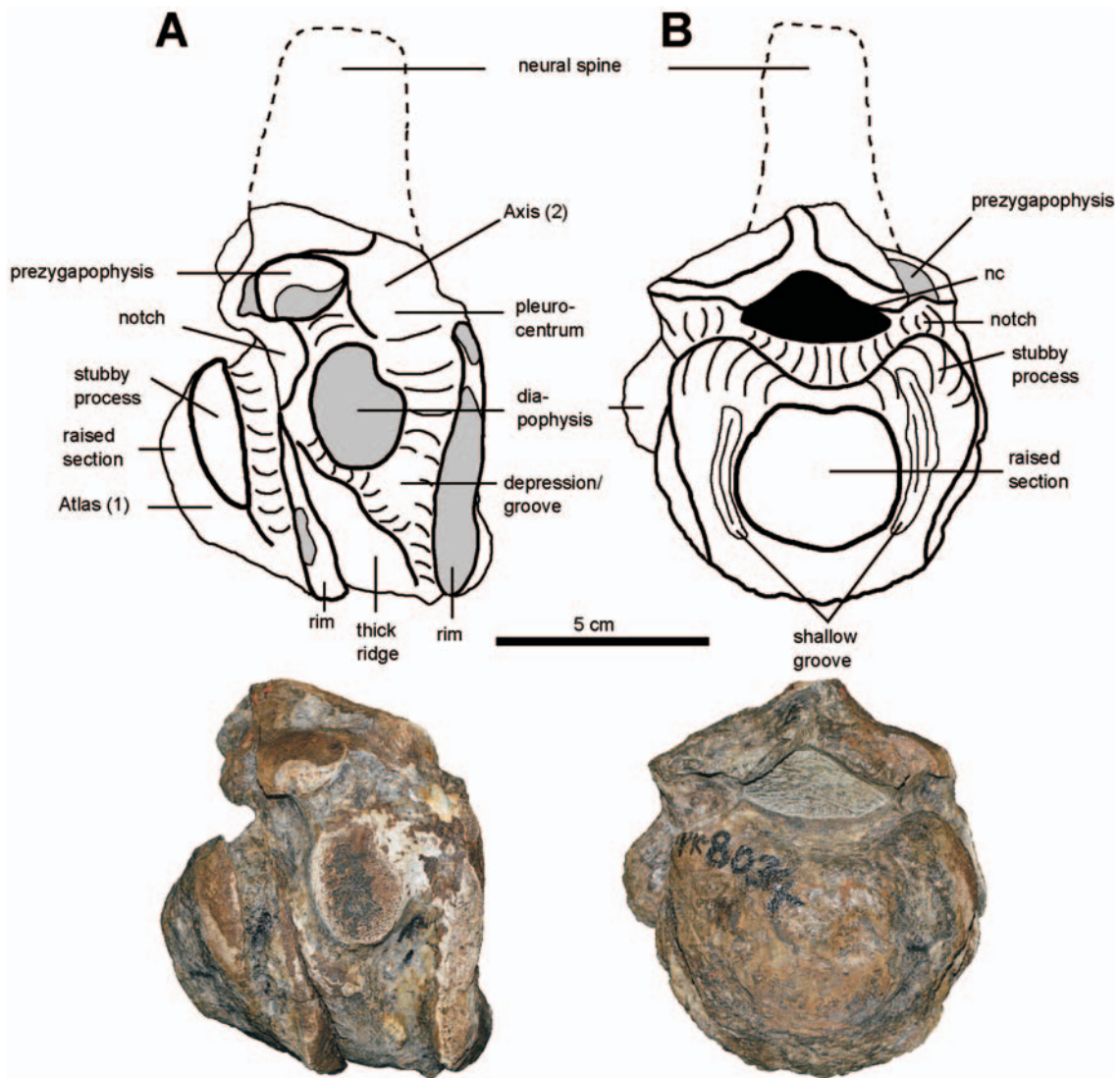


Figure 4. Photographs and interpretive drawings of the atlas and axis of the holotype of *Embrithosaurus schwarzi* (SAM-PK-8034), (A), in left lateral view, and (B), in anterior view. Dorsal to the top of the page. Scale bar equals 5 cm.

atlas is deeply concave. In *Embrithosaurus*, lateral to the raised central region, shallow curved grooves indicate where the atlantal neural arches were once present, and indicate a loose articulation with the atlas arch (Fig. 4). On the lateral surface of the atlas of both species, is a small, stubby, ovoid process, oriented anteroventrally, with a terminal convex facet. The posterior border of the atlas is sharply rimmed, apart from the posteroventral edge which is ventrally flattened. The dorsal surface of the atlas is concave and excavated by the flattened neural canal.

Axis

The axis of each of the three holotypes are incomplete: *Embrithosaurus*: Boonstra illustrated a complete neural arch and a tall and narrow spine on the axis, with a mediolaterally expanded dorsal end, and with a very sharp vertical anterior edge (Boonstra 1934c: 53, text-fig. 2; here Fig. 3). The neural spine of the axis of *Embrithosaurus*, illustrated by Boonstra, is no longer preserved and only a cross-sectional triangular break remains, anteriorly tapering, with concave sides. *Bradysaurus*: the neural arch and spine of the axis are not preserved and the neural canal is open (Fig. 5). *Nochelesaurus*: (axis is labelled as '1'

on the fossil) the neural arch of the axis is sheared-off at a very low level, leaving a posteriorly pointing, triangular bone break (Fig. 6).

In all three genera the amphicoelous pleurocentrum of the axis is anteroposteriorly flattened and dumbbell-shaped. Ventrally, the body of the pleurocentrum is anteroposteriorly short and the posterior border of the axis is much thicker and more robust than the anterior rim. Positioned posteroventrally either side of the midline, the posterior rim of the pleurocentrum of the axis of *Nochelesaurus* has anteroventrally facing, oval, faceted 'pad-like' surfaces (Fig. 6A,B).

The laterally facing diapophysial process is short and stubby, vertical to slightly anterodorsally oriented, and close to the anterior rim of the lateral pleurocentrum. It presents a flat and slightly concave, teardrop-shaped, diapophysial facet. Anterodorsal to the diapophysis, an upwardly directed process bears the prezygapophysis which is an oval, anterodorsally facing facet. In the holotype of *Embrithosaurus*, Broom (1903) noted the presence of a large, vertically elongated and curved axial intercentrum between the axis and the 3rd cervical vertebra, which is now no-longer preserved.

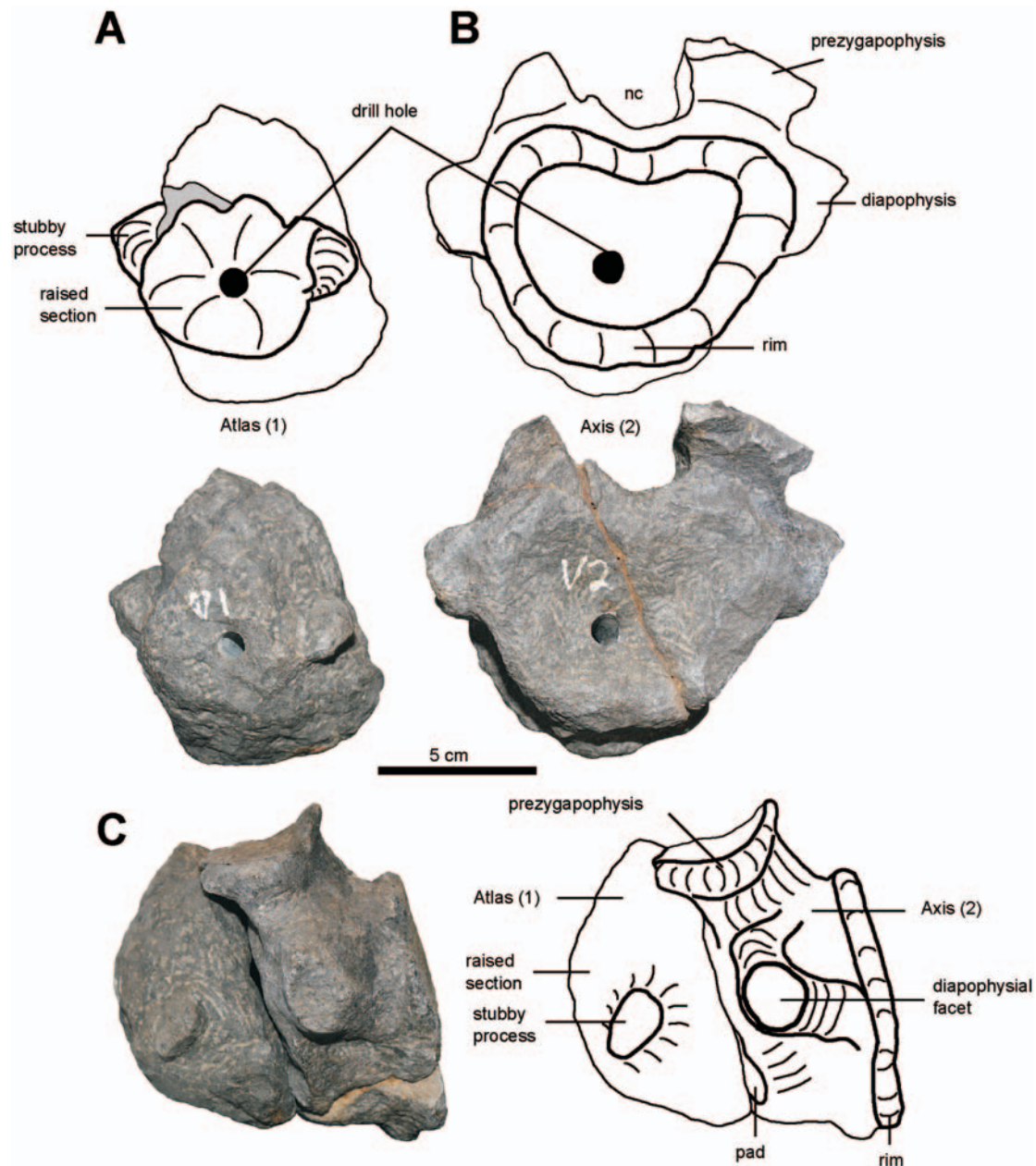


Figure 5. Photographs and interpretive drawings of the vertebrae of the holotype of *Bradysaurus baini* (NHMUK PVR 1971), (A), atlas in anterior view, (B), axis in anterior view, and (C), atlas and axis in left lateral view. Dorsal to the top of the page. Scale bar equals 5 cm.

Posterior cervical vertebrae (3rd–5th vertebrae)

The holotype of *Embrithosaurus* preserves the 3rd to 5th cervical vertebrae in articulation (Fig. 7). The holotype of *Nochelesaurus* has isolated 3rd to 5th vertebrae (but incorrectly labelled with '2', '3', and '4' on the vertebrae). The holotype of *Bradysaurus baini* has the 3rd to 5th vertebrae articulated in a long block containing ten vertebrae (3rd to 12th vertebrae).

The 3rd vertebra in all taxa is much smaller than the similarly sized 4th and 5th vertebra. The posterior cervical vertebrae share some characteristics. Compared to the dorsal vertebrae, they are taller than wide, very narrow, with very short and small pre- and postzygapophyses that do not extend far laterally, with tall, very narrow neural spines, and with differences in the parapophysis and the diapophysis (see below). The centra are amphi-coelous, square to round, and the bases are antero-posteriorly longer than the dorsal portion (Fig. 7). The

neural canal is large, ovoid in cross-section and slightly dorsoventrally flattened.

Laterally are two distinct processes with articulation facets for the heads of the ribs. The lower parapophyseal process and facet forms part of the anterior rim of each centrum and is laterally extended but short (10–14 mm) and stubby, and has a kidney-shaped facet (*Embrithosaurus*) or more rectangular, slightly vertically elongated, sharp-edged facet (*Nochelesaurus*). The higher diapophysial process and facet is situated slightly more posteriorly than the parapophyseal process, it is longer as it extends further posterolaterally, and has a vertically elongated oval facet (more elongated on the 4th and 5th vertebrae). These two processes are linked by the anterior rim of the centrum which is thickened into a ridge, with a deep notch behind the ridge creating a wide and clear separation between the two processes. Posteriorly, a vertical groove separates these processes from the posterior rim of

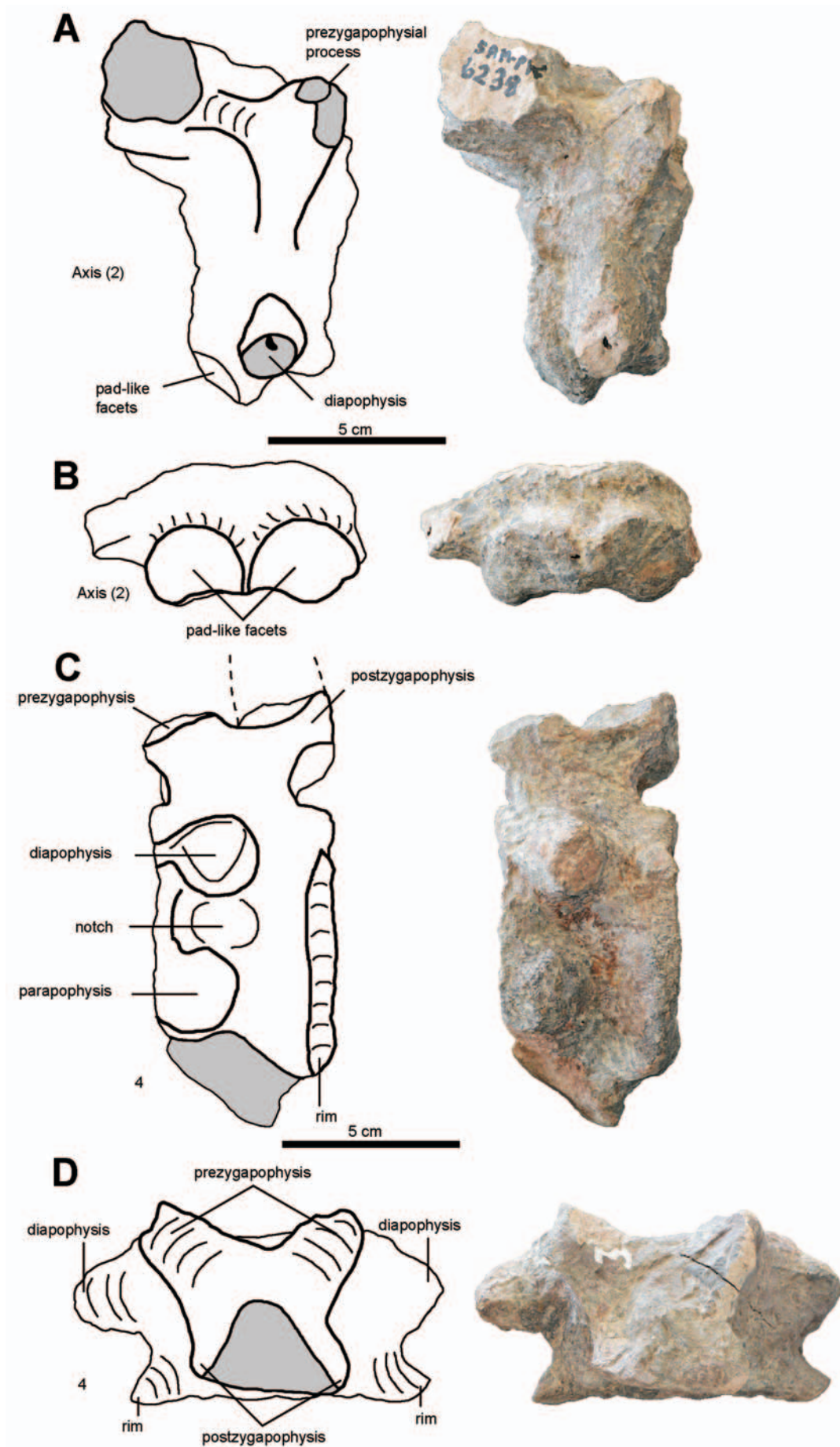


Figure 6. Photographs and interpretive drawings of the vertebrae of SAM-PK-6238 (*Nochelesaurus alexanderi*), (A) axis in right lateral view, (B) axis in ventral view, (C) 4th vertebra in left lateral view, and (D), 4th vertebra in dorsal view. Dorsal to the top of the page in (A) and (C), anterior to the top of the page in (B) and (D). Scale bar equals 5 cm.

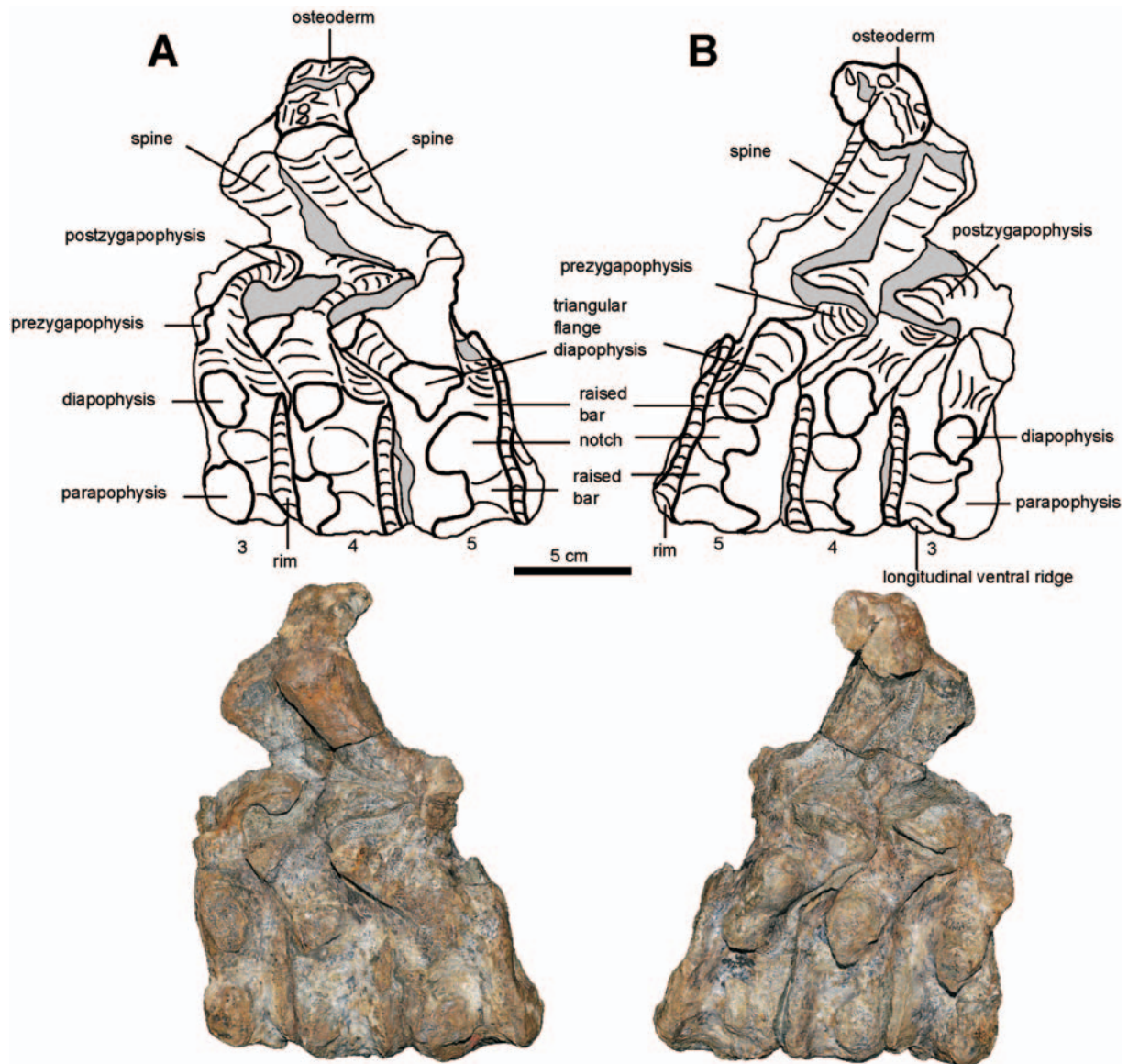


Figure 7. Photographs and interpretive drawings of the 3rd–5th vertebrae of the holotype of *Embrithosaurus schwarzi* (SAM-PK-8034), (A), in left lateral view, and (B), in right lateral view. Dorsal to the top of the page. Scale bar equals 5 cm.

the centrum, which is thickened and laterally flared. The posteroventral margin of each centrum is slightly swollen, producing a rounded posterior lip-like protrusion.

In *Bradysaurus* and *Embrithosaurus* the diapophysis on the 5th vertebra is much larger than that of the 3rd and 4th vertebrae, and extends laterally and dorsally to form a wall-like distinct triangular flange (Fig. 7). In *Bradysaurus* this diapophysial process is partially fused to the lower, irregular parapophysial process and facet on the 5th vertebra. This fusion is seen from the 6th vertebra backwards in *Embrithosaurus* (Fig. 9) and *Nochelesaurus*, where the separate and distinct parapophysial and diapophysial processes fuse into a single vertical flange, creating a transverse process with a single lateral facet, but with dorsal and ventral portions. The anteroventral border of the centrum has a small ventral process, which tapers posteriorly and forms a longitudinal midline ridge.

The prezygapophysial processes are very slender, small, short, and anterodorsally extended above the diapophysis, with dorsally and slightly anteriorly facing mediolaterally narrow and anteroposteriorly elongated articula-

tion facets. The small and short processes of the postzygapophyses are well developed on only the 5th vertebra and extend posterolaterally from the base of the neural spine, with flat, curved ventrally facing facets. The pre- and postzygapophyses gradually increase in overall size and robustness posteriorly.

Two articulated osteoderms partially obscure the dorsal surface of the 4th and 5th neural spines of the holotype vertebrae of *Embrithosaurus*. The complete 5th neural spine is slender and is slightly dorsoventrally shorter than the height of the centrum. As the spine extends dorsally it flares mediolaterally, to nearly twice the width of its base. The spine is diamond-shaped in cross-section, anteroposteriorly flattened and mediolaterally wide, matching the morphology of the 5th neural spine of *Bradysaurus*. The dorsal surfaces of the 5th neural spines of *Bradysaurus* and *Embrithosaurus* are deeply concave with a deep longitudinal groove that creates anterior and posterior notches in the dorsal margin of the neural spine. The spines on the 4th and 5th vertebra of *Embrithosaurus* and the 5th vertebra of *Bradysaurus* slant anteriorly. Benton (2016:

20) reported similar forward-leaning neural spines on the posterior cervical vertebrae of *Shihtienfenia* as 'most unusual'.

Dorsal vertebrae (6th–19th vertebrae)

The dorsal vertebrae are defined as those vertebrae supporting the ribs that form a continuous cage over the length of the torso (Tsuji 2010, 2013). In the basal South African pareiasaurs they extend from the 6th to the 19th vertebrae (Turner *et al.* 2015, character 80).

In the holotype of *Embrithosaurus* the 6th to 8th vertebrae are preserved in a single block (Fig. 9), the 9th, 10th (Fig. 10), 11th, 12th (Fig. 13), and 13th are single elements and the 14th to 16th (Fig. 14) and 17th to 21st (Figs 15, 16) are articulated in two large blocks. In *Nochelesaurus* specimen SAM-PK-6238 the dorsal vertebrae are preserved as isolated separated elements, apart from the 11th to 13th vertebrae (Fig. 11) which are articulated. Four large, isolated neural spines are also preserved, but, these do not appear to belong to any of the preserved fifteen vertebrae. The dorsal vertebrae of the holotype of *Bradysaurus baini* are preserved in two large blocks, i.e. a block containing the 3rd to 12th vertebrae and a block containing the 13th to 19th vertebrae.

We consider the dorsal vertebral column in two regions: anterior dorsal vertebrae (6th to 9th vertebrae) and posterior dorsal vertebrae (10th to 19th vertebrae). The entire dorsal vertebral sequence is united by a number of features that are different compared to the posterior cervicals.

All dorsal vertebrae are larger than the posterior cervicals and increase in size posteriorly. Mediolaterally they are much wider than the cervicals as a result of the expanded laterally projecting transverse processes, which form a vertical flange-like wall. The posteroventrally extended or swollen margins or rims of the centra are much more robust than in the cervical vertebrae. All centra are anteroposteriorly short (mediolaterally wider than anteroposteriorly long) (e.g. Fig. 12) apart from the posterior-most dorsal vertebrae which are as long as wide. The centra of the dorsals are amphicoelous with deep concave anterior articular facets, whereas the posterior facets have concave dorsal and a convex ventral halves, producing a posteroventrally extended overhanging 'lip-like' projection (Fig. 12). Centra of the dorsal vertebral are more mediolaterally constricted than those of the posterior cervicals and the vertical grooves on the sides are very deep. This constriction intensifies posteriorly on each subsequent vertebra, causing the anterior and posterior rims of each centrum to become more exaggerated and pronounced. Ventrally, the anterior and posterior rims of the posterior dorsal centra curve towards each other and the ventral surface of the centrum lacks the distinct longitudinal midline ridge of the posterior cervicals. Approximately half way up, the centrum is medially pinched, such that the ventral-most portion of each centrum forms a midline cylindrical swelling. From the 11th vertebrae backwards, the mediolateral constriction is so severe that centra are severely 'pinched in', creating an exaggerated hourglass-shape and below

this constriction the 18th and 19th vertebrae are wide and square-edged.

The processes bearing the prezygapophyses of the anterior dorsal vertebrae are small and extend only a short distance anterodorsally (Figs 9, 10). They present a slightly convex surface that faces dorsomedially and slightly anteriorly. On the posterior dorsal vertebrae, the prezygapophysial processes are more robust. On the 6th to 13th vertebrae the prezygapophyses are mediolaterally narrow and laterally they do not reach the level of the lateral articular surface of the transverse process. On the 14th to 19th vertebrae, the prezygapophyses are mediolaterally wider and extend laterally to just beyond the level of the articular surface of the transverse process.

The postzygapophysial processes on all dorsal vertebrae are very large, much larger than the prezygapophyses, and significantly increase in size, lateral extension, and overall robustness posteriorly (Figs 13, 14). They extend posterolaterally from the lateral base of the neural spine to far beyond the posterior border of the centrum, and laterally extend slightly further than the prezygapophyses with which they articulate. On the anterior dorsal vertebrae, the postzygapophysial processes are mediolaterally much narrower than the transverse processes (Fig. 10, SAM-PK-8034, 10th vertebra), but on the posterior dorsals they reach the level of the transverse processes (Fig. 13, SAM-PK-8034, 12th vertebra).

Additional preparation of the 6th to 16th vertebrae of the holotype of *Embrithosaurus* (SAM-PK-8034) reveals that these vertebrae have notochordal centra (Figs 10, 13), as have also been reported for a juvenile specimen of *Deltaojatia* (Tsuji 2010, 2013). Broom (1903: 129) suggested that intercentra were 'apparently' present between all the dorsal vertebrae of SAM-PK-8034. Boonstra (1934c) stated that small intercentra are found throughout the pareiasaurian presacral vertebral series, except in the first five vertebrae. We did not observe any intercentra in SAM-PK-8034, but the holotype of *Bradysaurus* (NHMUK PV R 1971) preserves several large, dorsoventrally flattened intercentra, positioned ventrally, from the 8th to 19th dorsal vertebrae. Superficially, the intercentra resemble osteoderms as they are ovoid, thin, disc-like, and convex with rugose ventral surfaces.

The four-sided, diamond-shaped neural spines are more robust, larger, and taller on the dorsal vertebrae than on the posterior cervicals. Dorsally, the neural spines are significantly mediolaterally flared, and typically wider than long. However, on the 11th to 13th vertebrae of *Nochelesaurus* (Figs 11, 12) the spines are mediolaterally wider (60–65 mm) than long (40–55 mm), whereas on the 14th to 16th vertebrae they are anteroposteriorly longer (55–60 mm) than mediolaterally wide (40–45 mm). Generally, the neural spines of the anterior dorsals are short (reaching ± 40 mm above the postzygapophyses) and are taller on the posterior dorsal vertebrae (± 60 –70 mm). However, in *Embrithosaurus*, the neural spines are short on the 12th to 16th vertebrae, and higher on the 17th to 19th. In *Embrithosaurus* the dorsal neural spines lean forward, probably the result of distortion as in *Bradysaurus* and *Nochelesaurus* the neural spines of all dorsal vertebrae

are vertical or only very slightly forward-leaning. The neural canals of the anterior dorsal vertebrae are larger than those of the posterior cervical vertebrae as the diameter of the canal decreases posteriorly.

Anterior dorsal vertebrae (6th–9th vertebrae)

All of the anterior dorsals (6th to 9th vertebrae) are similar in morphology and increase in size posteriorly. Most notably, the postzygapophyses increase in size and mediolateral extent. Dorsally, the transverse process extends further laterally than the ventral part, creating an oblique lateral edge in anterior or posterior view (e.g. Fig. 10) and this difference becomes more exaggerated on more posterior vertebrae, where the process also increases in mediolateral extent and general thickness. The process forms a flange that is vertical and slightly posterodorsally oriented, with the dorsal portion more posterodorsally oriented than the more vertical ventral portion.

The obliquely slanted lateral facet of the transverse process comprises a dorsal facet that is tall, narrow, flat, roughly rectangular, and faces laterally to ventrolaterally, and a ventral facet that is wide, round, shallow, gently concave and faces posterolaterally (Figs 8, 9). On the 6th to 9th vertebrae (e.g. right side of the 7th vertebra of SAM-PK-8034, Fig. 9) the flange is dorsoventrally high. On the lateral side of the vertebrae, the ventral facet is very low and almost indistinguishable from the side of the body of

the centrum, hardly protrudes from the lateral side of the centrum, and ventrally almost reaches the ventral surface of the centrum.

Posterior dorsal vertebrae (10th–19th vertebrae)

From the 10th vertebra backwards in *Embrithosaurus* (Fig. 10) and the 11th vertebra in *Bradysaurus*, the small, rounded, ventral facet on the lateral transverse process or flange shifts upwards to merge with the longer, vertical, dorsal facet, decreasing the height of the transverse process and the lateral facet. This can be seen on the 13th to 19th vertebrae (Figs 11, 12, 13, 14) where the transverse process continues to shorten in dorsoventral height on each subsequent posterior vertebrae and the lateral facet comprises two roughly equally sized lobes. The transverse process shifts significantly dorsally so that the dorsal edge reaches the level of the articular surface of the prezygapophyses and the ventral edge is several centimetres above the ventral edge of the centra (Figs 13, 14).

As in the anterior dorsals, the lateral facet of the transverse process is oblique as the dorsal portion of the transverse process extends further laterally than the ventral portion. Moving posteriorly the lateral facet becomes more vertically oriented and less oblique as the ventral portion extends further laterally from the centrum. Additionally, the almost vertical transverse process becomes more posterodorsally oriented over subsequent posterior vertebrae (Fig. 14).

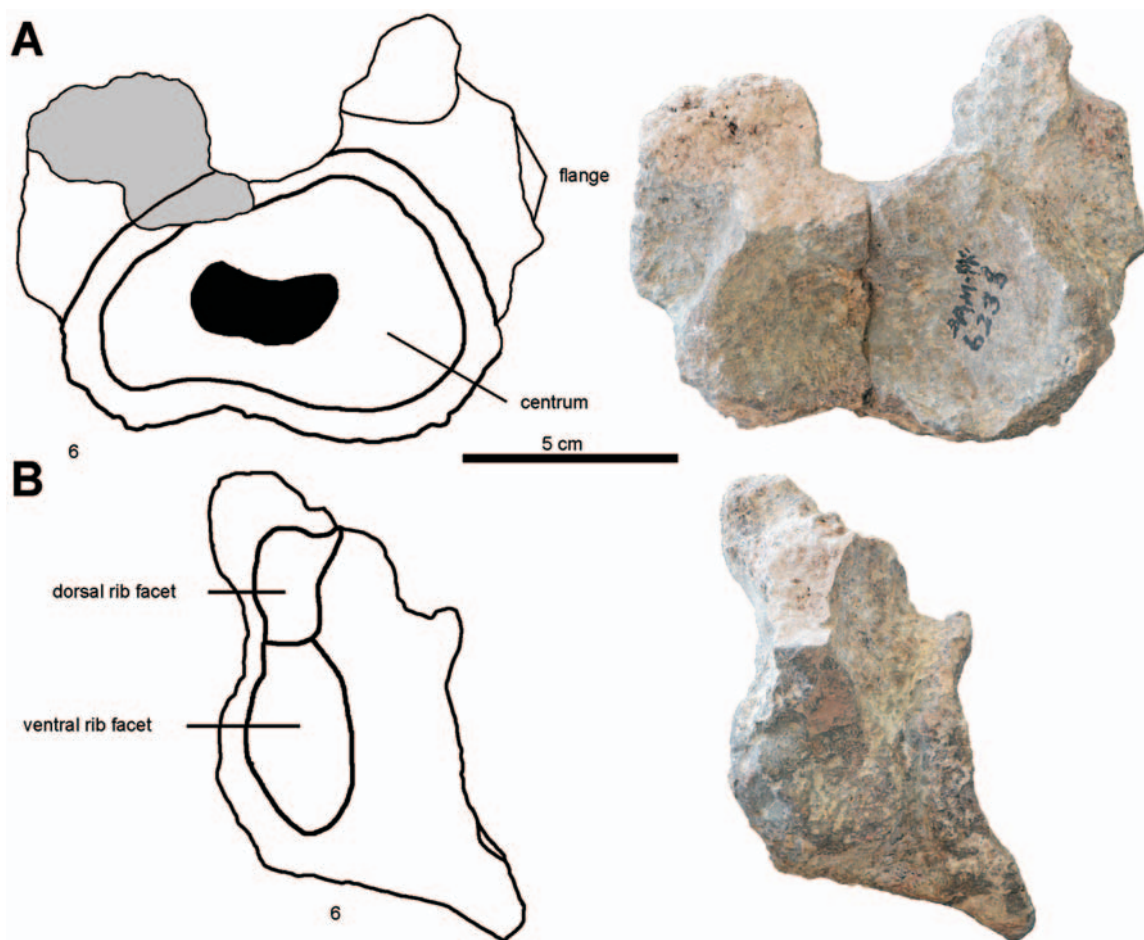


Figure 8. Photographs and interpretive drawings of the 6th vertebra of SAM-PK-6238 (*Nochelesaurus alexanderi*), (A), in anterior view, and (B), in left lateral view. Dorsal to the top of the page. Scale bar equals 5 cm.

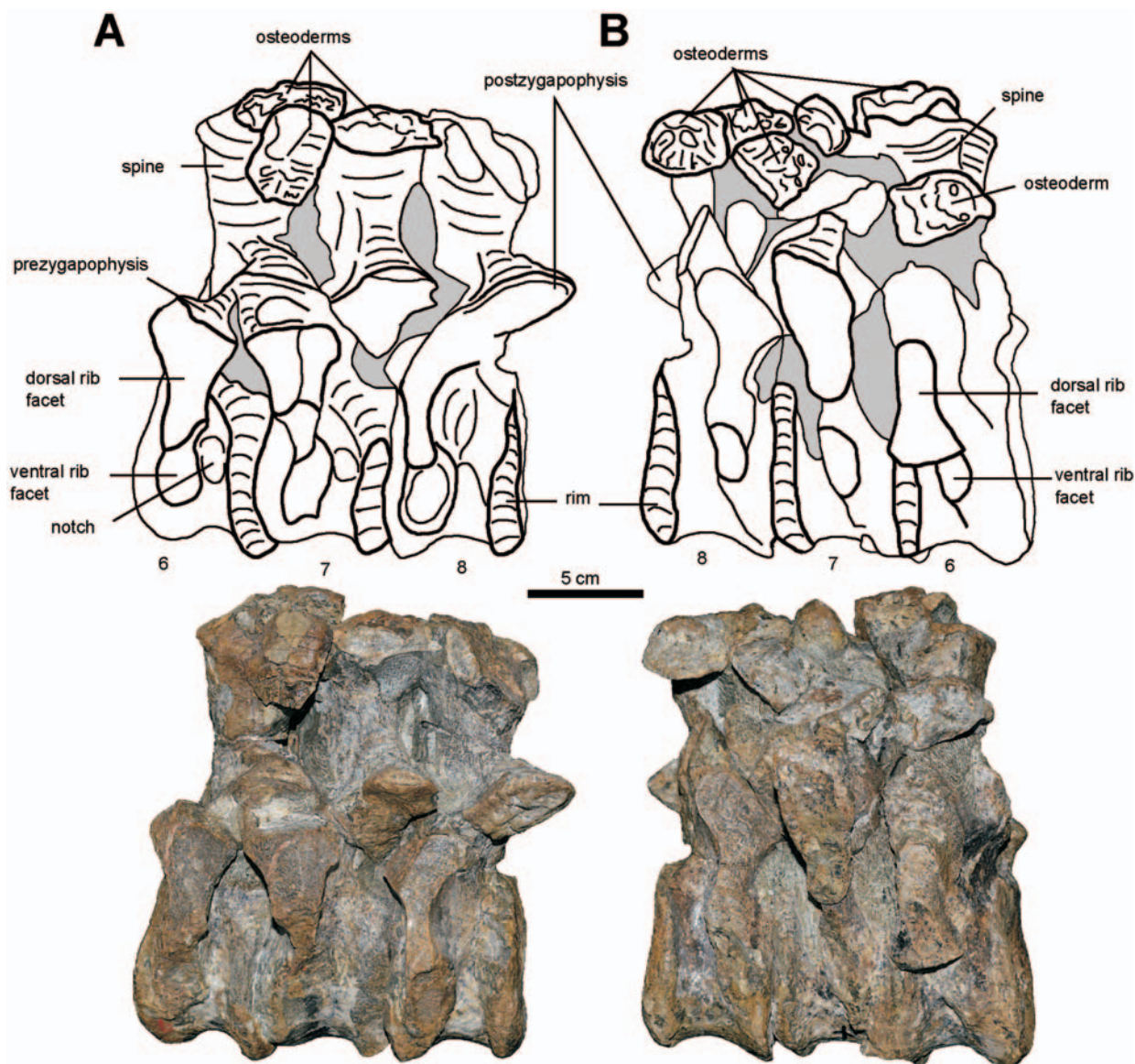


Figure 9. Photographs and interpretive drawings of the 6th–8th vertebrae of the holotype of *Embrithosaurus schwarzi* (SAM-PK-8034), (A), in left lateral view, and (B), in right lateral view. Dorsal to the top of the page. Scale bar equals 5 cm.

On the 18th dorsal vertebra of *Embrithosaurus* the lateral articular surface for the head of the rib is indistinct, and on the 19th vertebra only a very small lateral ventral facet is present (Fig. 15). The presence of these facets on the transverse processes shows that the 18th and 19th vertebrae bore ribs, and indeed lumbar vertebrae are absent in all pareiasaurs (Boonstra 1934c; Lee 1997b; Turner *et al.* 2015, character 81).

Mid dorsal vertebrae show that below the base of the neural spine is an upside-down V-shaped cavity, formed laterally by the arms of the prezygapophysial processes that sweep posteroventrally from the base of the neural spine (Figs 10, 12, 13). A vertical midline ridge divides the cavity into two triangular halves. On the posterior side of the vertebra, the cavity is separated from the neural canal by a low horizontal, bar-like hyposphene which articulates with the facet of the hypantrum on the anterior side of the adjacent vertebra. The hypantrum is much less robust than the hyposphene. The neural canal is very large. The prezygapophysial processes gradually increase in robustness and mediolateral width posteriorly.

The dorsal surface of the neural spines is simple anteriorly and more complex posteriorly. Anteriorly, they are concave with a deep longitudinal midline groove (9th to 13th vertebrae of the holotype of *Embrithosaurus*, Figs 10, 13; *Nochelesaurus* SAM-PK-6238, 11th to 13th vertebrae, Fig. 11; *Bradysaurus baini* holotype, 5th to 9th dorsal vertebrae, Fig. 74). Posteriorly, the dorsal surfaces of the spines are convex, with a rugose surface with small circular pitting (14th to 19th vertebrae of the holotype of *Embrithosaurus*, Fig. 16; *Nochelesaurus*, SAM-PK-6238, 14th to 16th vertebrae; *Bradysaurus baini* holotype, 10th to 18th vertebrae, Fig. 74, partially obscured by osteoderms). Along with the rugose convex surfaces, *Embrithosaurus* has a long, shallow midline groove outlined by a raised rim on these posterior vertebrae; *Nochelesaurus* SAM-PK-6238, has a large, central, shallow, rounded, pit, but no long anteroposterior midline groove; and *Bradysaurus baini* has no longitudinal midline groove and sometimes has a large, central, shallow, rounded pit.

In *Bradysaurus baini*, the 13th to 19th vertebrae are homogeneous. The centra are massive and deeply excavated

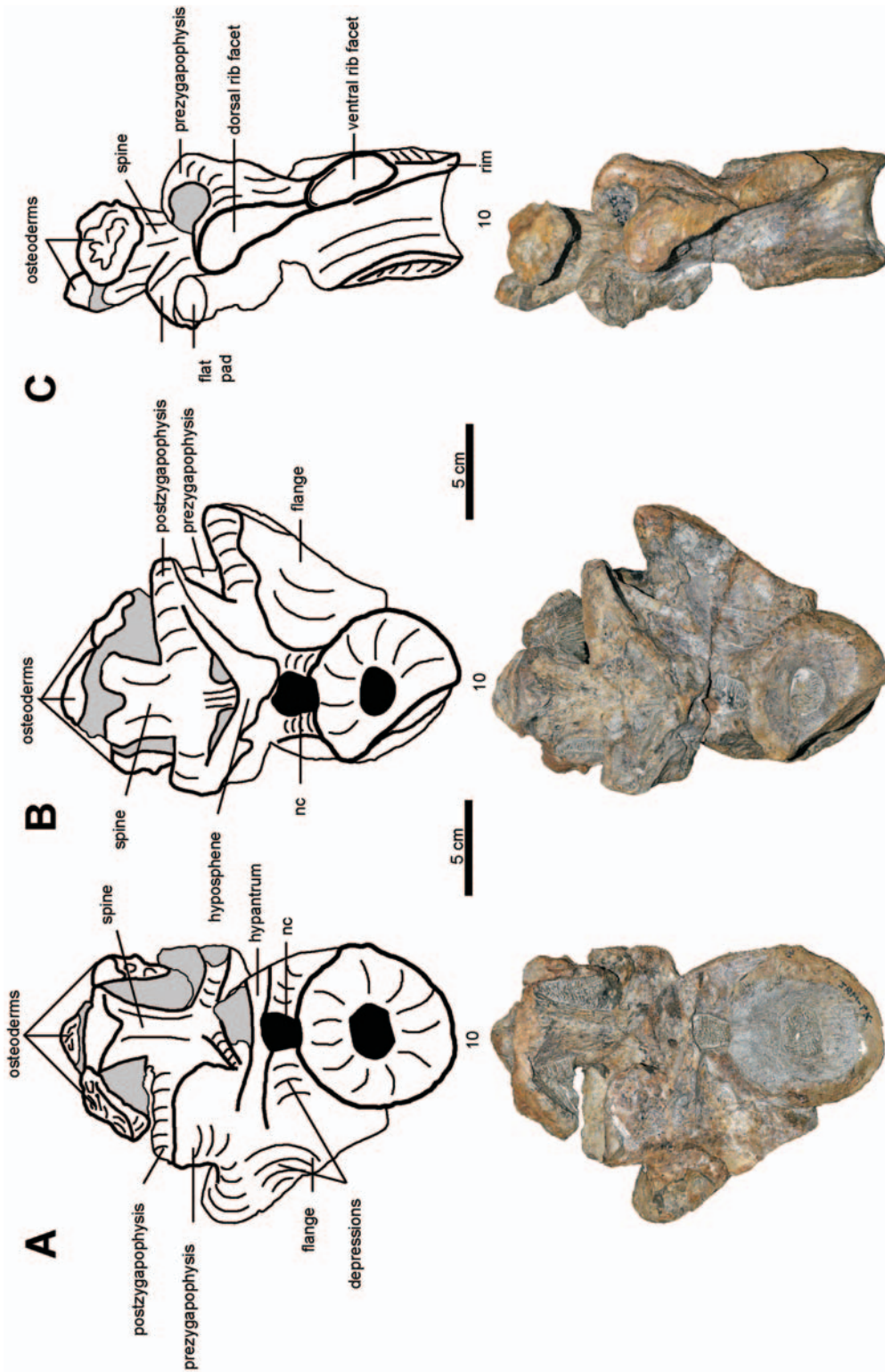


Figure 10. Photographs and interpretive drawings of the 10th vertebrae of the holotype of *Embriithosaurus schwarzi* (SAM-PK-8034), (A), in anterior view, (B), in posterior view, and (C), in left lateral view. Dorsal to the top of the page. Scale bar equals 5 cm.

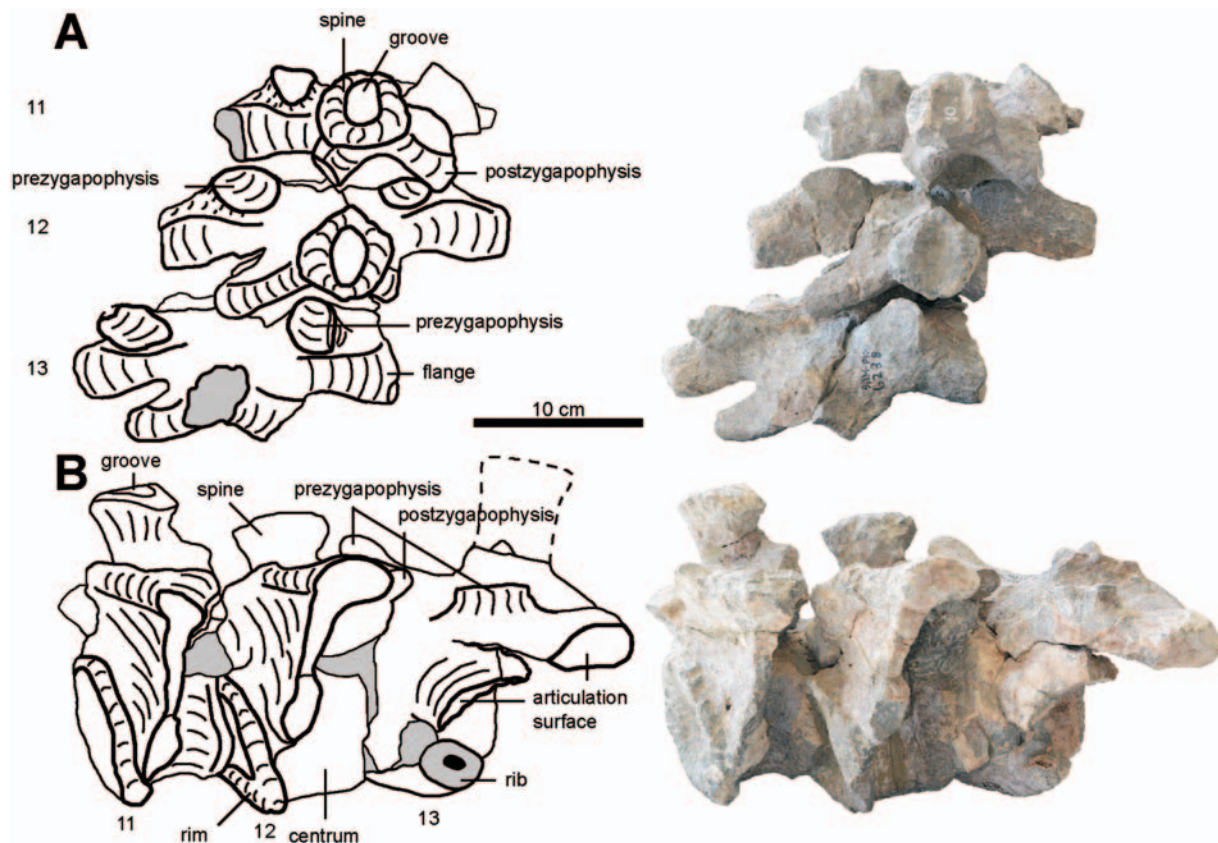


Figure 11. Photographs and interpretive drawings of the 11th–13th vertebrae of SAM-PK-6238 (*Nochelesaurus alexanderi*), (A), in dorsal view, and (B), in left lateral view. Anterior to the top of the page in (A), dorsal to the top of the page in (B). Scale bar equals 10 cm.

laterally, creating thick protruding anterior and posterior rims.

Sacral vertebrae (20th–23rd vertebrae)

There are four sacral vertebrae (20th–23rd vertebrae) (Turner *et al.* 2015, character 82). In *Embrithosaurus*, the first two sacral vertebrae (20th, 21st) are articulated in a large block containing the 17th to 21st vertebrae (Figs 15, 16) and the last two sacral vertebrae (22nd, 23rd) are preserved articulated in a small separate block (Fig. 17). The sacral vertebrae of *Bradysaurus baini* are preserved in a large block (Fig. 57).

All four sacral vertebrae of *Embrithosaurus* are damaged dorsally, with the neural spines and processes of the postzygapophyses sheared-off. In the *Bradysaurus baini* holotype the neural spines of the 20th and 21st vertebrae are the most massive on this individual (dorsally 70 mm wide, 65 mm long) and the slightly convex dorsal surface of the neural spines is covered with rugose ornamentation comprising several hundred irregular and raised ridges per spine, less than 1 mm thick and generally placed in a random pattern. There are also irregular and mottled tiny pits. A longitudinal, very shallow, midline, groove (10 mm wide, 25 mm long) is present. The neural spines decrease in size from the 22nd vertebrae backwards.

In *Embrithosaurus*, the first sacral vertebra (Figs 15, 16, 20th vertebra) is distinct from the last dorsal vertebra (19th) in several ways: 1) dorsally, behind the prezygapophyses, the first sacral is very robust and there is a wide, slightly concave region bordered laterally by a conspicu-

ous, sharp longitudinal ridge which supports the greatly expanded first sacral rib (Fig. 16); 2) the processes of the prezygapophyses of the first sacral are most robust and extend further anteriorly; and, 3) the breadth of the postzygapophyses is less than the breadth of the prezygapophyses on the first sacral vertebra.

In *Bradysaurus baini*, on the first sacral vertebra, there is a similarly wide and shallowly depressed region, bordered laterally by a sharp, raised longitudinal ridge that supports the expanded first sacral rib (Fig. 57) and the prezygapophyses are also very large. The first two sacral centra are the largest, decreasing significantly in size posteriorly on the last two sacra. The centra of the four sacral vertebrae are fused, evidenced by the fused ventral surface rims of adjacent vertebrae and the lack of matrix between these rims. Only in this taxon are intercentra which are ventrally convex and preserved posteroventral to the fused rims of the first and second sacral vertebrae.

Caudal vertebrae (24th vertebra backwards)

Broom (1903: 127) stated that there were ‘probably’ 30 caudal vertebrae in the holotype of *Embrithosaurus* (Turner *et al.* 2015, character 83). Broom (1903) noted that apart from a few anterior caudals following the sacrum, a block of nine caudal vertebrae and two additional very small articulated caudals were preserved. However, presently only a series of four articulated anterior caudal vertebrae (Fig. 17, 24th to 27th vertebrae) and the two small additional vertebrae are preserved. The nine articulated caudals reported by Broom (1903) are lost. Twenty-

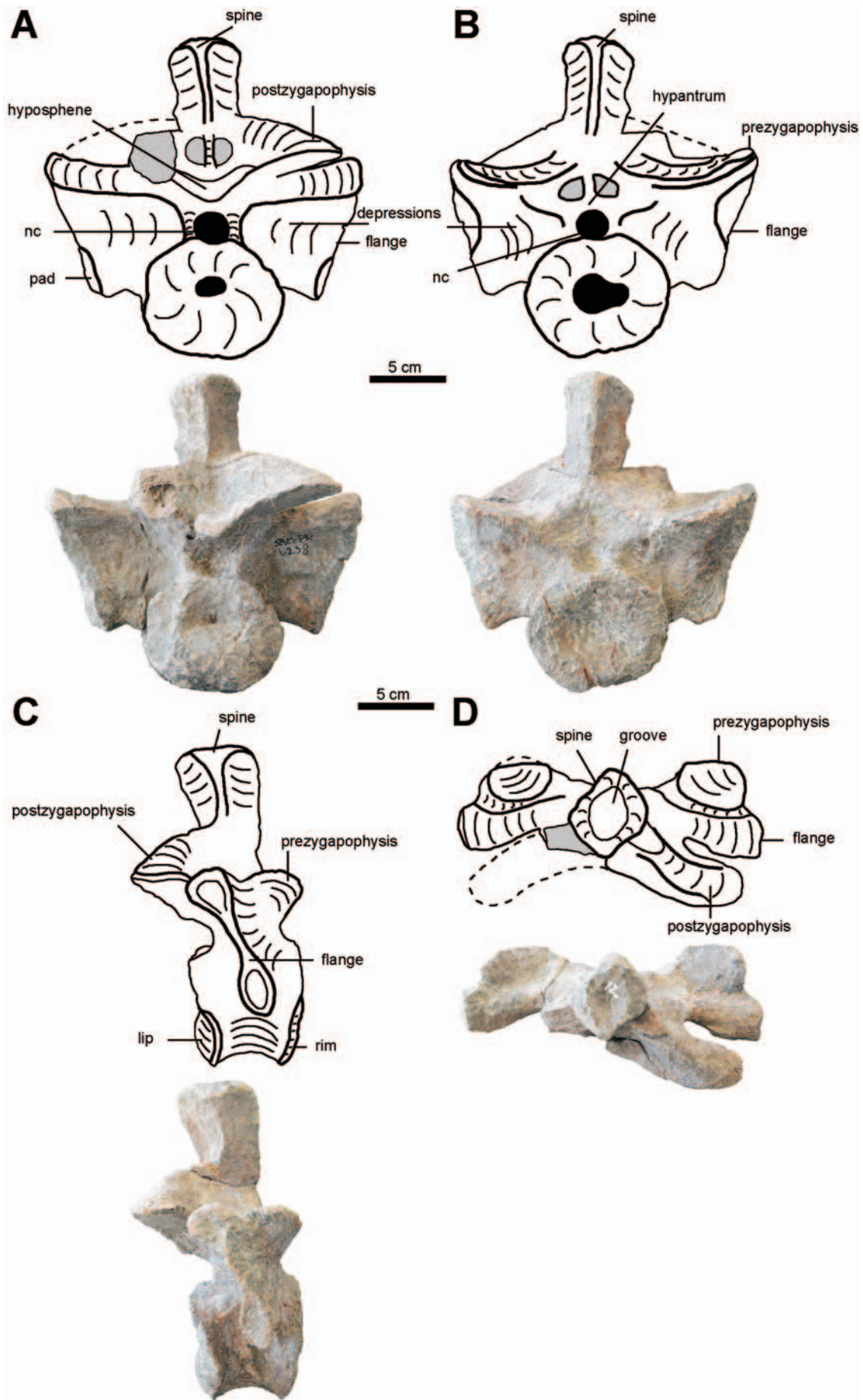


Figure 12. Photographs and interpretive drawings of the 13th vertebra of SAM-PK-6238 (*Nochelesaurus alexanderi*), (A), in anterior view, (B), in posterior view, (C), in right lateral view, and (D), in dorsal view. Dorsal to the top of the page in (A), (B) and (C). Anterior to the top of the page in (D). Scale bar equals 5 cm.

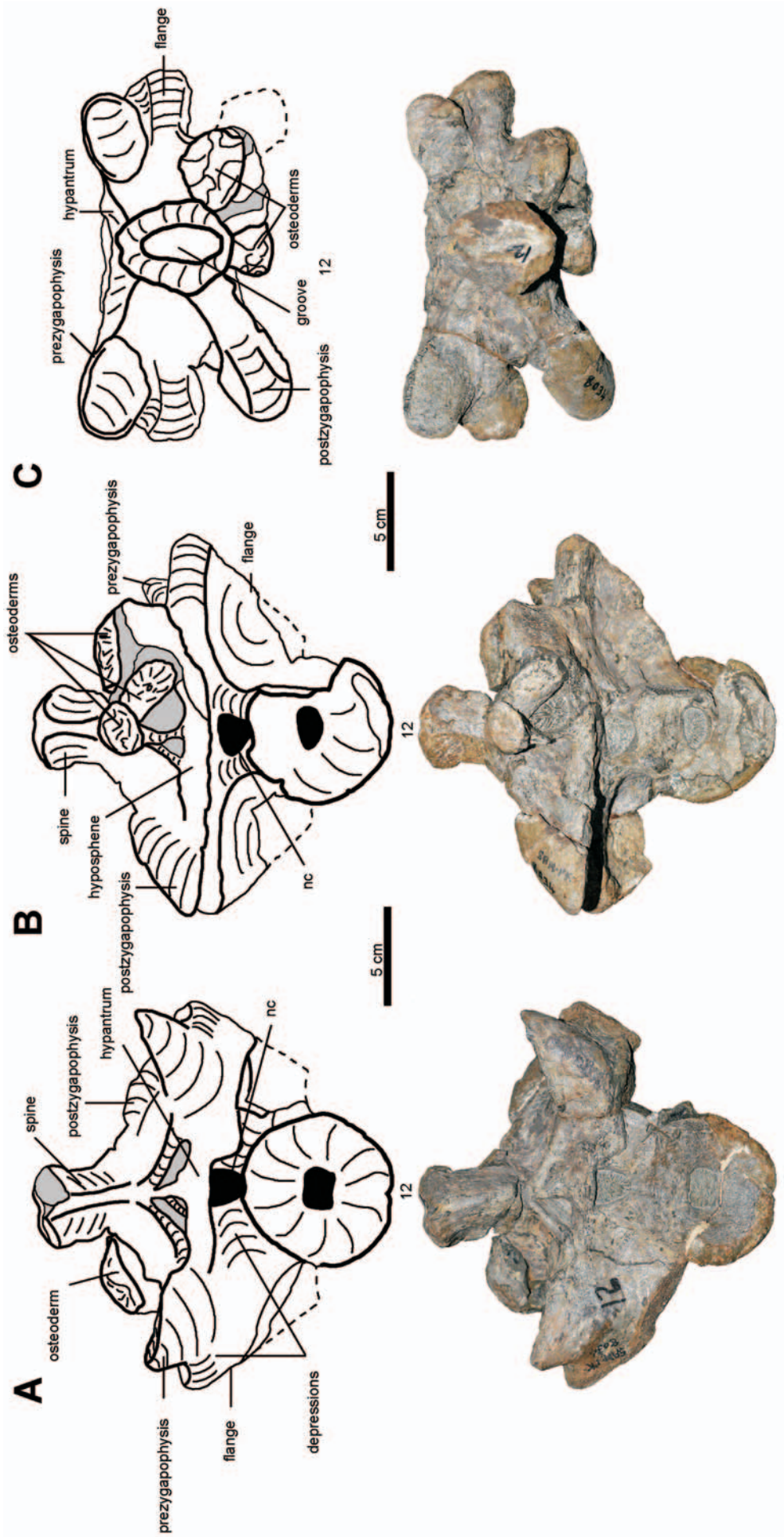


Figure 13. Photographs and interpretive drawings of the 12th vertebrae of the holotype of *Embriithosaurus schuurzi* (SAM-PK-8034), (A), in anterior view, (B), in posterior view, and (C), in dorsal view. Dorsal to the top of the page. Scale bar equals 5 cm.

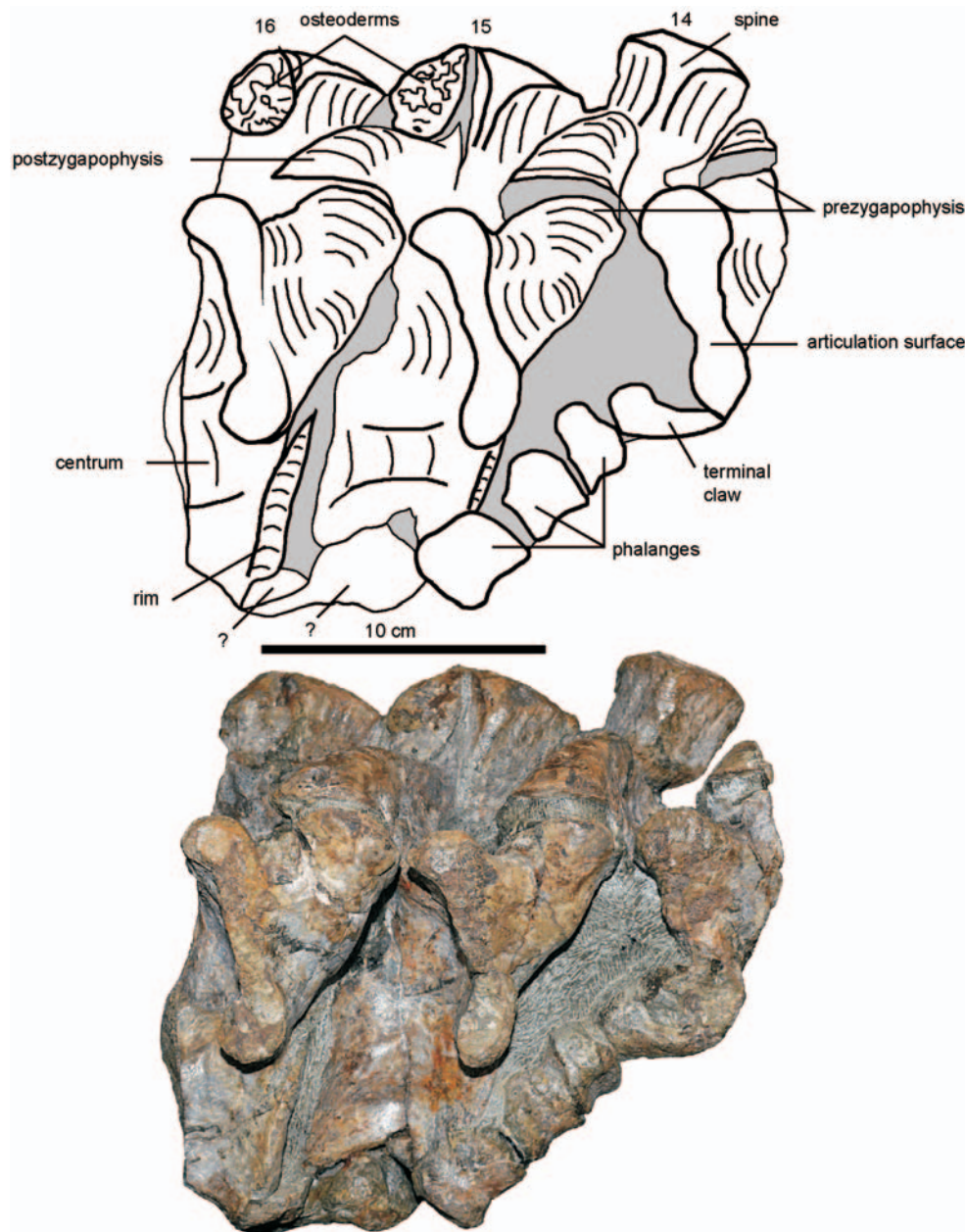


Figure 14. Photograph and interpretive drawing of the 14th–16th vertebrae of the holotype of *Embrithosaurus schwarzi* (SAM-PK-8034), in right lateral view. Dorsal to the top of the page. Scale bar equals 10 cm.

six caudal vertebrae are preserved in the holotype of *Bradysaurus baini* in three blocks: the 24th to 27th, the 28th to 37th, and the 38th to 49th (Fig. 18). Seeley (1892) considered that beyond the 49th vertebra there were several more vertebrae which are not preserved. No caudal vertebrae are preserved in any *Nochelesaurus* specimens.

The caudal vertebrae of *Bradysaurus* and *Embrithosaurus* show that the centra and size and length of the neural spines decrease rapidly posteriorly. In particular the processes of the postzygapophyses dramatically decrease in length and robustness. The prezygapophyses are also small, but twice as long as the very tiny postzygapophyses.

In *Embrithosaurus* the 24th to 27th vertebrae are short with straight lateral projections (transverse protuberances) on either side of each centrum (Fig. 17B) (Turner *et al.* 2015, characters 84, 85). These have damaged tips and are slightly posteriorly directed and short. They extend

over the anteroposterior extent of the lateral centra and shift ventrally and decrease in size on more posterior vertebrae. A deep notch is present laterally, below these lateral projections.

In *Bradysaurus baini*, the transverse processes are largest on the 24th and 25th vertebrae and are dorsoventrally elongated with a dorsal and a ventral lobe. From the 26th vertebra backwards, the transverse process is cylindrical and long and there are no lateral articulation surfaces as the processes end in a rounded stub and form an 'L' as their distal portions are recurved posteriorly parallel to the axis of the body (Fig. 18) (Turner *et al.* 2015, characters 84, 85).

The complete neural spine of the 27th vertebra of *Bradysaurus baini* is dorsoventrally high (65 mm) and triangular in cross-section (Fig. 18) with a sharp anterior side, and a straight to gently convexly curved posterior side. The dorsal surface is convex and slightly rugose. More posteri-

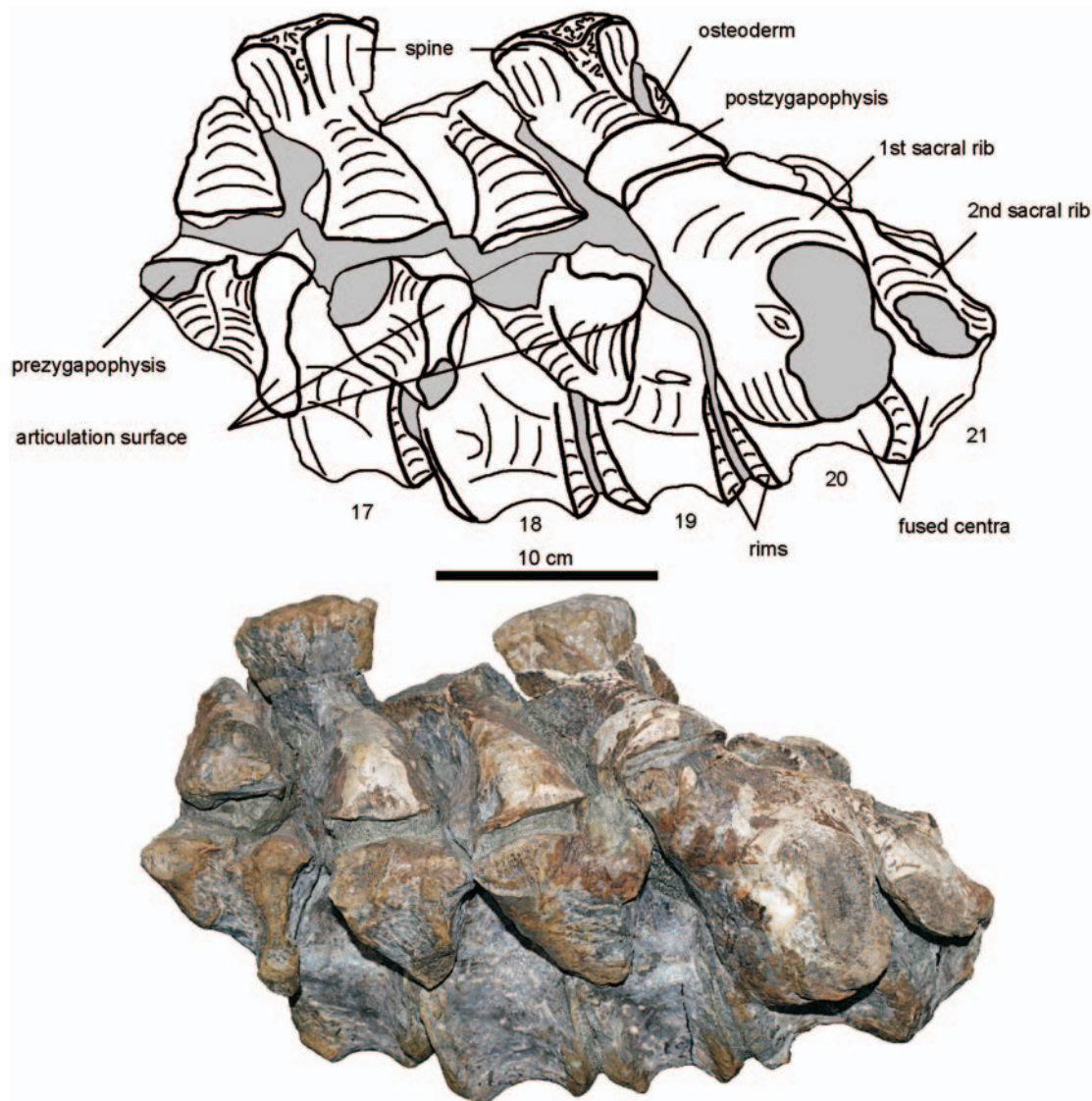


Figure 15. Photograph and interpretive drawing of the 17th–21st vertebrae of the holotype of *Embrithosaurus schwarzi* (SAM-PK-8034), in left lateral view. Dorsal to the top of the page. Scale bar equals 10 cm.

only, from about the 35th vertebrae backwards, the small neural spines have diamond-shaped four-sided dorsal surfaces and are anteroposteriorly longer than mediolaterally wide (Fig. 18). The 24th to 27th vertebrae of *Embrithosaurus* are poorly preserved and partially sheared-off and the neural spines are also triangular in cross-section.

V-shaped haemal arches are present on the ventral surfaces of most of the preserved caudal vertebrae of *Bradysaurus baini* and decrease in size posteriorly. As seen on the 38th to 49th vertebrae, the haemal arches articulate with two slightly concave facets, one either side of the midline, on the posteroventral rim of each centrum.

Broom (1903) described and illustrated long chevrons on the (now missing) 32nd to 40th caudal vertebrae of *Embrithosaurus*, stating that they developed from about the 5th caudal vertebrae (i.e. 27th or 28th vertebra) backwards and continue posteriorly to at least the 47th vertebrae. Chevrons are not present on the preserved 24th to 27th vertebrae. Boonstra (1934c) concluded that chevrons develop from the 4th caudal vertebrae backwards in *Embrithosaurus*. The posteroventral rim of the 4th caudal

vertebrae of *Embrithosaurus* (27th vertebra) appears to have short flat facets either side of the midline, possibly for articulation with the missing paired chevrons, but poor preservation makes this conclusion tentative. The posteroventral rim of the centrum of the first of the two small articulated caudal vertebra appears to show small notches either side of the midline for possible chevron articulation, but these notches may be the result of damage to the posterior rim.

Ribs

Broom's (1903) skeletal restoration of the holotype of *Embrithosaurus* (plate XVI; and here Fig. 1) shows that only three partial ribs were preserved, with the 12th rib almost complete and preserving the head. Presently only a single rib head is preserved in this specimen, presumably the 12th rib as per Broom. *Nochelesaurus* specimen SAM-PK-6238 preserves several dozen large, disarticulated, and isolated partial rib fragments, including several well-preserved rib heads, all holocephalous. For *Bradysaurus baini*, five complete but shifted and disarticulated ribs are preserved along the left side of the 8th, 9th and 10th verte-

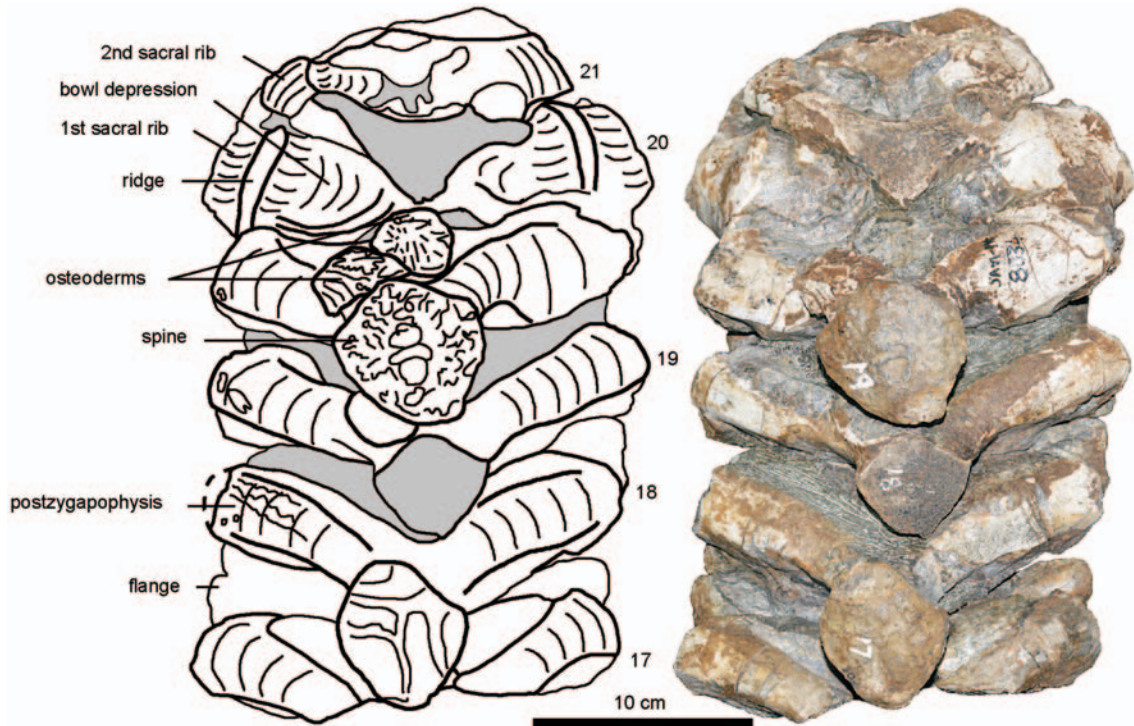


Figure 16. Photograph and interpretive drawing of the 17th–21st vertebrae of the holotype of *Embrithosaurus schwarzi* (SAM-PK-8034), in dorsal view. Posterior to the top of the page. Scale bar equals 10 cm.

brae, and a few almost complete ribs are disarticulated but preserved in the block containing the 13th to 19th vertebrae.

Cervical ribs (2nd–5th vertebrae)

As noted by Boonstra (1934c: 59) the holotype of *Embrithosaurus* shows that all presacral vertebrae, except the atlas, possess facets for rib articulation (see vertebrae).

Dorsal ribs (6th–19th vertebrae)

Most of the rib fragments of the large, single-headed dorsal ribs of *Nochelesaurus* (SAM-PK-6238) are thick (35 mm wide) with long (410–560 mm) and gently curved shafts. They have dorsoventrally elongated heads, that form ‘figure-of-eight’ articular facets. All the long rib fragments taper distally and are oval in cross-section. In the holotype of *Bradysaurus baini*, the five complete and

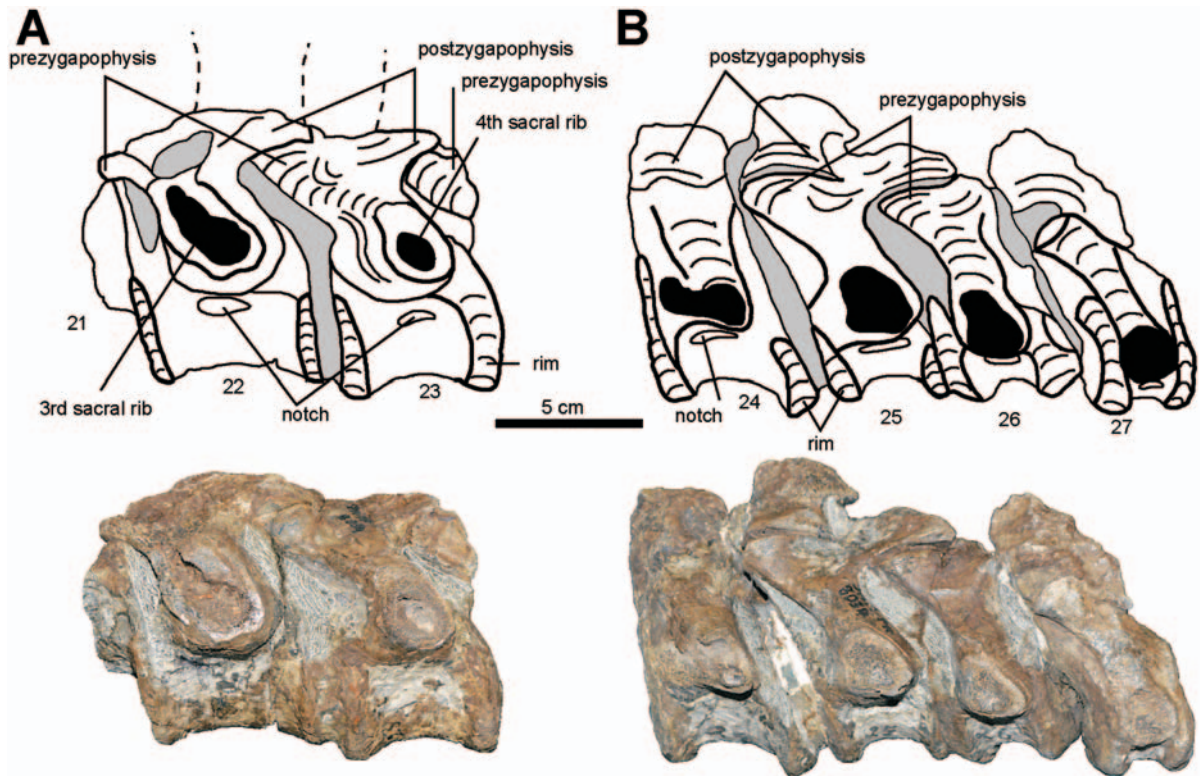


Figure 17. Photograph and interpretive drawing of the 22nd–27th vertebrae of the holotype of *Embrithosaurus schwarzi* (SAM-PK-8034), in left lateral view. Dorsal to the top of the page. Scale bar equals 5 cm.

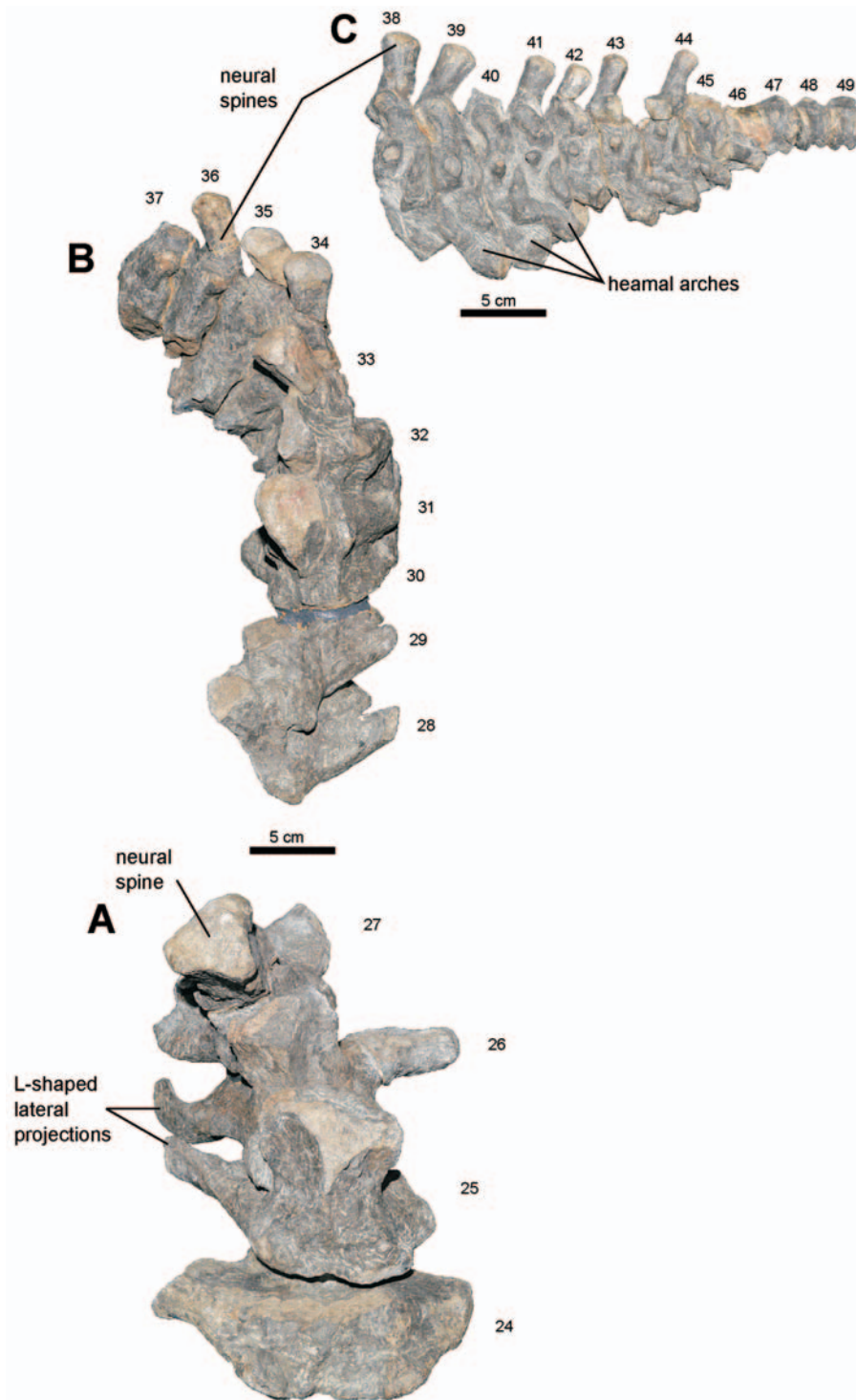


Figure 18. Photographs of the caudal vertebrae of the holotype of *Bradysaurus baini* (NHMUK PV R 1971), (A), anterior caudals 24–27 in dorsal view, (B), caudals 28–37 in dorsal view, and (C), posterior caudals 38–49 in left lateral view. Posterior to the top of the page in (A) and (B). Dorsal to the top in (C). Scale bar equals 5 cm.

shifted ribs preserved along the left side of the 8th, 9th, and 10th dorsal vertebrae are approximately 600 mm long, with large, single heads that have long and bilobed articulation surfaces.

Sacral ribs (20th–23rd vertebrae)

The holotypes of *Embrithosaurus schwarzi* and *Bradysaurus baini* each preserve four, nearly complete, sacral ribs and the holotype of *Nochelesaurus alexanderi* has no sacral ribs preserved.

In the holotype of *Embrithosaurus* the first sacral rib is

very large, dorsoventrally elongated, and laterally occupies the entire dorsoventral height of the iliac blade (Figs 51, 54). It is oriented anterodorsally at about 45° above the horizontal plane. The ventral margin of the rib is convex. The dorsal margin has a concave anterior side and a much more concave posterior side to accommodate the adjacent second sacral rib. The medial end of the first sacral rib measures 90 mm dorsoventrally and 70 mm anteroposteriorly (Fig. 15) and covers most of the lateral surface of the centrum. The rib is severely constricted midway. The lateral end of the rib is much larger than the

medial end, and measures 230 mm anteroposteriorly and extends over the longitudinal level of the 20th to 23rd vertebrae. The first sacral rib of *Bradysaurus baini* (20th vertebra) is much smaller than that of *Embrithosaurus*, and for example, measures medially only 50 mm dorsoventrally and 60 mm anteroposteriorly.

In *Embrithosaurus*, the second sacral rib is much smaller than the first, medially only dorsoventrally 20 mm high and anteroposteriorly 50 mm long. The rib is anterodorsal, but more horizontally oriented and with the midway constriction less severe than in the first sacral. The second sacral rib is relatively flat and sheet-like. The articulation of the second rib against the ilium is positioned high on the iliac blade, above and behind the articulation of the first sacral rib and is only half the anteroposterior length of the first sacral rib. In *Bradysaurus baini* the second sacral rib is the largest and medially the rib is dorsoventrally 110 mm high and anteroposteriorly 50 mm long. Laterally, the rib terminates with a deep, concave, lateral facet for articulation with the corresponding convex bulge of the medial iliac blade, best seen on the right (Fig. 57A).

Short medial portions of the third and fourth sacral ribs are preserved on the 22nd and 23rd vertebrae of the holotype of *Embrithosaurus* (Fig. 17). The fourth sacral rib is the smallest of the series and unlike the first three sacral ribs, it is not flattened or plate-like but is oval in cross-section. Boonstra (1934c) notes that the fourth pareiasaurian sacral rib does not reach the ilium, and was likely attached to it by a ligament. In *Bradysaurus baini* the third and fourth sacral ribs are much smaller than the first two, oriented almost horizontally, and appear dorsoventrally flattened, or 'sheet-like' (Turner *et al.* 2015, character 108).

Shoulder girdle and forelimb

The shoulder girdle of pareiasaurs comprises paired scapulocoracoids, cleithra, clavicles, and a single median interclavicle (Boonstra 1932b). The holotype of *Embrithosaurus* preserves a partial left scapulocoracoid with articulated partial proximal cleithrum and a partial lateral clavicular fragment (Fig. 25). A separate partial right interclavicle and articulated clavicle are preserved (Fig. 19). The holotype of *Nochelesaurus* preserves a partial right scapulocoracoid (Fig. 26) and separately the base of the left scapula blade (Fig. 26). Most of the interclavicle is preserved, apart from the median stem, and the medial halves of each clavicle are tightly articulated to the interclavicle. SAM-PK-6238 preserves an almost complete right scapulocoracoid (Fig. 27), and separately an isolated fragment of the dorsal left scapula blade (Fig. 27C) and the complete right clavicle (Fig. 22). The holotype of *Bradysaurus baini* preserves a virtually complete left scapulocoracoid and cleithrum (Fig. 28). Most of the right coracoid plate is damaged and the right distal scapula blade is missing (reconstructed in plaster) whereas most of the interclavicle and both clavicles are preserved.

Interclavicle

As in all pareiasaurs, the interclavicle is T-shaped, comprising a thin, flat median stem and two laterally projecting thin flat extensions ('lateral arms') on a trans-

verse bar. The right and left lateral arms of the transverse bar of the interclavicle of the holotype of *Nochelesaurus* are preserved but not the posterior portion of the median stem (Fig. 20) whereas the interclavicle of SAM-PK-6238 preserves the entire median stem and the right lateral arm (Fig. 21). These two *Nochelesaurus* specimens are used as the basis for describing the interclavicles of the group.

The median stem of the interclavicle of SAM-PK-6238 is thin and dorsoventrally flat. It is slightly dumbbell-shaped being anteriorly (80 mm wide), narrowing posteriorly to 50 mm, before widening to 70 mm near the posterior end of the bone (Fig. 21A,B). Anteriorly, behind the transverse bar, the median stem has a flat dorsal surface (Fig. 21B), and ventrally is raised to form a swollen median ridge (Fig. 21A). The midline ridge is higher and narrower anteriorly, and posteriorly it widens and flattens to form a gentle convex ventral surface and a rugose and concave dorsal surface.

The transverse bar of the interclavicle is robust (Figs 20A, 21A) and the anterior surface is deeply grooved for the articulation of the sharp posterior process of the clavicles. There is a ridge on the anterior surface, below the groove (Fig. 21C). The lateral extensions of the interclavicle flatten anteroposteriorly and the strongly convex posterior sides curve and flatten laterally to a rounded 'cup-shaped' tip.

The holotype of *Embrithosaurus* preserves only the lateral end of the right interclavicle (Fig. 19). Its morphology is typical for the group: the bone is anteroposteriorly flattened, the anterior surface is deeply grooved, the posterior side convex and has a rounded lateral edge. The anterior surface is bowl-shaped to accommodate the ventral process of the clavicle (Fig. 19). The interclavicles of the holotype of *Bradysaurus baini* are very typical for the group, share all salient morphology, and offer no unique features.

Clavicle

The clavicles are long, flat bones which extend laterally from their median articulation with the interclavicle, to reach laterally just beyond the dorsal edge of the acromion process of the scapula.

The holotype of *Embrithosaurus* preserves only small, partial left (Fig. 25) and partial right (Fig. 19) clavicular fragments. On the holotype of *Bradysaurus*, the left clavicle is complete, with the medial portion articulated with the left lateral extension arm of the interclavicle (Fig. 23) and the lateral end attached to the left scapula (Fig. 28). The complete right clavicle of *Nochelesaurus* specimen SAM-PK-6238 is beautifully preserved (Fig. 22), 520 mm long, and gently upwardly curved laterally along its length, oriented as a thin, flattened, vertical wall (anteroposteriorly flat, dorsoventrally high). In all three species, the mid anterior surface is overall slightly convex, flattened in the centre but more convex towards the dorsal and ventral anterior edges.

The posterior surface of the clavicle has a number of features. Medially, in all species, the clavicle narrows dorsoventrally towards the midline to become triangular in cross-section as it forms a sharp, wedge-shaped, posterior process (Fig. 22B) that fits into the corresponding

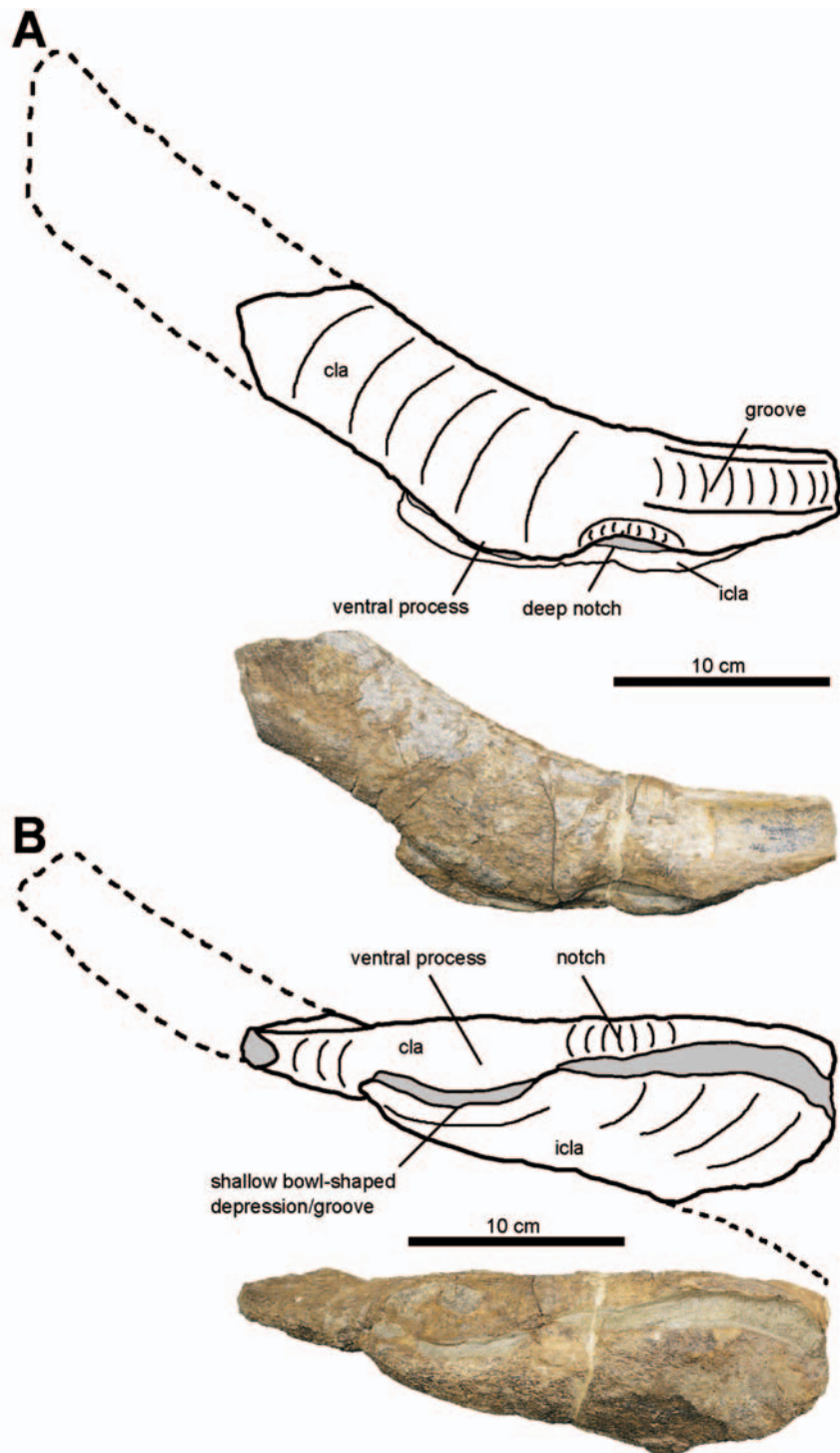


Figure 19. Photographs and interpretive drawings of the right clavicle and interclavicle of the holotype of *Embrithosaurus schwarzi* (SAM-PK-8034), (A), in anterior view, and (B), in ventral view. Dorsal to the top of the page. Scale bar equals 10 cm.

deep groove on the anterior side of the interclavicle (Fig. 21C). All species have a deep groove on the anterior surface of the interclavicle, which is deeper medially and shallower laterally (e.g. in *Embrithosaurus*, Fig. 19, and *Nochelesaurus*, Fig. 21). Below the posterior process of the median clavicle (e.g. *Nochelesaurus*, SAM-PK-6238, Fig. 22) is a shallow, rounded depression. Laterally, the posterior clavicle of *Nochelesaurus* (SAM-PK-6238) and *Bradysaurus* (NHMUK PV R 1971) have a long sharp dorsal ridge which also gives the lateral end a triangular cross-section (Fig. 22).

The anterior surface of the clavicle, medially, has a dorsal

thickened bar which is thicker and larger in *Nochelesaurus* (Fig. 22A), than *Embrithosaurus* (Fig. 19) and *Bradysaurus* (Fig. 23). Laterally, the right clavicles of *Nochelesaurus* and *Bradysaurus* are concave and forms a flat, thin, flange of bone between a swollen cylindrical bar-like dorsal border and a thickened ventral border (e.g. *Nochelesaurus*, SAM-PK-6238, Fig. 22A). The distal end of the clavicle of SAM-PK-6238 terminates with a sharp tip (Fig. 22) and the tip is also relatively sharp in *Bradysaurus baini* (Fig. 28), whereas in *Embrithosaurus* the distal end is blunt and convexly rounded (Fig. 25). The lateral end of the left clavicle of the holotype of *Embrithosaurus* is attached to the

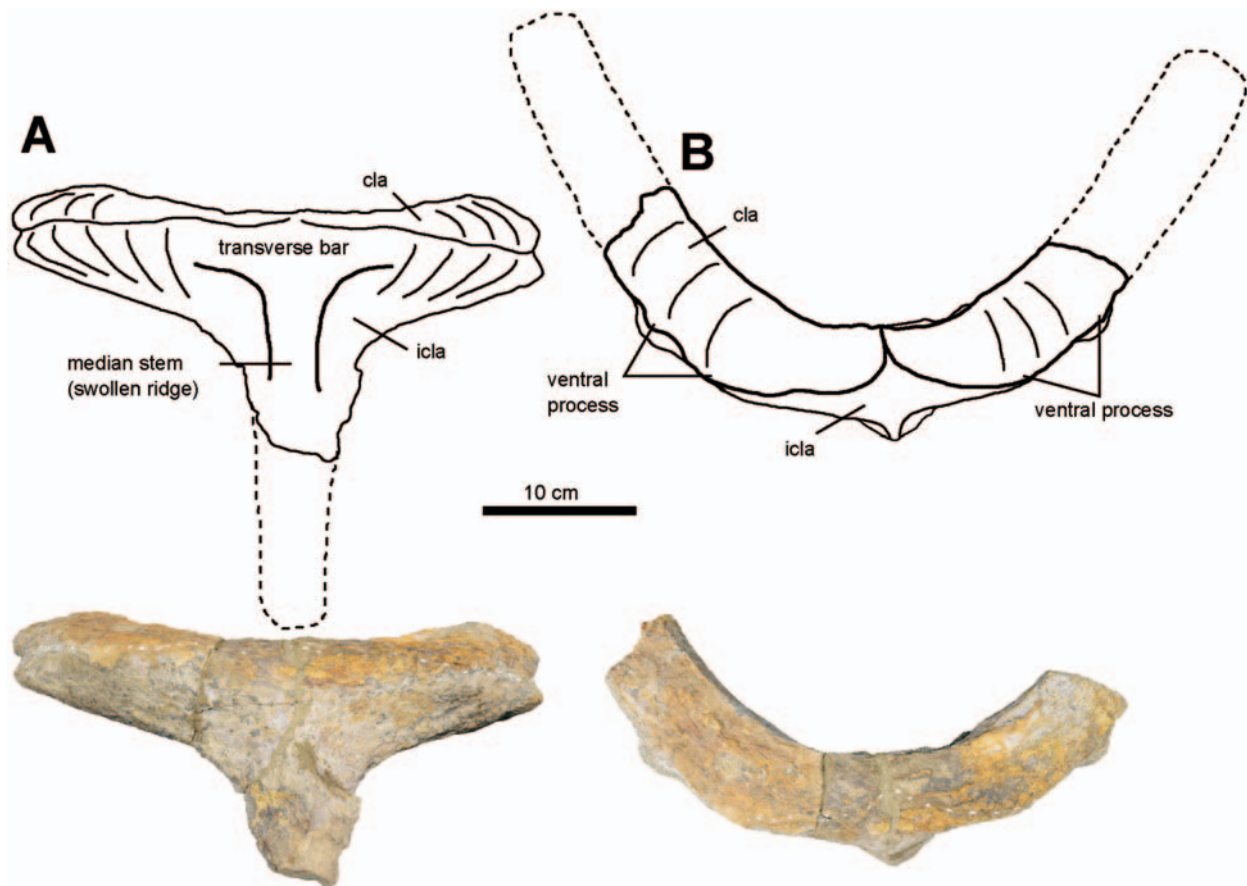


Figure 20. Photographs and interpretive drawings of the partial interclavicle, and partial right and left clavicles of the holotype of *Nochelesaurus alexanderi* (SAM-PK-6239), (A), in ventral view, and (B), in anterior view. Anterior to the top of the page in (A), dorsal to the top of the page in (B). Scale bar equals 10 cm.

scapulocoracoid (Fig. 25), primarily articulating with the acromion process which is not well preserved apart from the dorsal-most edge of the acromion process. Dorsal to the acromion process, the dorsal tip of the clavicle has small articulations with the cleithrum and the scapula blade.

A wide and deep notch is present on the ventral edge of the clavicle of the holotype of *Embrithosaurus* and referred specimen CGP CBT 112 (Fig. 19). Lateral to this notch is a prominent ventral process (80 mm wide, 20 mm high on the holotype) which articulates tightly with a corresponding shallow rounded depression at the lateral end of the anterior side of the interclavicle (Fig. 19B). On the ventral border of both clavicles of the holotype of *Nochelesaurus* (Fig. 20) and the right clavicle of SAM-PK-6238 (Fig. 22) the ventral process is similarly wide (90 mm) but is lower, projecting only 10 mm posteroventrally. On the holotype of *Bradysaurus baini* this process is very wide, but low (110 mm mediolaterally wide, 10–15 mm high). Interestingly and perhaps diagnostically, both *Bradysaurus baini* (NHMUK PV R 1971, SAM-PK-5002) and *Nochelesaurus* (SAM-PK-6239, SAM-PK-6238) lack the distinct notch medial to the posteroventral process in *Embrithosaurus* (SAM-PK-8034).

Cleithrum

The holotype of *Bradysaurus baini* preserves a complete left cleithrum which is articulated to the anterolateral margin of scapula blade (Fig. 28). It is 220 mm long,

thin, and gently curved. Dorsally, the cleithrum thins mediolaterally to fuse with the scapula blade, such that it is difficult to identify its dorsal extent with certainty, but it does not reach the dorsal edge of the scapula (Turner *et al.* 2015, character 91). The ventral base of the cleithrum rests on the short dorsal surface of the acromion process and articulates with the lateral tip of the clavicle. The holotype of *Embrithosaurus* has only the ventral-most portion of the right cleithrum preserved, as a thin plate of bone partially fused to the anterolateral margin of the base of the scapula blade (Fig. 25). As in the holotype of *Bradysaurus baini*, the cleithrum of *Embrithosaurus* is larger and thicker ventrally, just above the dorsal edge of the acromion process and narrows and thins dorsally to fuse almost indistinguishably with the scapula blade. Its dorsal end is not preserved but the figures provided by Broom (1903: plate XV, fig. 1; here Fig. 24A) and Boonstra (1932b: fig. 18; here Fig. 24B) indicate that it did not reach the dorsal edge of the scapula (Turner *et al.* 2015, character 91) as is the case in the holotype of *Bradysaurus baini*, and this may be taken as characteristic of the group. Only the distal-most portion of the cleithrum is fused to the left scapula blade fragment of the holotype of *Nochelesaurus* and it is consistent with the morphology in the rest of the group (Fig. 26).

Scapulocoracoid

In pareiasaurs, the scapulocoracoid comprises the elongated scapula blade and the anterior and posterior coracoids that form most of the flat coracoid plate. Apart

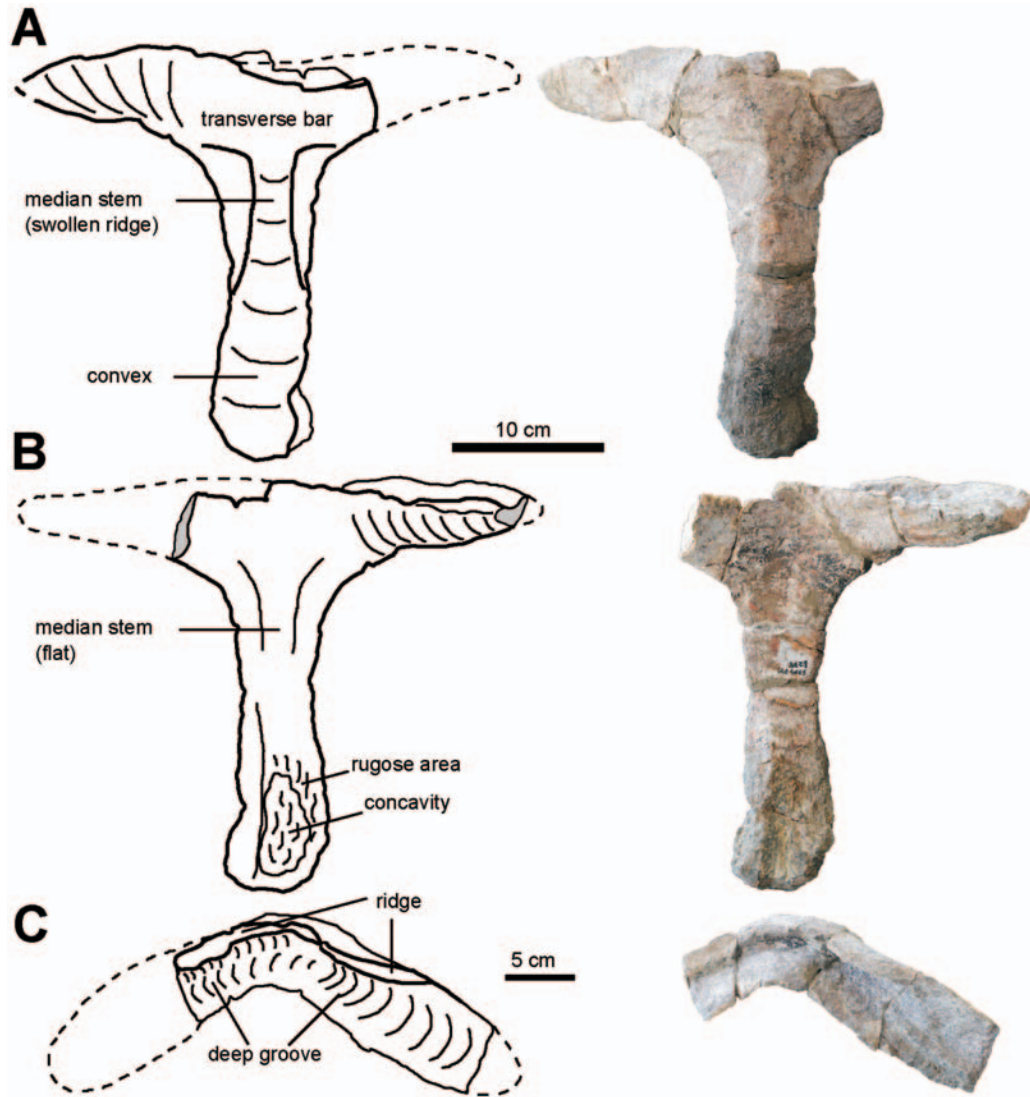


Figure 21. Photographs and interpretive drawings of the interclavicle of SAM-PK-6238 (*Nochelesaurus alexanderi*), (A), in ventral view, (B), in dorsal view, and (C), in anterior view. Anterior to the top of the page in (A) and (B), ventral to the top of the page in (C). Scale bars equal: A, 10 cm; B, 10 cm; C, 5 cm.

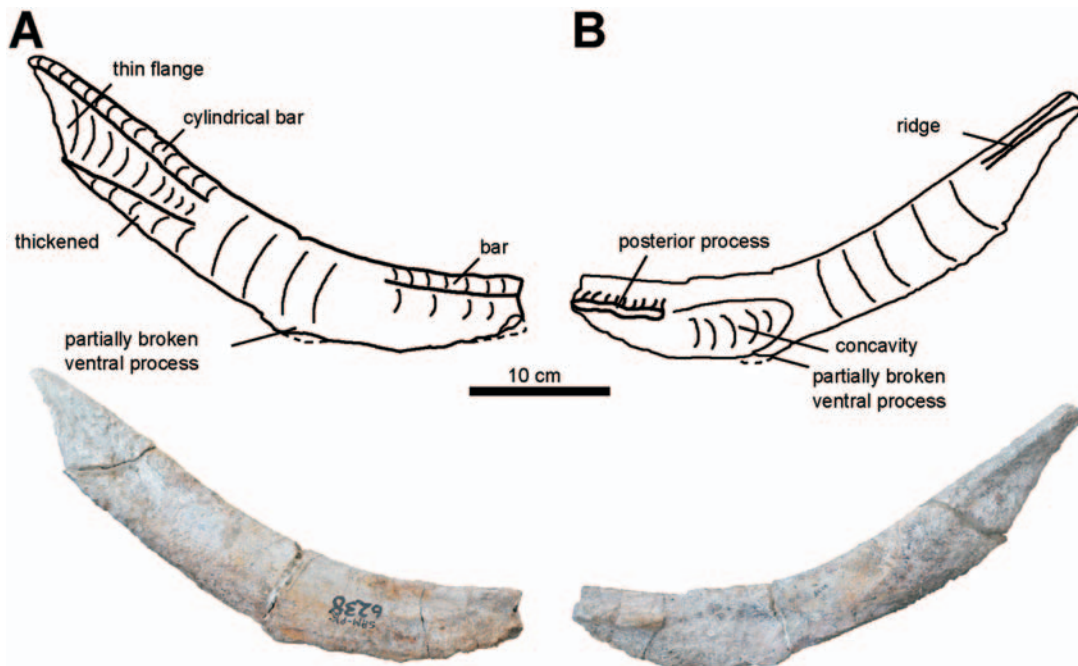


Figure 22. Photographs and interpretive drawings of the right clavicle of SAM-PK-6238 (*Nochelesaurus alexanderi*), (A), in anterior view, and (B), in posterior view. Dorsal to the top of the page. Scale bar equals 10 cm.



Figure 23. Photograph of the partial left clavicle and interclavicle of the holotype of *Bradysaurus baini* (NHMUK PV R 1971), in anterior view. Dorsal to the top of the page. Scale bar equals 10 cm.

from the vertical suture between the anterior and posterior coracoid on the lateral surface of *Embrithosaurus* (Fig. 25), the scapulocoracoid elements are strongly fused in all specimens and sutures cannot be determined, as is often the case in adult pareiasaurs (Benton 2016; Boonstra 1932b).

As in all large basal South African pareiasaurs, the acromion process of *Nochelesaurus* (SAM-PK-6238) is large and forms a wide, rectangular, plate-like flange. It is 120 mm (holotype SAM-PK-6239) to 125 mm (SAM-PK-6238) in dorsoventral length, 15 mm mediolaterally thick, and extends 40 mm beyond the anterior border of the scapula. The anterior margin is long, thin and gently convex. The dorsal and ventral margins are short: concave dorsally, and straight ventrally, emerging from the anterior border of the scapula at a right angle. The plate-like acromion flange has a gently convex lateral side and is concave medially (Turner *et al.* 2015, character 89). The rectangular flange of the acromion process of *Bradysaurus baini* is the largest in this group, 145 mm long, 45 mm higher than the anterior border of the scapula. The short dorsal margin is deeply concave, the short ventral margin slightly concave and straighter, being at a right angle to the scapula blade. The flange is gently convex laterally and concave medially. Broom (1903: plate XV, fig. 1; here Fig. 24A) and Boonstra (1932b: fig. 18; here Fig. 24B) figured the complete left scapula blade and a large acromion process in the holotype of *Embrithosaurus*, but the acromion process and most of the blade is now lost (Fig. 25). From Broom's (1903: plate XV, fig. 1; here Fig. 24A) and Boonstra's (1932b: fig. 18; here Fig. 24B) illustrations, the acromion process of *Embrithosaurus* shares all the features of the other basal pareiasaurian taxa and we estimate it was approximately 100 mm long dorsoventrally.

The base of the scapula blade of these animals, just above the dorsal edge of the acromion process is constricted, oval in cross-section and narrow in all species (anteroposteriorly 90 mm and mediolaterally 50 mm in *Nochelesaurus*, 100 mm × 50 mm in *Embrithosaurus* and 100 mm × 50 mm in *Bradysaurus baini*). The mid scapula blade of *Nochelesaurus* flares significantly less anteroposteriorly than the other taxa and is very narrow.

At the level just above the swollen process of the medial surface, the isolated left scapula blade fragment of the holotype of *Nochelesaurus* measures only 115 mm anteroposteriorly, which is much narrower than *Embrithosaurus* (150 mm) and *Bradysaurus baini* (130–140 mm). Similarly, the distal left scapula blade of *Nochelesaurus* SAM-PK-6238 (Fig. 27C) is very narrow and only slightly flared (anteroposteriorly only 171 mm) and the preaxial and postaxial margins are straight and not very curved (Turner *et al.* 2015, character 88). This is significantly narrower than the wide and extremely flared distal ends of the scapula blades of *Embrithosaurus* (estimated at 200 mm, Broom 1903; plate XV, fig. 1; here Fig. 24A; and Boonstra 1932b, fig. 18; here Fig. 24B) and *Bradysaurus baini* (200 mm). It is important to note that compared to the longer, anteroposteriorly narrower and only very slight distal flaring of *Nochelesaurus*, the scapula blades of *Embrithosaurus* and *Bradysaurus baini* are short and wide, distally flared to almost twice their basal anteroposterior width, with strongly curved preaxial and postaxial margins (Turner *et al.* 2015, character 88).

As noted by Boonstra (1932b: 469) the dorsoventrally complete right scapula blade of *Nochelesaurus* specimen SAM-PK-6238 is very long (490 mm, including the acromion process) compared to the much shorter blades of *Embrithosaurus* (estimated to 425 mm, Broom 1903: plate XV, fig. 1; here Fig. 24A; and Boonstra 1932b: fig. 18; here Fig. 24B) and *Bradysaurus baini* (440 mm). The length of the scapula blade of *Nochelesaurus* is two and a half times the anteroposterior diameter of the glenoid fossa (190 mm) (Turner *et al.* 2015, character 87). The ratio is well above two in *Nochelesaurus*, but less than three (SAM-PK-6238: 490 mm blade and 190 mm glenoid). The glenoid fossa of *Bradysaurus baini* is anteroposteriorly long (180 mm left, 200 mm right) and the relatively short scapula blade is only a little over two times the anteroposterior diameter of the glenoid fossa (440 mm) (Turner *et al.* 2015, character 87) similar to *Embrithosaurus* (blade length of approximately 425 mm long and anteroposterior diameter of the glenoid fossa of 210 mm).

Distally, the lateral and medial surfaces of the scapula blades of all species are covered with densely packed, long and thin, rugose striations or ridges.

On the medial surface of the isolated left scapula blade fragment of the holotype of *Nochelesaurus* (Fig. 26D) and SAM-PK-6238 is a wide, low process (50 mm anteroposteriorly wide, 20 mm high) covering the anterior half of the medial blade, just above the depression of the distal articulation of the clavicle. This process is common to all large co-occurring pareiasaurian taxa, but are somewhat lower and less distinct in *Embrithosaurus* (Fig. 25B) and *Bradysaurus* (Fig. 28B) (only 10 mm high in each).

The coracoid plates are anteroposteriorly elongated and flat. The ventral border is almost straight, slightly curved and the anterior and posterior sides very curved. The coracoid plate of the holotype of *Nochelesaurus* is severely damaged. Referred *Nochelesaurus* specimen SAM-PK-6238 is much more complete, except anteriorly (Fig. 27). In all middle Permian South African pareiasaurs, the lateral surface of the coracoid plate (ventral to the glenoid fossa)

undulates with two to three bulging areas with three to four corresponding lower depressed regions between.

The sigmoidal glenoid fossa is an irregular concavity. It is anteroposteriorly elongated (*Embrithosaurus*: 210 mm long, 80 mm high; *Nochelesaurus*: 150 mm, 80 mm in the holotype; 190 mm and 110 mm in SAM-PK-6238; *Bradysaurus baini*: 180 mm long in the left, 200 mm long in the right) and obliquely anterodorsally oriented (*Embrithosaurus*: 20° above the horizontal ventral border of the coracoid plate; *Nochelesaurus*: 30°; *Bradysaurus baini*: 25°). The border of the glenoid is thickened, especially anterodorsally, to form the supraglenoid buttress which is curved and rounded with a sharp ventral edge and. The swollen supraglenoid buttress tapers dorsally into the base of the scapula blade. Behind this tapering is a vertical groove or notch bordered posteriorly by a raised ridge emanating dorsally from the posterodorsal rim of the glenoid fossa.

The glenoid fossa is bipartite as it comprises two main internal facets for articulation with the head of the humerus: 1) an anterior facet beneath the supraglenoid buttress, on the internal dorsal surface of the glenoid, that faces posteroventrolaterally, and 2) a posterior facet on the internal ventral surface. The posterior facet is horizontally flat, with a posterior portion facing dorsolaterally and an anterior portion facing more dorsally. The posterior facet is supported ventrally by a particularly robust and thick shelf-like buttress (only slightly smaller than the supraglenoid buttress) that forms a ventral swelling under the facet. Between the anterior and posterior facets, the glenoid has a low (<10 mm high), oblique anterodorsal ridge (30 mm wide, 60 mm long) that does not cover the flat posterior facet.

Broom (1903) noted an extremely unusual 'vertical dividing ridge' (Broom 1903: 131) in the left glenoid fossa of the holotype of *Embrithosaurus*. Additional recent preparation revealed that this vertical ridge is a dislodged piece of the distal head of the left humerus (Fig. 25A), and it matches perfectly with bone break marks on the left humeral head. *Embrithosaurus* specimen CGP CBT 112 shows the typical low, oblique ridge in the centre of the glenoid fossa, present in the holotypes of *Nochelesaurus* and *Bradysaurus*.

The lateral exit of the large coracoid foramen is present 20–40 mm below the anteroventral corner of the glenoid fossa in all species. It is a rounded to elongated oval foramen and sometimes 'teardrop'-shaped laterally. The foramen passes through the coracoid plate obliquely (quite vertically) to exit at a higher level on the medial surface where the oval coracoid foramen is positioned in the ventral-most portion of the subscapular fossa. Turner *et al.* (2015) in their description of *Bunostegos*, consider that the orientation of the path of the foramen may be phylogenetically important as it varies between a lateral or a more ventral orientation in different pareiasaurs.

The medial surface of the scapulocoracoid shows the prominent dorsoventral groove of the subscapular fossa, which is largest in *Bradysaurus baini* (80 mm long, 20 mm wide, 20 mm deep). In *Embrithosaurus* the groove is slightly smaller (60 mm high, 30 mm wide, 10 mm in the

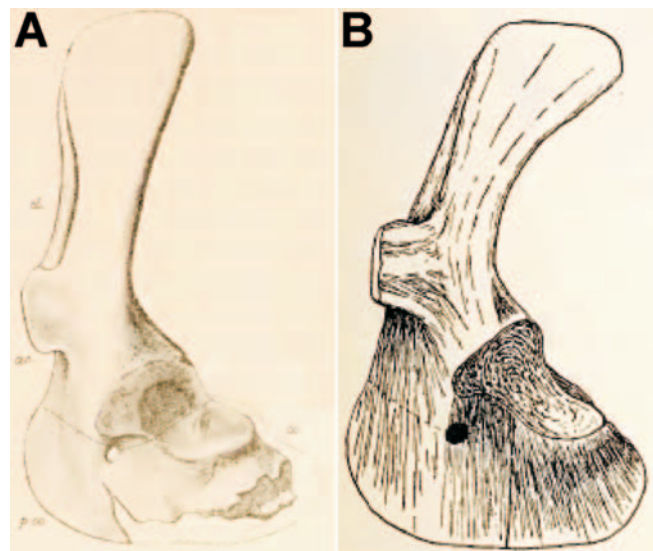


Figure 24. Interpretive drawings of the left scapulocoracoid of the holotype of *Embrithosaurus schwarzi* (SAM-PK-8034) in lateral view, (A), by Broom (1903), ac, acromion; cl, cleithrum; co, coracoid; p.co, precoracoid, and (B), by Boonstra (1932b). Note the acromion process (ac) and dorsal scapula blade are no longer preserved. Scapulocoracoid approximately 65 cm high.

holotype; 90 mm high, 35 mm wide and 20 mm deep in CGP CBT 112) but in *Nochelesaurus* (50 mm high, 15 mm wide, 5 mm deep in the holotype) the groove is much smaller than in *Bradysaurus baini*. In all species, the groove is located immediately posterior to a 45 mm thick convex cylindrical 'bar-like' swelling of the anterior border of the scapula. The subscapular fossa of *Embrithosaurus* and *Nochelesaurus* is positioned slightly more anteriorly than in *Bradysaurus baini*, but this is not significant or diagnostic (see Discussion).

The ventral and anterior margins of the coracoid plate of *Embrithosaurus* are relatively smooth and lack the numerous small thickenings (coracoid rim buttresses) reported for *Bunostegos* (Turner *et al.* 2015). In the holotype of *Bradysaurus baini*, however, the ventral edge of the anterior and posterior coracoid plate is irregular and uneven with numerous small notches and indentations. The anterior coracoid rim is swollen and thickened, producing a knob-like process. This region is not preserved on the holotypes of *Embrithosaurus* or *Nochelesaurus*, but referred *Embrithosaurus* specimen CGP CBT 112 has a similar swollen process, so it is most likely common to this group of pareiasaurs. On the anterior rim, laterally, between the knob-like process and the acromion process, the anterior coracoid is very concave in all species.

Assuming the posterior edge of the scapula blade is vertical, the dorsal edge of the posterior coracoid is relatively horizontal in all taxa, forming an angle of about 120° with the posterior border of the scapula in *Embrithosaurus* (SAM-PK-8034, holotype, Fig. 25) or 125° (CGP CBT 112), 130–135° in *Nochelesaurus* (SAM-PK-6238, Fig. 27), and 125° in *Bradysaurus baini* (NHMUK PV R 1971, holotype, Fig. 28) (Turner *et al.* 2015, character 90).

Humerus

All middle Permian South African pareiasaurs have previously been reconstructed in a sprawling posture

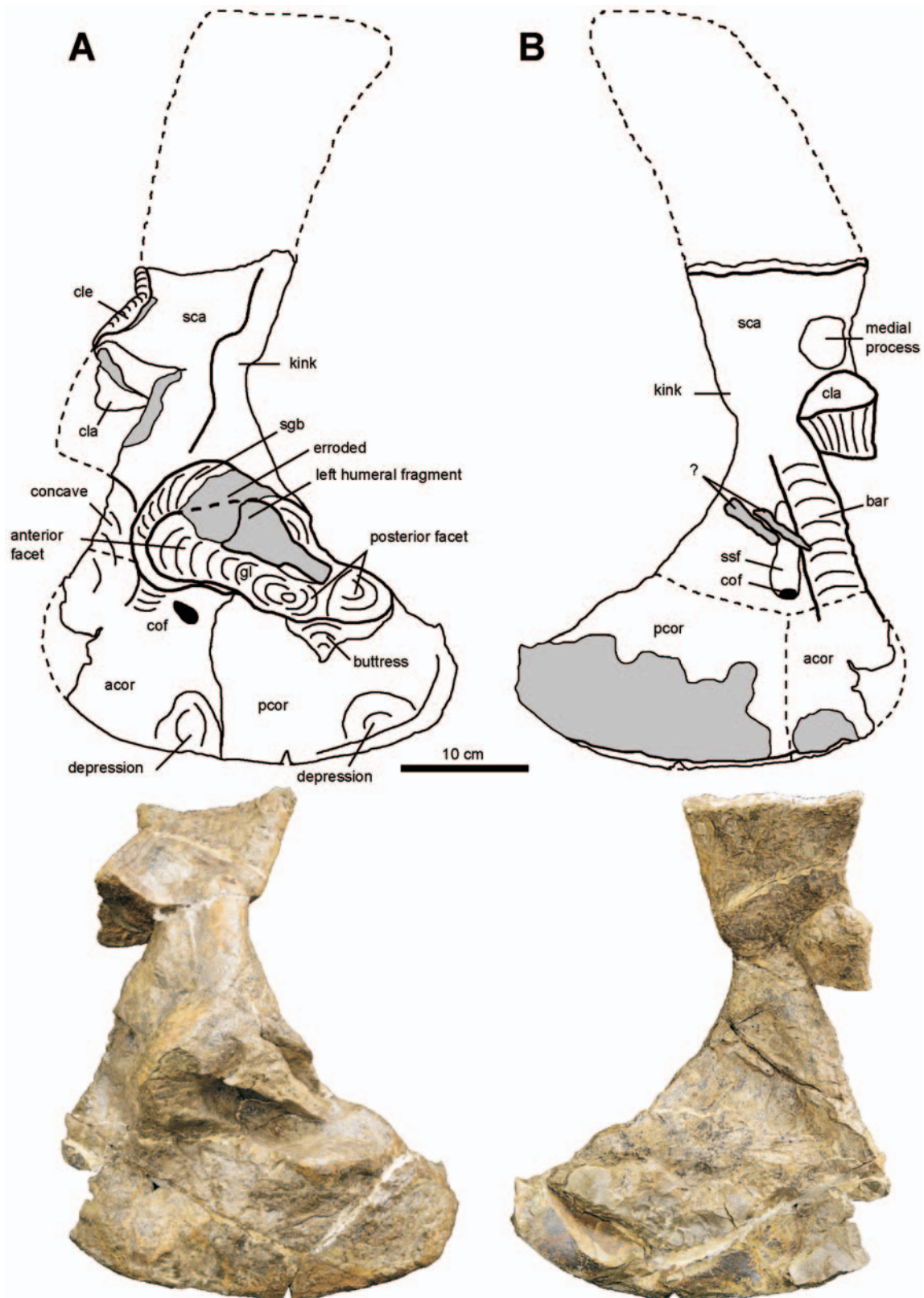


Figure 25. Photographs and interpretive drawings of the left scapulocoracoid of the holotype of *Embrithosaurus schwarzi* (SAM-PK-8034), (A), in lateral view, and (B), in medial view. Dorsal to the top of the page. Scale bar equals 10 cm.

with the humerus horizontal, parallel to the ground (e.g. Boonstra 1932b; Lee 1997a). We therefore use the directional vector terms proximal, distal, dorsal, ventral, post-axial (posterior) and preaxial (anterior) in terms of a horizontal orientation for the humerus, with the intercondylar fossa (ulnar fossa, olecranon fossa) of the distal humerus facing dorsally.

These humeri are very robust, with a short and narrow cylindrical shaft and widely expanded proximal and distal ends. The proximal end has a flattened area for articulation with the glenoid cavity, and the distal end comprises the complex trochlear joint with facets on the dorsal and ventral surfaces for the articulation of the radius and ulna.

The right humerus of the holotype of *Embrithosaurus* is

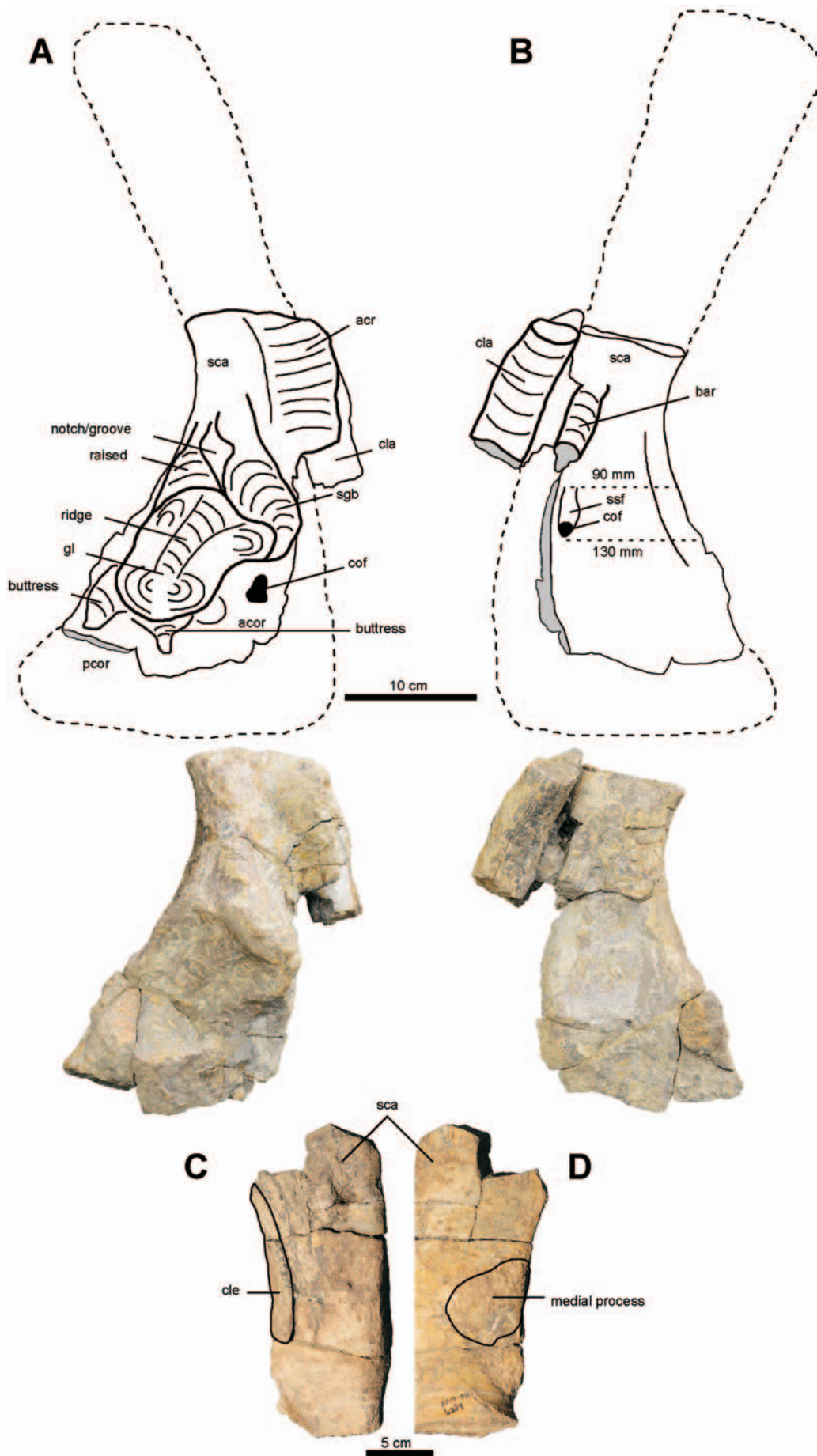


Figure 26. Photographs and interpretive drawings of the scapulocoracoid of the holotype of *Nochelesaurus alexanderi* (SAM-PK-6239), (A), right scapulocoracoid, in lateral view, and (B), in medial view. Base of the left scapula blade in (C), lateral view, and (D), medial view. Dorsal to the top of the page. Scale bars equal: A, 10 cm; B, 10 cm; C, 5 cm; D, 5 cm.

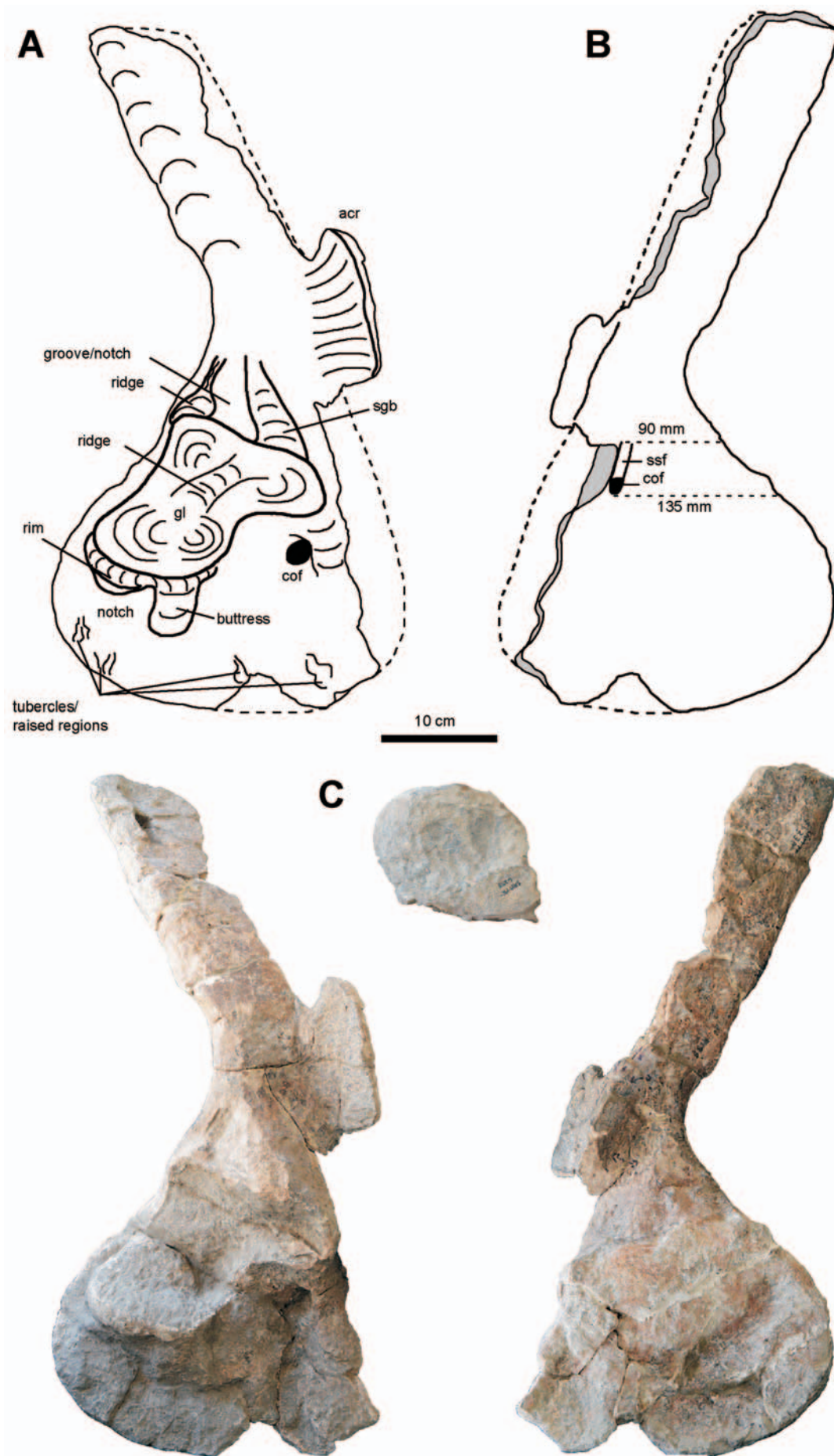


Figure 27. Photographs and interpretive drawings of the scapulocoracoid of SAM-PK-6238 (*Nochelesaurus alexanderi*), (A), right scapulocoracoid in lateral view, (B), right scapulocoracoid in medial view, and (C), dorsal end of the left scapula blade in lateral view. Dorsal to the top of the page. Scale bar equals 10 cm.

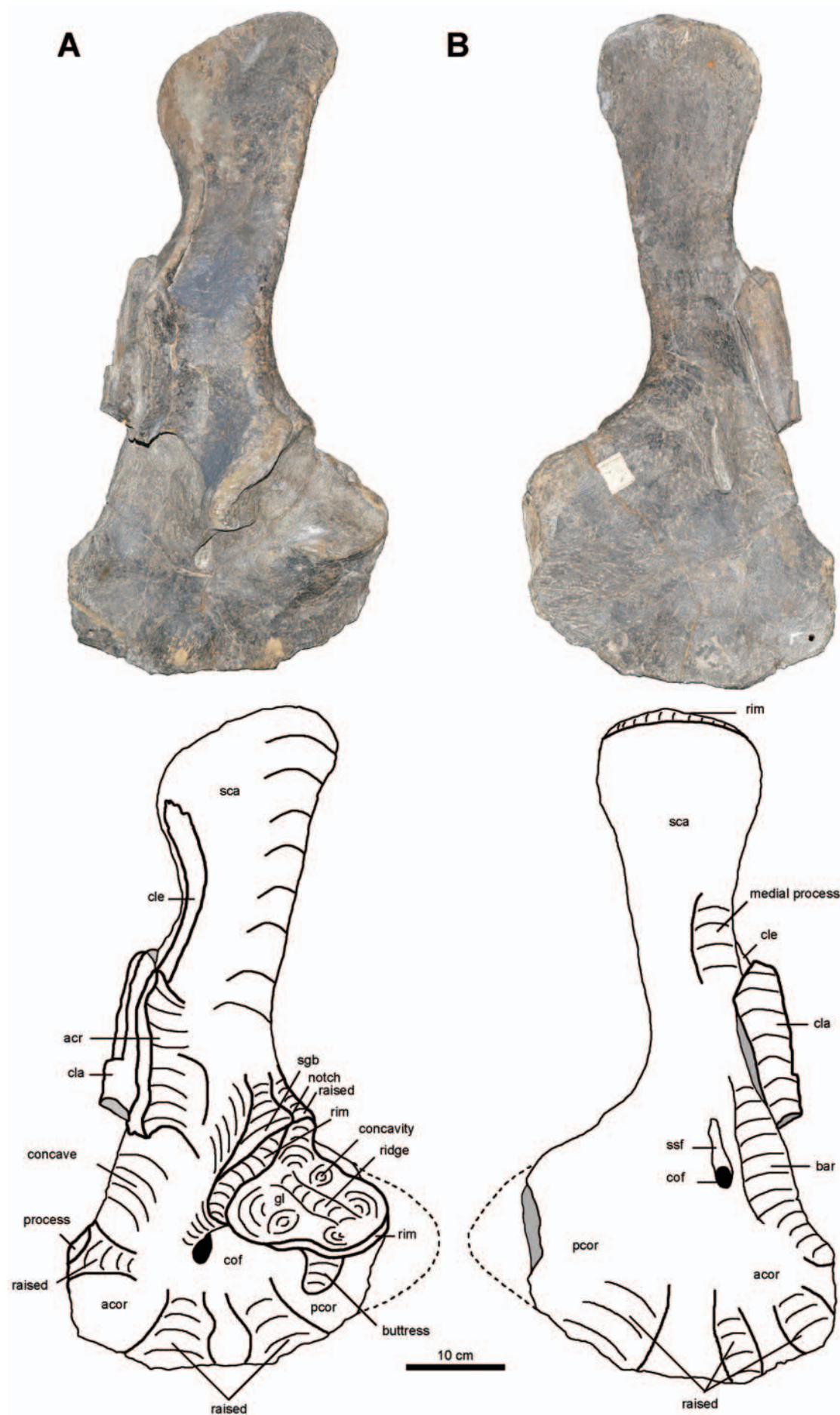


Figure 28. Photographs and interpretive drawings of the left scapulocoracoid of the holotype of *Bradysaurus bairi* (NHMUK PV R 1971), (A), in lateral view, and (B), in medial view. Dorsal to the top of the page. Scale bar equals 10 cm.

very well preserved (Figs 29, 30, 31), and only about half of the left is preserved. For *Nochelesaurus*, we use the left humerus of the holotype, missing a large section of the preaxial proximal blade and a section of the distal postaxial entepicondyle (Figs 32, 33, 34); and the right humerus of SAM-PK-6238 which is nearly complete, apart from a section of the ectepicondyle and part of the postaxial flange of the entepicondyle (Figs 35, 36, 37). The right humerus of the holotype of *Bradysaurus baini* is very complete apart from a postaxial piece of the entepicondyle and most of the short shaft of the humerus (Fig. 38). The left humerus consists of only the distal expansion and the proximal expansion has been reconstructed in plaster. It is important to recognize that Seeley (1892: 360) specifically noted that the shaft of the right humerus was broken during preparation and that he could not be certain as to the original alignment of the proximal and distal ends. Seeley attached the distal and proximal ends in virtually the same plane, with a torsion of only 10°. Therefore, the holotype of *Bradysaurus baini* does not reveal the torsion in the humerus of the species. *Bradysaurus* specimen SAM-PK-5624 shows humeral torsion of 70–80° in both humeri and SAM-PK-3718 shows 60–70° torsion in its right humerus. Similarly, the proximal and distal expansions of both humeri of the holotype of *Embrithosaurus* are twisted at nearly at right angles to each other, forming an angle of 70–80° (Fig. 31) (Turner *et al.* 2015, character 92) and referred *Embrithosaurus* FMNH UR 2443 shows twisting of 60°. In contrast, the distal and proximal expansions of the humerus of the holotype of *Nochelesaurus* are nearly on the same plane and only offset by 20° (Fig. 34), also noted by Boonstra (1932b: 466). Referred *Nochelesaurus* SAM-PK-6238 shows 30–40° twisting. The torsion angle in *Nochelesaurus* is thus much less than in *Embrithosaurus* and *Bradysaurus*.

In middle Permian South African pareiasaurs, the ectepicondyle is swollen, large, and robust and dorsoventrally more than twice as thick as the entepicondyle (Turner *et al.* 2015, character 99). *Bradysaurus* has the widest distal humerus, across the ectepicondyle and entepicondyle (290 mm), wider than the range of *Nochelesaurus* (235–260 mm) and much wider than the holotype of *Embrithosaurus* (230 mm).

The large ectepicondyle is a thin, expanded and widely flared flange (Turner *et al.* 2015, character 93) in all species, and the anterior margin of the flange is irregular and notched. The holotype of *Nochelesaurus* and SAM-PK-6238 (Figs 32, 33, 35, 36) show the small ectepicondylar foramen (present in all pareiasaurs according to Lee 1997b: 237) on the flange, visible in distal dorsal view, at a level just proximal to the triangular proximal edge of the intercondylar fossa (Turner *et al.* 2015, character 94). *Embrithosaurus* and *Bradysaurus* present an irregular notch on the ectepicondylar flange which represents the vestiges of the foramen (Figs 30, 38).

The smaller entepicondyle also has a flared flange that extends far posteriorly and is much thicker and wider than that of the ectepicondyle. It is wide, thick, and slightly curled over and in the complete flanges of *Embrithosaurus* and *Nochelesaurus* is square-edged with a

notable sharp, right-angled edge on the postaxial proximal corner (Turner *et al.* 2015, character 95). A large and completely enclosed entepicondylar foramen is present in the entepicondylar flange (40 mm long, 20 mm wide, 20 mm deep approximate dimensions in *Embrithosaurus* and *Nochelesaurus*). This foramen is characteristically slit-like and elongated, with a very thin and delicate, flattened, medial bridge-like margin (Turner *et al.* 2015, character 96). The entepicondylar foramen is positioned so that it is visible (completely open) when the distal expansion of the humerus is viewed dorsally (Figs 30A, 33A, 36A) (Turner *et al.* 2015, character 97). Both humeri in the holotype of *Bradysaurus baini* are damaged and do not preserve the entepicondylar flange.

The ectepicondyles of the holotype of *Bradysaurus baini* project distally much further beyond the radial and ulnar articulation surfaces, appearing forked (44 mm left humerus, 49 mm right humerus) than do the holotype of *Embrithosaurus* (25 mm) or *Nochelesaurus* (Holotype: left humerus, 35 mm; SAM-PK-6238: right humerus, 35 mm, left humerus, 40 mm) (Turner *et al.* 2015, character 98).

The intercondylar fossa (olecranon fossa) is a large and wide triangular depression, on the dorsal distal surface of the humerus, between the two epicondyles, for articulation of the olecranon process of the ulna. The intercondylar fossa forms a deep depression on the humerus of *Bradysaurus baini* (50 mm/40 mm deep on the right/left humerus) and in *Nochelesaurus* (40 mm deep in the holotype left humerus, 35 mm/50 mm deep on the right/left humerus of SAM-PK-6238) (Turner *et al.* 2015, character 103). The fossa is much shallower in *Embrithosaurus* (SAM-PK-8034: 20 mm) (Turner *et al.* 2015, character 103). In all species, the intercondylar fossa is much wider than the width of the olecranon process of the proximal ulna (Turner *et al.* 2015, character 104) and is demarcated by straight, raised edges preaxially and postaxially, and a gently curved, wide and low, transverse intercondylar ridge on the dorsal distal margin of the humerus. The intercondylar ridge separates the intercondylar fossa from the radial facet and the ulnar facet of the humerus, and does not extend onto the distal side of the humerus (Turner *et al.* 2015, character 102).

The maximum width of the proximal right humerus of *Bradysaurus baini* is 305 mm, closer to *Nochelesaurus* (SAM-PK-6238: 275 mm right humerus, 284 mm left humerus) and much wider than the in the holotype of *Embrithosaurus* (250 mm). Similarly, the distal humerus is wider in *Bradysaurus* (290 mm holotype) than in *Nochelesaurus* (SAM-PK-6238: 245 mm right humerus, 235 mm left humerus) or *Embrithosaurus* (230 mm).

A large and distinct tubercle is present midway on the straight posterior margin of the intercondylar fossa of the right humerus of SAM-PK-6238 (Figs 35, 36). The anterior and posterior margins of the tubercle are sharp-edged perpendicular to the postaxial margin and 35 mm apart, but the proximal and distal margins show rising sides and are slightly further apart (45 mm). The dorsal surface of the tubercle is slightly convex and there is a small notch on the distal margin. The left humerus of SAM-PK-6238 shows the entire dorsal surface of the entepicondyle as

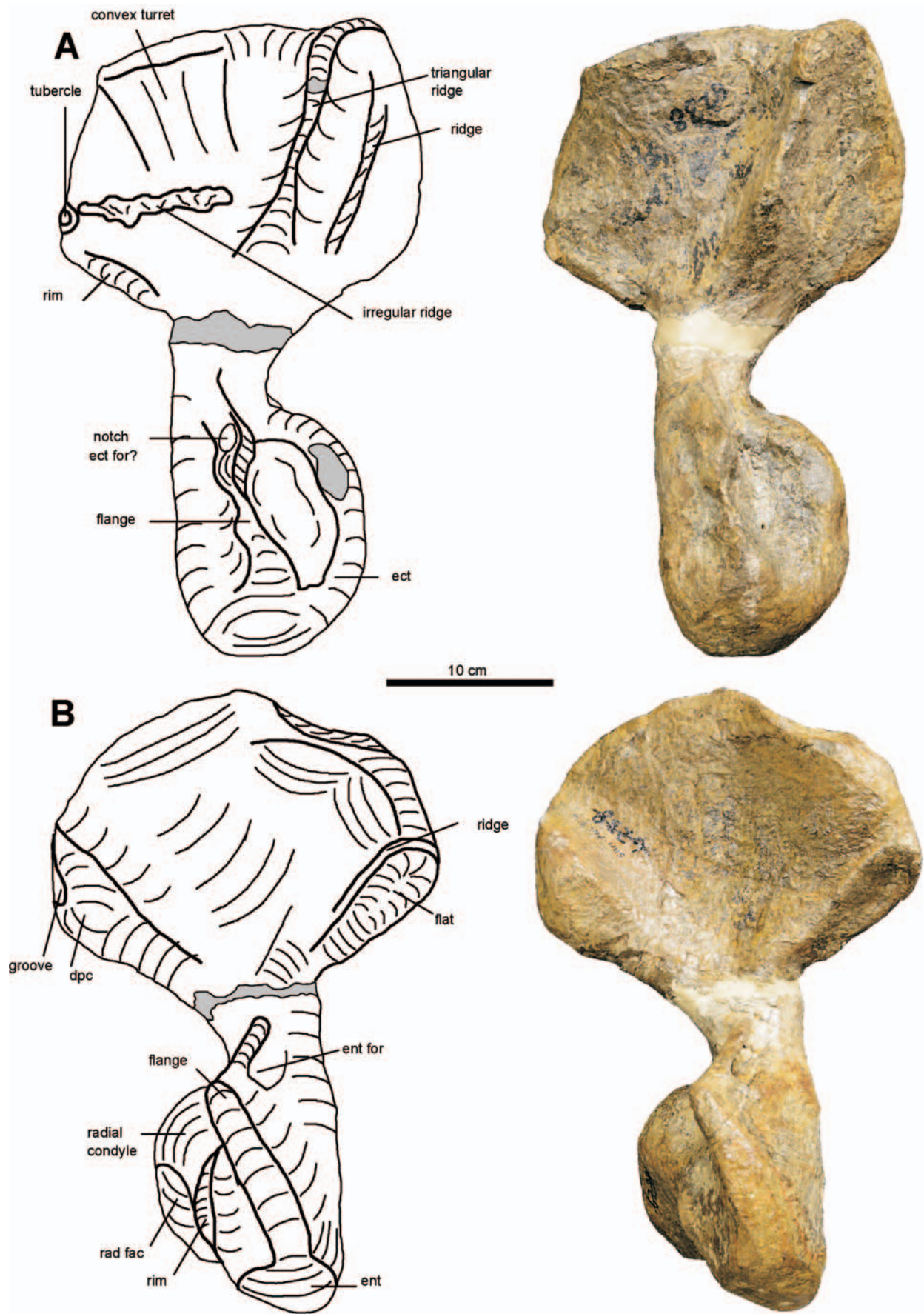


Figure 29. Photographs and interpretive drawings of the right humerus of the holotype of *Embrithosaurus schwarzi* (SAM-PK-8034), (A), in anterior view, and (B), in posterior view. Medial to the top of the page. Scale bar equals 10 cm.

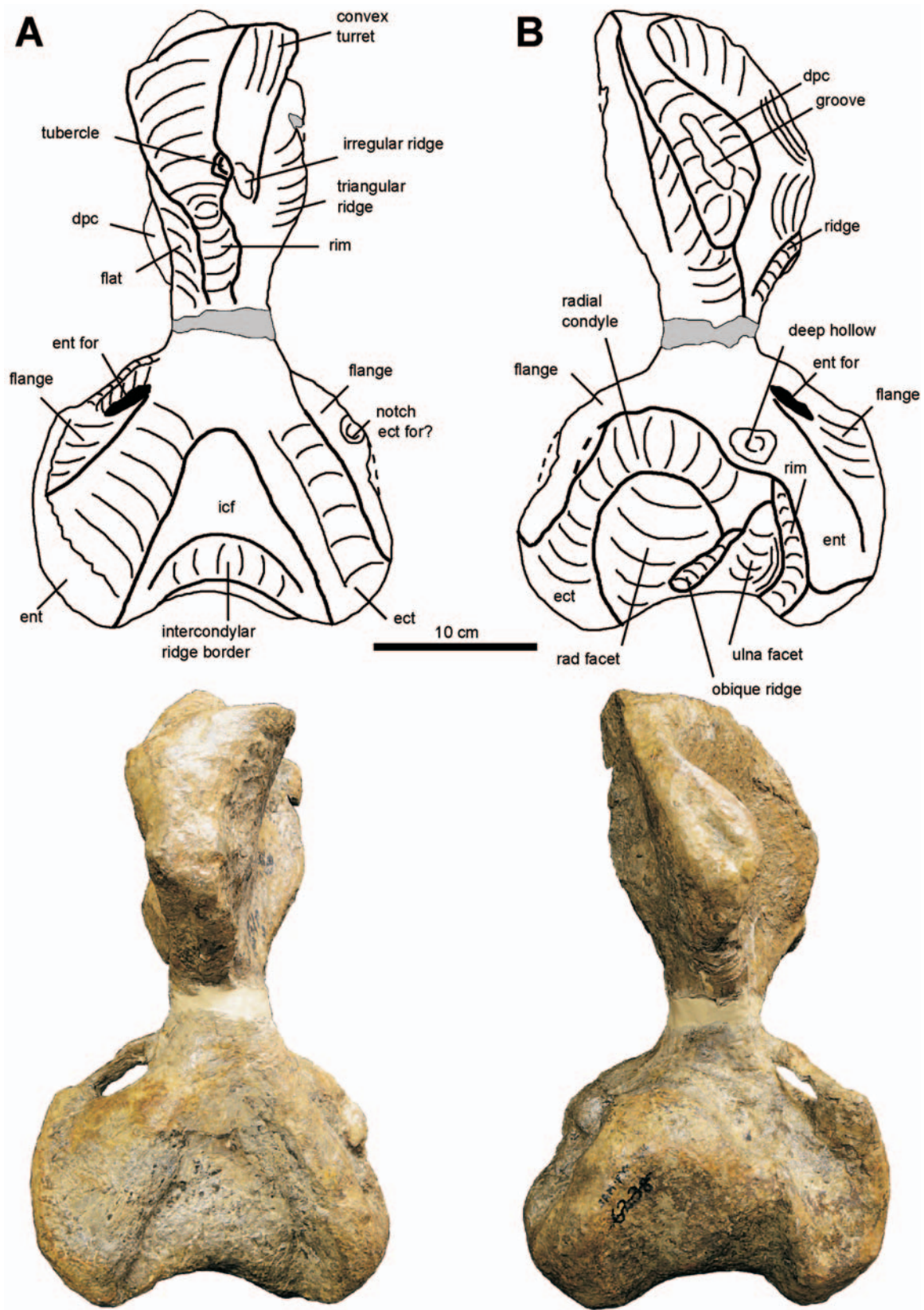


Figure 30. Photographs and interpretive drawings of the right humerus of the holotype of *Embrithosaurus schwarzi* (SAM-PK-8034), (A), in dorsal view, and (B), in ventral view. Medial to the top of the page. Scale bar equals 10 cm.

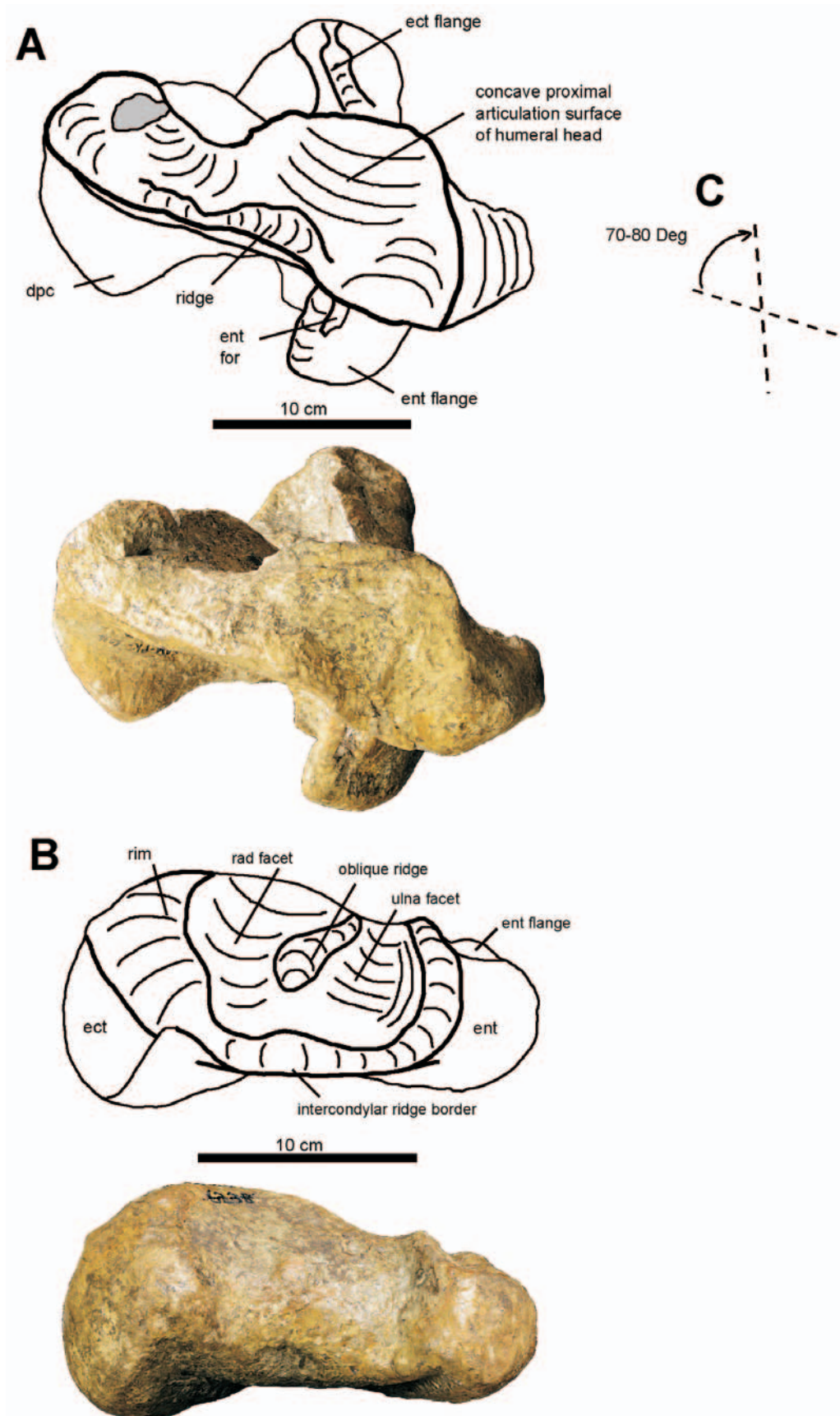


Figure 31. Photographs and interpretive drawings of the right humerus of the holotype of *Embriithosaurus schwarzi* (SAM-PK-8034), (A) and (C), in proximal view, and (B), in distal view. (C) illustrates the angle between the proximal and distal expansions as 70–80°. Ventral to the top of the page. Scale bar equals 10 cm.

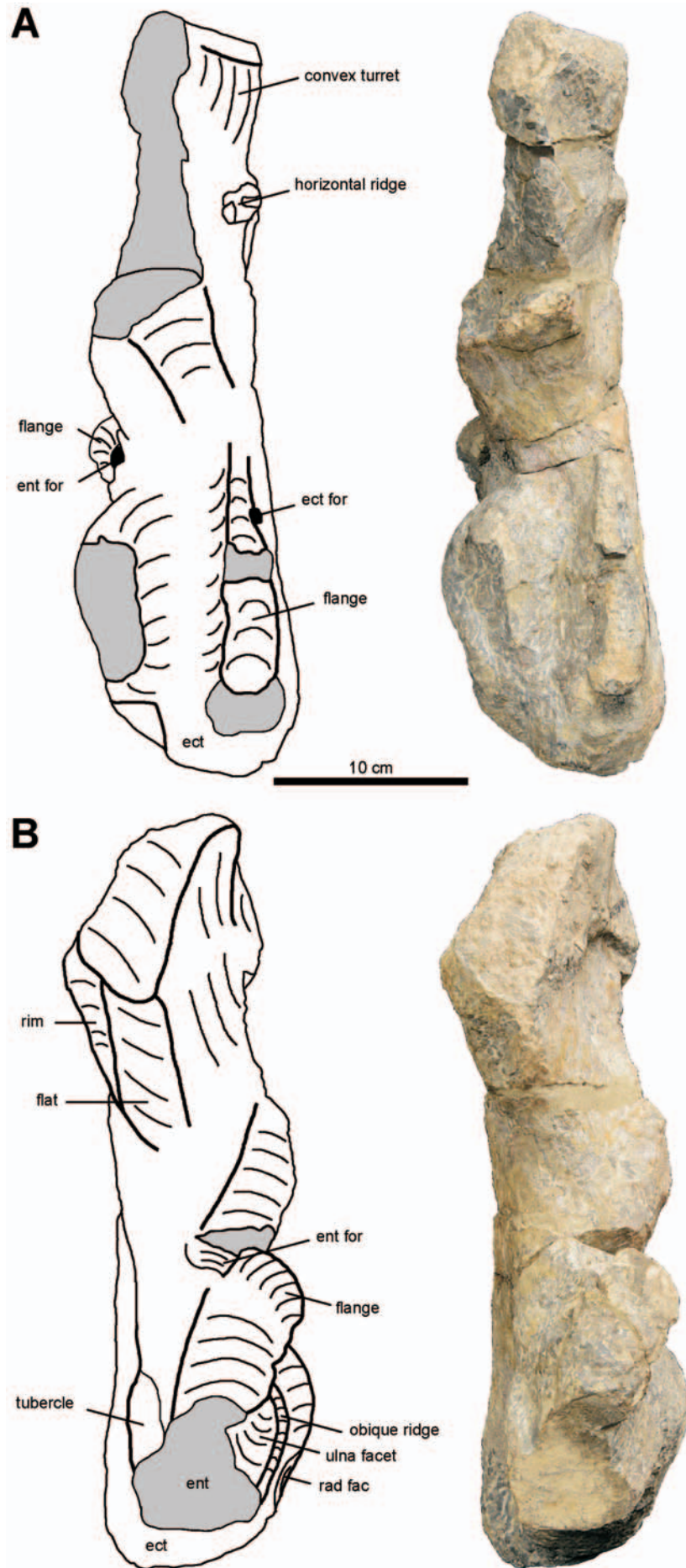


Figure 32. Photographs and interpretive drawings of the left humerus of the holotype of *Nochelesaurus alexanderi* (SAM-PK-6239), (A), in anterior view, and (B), in posterior view. Medial to the top of the page. Scale bar equals 10 cm.

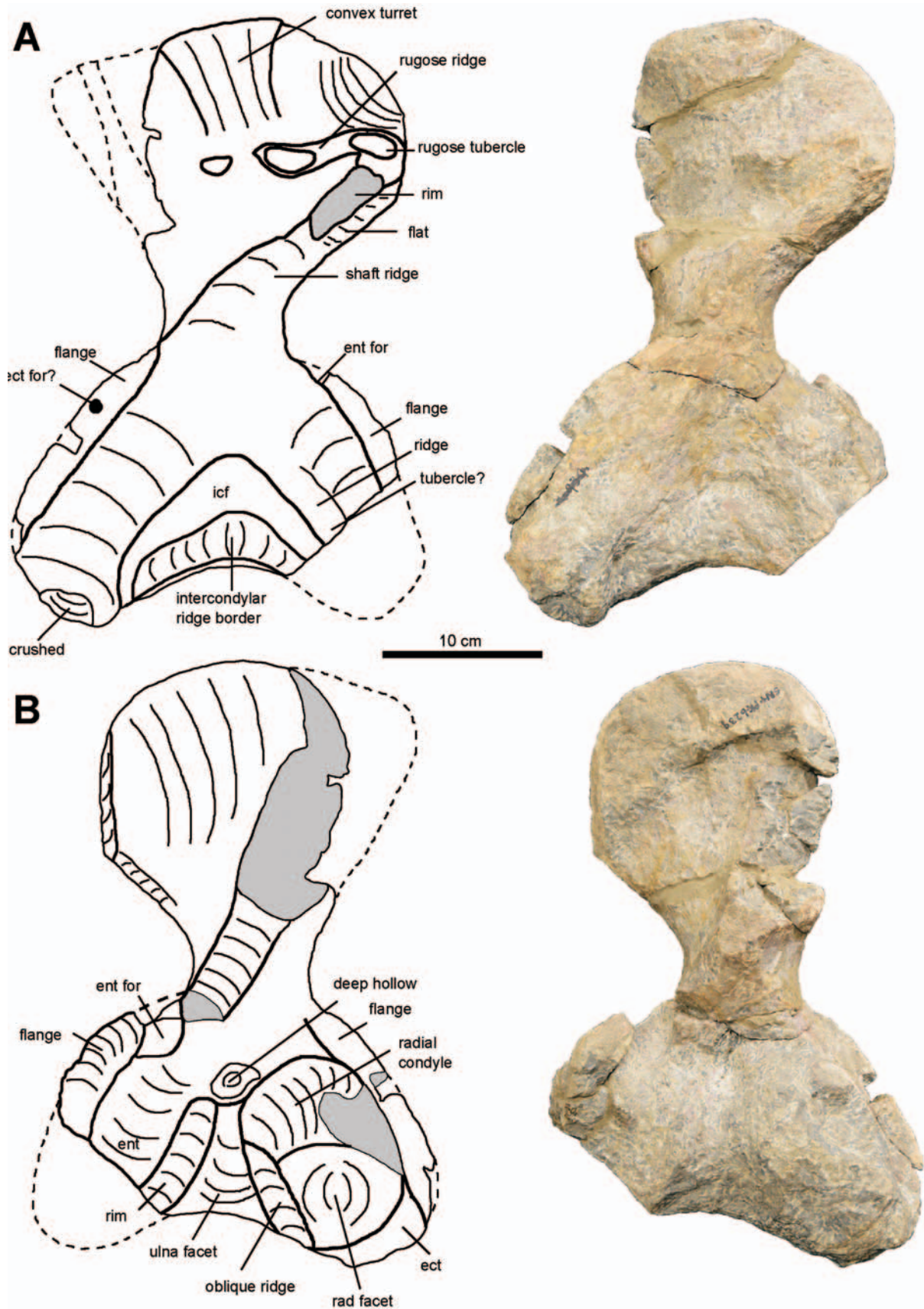


Figure 33. Photographs and interpretive drawings of the left humerus of the holotype of *Nochelesaurus alexanderi* (SAM-PK-6239), (A), in dorsal view, and (B), in ventral view. Medial to the top of the page. Scale bar equals 10 cm.

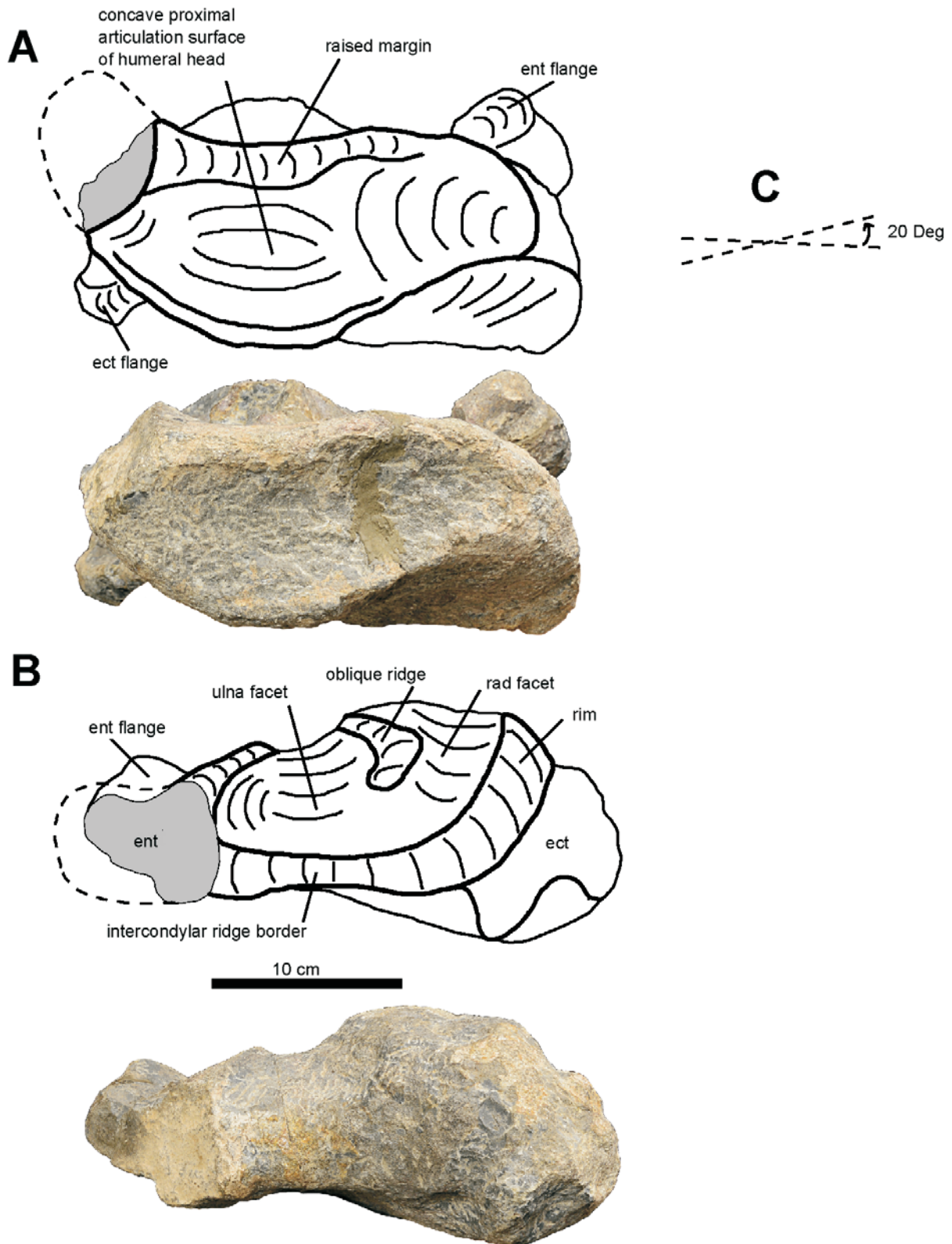


Figure 34. Photographs and interpretive drawings of the left humerus of the holotype of *Nochelesaurus alexanderi* (SAM-PK-6239), (A) and (C), in proximal view, and (B), in distal view. (C) illustrates the angle between the proximal and distal expansions as 20°. Ventral to the top of the page. Scale bar equals 10 cm.

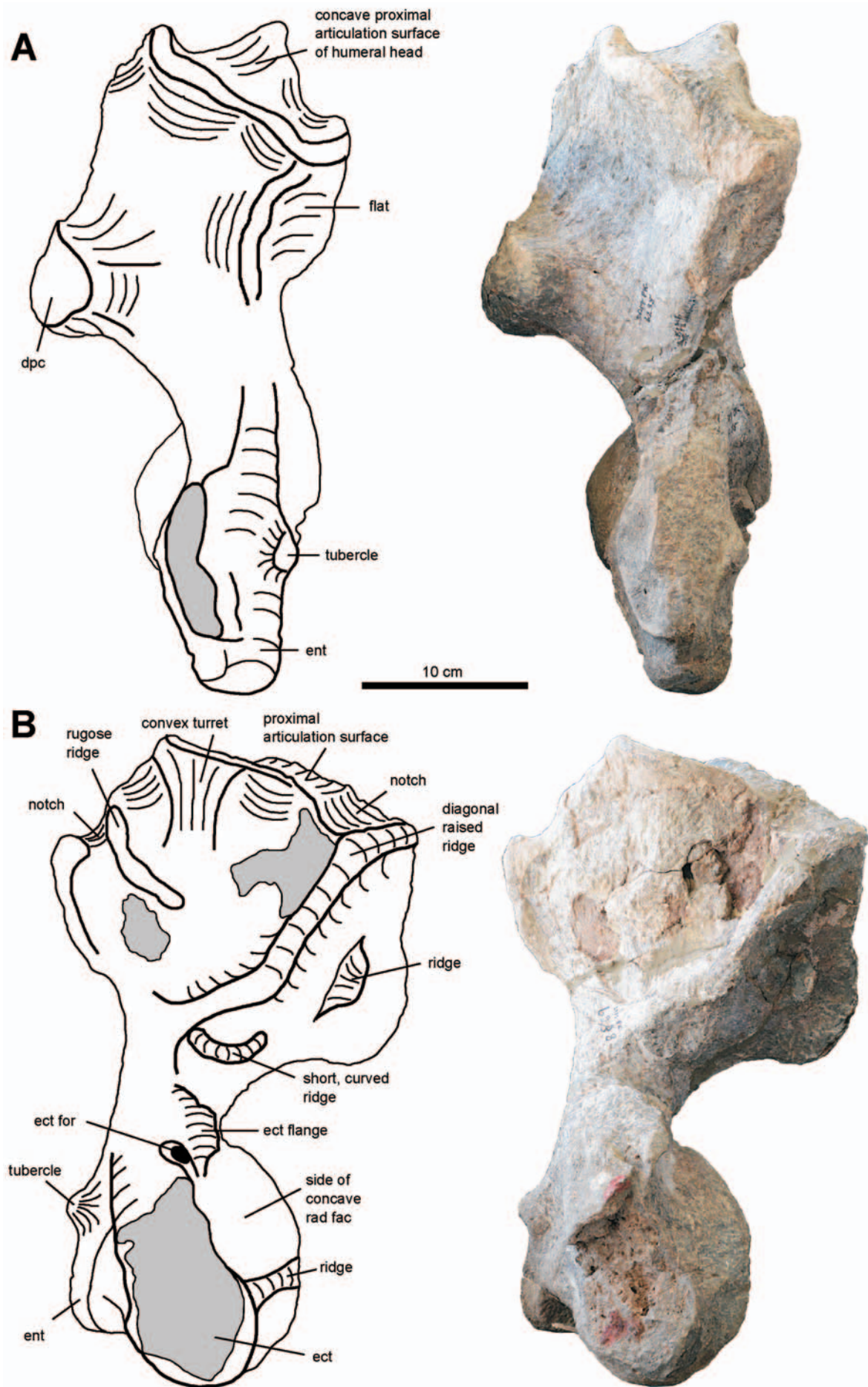


Figure 35. Photographs and interpretive drawings of the right humerus of SAM-PK-6238 (*Nochelesaurus alexanderi*), (A), in anterior view, and (B), in posterior view. Medial to the top of the page. Scale bar equals 10 cm.

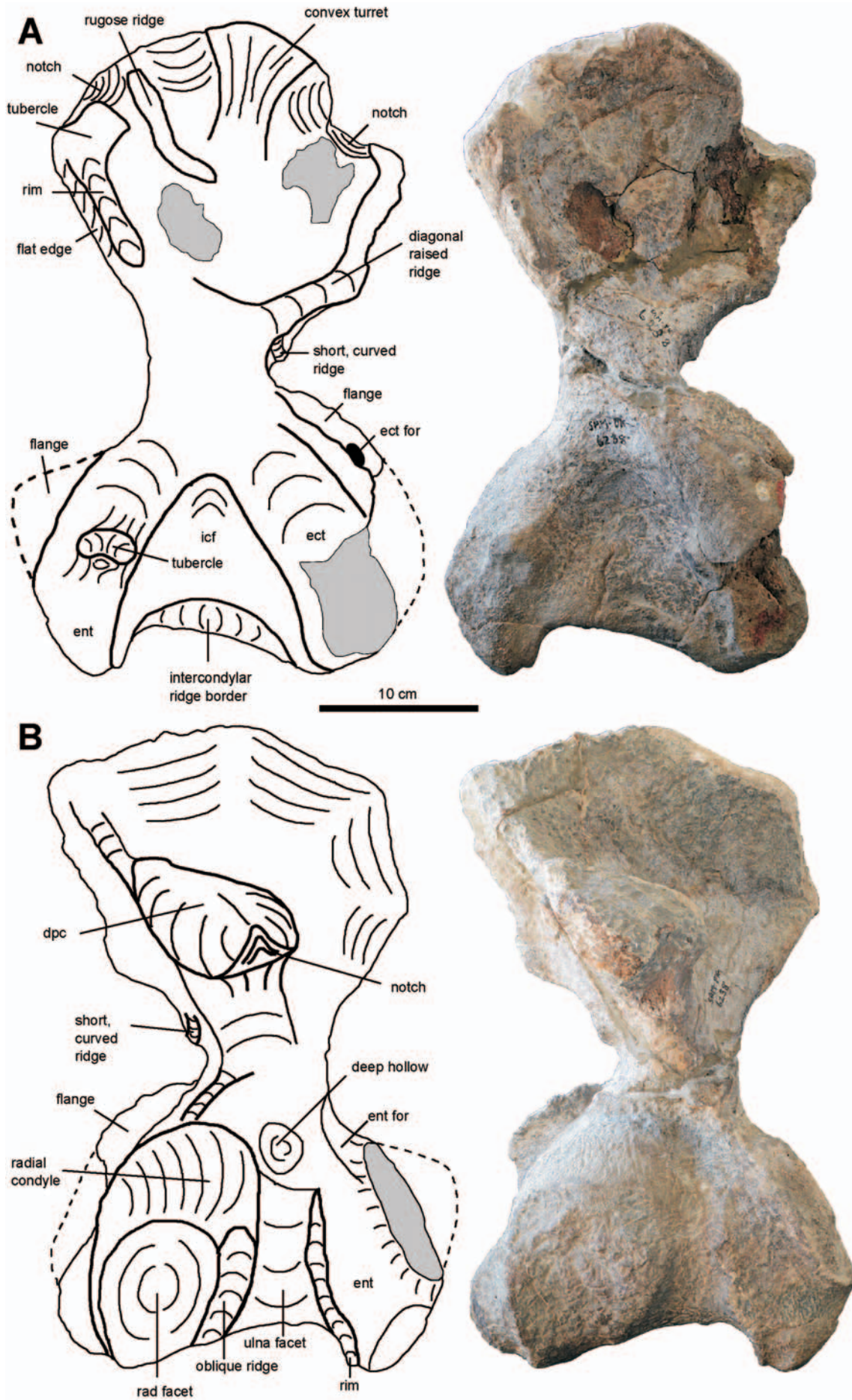


Figure 36. Photographs and interpretive drawings of the right humerus of SAM-PK-6238 (*Nochelesaurus alexanderi*), (A), in dorsal view, and (B), in ventral view. Medial to the top of the page. Scale bar equals 10 cm.

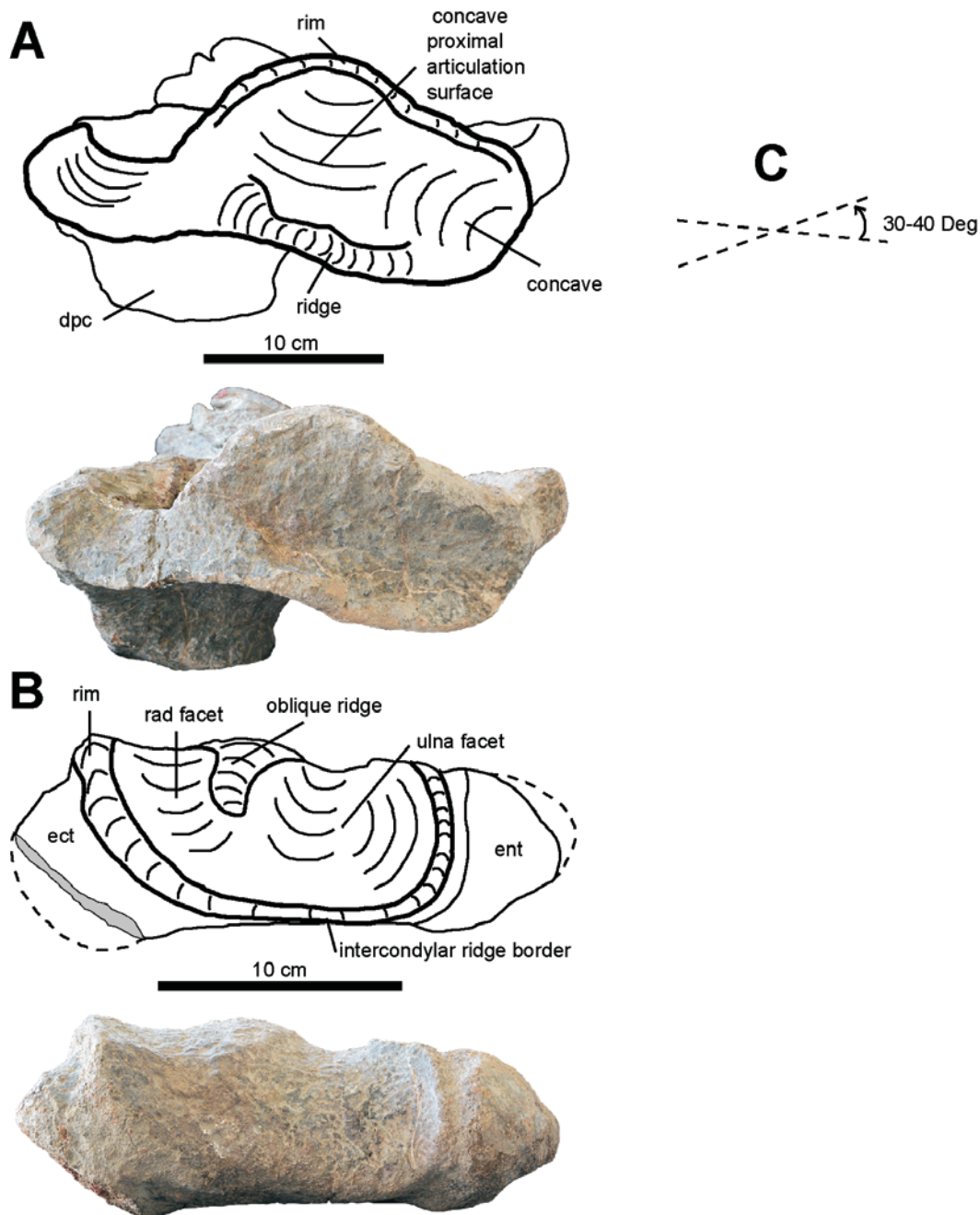


Figure 37. Photographs and interpretive drawings of the right humerus of SAM-PK-6238 (*Nochelesaurus alexanderi*), (A) and (C), in proximal view, and (B), in distal view. (C) illustrates the angle between the proximal and distal expansions as 30–40°. Ventral to the top of the page. Scale bar equals 10 cm.

deeply weathered and it appears that the low, eroded remnants of a similarly sized round tubercle are present. The distal end of the entepicondyle of the left humerus of the holotype of *Nochelesaurus* is missing (Fig. 33). Proximal to the missing section, the straight, swollen posterior border of the intercondylar fossa forms a raised ridge (25 mm wide, 50 mm long) which may be interpreted as part of a tubercle, or this feature may be the swollen, ridge-like postaxial border of the intercondylar fossa, a morphology often seen in middle Permian South African pareiasaurs (e.g. *Embrithosaurus* holotype). Referred *Nochelesaurus* specimens FMNH UR 2436 and FMNH UR 2480 also appear to show the humeral tubercle, but this is uncertain.

The radial condyle is located entirely on the ventral surface of the humerus, positioned preaxially and is a

large, round, convex, bulbous swelling proximally, with an oval, concave, shallow depression, the radial facet, distally (Figs 30, 33, 36, 38). Medial to the radial facet is a small hollow depression. The adjacent ulnar facet (trochlear ulnar groove) is positioned postaxially, is much smaller than the radial condyle and facet, and comprises a proximally tapering, elongated triangular groove or depression, much deeper than the radial facet, with the posterior margin formed by a distinct, raised, sharp-tipped pointed rim (Turner *et al.* 2015, character 101). The triangular ulnar facet and its raised postaxial rim together form the trochlea for the ulna (Lee 1997b: 238). An oblique, low ridge separates the radial and ulnar facets, but dissipates distally and does not reach the intercondylar ridge border on the dorsal edge of the humerus (Fig. 31B). The radial and ulnar facets are prevented from extending onto

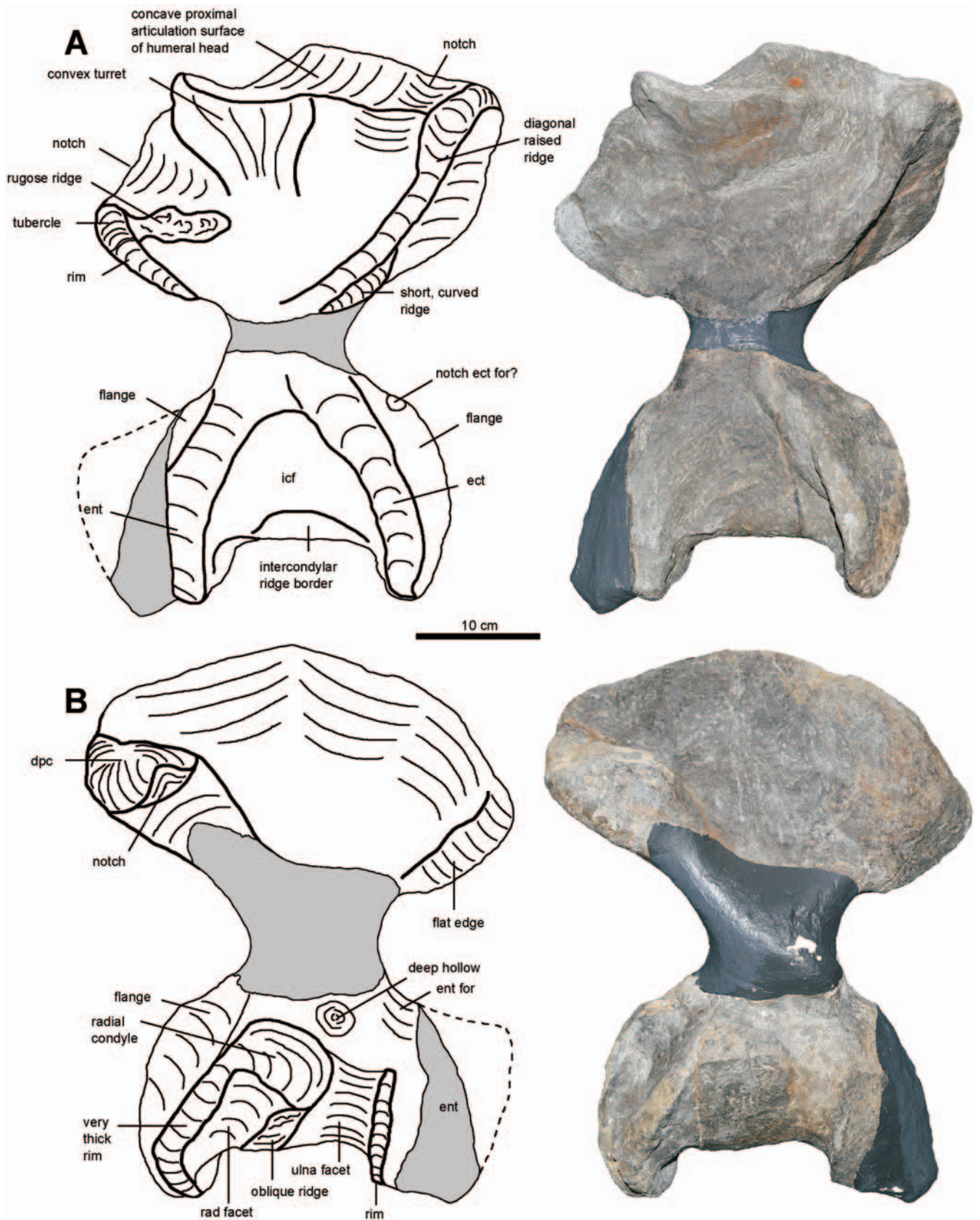


Figure 38. Photographs and interpretive drawings of the right humerus of the holotype of *Bradysaurus baini* (NHMUK PV R 1971), (A), in dorsal view, and (B), in ventral view. Medial to the top of the page. Scale bar equals 10 cm.

the distal side of the humerus by the transverse intercondylar ridge border at the dorsal edge of the humerus (Figs 34B, 37B) (Turner *et al.* 2015, character 100). In *Nochelesaurus* specimen SAM-PK-6238 the radial condyle and facet are demarcated by very distinct sharp edges.

The proximal half of the humerus forms a wide, plate-like, roughly square blade. The dorsal side of the proximal blade is convex overall and dominated by a prominent, thick, diagonal, oblique ridge that extends from the anterodorsal edge of the proximal articular

surface, fading away distally before reaching the shaft of the humerus (Fig. 29A). Preaxially is a thin, straight ridge, in the same orientation as the oblique ridge. Almost perpendicular to the oblique ridge is an irregular rugose ridge, leading to a tubercle and a notch of the proximal-postaxial corner rim of the humerus. The anterior proximal blade is swollen and bulged to form a convex turret and is shallowly concave either side of the turret. The preaxial edge of the proximal blade is flat or slightly concave, with very sharp 90° angular edges. A short (45 mm long) crescent-shaped ridge for muscle attachment is present on the humeral shaft, distal to the dominant oblique ridge in *Nochelesaurus* and *Bradysaurus* (absent in *Embrithosaurus*). Ventrally, the proximal blade is deeply concave, and featureless apart from the postaxial edge that forms the deltopectoral crest extending distally from the proximal head of the humerus and curving postaxially. In *Embrithosaurus* the deltopectoral crest forms a narrow knob-like structure (70 mm wide) with straight preaxial margin and curved postaxial margin. It has a gently convex ventral surface with a long, shallow groove (Fig. 30B). In *Nochelesaurus* and *Bradysaurus*, the deltopectoral crest is massive and robust (e.g. *Nochelesaurus* SAM-PK-6238: 90 mm wide) whereas it is narrow in *Embrithosaurus*. The ventral surface of the crest is irregular, roughly convex and heart-shaped. It lacks the long, central, ventral groove of *Embrithosaurus*.

The proximal articulation surface of the head of the humerus forms an s-shaped surface, as the anterior portion curves ventrally and the posterior portion extends dorsally (Fig. 31A). The articular surface widens anteriorly to more than twice the posterior width and the proximal blade is swollen to form a convex turret (Fig. 29A). The proximal articulation surface is generally flat, but concave preaxially where the blade is the thickest, and the central ventral margin forms a ridge that is raised well above the concave surface. Turner *et al.* (2015) consider a similar concave surface in *Bunostegos* to be evidence of a large cartilaginous cap.

Radius

The right radius of *Embrithosaurus* is well preserved (Fig. 39), the left is deeply weathered. The holotype of *Nochelesaurus* preserves no radius, but SAM-PK-6238 preserves an almost complete right radius (Fig. 40) apart from a small proximal lateral section. *Bradysaurus baini* has a well-preserved right radius (Fig. 41).

The morphology of the radii of all the middle Permian South African pareiasaur genera is very similar, short and stout (significantly shorter than the ulna) with an oval to roughly rectangular cross-sectional shaft. The proximal and distal ends are mediolaterally expanded to a little more than twice the width of the shaft and the bone is anteroposteriorly slightly flattened. The torsion (twisting) between the long axis of the proximal and distal expansions is about 45° in all three genera. The radius is straight, but slightly curved to bulge slightly anteriorly. Assuming an upright vertical shaft and a horizontal proximal articulation surface, the distal articulation surface is oblique, at an angle of about 20° below a horizontal plane in all three

genera (exaggerated to 35° in *Bradysaurus baini* as a result of the distortion of the specimen, which also causes a distinct and unnatural bend on the posterior side (Fig. 41C).

In cross-section, the dorsal articulation surface of the radius is ovoid, with a deep concavity for articulation with the radial condyle/facet of the humerus (Figs 39E, 40E, 41E). The edges are slightly raised and a small notch for articulation with the sigmoid notch of the ulna is present on the posterolateral corner. The ventral articulation surface forms a triangle and is also concave (Figs 39F, 40F, 41F). The posterior side is straight, or slightly concave, and slightly longer than the anteromedial and anterolateral sides which are roughly equal and convexly bulging.

In general morphology, the radii of *Bradysaurus baini* and *Embrithosaurus* are more similar to each other. In *Bradysaurus* and *Embrithosaurus*, the proximal expansion is slightly wider than the distal expansions, whereas in *Nochelesaurus* the situation is reversed, but this difference may not be significant. *Bradysaurus* and *Embrithosaurus* also present symmetrical proximal and distal radii (Figs 39, 41), whereas in *Nochelesaurus* the distal half of the radius is ventrolaterally expanded and stretched (SAM-PK-6238, Fig. 40A,B). As a result, the distal end of the radius of *Nochelesaurus* is mediolaterally wider than those of *Embrithosaurus* and *Bradysaurus baini*.

Anteriorly there is a small, triangular, anterior process on the radius of all three genera, about 10 mm above the ventral edge. In *Nochelesaurus* the anterior process is larger than that of *Embrithosaurus* and *Bradysaurus*. On the lateral side of the radii of *Embrithosaurus* (Fig. 39C) and *Nochelesaurus* (Fig. 40C) are rugose scars for the articulation with the ulna and on the medial side of the radii of *Nochelesaurus* (Fig. 40D) and *Bradysaurus* (Fig. 41D) are distinct and long vertical ridges, located posteriorly, which do not appear to be present in *Embrithosaurus*.

The posterior radius has a large shallow concave region with sharp vertical medial and lateral borders over the distal half of the bone in all genera. In *Nochelesaurus* alone, there is a low rugose tubercle near the distal edge of the lateral posterior ridge (Fig. 40B,C) and proximally two rugose areas (Fig. 40B), all of which are not apparent in the other genera, probably as a result of poor preservation.

Ulna

The right ulna of the holotype of *Embrithosaurus* is well preserved (Figs 42, 43, 44) but the left is badly weathered. *Embrithosaurus* specimen FMNH UR 2443 (Fig. 42C) preserves the articulated proximal right ulna and radius. *Nochelesaurus* specimen SAM-PK-6238 has a well-preserved right ulna (Figs 45, 46, 47). The right ulna of the holotype of *Bradysaurus baini* is complete and well preserved (Figs 48, 49, 50) and the left ulna is damaged and partially reconstructed. In all three genera the ulna is mediolaterally narrow, with a much thicker proximal half to support the large proximal articulation surface.

In all middle Permian South African pareiasaurs, the straight posterior border of the ulna is thickened and swollen to form a proximally thickening cylindrical bar covered by long, straight rugose ridges for muscular

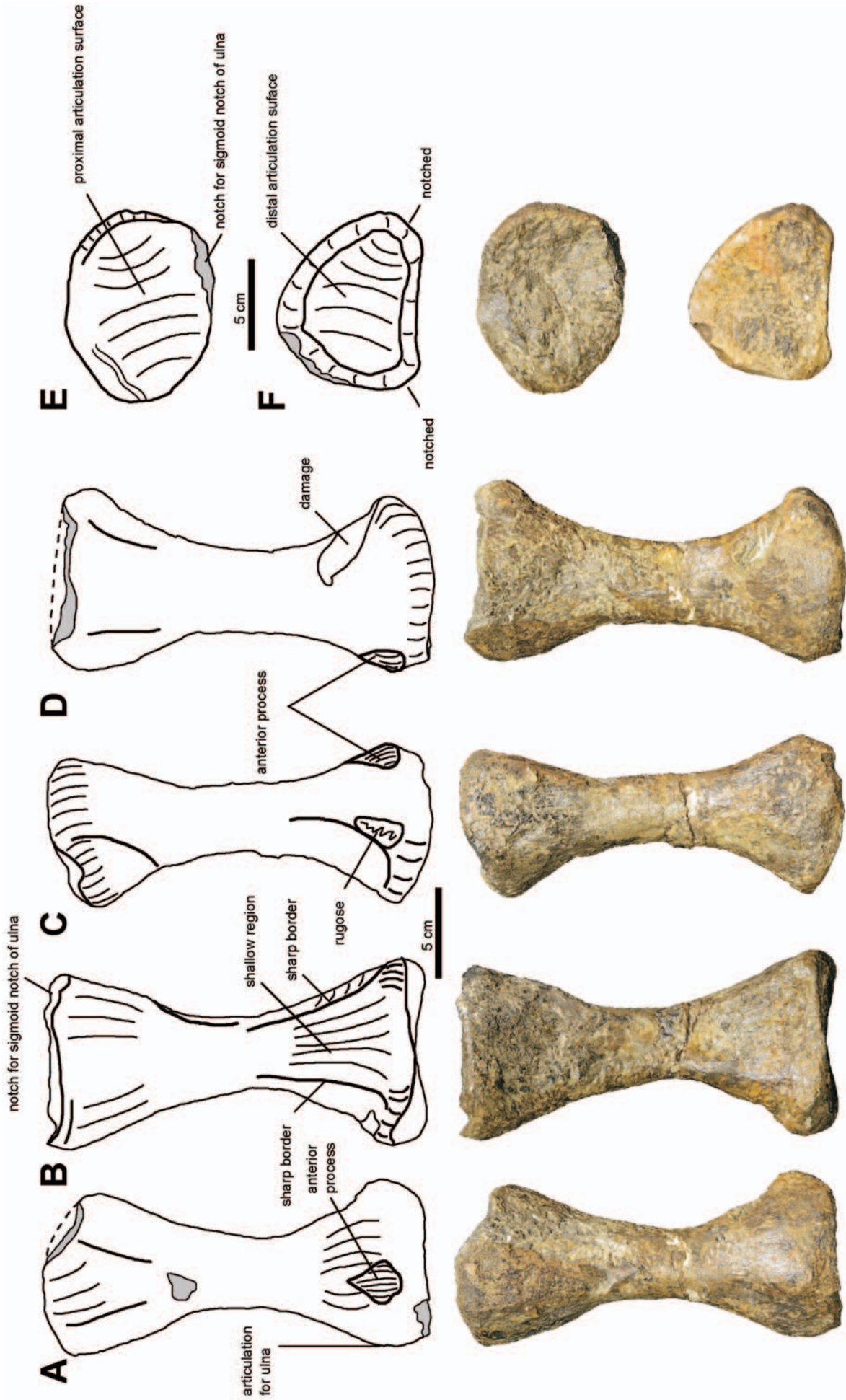


Figure 39. Photographs and interpretive drawings of the right radius of the holotype of *Embriothosaurus schwarzii* (SAM-PK-8034), (A), in anterior view, (B), in posterior view, (C), in lateral view, (D), in medial view, (E), in dorsal view, and (F), in ventral view. Dorsal to the top of the page in (A), (B), (C) and (D). Anterior to the top of the page in (E) and (F). Scale bar equals 5 cm.

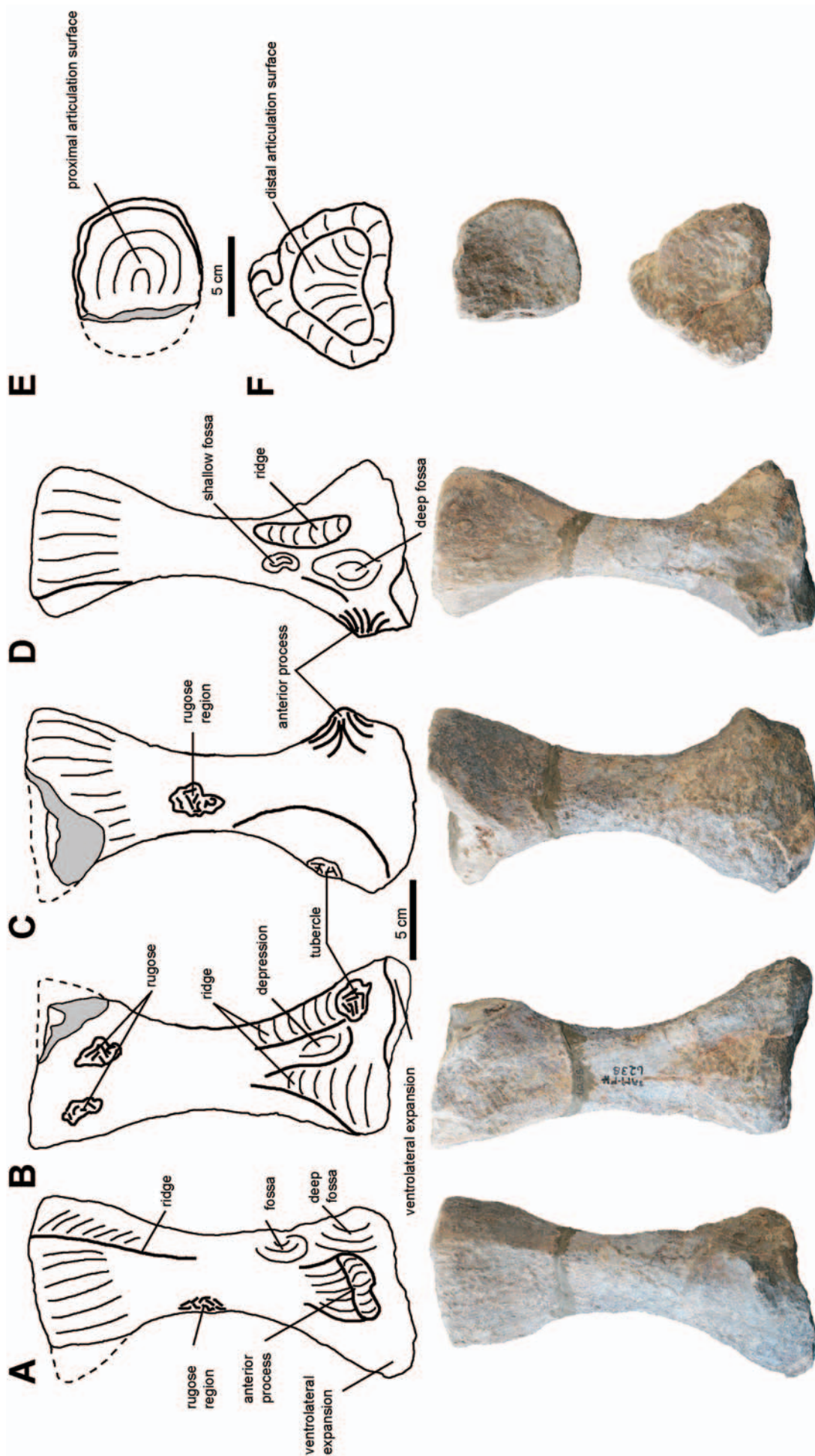


Figure 40. Photographs and interpretive drawings of the right radius of SAM-PK-6238 (*Nochthesaurus alexanderi*), (A), in anterior view, (B), in posterior view, (C), in lateral view, (D), in medial view, (E), in dorsal view, and (F), in ventral view. Dorsal to the top of the page in (A), (B), (C) and (D). Anterior to the top of the page in (E) and (F). Scale bar equals 5 cm.

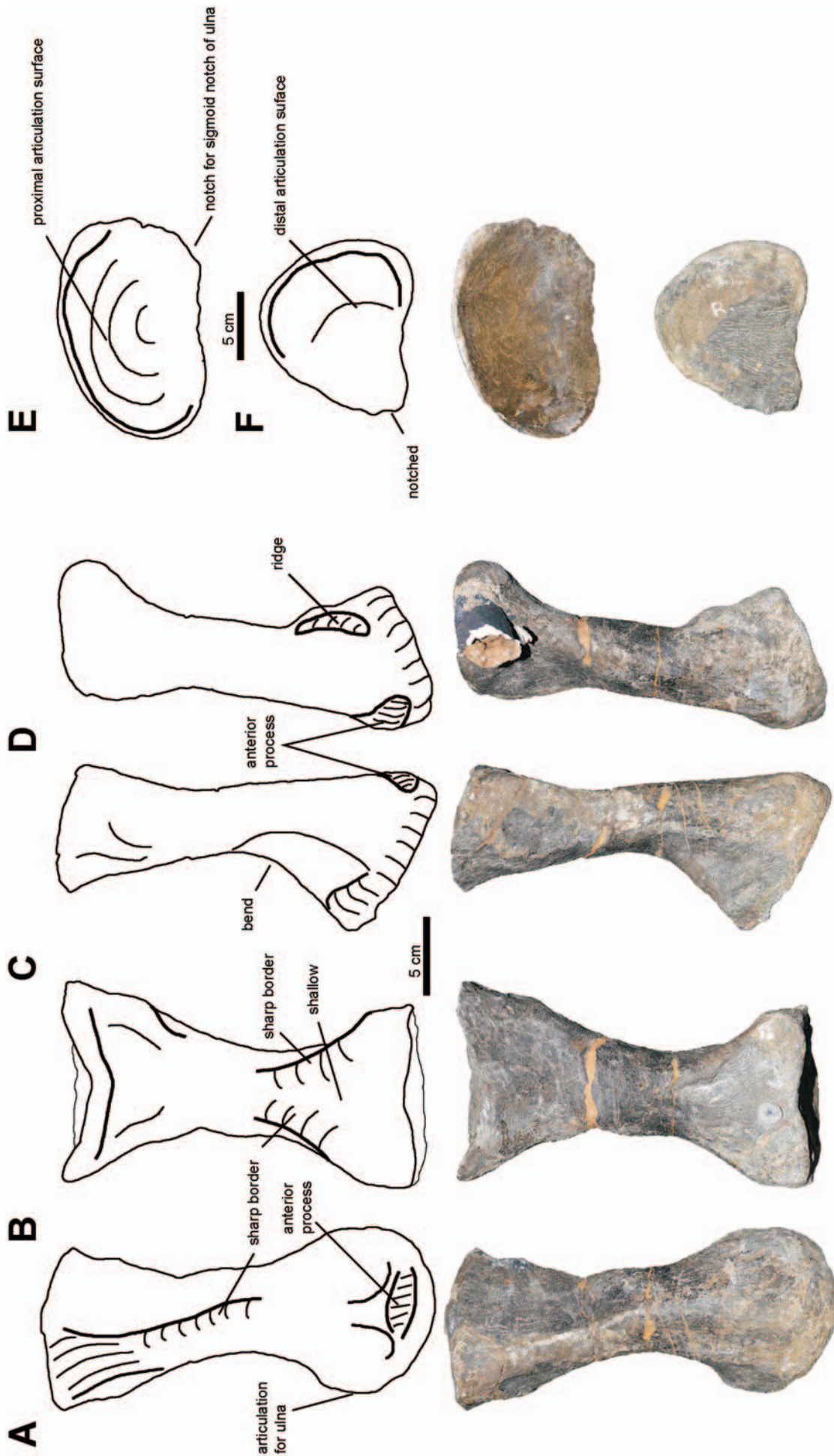


Figure 41. Photographs and interpretive drawings of the holotype of the right radius of the holotype of *Bradysaurus bairdi* (NHMUK PV R 1971), (A), in anterior view, (B), in posterior view, (C), in lateral view, (D), in medial view, (E), in dorsal view, and (F), in ventral view. Dorsal to the top of the page in (A), (B), (C) and (D). Anterior to the top of the page in (E) and (F). Scale bar equals 5 cm.

attachment (Boonstra 1932b). The medial and lateral sides have vertical concave regions anterior to the bar. The posterior bar consists of distal and proximal portions, separated by a distinct posterior bend. The distal portion is rounded and almost cylindrical, gently rugose, narrow, and gradually widens towards the proximal end. The proximal portion is much wider, more angular with sharper, square-edged sides, and prominent rugose ridges. The proximal and distal portions of the posterior bar are roughly of equal length in the ulnae of *Bradysaurus baini* and *Nochelesaurus* which have olecranon processes, but when no olecranon is present on the ulna (e.g. *Embrithosaurus* holotype SAM-PK-8034) the proximal portion is very short. The ulnae of *Nochelesaurus* and *Bradysaurus* are dorsoventrally long (370 mm), significantly longer than the short right ulna of the holotype of *Embrithosaurus* (295 mm). The proximal articulation surface is also dorsoventrally higher in *Nochelesaurus* and *Bradysaurus baini* (both 130 mm) than in *Embrithosaurus* (90 mm). The small distal articulation surfaces are roughly triangular. In *Embrithosaurus* the anterior two-thirds is concave and the posterior rim is convex (Fig. 44B). In *Nochelesaurus* (SAM-PK-6238) most of the surface is convex.

The proximal articulation surface of the ulna forms a gently convex rectangular surface which faces anterodorsally and has sharp-edged margins. It articulates with the groove-like, triangular, ulnar facet of the humerus. The proximal articular surfaces of the ulnae of *Nochelesaurus* (SAM-PK-6238), *Bradysaurus* (NHMUK PV R 1971), and *Embrithosaurus* (FMNH UR 2443) are complex (Figs 43, 46, 49). A swollen, oblique ridge in *Nochelesaurus* which is more vertical in *Bradysaurus* and *Embrithosaurus*, divides the surface into roughly equal-sized medial and lateral portions. Each portion is gently concave, the lateral side facing anterolaterally and the medial portion more anteriorly (Turner *et al.* 2015, character 105). The large *Embrithosaurus* ulna of FMNH UR 2443 has this vertical dividing ridge, with medial and lateral concave portions on the proximal articulation surface. However, the smaller ulna of the holotype of *Embrithosaurus* has a much simpler proximal articulation surface, which is short, gently convex, lacks any central dividing ridge, and is not bounded dorsally by an olecranon process.

A large, 50–60 mm deep sigmoidal (radial) notch is present, bordered dorsally by the lateral and medial sigmoidal processes. These triangular, ledge-like, sigmoidal processes form the distal edges of the proximal articulation surface. The medial process is larger and extends further anteriorly than the lateral process. The processes show slightly different shapes between the three species, but these are not significant and are at least partially the result of deformation, poor preparation, and damage. In *Nochelesaurus* the medial process tapers to a rounded tip and the lateral process ends in a blunt bilobed projection, with a notch between the lobes. In *Bradysaurus* the medial process is massive and both processes end in rounded tips. In all species, there is an additional small, medially extending process, on the medial rim of the proximal articular surface, a little above the posterior base of

the medial sigmoidal process, with an indentation above it.

In *Bradysaurus baini* a large olecranon process is present above the proximal articulation surface, formed anterodorsally by two overhanging ledges or concavely curved projections of the lateral and medial sides of the ulna that meet each other anteriorly. Dorsally the olecranon process is convex. The left and right olecranon processes of the holotype of *Bradysaurus baini* are morphologically very different from each other. The right olecranon process is very large (Figs 48, 49, 50) (45 mm in dorsoventral height, extending anteriorly 30 mm beyond the proximal articular surface) (Turner *et al.* 2015, character 106). The right process abruptly ends the proximal articular surface, forming a distinct lip-like overhanging ledge that prevents the hooked anterior facing articular surface from passing over onto the proximal side of the ulna. The left olecranon process is significantly smaller (Fig. 49C) extending only 15 mm dorsoventrally above the articular surface, one third as much as the right ulna, indicating a lack of bilateral symmetry. A posterodorsal transverse limiting ridge is present at the posterodorsal corner of the ulna of *Bradysaurus* and separates the proximal olecranon process from the posterior bar (Turner *et al.* 2015, character 105).

Nochelesaurus specimen SAM-PK-6238 has a low olecranon process (20 mm high) and the morphology is very different from those of the holotype of *Bradysaurus baini*. At the anterodorsal corner of the ulna of *Nochelesaurus* the proximal articulation surface is constricted or pinched-in. The lateral surface is concave and curved, and the medial surface only slightly so, which together narrow and constrict the articular surface, but not meeting anteriorly to form a ledge above the articulation surface. Instead, the constricted lateral and medial rims of the proximal articulation surface are slightly raised (5 mm high) to form small, short olecranon crests with the articular surface extending proximally as a wide shallow groove between the crests. Above the constriction point, the proximal ulna is bulbous, convex and curved to form a low (20 mm high) olecranon process, which terminates posteriorly on the posterodorsal corner of the ulna, at a square-edged, transverse ridge. This ridge separates the olecranon process from the rugose, proximal portion of the posterior cylindrical bar. Boonstra (1932b: 472) noted that the ulna of SAM-PK-6238 had 'hardly any olecranon process'. The olecranon process is low (only 20 mm high), convex on the proximal end of the ulna only, and does not extend anteriorly beyond the articulation surface at all (Turner *et al.* 2015, character 106).

Large *Embrithosaurus* specimen FMNH UR 2443 (unambiguously identified as *Embrithosaurus* through the shape of the pelvis, see Fig. 56) has a large and prominent olecranon process (Figs 42C, 43C) 40 mm dorsoventrally high, extending anteriorly 20 mm, which is similar to that of the right ulna of the holotype of *Bradysaurus baini*. The olecranon process is formed anterodorsally by two overhanging, concavely curved projections of the lateral and medial surfaces that meet anteriorly, forming a limiting ridge (overhanging ledge) above the proximal articulation surface of the ulna (Turner *et al.* 2015, character 105).

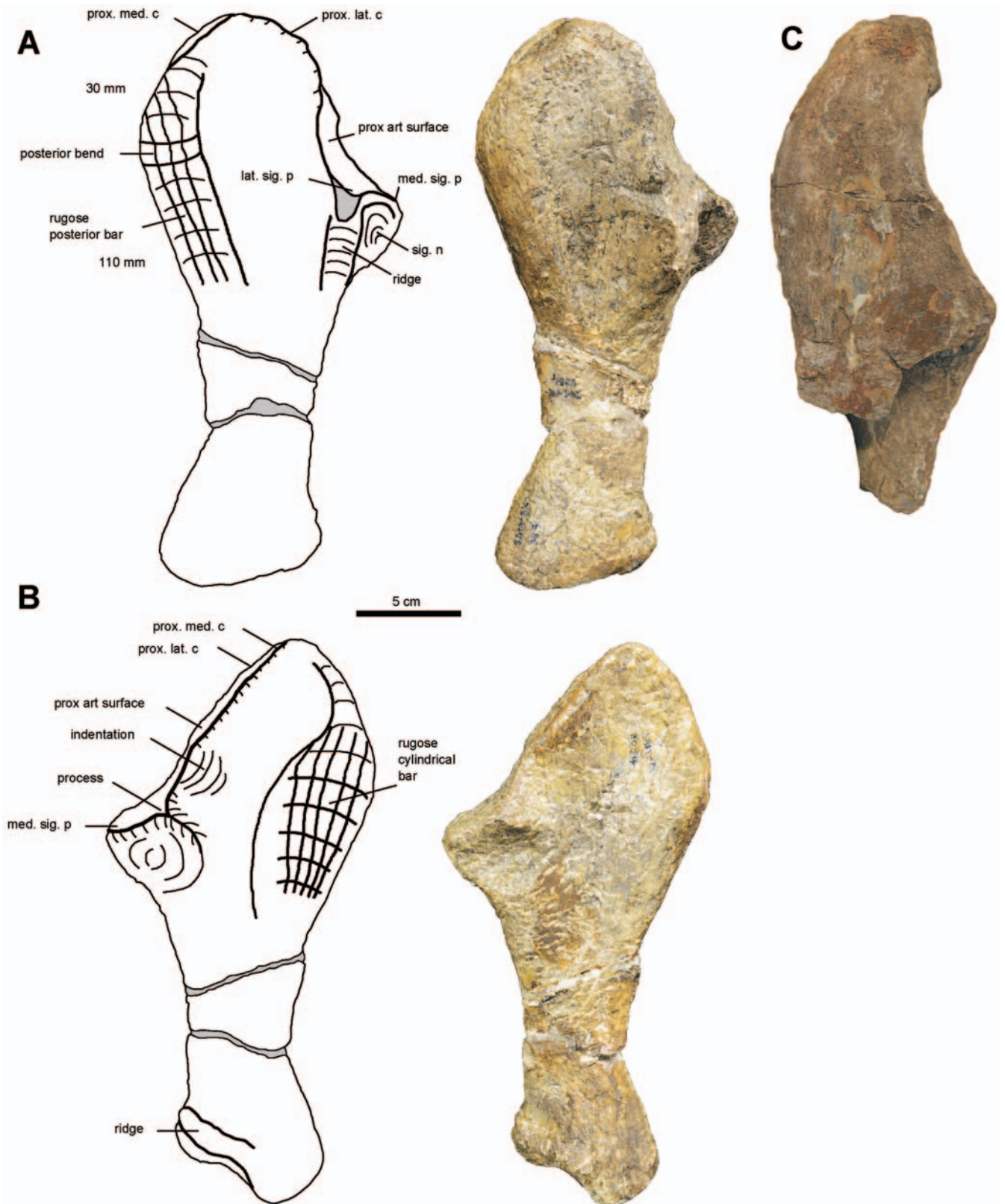


Figure 42. Photographs and interpretive drawings of right ulnae of *Embrithosaurus schwarzi*, (A), the holotype (SAM-PK-8034) in lateral view, (B), the holotype (SAM-PK-8034) in medial view, and (C), FMNH UR 2443 in lateral view (note the olecranon process, with partial right radius attached). Proximal to the top of the page. Scale bar equals 5 cm.

Embrithosaurus CGP CBT 112 also has a large, prominent olecranon process on the right ulna, 25 mm dorso-ventrally high, extending anteriorly 15 mm beyond the articular surface.

The ulnae of the holotype of *Embrithosaurus* are smaller than those of most other specimens and there is no

olecranon process. Instead, the anterodorsally articular surface forms a shallow, concave groove between two sharp, raised olecranon crests dorsally and posteriorly (Figs 42, 43, 44) (Turner *et al.* 2015, character 105). As noted by Boonstra (1932b), there is no anterodorsal limiting ridge, and no olecranon process (shelf or ledge) prevent-

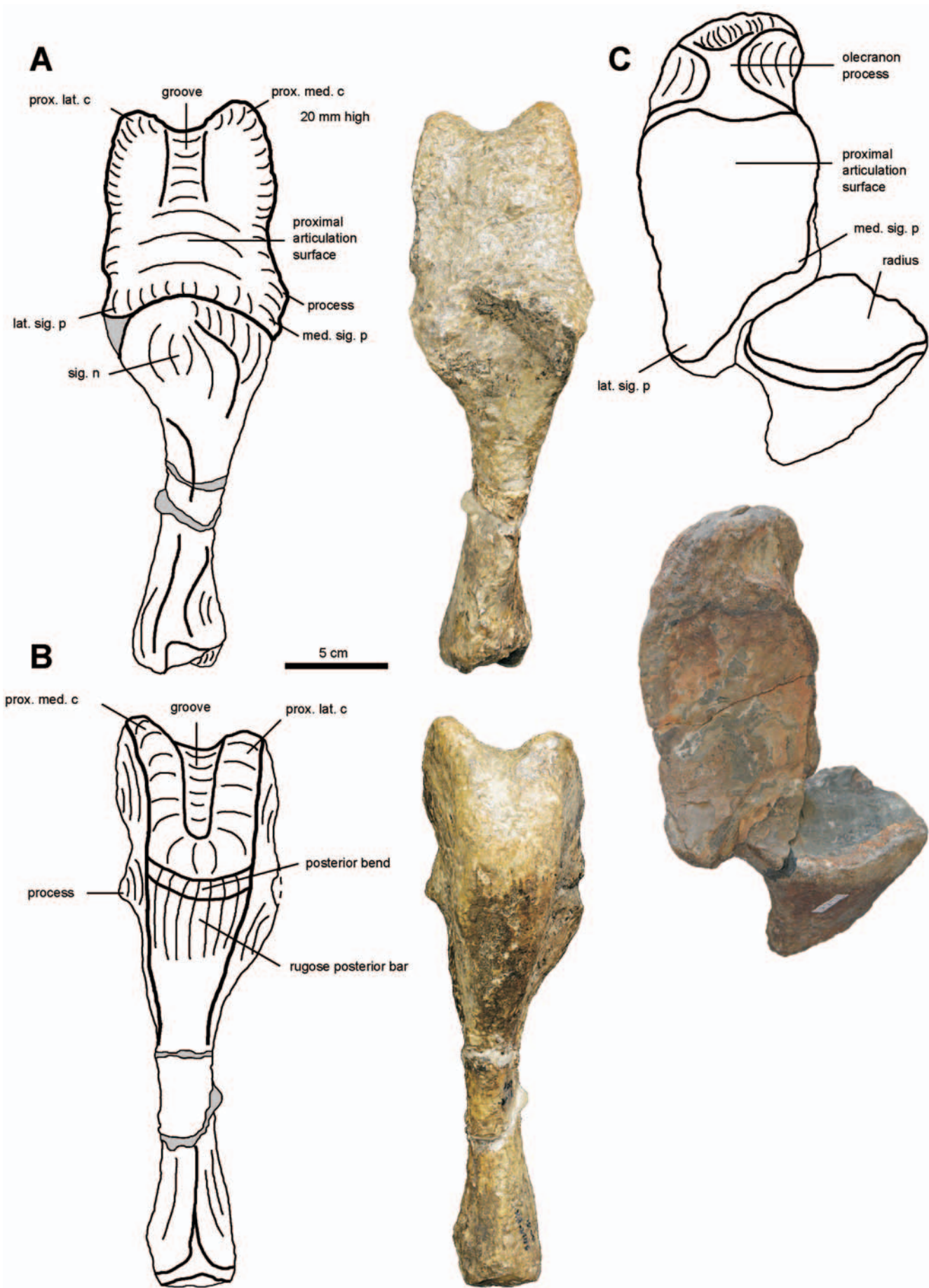


Figure 43. Photographs and interpretive drawings of right ulnae of *Embrithosaurus schwarzi*, (A), the holotype (SAM-PK-8034) in anterior view, (B), the holotype (SAM-PK-8034) in posterior view, and (C), FMNH UR 2443 in anterior view (with partial right radius attached). Proximal to the top of the page. Scale bar equals 5 cm.

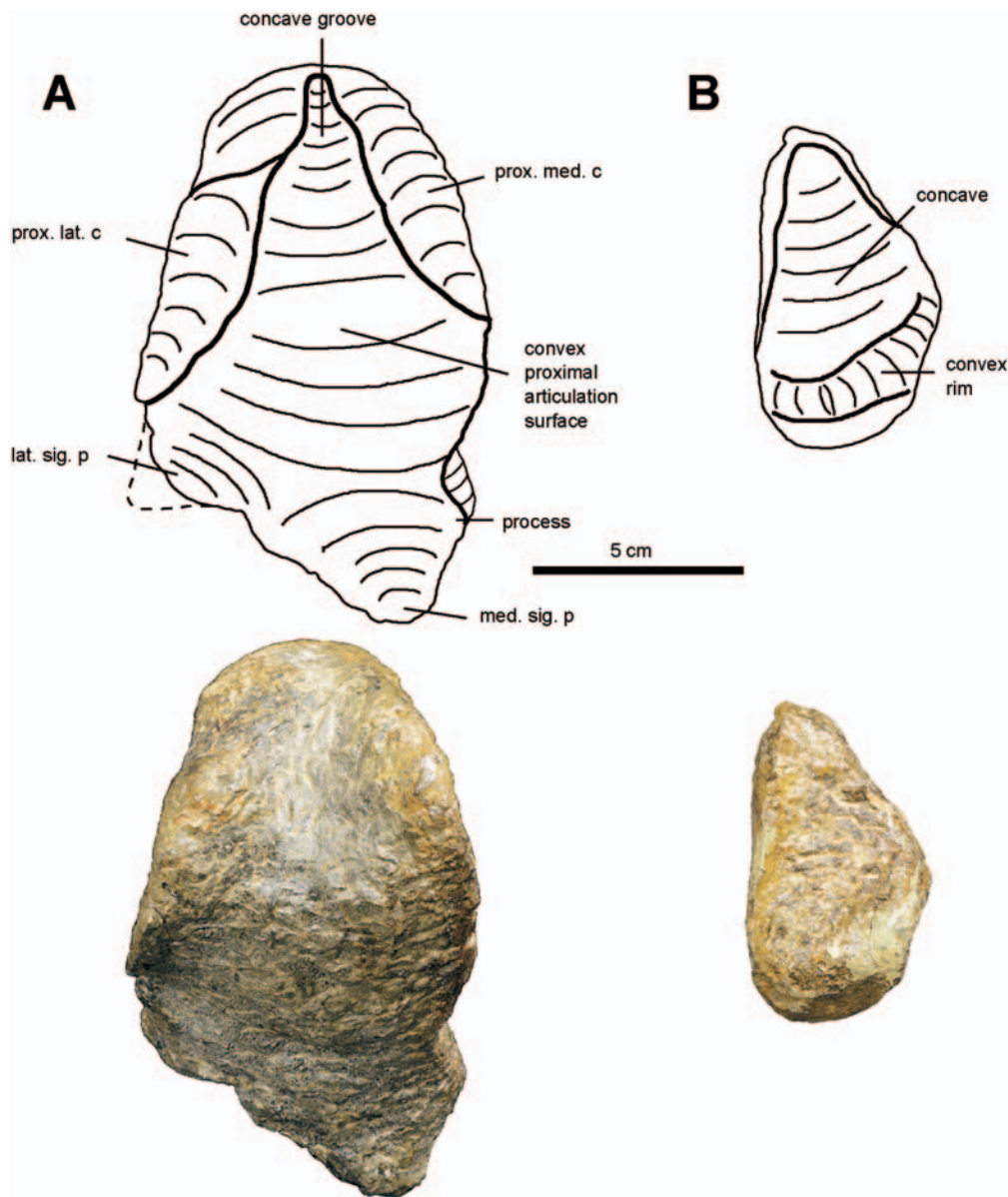


Figure 44. Photographs and interpretive drawings of the right ulna of the holotype of *Embrithosaurus schwarzi* (SAM-PK-8034), (A), in proximal view, and (B), in distal view. Posterior to the top of the page in (A). Anterior to the top of the page in (B). Scale bar equals 5 cm.

ing the anterodorsal articular surface from extending proximally onto the proximal end of the ulna. The proximal lateral and the slightly larger proximal medial crests are 40 mm apart and the groove between them is up to 20 mm deep. The proximal groove extends 30–40 mm onto the posterior side of the ulna (Fig. 44A), where the distance between the crests narrows to 20 mm before the crests and the groove disappear just before reaching the posterior bending of the cylindrical posterior bar. There is no posterodorsal limiting ridge. There is no dorsally projecting olecranon process on the proximal end of the ulna (Turner *et al.* 2015, character 106). It appears that the olecranon processes of these pareiasaurs are highly variable and that ontogenetic effects may account for the differences (see Discussion).

Carpus and manus

Broom (1903: 132) reported for the holotype of *Embrithosaurus* that 'a considerable number of isolated phalanges and metacarpals were found with, but with no

indication as to which digits they belong'. Two complete isolated digits with articulated phalanges, which Broom referred to the second and third digits, are preserved in SAM-PK-8034 as well as several misplaced phalanges and small carpal bones. Boonstra (1929a) published a labelled photograph of these two isolated digits (Boonstra 1929a: plate VII, fig. 2) indicating that each comprises a metacarpal and three phalanges, including the terminal claws.

Boonstra's (1929a) study remains the most extensive work done on South African pareiasaurian manus and he based most of his conclusions on a perfect left manus of a *Tapinocephalus* AZ pareiasaur (SAM-PK-8941). According to Boonstra (1929a) the digits decrease in size from the first to fifth, with a tiny, almost rudimentary fifth digit. The phalangeal formula of the manus is given as 2, 3, 3, 3, 2, which is the same in all known pareiasaurs (Turner *et al.* 2015, character 107).

The holotype of *Bradysaurus baini* preserves most of the right carpus and manus which were arranged by Seeley (1892) into five digits. The principal carpus is a large

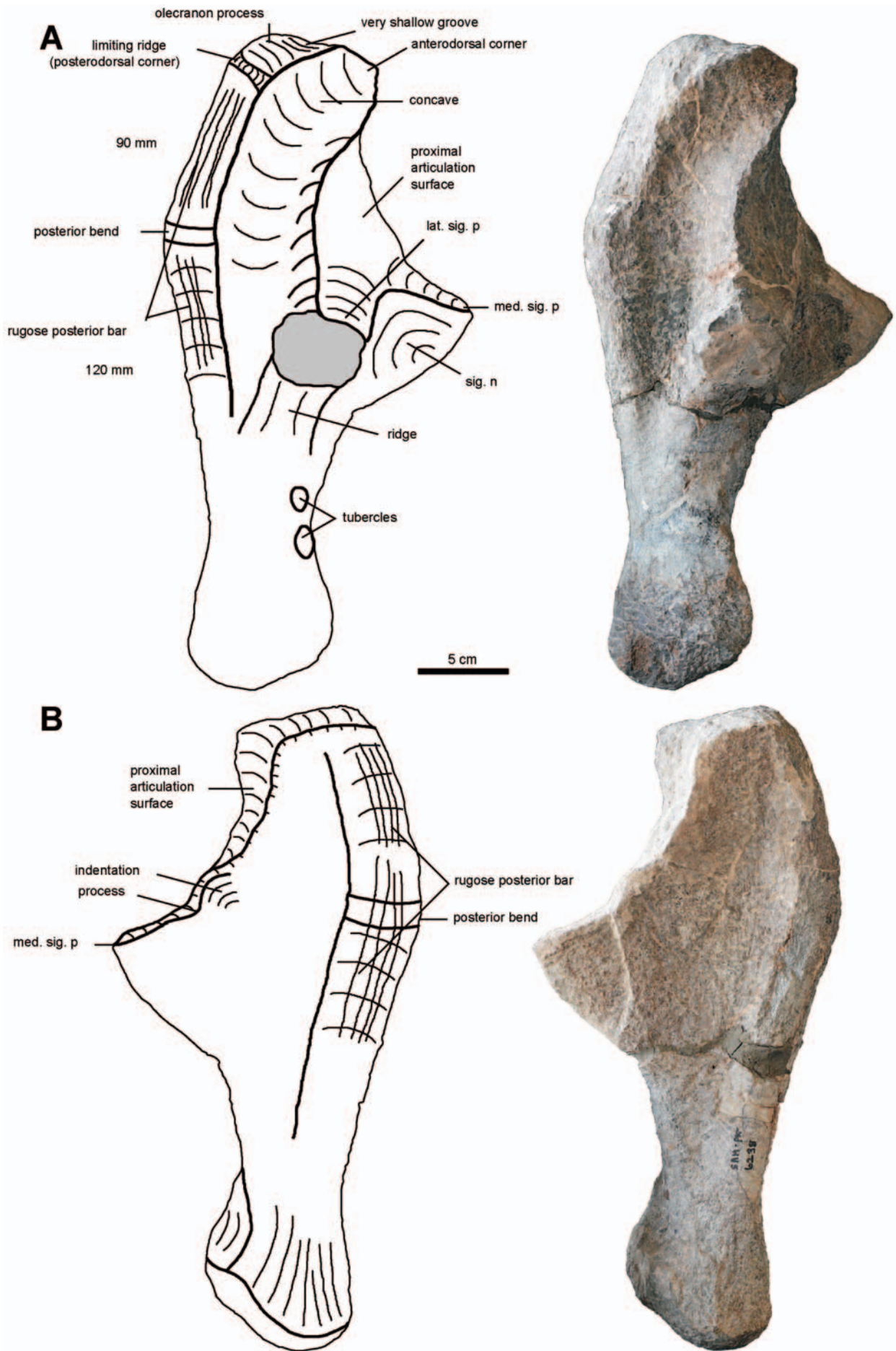


Figure 45. Photographs and interpretive drawings of the right ulna of SAM-PK-6238 (*Nochelesaurus alexanderi*), (A), in lateral view, and (B), in medial view. Proximal to the top of the page. Scale bar equals 5 cm.

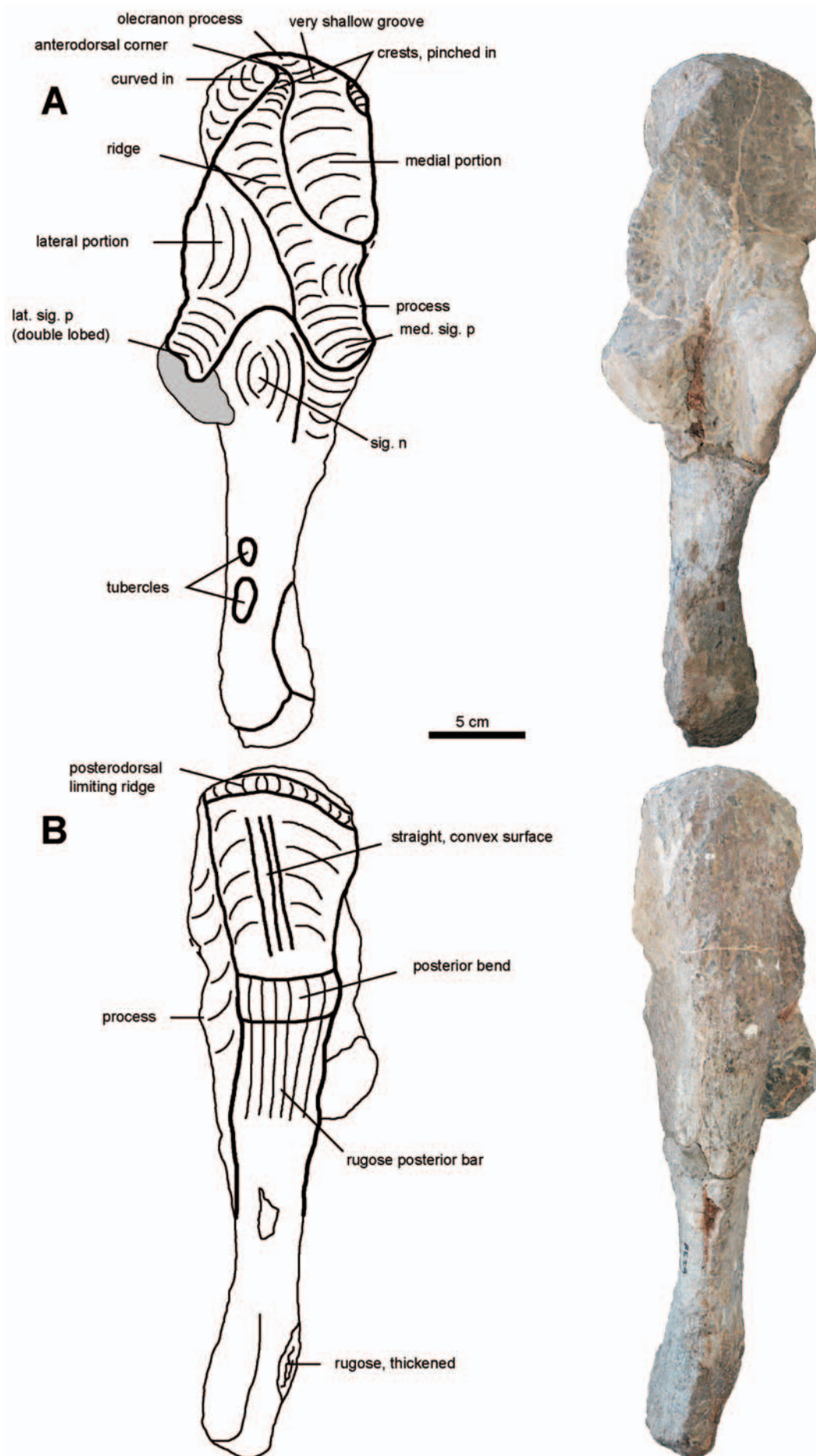


Figure 46. Photographs and interpretive drawings of the right ulna of SAM-PK-6238 (*Nochelesaurus alexanderi*), (A), in anterior view, and (B), in posterior view. Proximal to the top of the page. Scale bar equals 5 cm.

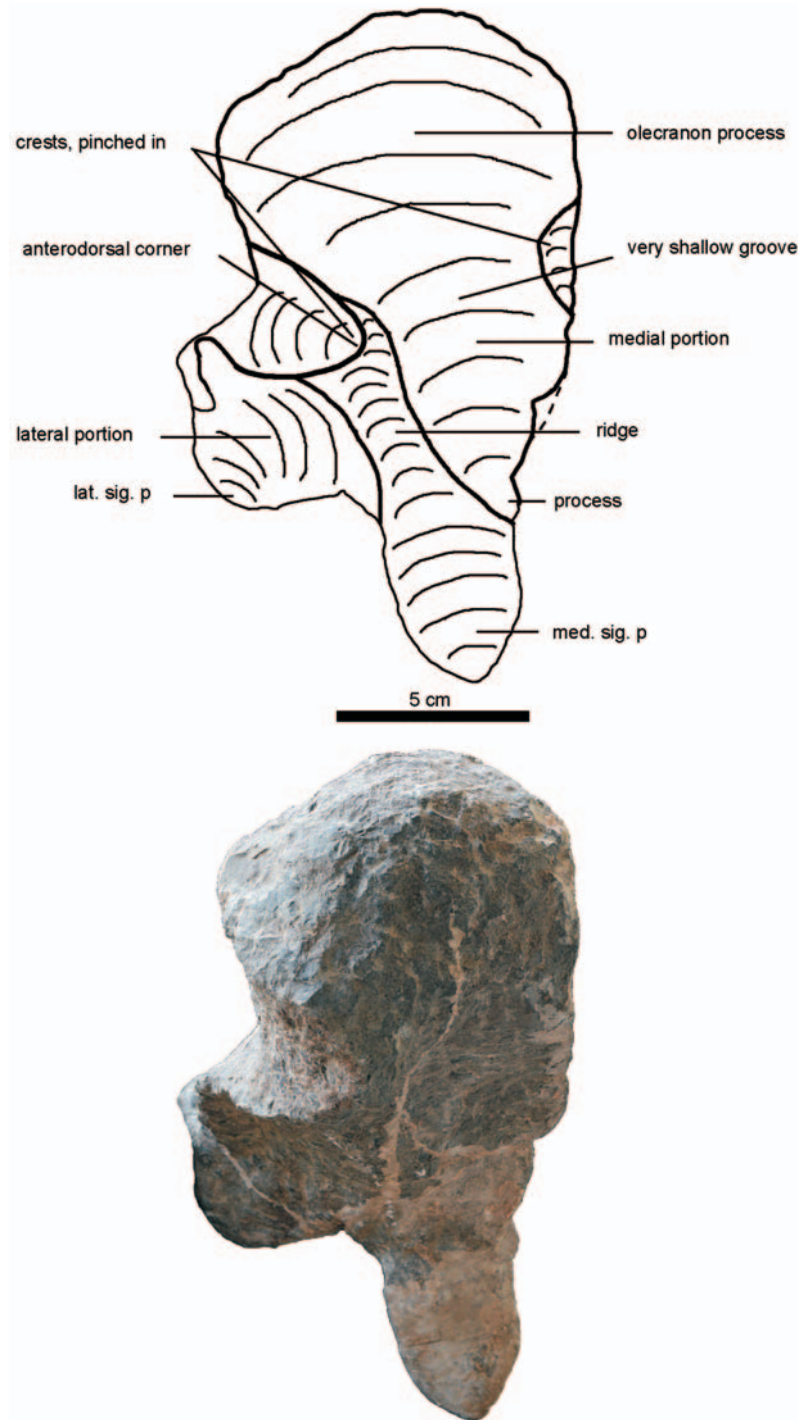


Figure 47. Photograph and interpretive drawing of the right ulna of SAM-PK-6238 (*Nochelesaurus alexanderi*), in proximal view. Posterior to the top of the page. Scale bar equals 5 cm.

rounded element, dorsally convex for articulation with the corresponding concave articulation surface of the distal radius (Seeley 1892; Boonstra 1929a) with two small carpals attached to it. As arranged by Seeley (1892) there are five digits of one metacarpal and three phalanges each still preserved, including a large terminal claw per row.

Pelvic girdle and hindlimb

Pelvic girdle

The pelvic girdle of pareiasaurs comprises a paired ilium, ischium, and pubis, all strongly fused to form two innominate bones that are themselves fused along the

midline (Haughton & Boonstra 1930). For the description of *Embrithosaurus* we used the innominates of SAM-PK-8034, FMNH UR 2443, FMNH UR 2486, and CGP CBT 112. In the holotype, SAM-PK-8034, the pelvis is nearly complete (Figs 51, 52, 54, 56), except for distal portions of both iliac blades, and small pieces of the left pubis and the right ischium (see below). As pointed out by Haughton & Boonstra (1930) the pelvis of SAM-PK-8034 is remarkably high and mediolaterally narrow, with a very narrow pelvic floor. The pelvis of the holotype of *Bradysaurus baini* is complete, well preserved, and well prepared (Figs 53, 55, 57), with only a few small isolated pieces crushed and filled with plaster. Compared to *Embrithosaurus*, the pelvis

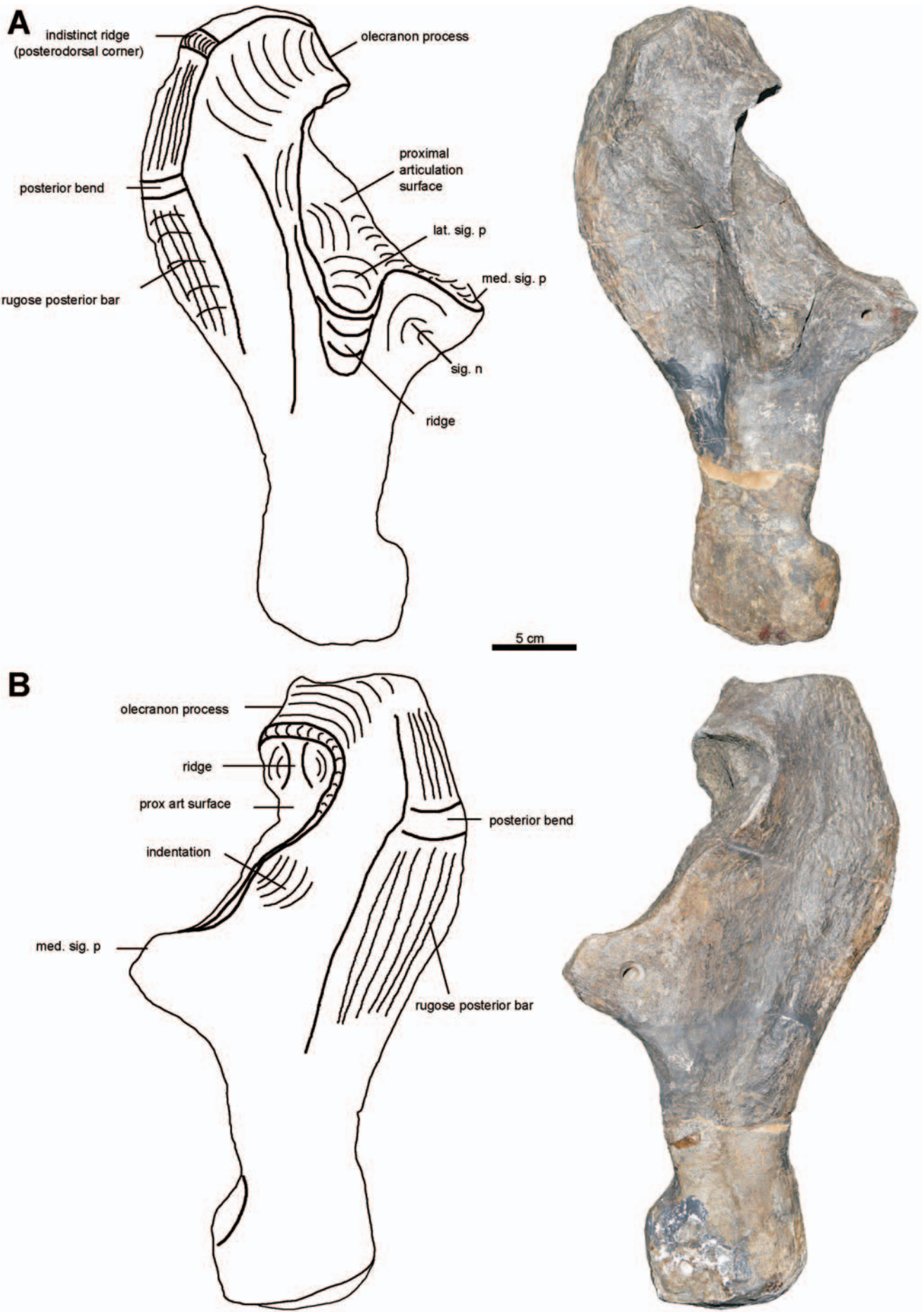


Figure 48. Photographs and interpretive drawings of the right ulna of the holotype of *Bradysaurus baini* (NHMUK PV R 1971), (A), in lateral view, and (B), in medial view. Proximal to the top of the page. Scale bar equals 5 cm.

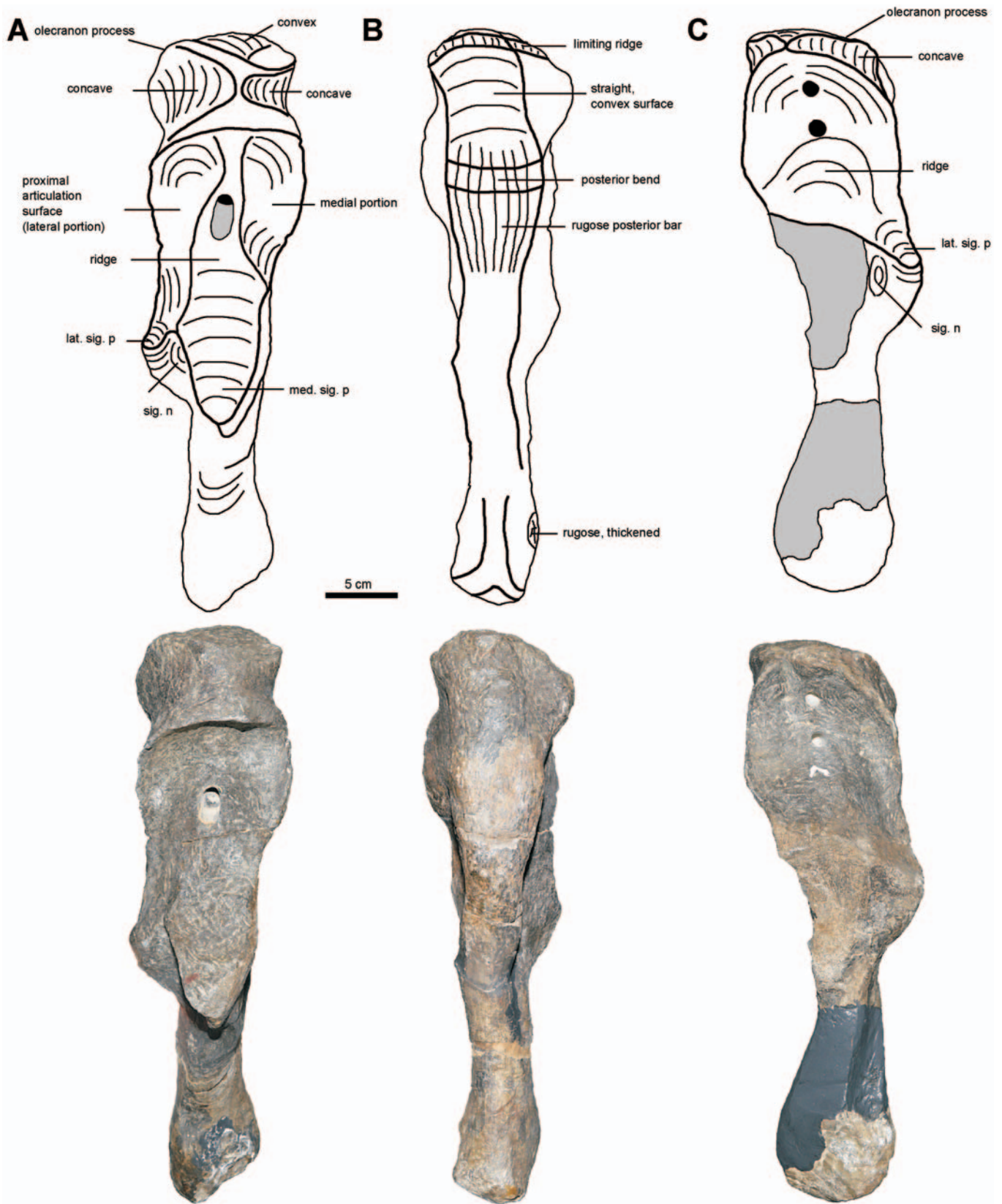


Figure 49. Photographs and interpretive drawings of the ulnae of the holotype of *Bradysaurus bairi* (NHMUK PV R 1971), (A), right ulna in anterior view, (B), right ulna in posterior view, and (C), left ulna in anterior view. Proximal to the top of the page. Scale bar equals 5 cm.

of *Bradysaurus* is noticeably low and wide. The holotype of *Nochelesaurus* preserves no pelvis. The sutures between the ilium, ischium, and pubis are strongly fused and not discernible in any specimens or species; however, in the following descriptions the region occupied by each bone is described separately.

Ilium

The ilium forms the entire iliac blade, the shaft below the blade, and the dorsal portion of the acetabulum. The large blade is a thin, elongated plate, anterodorsally directed, consisting of an elongated anterior process, and a shorter posterior process. In the holotype of *Embrithosaurus* the

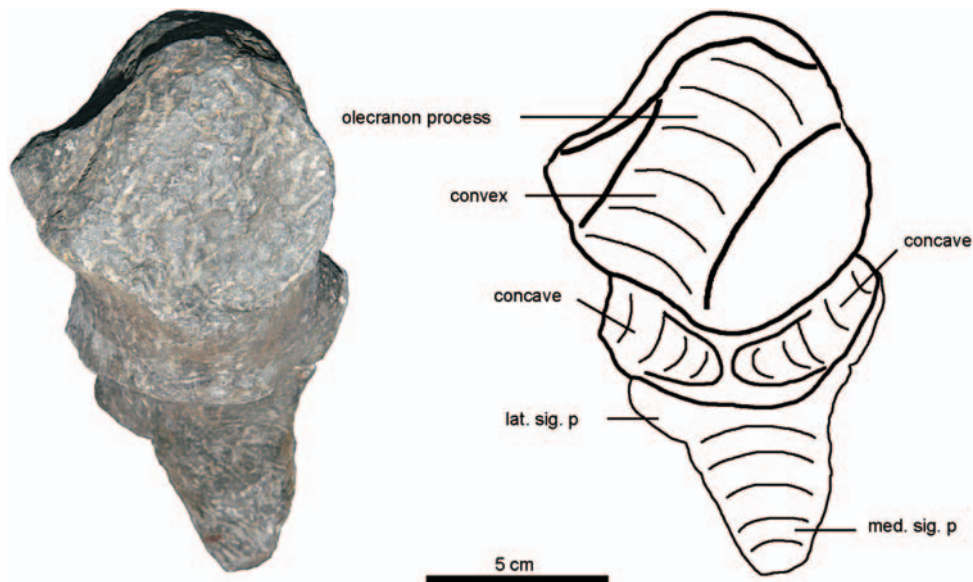


Figure 50. Photograph and interpretive drawing of the right ulna of the holotype of *Bradysaurus baini* (NHMUK PV R 1971), in proximal view. Posterior to the top of the page. Scale bar equals 5 cm.

anterior process of the right iliac blade is complete, but the posterior process is mostly missing. The left iliac blade is very poorly preserved and deeply eroded, consisting of only the shaft and a remnant internal core of bone.

The iliac blade of *Embrithosaurus* is more gracile than that of *Bradysaurus baini*: 1) anteriorly and dorsally the blades are mediolaterally narrower in *Embrithosaurus* (15–20 mm) and wider in *Bradysaurus baini* (25–30 mm); 2) although both species have well anteriorly expanded anterior processes, the anteroposterior length of the anterior process (from the anterior border of the shaft to the anterior tip of the anterior process) is shorter in *Embrithosaurus* (60–90 mm) and longer in *Bradysaurus baini* (130 mm) (Turner *et al.* 2015, character 110); and 3) the anteroposterior length of the dorsal sacral blade (anterior and posterior process) is shorter in *Embrithosaurus* (estimated 260–290 mm) and longer in *Bradysaurus baini* (290–310 mm). The posterior processes are short in all species, about 30 mm in *Embrithosaurus* specimens and 35–50 mm in *Bradysaurus baini* specimens (Turner *et al.* 2015, character 112).

Our research verifies unique features in the shape and orientation of the iliac blades of *Embrithosaurus*, which we take as genuine features, unaffected by ontogeny, as they are found in both the late subadult-sized holotype and large adult specimens (e.g. FMNH UR 2443, FMNH UR 2486, CGP CBT 112). The morphology of the iliac blades of *Embrithosaurus* is simple (Fig. 56). The entire blade is almost perfectly flat and straight (e.g. SAM-PK-8034, FMNH UR 2443), and on only some specimens is the blade laterally slightly and evenly concave (e.g. FMNH UR 2486, CGP CBT 112). The entire blade is oriented almost perfectly vertically, except for the anteroventral margin or tip of the anterior process, which is very slightly curved or bent upwards (curved less than 10° outwards and upwards from a vertical plane), and everted laterally (extending only 10 mm laterally outwards from the main body of the blade). We thus confirm an autapomorphy of *Embrithosaurus* proposed by Lee (1994, 1997a), that the

anterior portion of the iliac blades is flat and vertical/dorsoventral (not everted or upturned) (Turner *et al.* 2015, character 111).

In contrast, the iliac blades of *Bradysaurus baini* are complex (Fig. 57). Anteriorly, they are severely laterally concave, curved or bent upwards and everted outwards, as the anterior process bends upwards (facing the blades more upwards) forming an angle of 55–60° outwards from a parasagittal vertical plane (Fig. 55A: NHMUK PV R 1971, SAM-PK-5002) (Turner *et al.* 2015, character 111). The posterior half of the iliac blade is vertically oriented, flat and thin, and the dorsal margin of the posterior process curves medially inwards a short distance (25 mm) towards the midline, giving the posterior blade a convex shape posterodorsally (Fig. 57, NHMUK PV R 1971, SAM-PK-5002).

In dorsal view, the thin iliac blades of the holotype of *Embrithosaurus* are not parallel, and instead are oriented 45° off the sagittal midline plane, diverging anteriorly (Fig. 56A). Specimens FMNH UR 2443 and FMNH UR 2486 show a similar degree of anterior divergence (Fig. 56C,D). *Embrithosaurus* specimen CGP CBT 112 shows an extreme 60° divergence. We thus confirm another autapomorphy of *Embrithosaurus* proposed by Lee (1994, 1997a) that the iliac blades diverge anteriorly and are oriented 45–60° off the sagittal plane.

In contrast, in *Bradysaurus baini*, the iliac blades are oriented parallel or at most very slightly anteriorly divergent to each other and to the parasagittal plane (Fig. 57: NHMUK PV R 1971, SAM-PK-5002). In the holotype, the left blade is aligned with the parasagittal plane, whereas the right blade is directed slightly laterally outwards by 10° off a parasagittal plane, diverging anteriorly. Anteriorly, the blades are not parallel to the parasagittal plane but are sharply concavely curved outwards and the anterior third of the blade is directed roughly 45° off the parasagittal plane, diverging anteriorly, and the anterior tip of the anterior process extends up to 80 mm laterally from the sagittal plane or main body of the blade in

NHMUK PV R 1971 (Fig. 57) and SAM-PK-5002 (Turner *et al.* 2015, character 111).

The shaft of the ilium of *Embrithosaurus* is more vertically oriented than that of *Bradysaurus baini*. In *Embrithosaurus* the shaft is oriented anterodorsally, only about 30° off the transverse vertical plane (Figs 51, 52) (Turner *et al.* 2015, character 113). This contrasts with *Bradysaurus baini* specimens that have much more horizontally oriented shafts, anterodorsally oriented about 60° from the transverse vertical plane (Fig. 53) (Turner *et al.* 2015, character 113). The orientation of the shaft described here assumes that the dorsal edge of the anterior process of the sacral blade is oriented slightly below a horizontal plane, such that the orientation of the sacral vertebrae is horizontal and slightly ventral, as they would have been in life position (Turner *et al.* 2015, character 113).

In *Bradysaurus* and *Embrithosaurus*, the medial side of the iliac blade has a thick, vertically elongated medial ridge that articulates with the first sacral rib (Fig. 56). This ridge is medially convex, thickens ventrally, and forms a well-fitting counterpart for articulation with the deeply concave lateral side of the first, large, sacral rib in *Embrithosaurus*. Some unprepared matrix fills a cavity between the concave lateral first left sacral rib and the convex articulation of the medial iliac process or ridge (Fig. 56). In *Bradysaurus*, the medial ridge of the iliac blade which articulates with the largest sacral rib is anterodorsally oriented and is prominent (Fig. 57), extending 40 mm medially from both the main body of the iliac blades, a similar morphology to that seen in *Embrithosaurus*.

The acetabulum is almost perfectly round in *Embrithosaurus* (Figs 51, 52) and more oval in *Bradysaurus* (Fig. 53). The oval shape in *Bradysaurus* appears to be the result of dorsoventral crushing and is probably not a true morphological difference. Three thickened regions are present around the acetabulum, each forming a buttress. The dorsal supra-acetabular buttress under the shaft of the ilium is the most prominent. It protrudes laterally, forming an almost perfect semi-circular overhanging dorsal lip to the acetabulum, with a ventrolaterally facing internal surface (Turner *et al.* 2015, character 114). The ischial buttress on the posteroventral corner of the acetabular rim forms a smaller, sharp-edged buttress, faces anterodorsally internally, and supports the posterior puboischiatic plate. The pubic buttress is the least robust of the three, and is low and flattened. A shallow notch on the anterior acetabular rim just above the dorsal edge of the pubic buttress, is present in the holotype of *Embrithosaurus*, in *Embrithosaurus* specimen CGP CBT 112 and the holotype of *Bradysaurus baini* (Turner *et al.* 2015, character 115). This notch has also been reported in *Pareiasuchus peringueyi* and *Pareiasuchus nasicornis* by Lee (1997b). Additionally, in CGP CBT 112, there is a very distinct, large, and deep notch on the posterior border of the acetabulum, just above the ischial buttress.

Pubis

The puboischiatic plate of the pelvis of *Embrithosaurus* is mediolaterally narrow. Anteriorly, in the holotype, it measures 305 mm between the anterolateral edges of the

lateral pubic processes, and posteriorly 290 mm between the posterolateral edges of the puboischiatic plate (Fig. 56). In contrast, the puboischiatic plate of *Bradysaurus baini* is very wide, anteriorly and posteriorly 360 mm wide (Fig. 57).

The puboischiatic plate of the pelvis of *Embrithosaurus* is not horizontally flat: the dorsal surface is strongly and evenly concavely curved, rising steeply laterally to meet the ischium, and here, between the blades, the curved plate is narrow, measuring 95 mm wide anteriorly, and 130 mm wide posteriorly (Fig. 54). In contrast, the puboischiatic plate of *Bradysaurus* is horizontally flat, and dorsally slightly raised along the midline (especially anteriorly). The wider pelvis of *Bradysaurus baini*, measures about twice the width of *Embrithosaurus* between the iliac blades, (210 mm anteriorly and 230 mm posteriorly, Fig. 55). Posteriorly wide and shallow longitudinally elongated depressions are present on either side of the bulged dorsal midline in *Bradysaurus baini*. *Embrithosaurus* lacks dorsal depressions posteriorly on its deeply concave dorsal puboischiatic plate.

The puboischiatic plate of *Embrithosaurus* SAM-PK-8034 is anteroposteriorly short (Fig. 56) and dorsoventrally very thick through the pelvic symphysis midway between the anterior and posterior edges of the plate (SAM-PK-8034, 90 mm; FMNH UR 2443, 106 mm; FMNH UR 2486, 110 mm; CGP CBT 112, 110 mm) (Fig. 54) (Turner *et al.* 2015, characters 118, 119). We thus confirm the final autapomorphy of *Embrithosaurus* proposed by Lee (1995, 1997a), that the pelvic symphysis very thick dorsoventrally (Turner *et al.* 2015, character 119). However, the maximum dorsoventral thickness (80 mm) of the pelvic symphysis of *Bradysaurus baini* NHMUK PV R 1971 is almost as thick as that of the holotype of *Embrithosaurus* (90 mm). Late subadult *Bradysaurus baini* SAM-PK-5002, measures 70 mm (Turner *et al.* 2015, character 119). Compared to *Embrithosaurus*, the puboischiatic plate of *Bradysaurus baini* is anteroposteriorly extremely long, measuring 325 mm (Fig. 57), compared to the much shorter 220 mm in *Embrithosaurus* (Fig. 56) (Turner *et al.* 2015, character 118).

The dorsoventral thickness of the pelvic symphysis of *Embrithosaurus* is formed by a midline V-shaped, ventrally directed elongated keel (Figs 52, 54, 56) forming most of the ventral surface of the puboischiatic plate. The keel measures at least 100 mm wide anteriorly and posteriorly and narrows midway. From the sharp midline edge, the keel extends dorsolaterally upwards at 50° above the horizontally flat plane (Fig. 54B) which is steeper than other middle Permian South African pareiasaurs. In contrast, the ventral surface of the puboischiatic plate of *Bradysaurus* is flat and forms a broad plate, interrupted by a very narrow (only 60–70 mm wide at most anteriorly and posteriorly) midline, ventrally directed v-shaped keel, with a low longitudinal ridge on either side of the keel (Fig. 57B). *Embrithosaurus* lacks longitudinal ventral ridges either side of the keel. In both *Bradysaurus* and *Embrithosaurus*, the ventral keel narrows in the middle of its length (Figs 56B, 57B).

The ventral surfaces of the keels of *Embrithosaurus* and

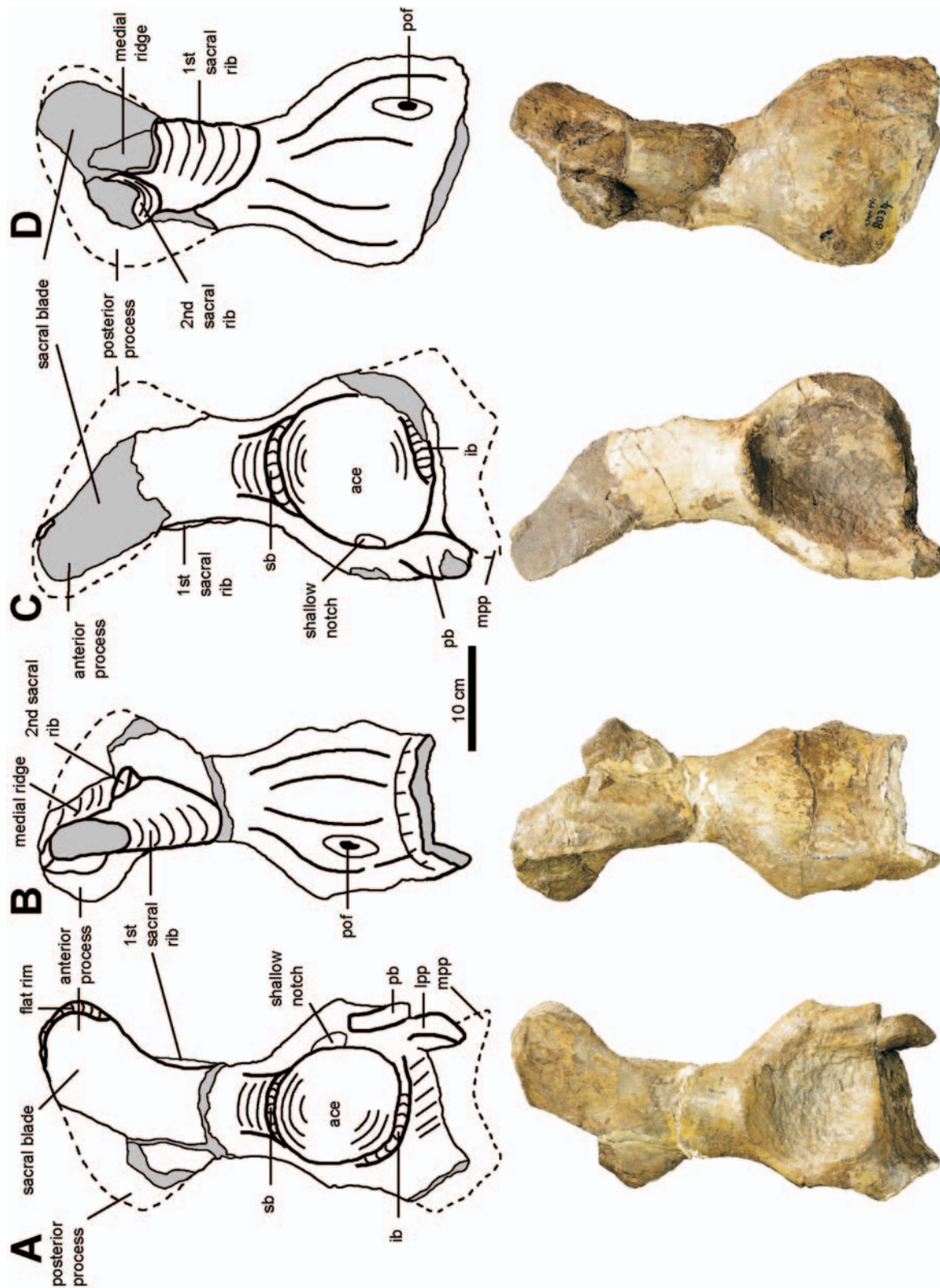


Figure 51. Photographs and interpretive drawings of the pelvis of the holotype of *Embriithosaurus schtorrzi* (SAM-PK-8034), (A), in right lateral view, (B), in right lateral view, (C), in left lateral view, and (D), in left medial view. Dorsal to the top of the page. Scale bar equals 10 cm.

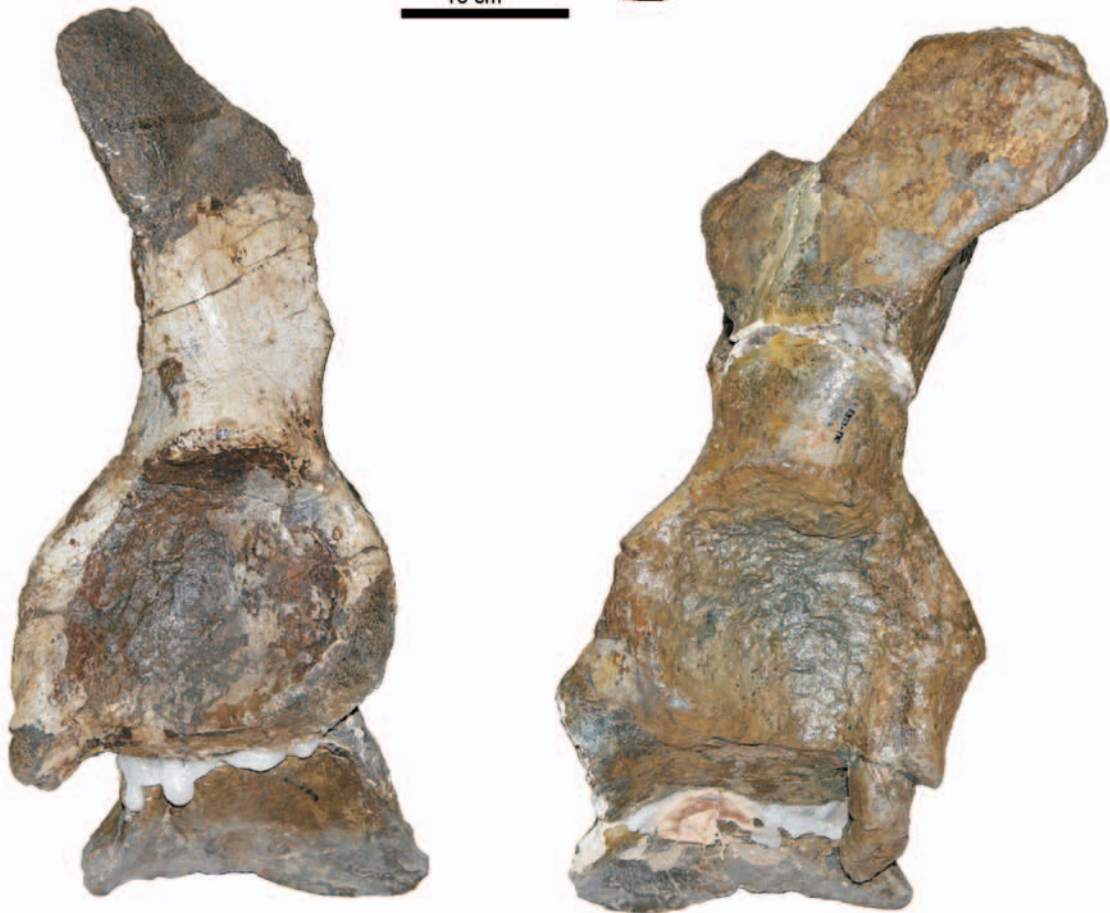
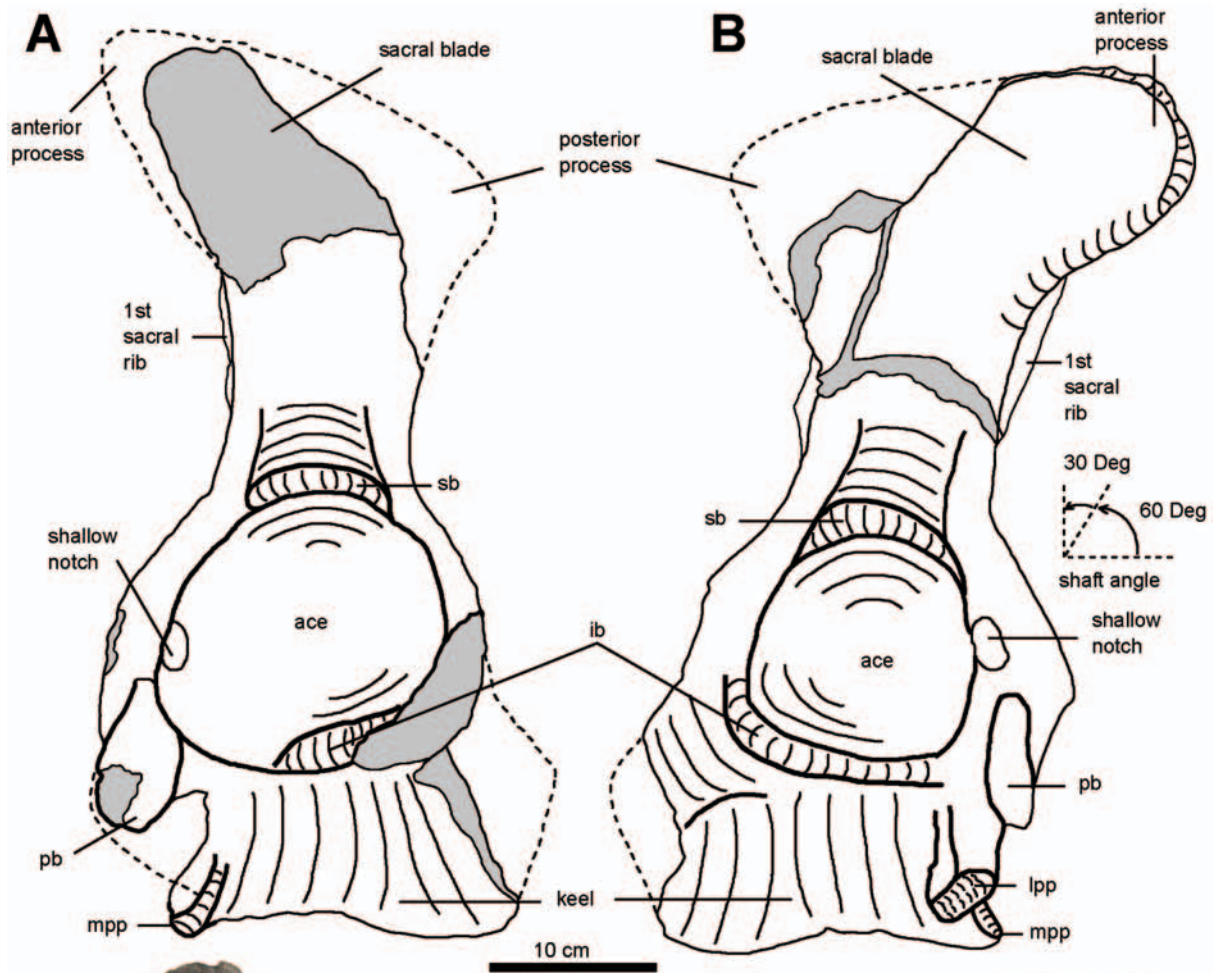


Figure 52. Photographs and interpretive drawings of the innominates of the holotype of *Embriithosaurus schwarzi* (SAM-PK-8034), (A), left innominate in lateral view, and (B), right innominate in lateral view. Dorsal to the top of the page. Scale bar equals 10 cm.

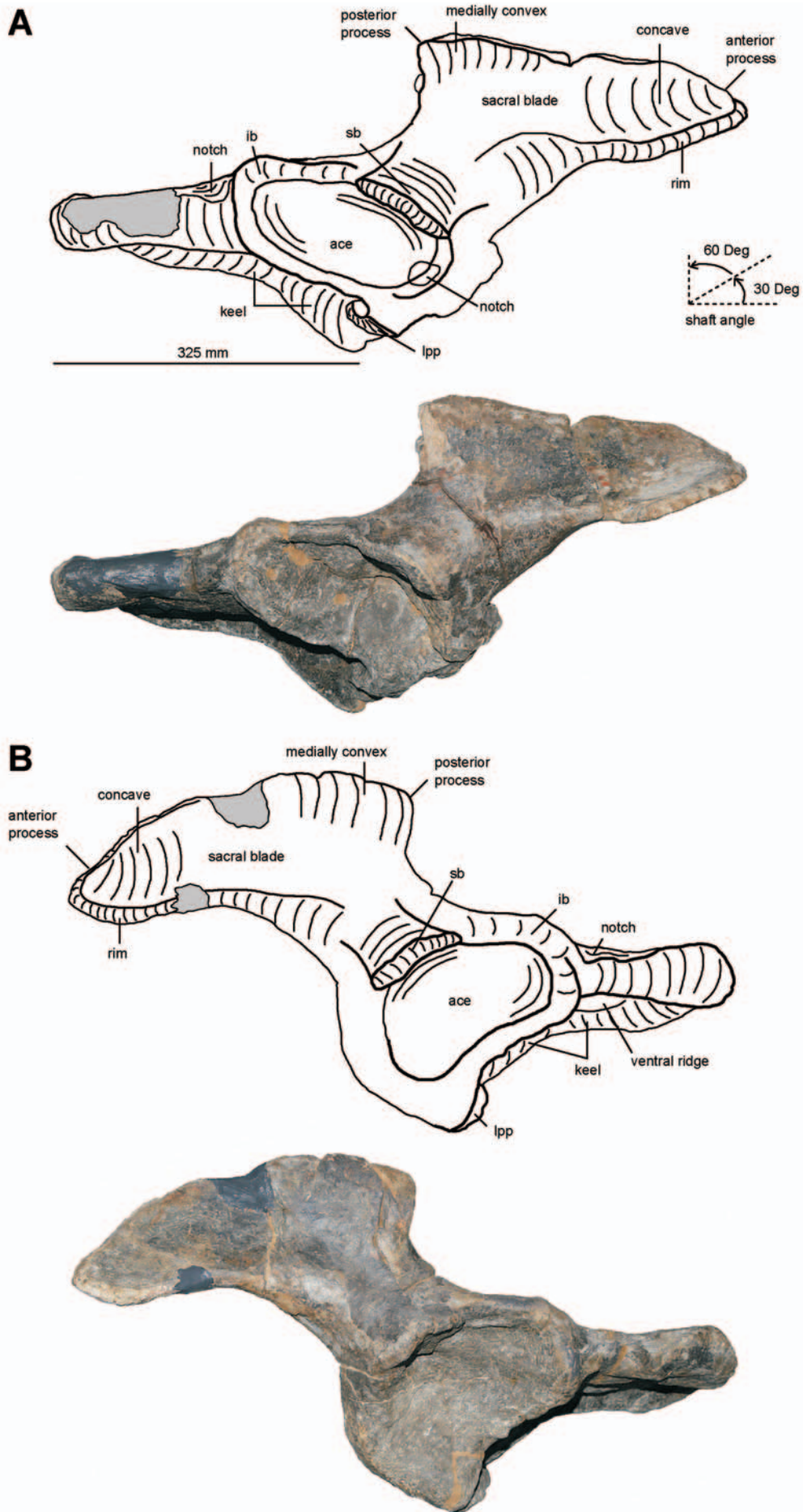


Figure 53. Photographs and interpretive drawings of the pelvis of the holotype of *Bradysaurus baini* (NHMUK PV R 1971), (A), in right lateral view, and (B), in left lateral view. Dorsal to the top of the page. Scale bar equals 325 mm.

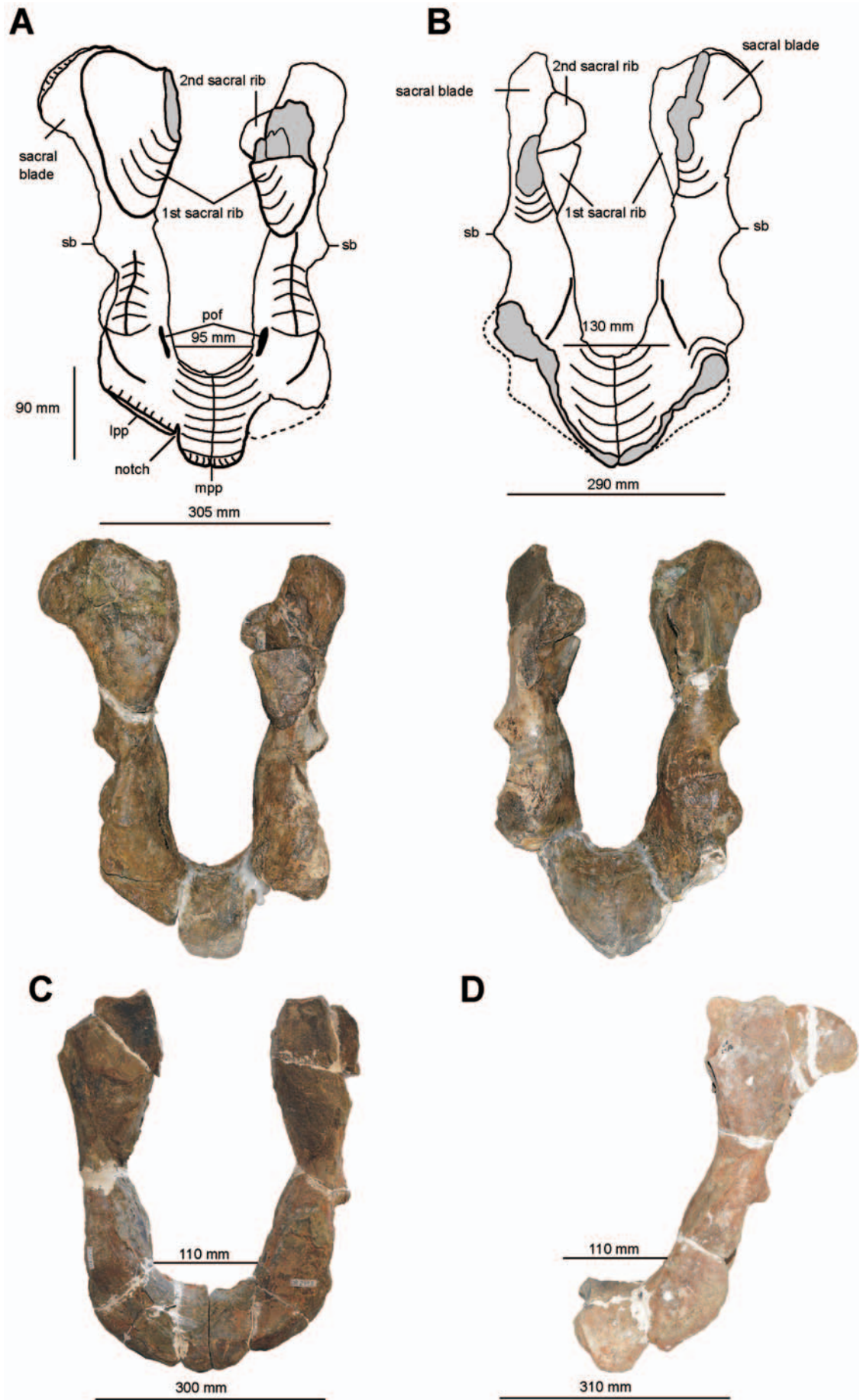


Figure 54. Photographs and interpretive drawings of the pelvis of *Embrithosaurus schwarzi*. The holotype (SAM-PK-8034) in (A), anterior view, and (B), posterior view. (C), FMNH UR 2443 in anterior view, and (D), FMNH UR 2486 in anterior view. Dorsal to the top of the page. Scale bars equal: A, 305 mm; B, 290 mm; C, 300 mm; D, 310 mm.

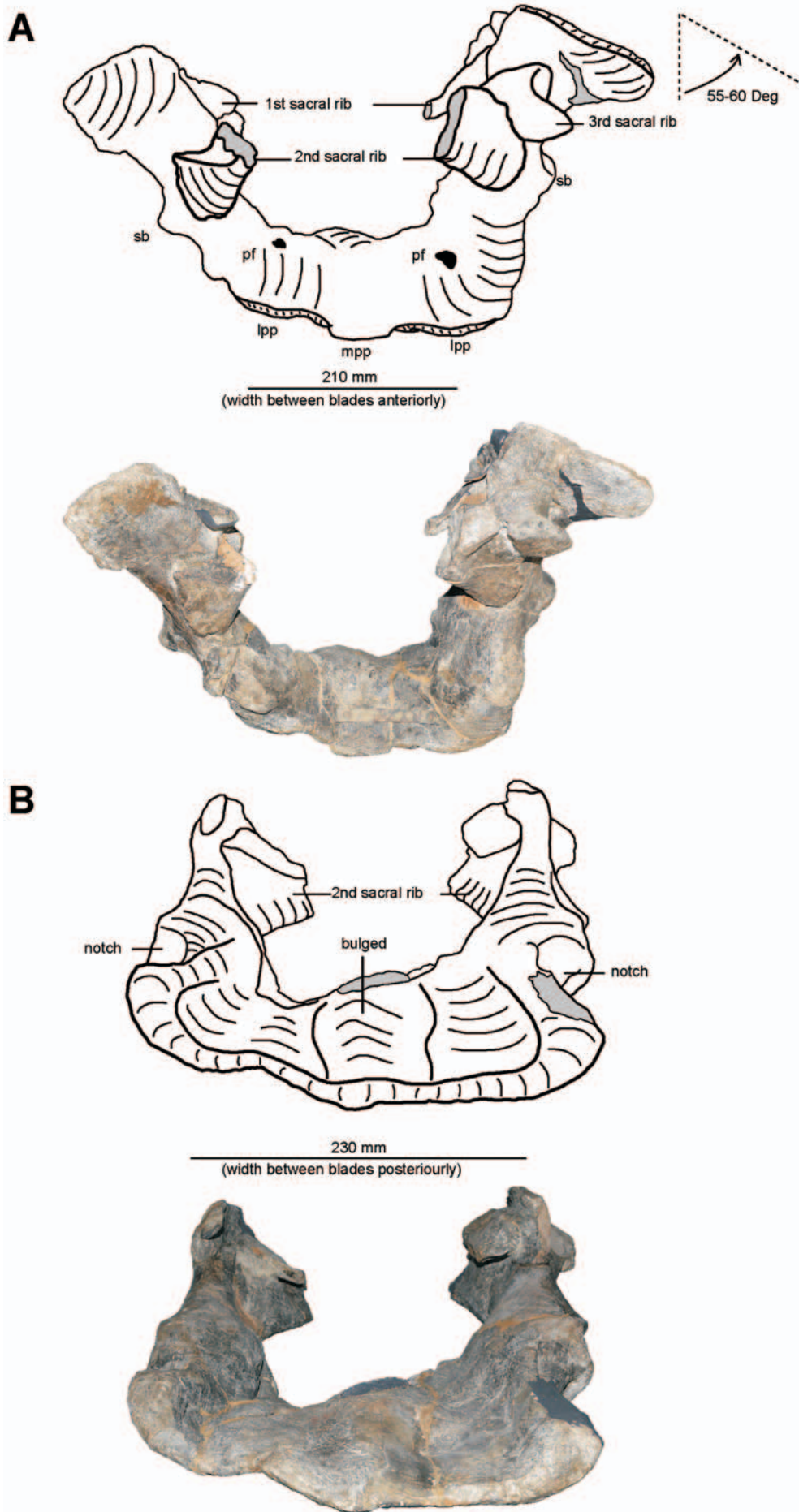


Figure 55. Photographs and interpretive drawings of the pelvis of the holotype of *Bradysaurus baini* (NHMUK PV R 1971), (A), in anterior view, and (B), in posterior view. Dorsal to the top of the page. Scale bars equal: A, 210 mm; B, 230 mm.

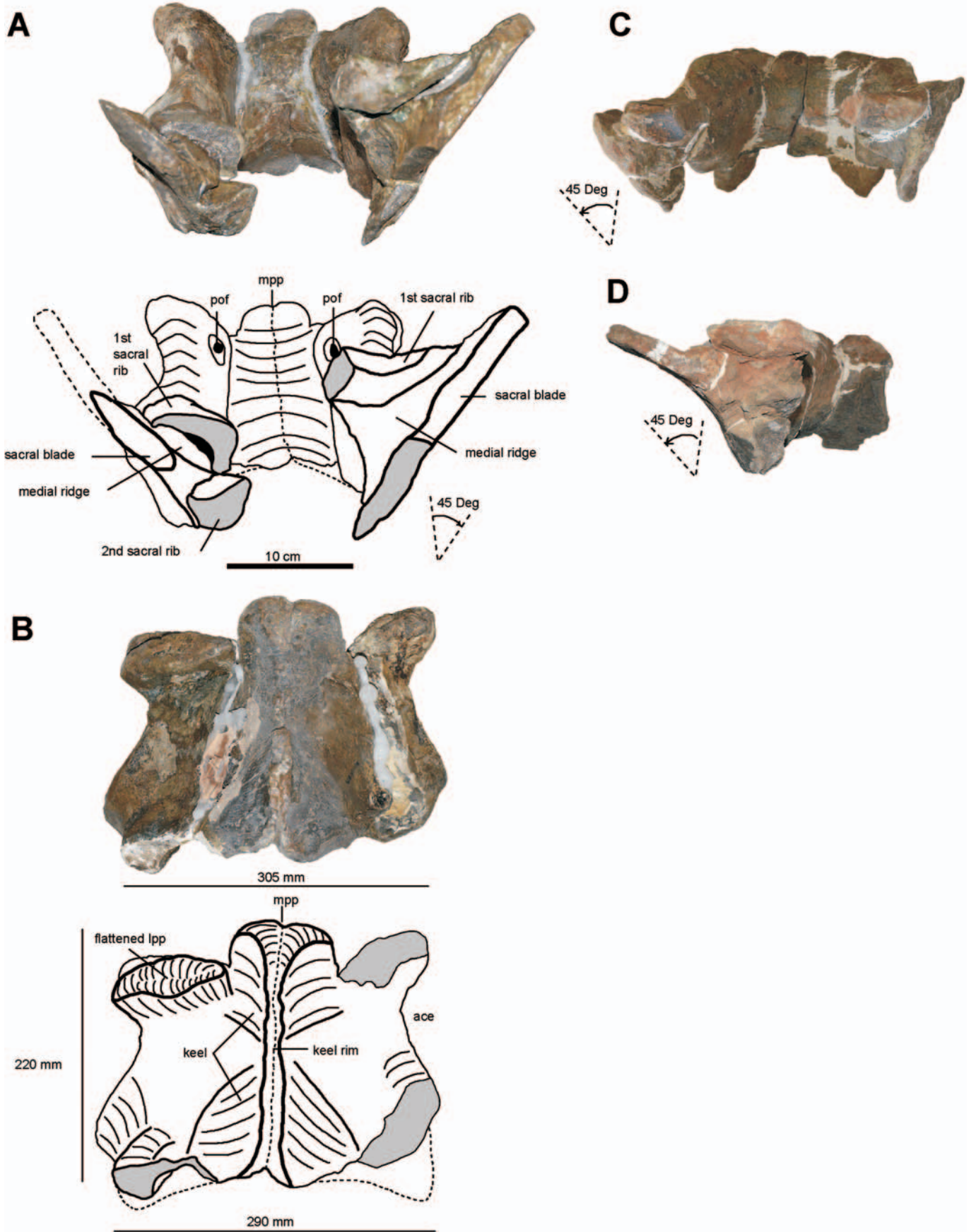


Figure 56. Photographs and interpretive drawings of the pelvis of *Embrithosaurus schwarzi*. The holotype (SAM-PK-8034), (A), in dorsal view, and (B), in ventral view. (C), FMNH UR 2443, in dorsal view, and (D), FMNH UR 2486, in dorsal view. Anterior to the top of the page. Scale bar equals 10 cm.

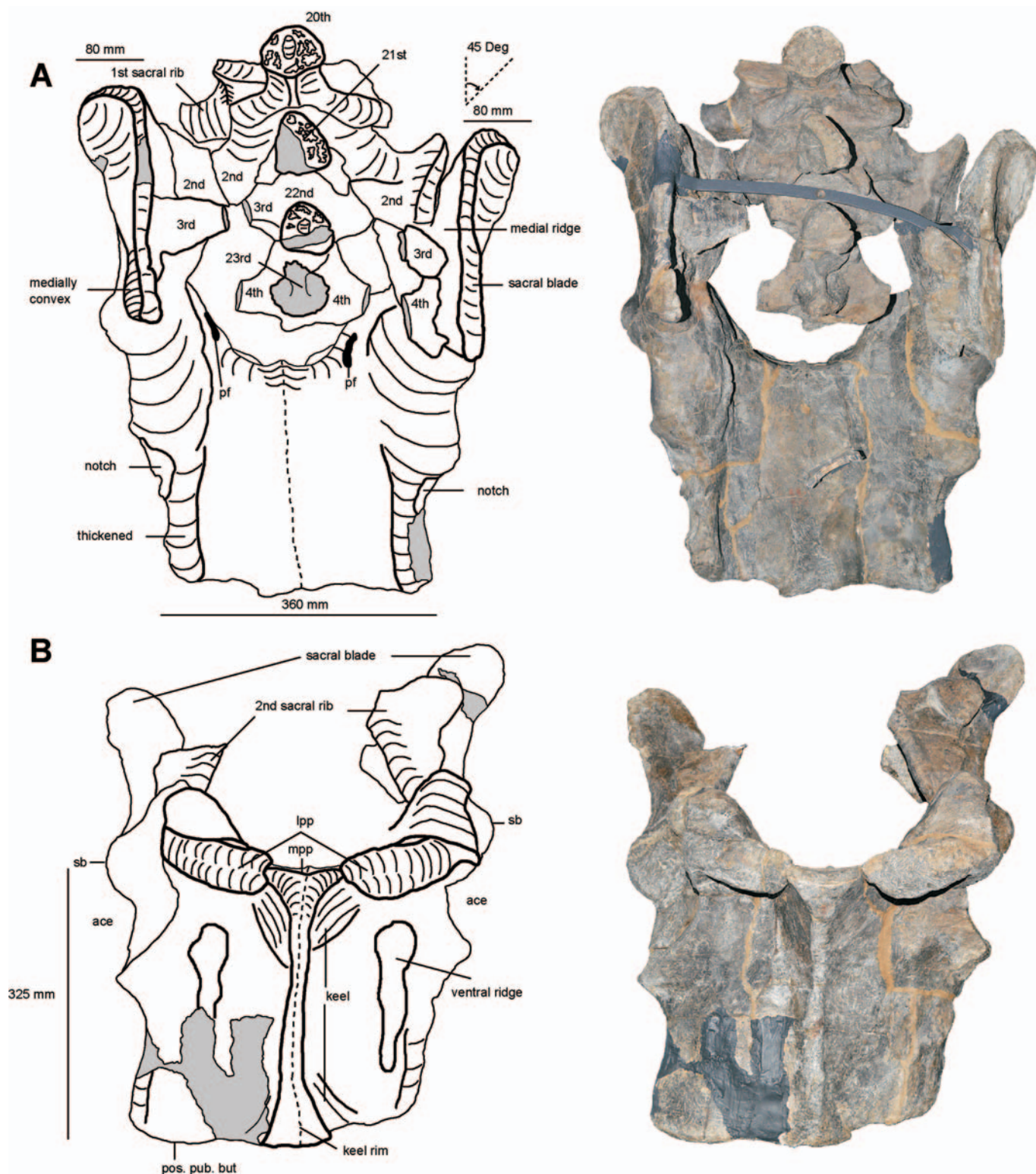


Figure 57. Photographs and interpretive drawings of the pelvis of the holotype of *Bradysaurus baini* (NHMUK PV R 1971), (A), in dorsal view, and (B), in ventral view. Anterior to the top of the page. Scale bars equal: A, 360 mm; B, 325 mm.

Bradysaurus are not level: the posterior half of the plate is horizontal, but the anterior half is oriented anteroventrally 25° below the horizontal plane (Figs 51, 52, 53).

An anteroventrally extending median pubic process (80 mm wide) is present on the anterior margin of the pubis of NHMUK PV R 1971 is about as wide (75 mm wide) as that of *Embrithosaurus*. However, in *Bradysaurus*, the median pubic process is rectangular to square with perpendicular sides, and extends only 10 mm ventrally below the lateral pubic processes, and not anteriorly at all

with the square edges in *Bradysaurus* and is directed anteroventrally compared to ventrally in *Bradysaurus*. It also extends further anteriorly than in *Bradysaurus* and has a notch either side. The median pubic process of the pubis of NHMUK PV R 1971 is about as wide (75 mm wide) as that of *Embrithosaurus*. However, in *Bradysaurus*, the median pubic process is rectangular to square with perpendicular sides, and extends only 10 mm ventrally below the lateral pubic processes, and not anteriorly at all

(Turner *et al.* 2015, character 117). In *Embrithosaurus*, it forms a curved 'tongue' and extends anteroventrally much further (50 mm). Laterally, a wide (120 mm) lateral pubic process is present either side of the median pubic process of SAM-PK-8034 (Turner *et al.* 2015, characters 116, 117). The lateral process is characterized by a rectangular, flattened to slightly convex, ventral surface (Fig. 56) that curve or direct upwards over their entire length. *Bradysaurus baini* has mediolaterally wider lateral pubic processes (140 mm wide) which are horizontally flattened over the entire ventral surface and only curve upwards at the lateral extremes.

Unique to the puboischiatic plate of *Bradysaurus baini*, anteriorly, the dorsal surface of the plate curves sharply downwards, forming an 80 mm high vertical wall that supports each lateral pubic process (Fig. 55A) (Turner *et al.* 2015, character 116). The holotype of *Embrithosaurus* lacks this high vertical wall supporting the lateral pubic process. In all species and specimens, the pubic/obturator foramen is large and distinct on the medial surface of the pubis and occupies the medial portion of a larger surrounding oval slit-like depression.

Ischium

The ischium forms the posterior portion of the puboischiatic plate, which has been fully described (see pubis) and part of the acetabulum (see Ilium). The posterior rim of the ischium is very thin in *Embrithosaurus* (<10 mm thick, Fig. 54) whereas in *Bradysaurus baini* it is thicker (15 mm, Fig. 55) and is much higher, thicker and robust on the lateral sides of the posterior pubic buttress, which form longitudinally thickened bars, measuring 30 mm wide, 40 mm high.

Femur

The right femur of the holotype of *Embrithosaurus* is well preserved, was illustrated by Broom (1903: plate XV, figs 15, 16), and forms the basis of this description (Figs 58, 59, 60). The right femur of the holotype of *Nochelesaurus* is almost completely preserved apart from a long, narrow piece of the postaxial flange and a small piece of the articular facet of the medial condyle (Figs 61, 62, 63). The right femur of the holotype of *Bradysaurus baini* is complete, but severely dorsoventrally crushed compared to the undistorted left femur (Fig. 64). For descriptive purposes we accept the 'obliquely outwardly oriented' life position for the femur, applied to all middle Permian South African pareiasaurs as a result of a 'permanently bent knee' (Haughton & Boonstra 1930: 303).

The femurs of the holotypes of the middle Permian South African pareiasaurs are very similar in length (415 mm *Bradysaurus*, 410 mm *Embrithosaurus*, 420 mm *Nochelesaurus*) and the mediolaterally width of the expanded proximal ends (200 mm *Bradysaurus* and *Nochelesaurus*, 210 mm *Embrithosaurus*). The shafts are similarly narrow (135 mm *Bradysaurus*, 110 mm *Embrithosaurus*, 120 mm *Nochelesaurus*). The femur is antero-posteriorly wider across the robust distal condyles in *Embrithosaurus* (170 mm) and *Bradysaurus* (190 mm), than the narrower condition in *Nochelesaurus* (155 mm).

Torsion of the planes between the proximal and distal articulations is 30° in all species (10° on the crushed right femur of *Bradysaurus*, the result of dorsoventral crushing, 30° in the undistorted left femur).

The head of the femur is large and robust, and the proximal articulation surface is generally convex (but slightly concave in *Nochelesaurus*) and was covered by a cartilage cap in life. In proximal view (Figs 60B, 63B) the borders of the articulation surface are well-defined, raised and rimmed and the head is elongated and dorsoventrally flattened (and very narrow in *Nochelesaurus*).

Medially the femoral head curves strongly as it expands anteriorly (preaxially) away from the shaft, until terminating at a right-angle (Figs 58, 61, 64) (Turner *et al.* 2015, character 120). In middle Permian South African pareiasaurs, the anterior (preaxially) expanded femoral head is directed out of the shaft of the femur at an angle of 40° from the femoral shaft plane (Figs 58, 61, 64). Haughton & Boonstra (1930) consider this relatively low and flat femoral head expansion, only 40° diverging from the shaft plane, to be the primitive tetrapod condition which supports an oblique femur and a sprawling hindlimb posture.

The postaxial (posterior) flange is about 20 mm thick in all middle Permian South African pareiasaurian specimens. On the flange, the major (external) trochanter is dorsoventrally thick (about 35 mm). In *Embrithosaurus*, the major trochanter is the most distinct, forming a knob-like swelling that extends posteriorly the furthest beyond the shaft of the femur (30 mm) postaxially (posteriorly) on the postaxial flange (Turner *et al.* 2015, character 121). The major trochanter of *Nochelesaurus* is very small as it hardly protrudes (less than 5 mm) beyond the postaxial shaft of the femur. This is also the case in *Bradysaurus baini* with a small trochanter, protruding posteriorly only 10 mm (NHMUK PV R 1971, SAM-PK-5002).

The major trochanter is formed between two notches: a notch on the proximal-postaxial corner of the femur separates the trochanter from the proximal articulation surface of the head, and a notch distal to the trochanter. The proximal notch is present in *Embrithosaurus*, deep in *Bradysaurus* and very shallow and almost absent in *Nochelesaurus*. Similarly, the distal notch is deepest in *Embrithosaurus* and *Bradysaurus*, and it absent in *Nochelesaurus*. The tubercle present on the posterodorsal corner of the femur of *Nochelesaurus* (Figs 61A, 62A) immediately dorsal to the major trochanter, is not present in *Bradysaurus baini* and *Embrithosaurus*.

The postaxial (posterior) flange forms a wide, flat plate, which proximally includes the major trochanter. This flange is posteriorly and slightly ventrally directed in all three species. It extends distally from the major trochanter over the entire length of the shaft of the femur and terminates at the large lateral condyle (Turner *et al.* 2015, character 123). The postaxial edge of the flange is slightly convex (*Bradysaurus* and *Embrithosaurus*) or straight (*Nochelesaurus*), in dorsal and ventral view. In *Embrithosaurus* the postaxial edge is not slightly concave contra Lee (1997b: 247), and the preaxial edge of the shaft of the femur is straight. Therefore the shaft of the femur is antero-

posteriorly consistently wide along its entire length and is not constricted in any of the studied species (Turner *et al.* 2015, character 124). Proximally, the flange is 20 mm thick dorsoventrally and thickens distally to 40 mm.

A broad, low, and rugose triangular ridge for muscular attachment dominates the dorsal surface of the proximal portion of the femur. This ridge is lower proximally and higher distally. A low and irregular tubercle is present anterior to this ridge, near its preaxial border (Figs 58, 61, 64). In ventral view, the proximal portion of the femur is deeply concave, forming the intertrochanteric fossa between the major trochanter and the internal trochanter.

It is important to note the morphology of the highly diagnostic internal (minor) trochanter. In *Nochelesaurus* it is simple, straight, or very slightly curved over its entire length (Turner *et al.* 2015, character 125). The internal trochanter is dorsoventrally low, extending only 10 mm beyond the shaft the femur, and the proximal edge of the internal trochanter emerges obliquely from the femur. Distally, the curved anterior process seen in *Bradysaurus* and *Embrithosaurus* (see below) is absent.

In *Bradysaurus* and *Embrithosaurus* the proximal region of the internal trochanter is curved (concave anteriorly and convex posteriorly), moderately or gently curved in *Embrithosaurus* and strongly curved in *Bradysaurus*. Most of the internal trochanter of the holotype of *Embrithosaurus* has been sheared-off and only a long broken edge remains (75 × 22 mm). However, Broom's illustrations (Broom 1903: plate XV, figs 16, 17; here Figs 58C, 59C) and Haughton & Boonstra's illustrations (Haughton & Boonstra 1930: text-fig. 34A; here Figs 58D, 59D) of the undamaged internal trochanter in ventral view show the gently proximal curvature (confirmed in *Embrithosaurus* specimens FMNH UR 2443 and CGP CBT 112). In *Bradysaurus* and *Embrithosaurus* the proximal region of the internal trochanter is high and extends ventrally far beyond the shaft the femur (*Bradysaurus*: NHMUK PV R 1971, 40 mm; SAM-PK-5002, 30 mm; *Embrithosaurus* holotype, 30 mm estimate based on Broom 1903: plate XV, fig. 17; here Fig. 59C), and the proximal edge of the internal trochanter emerges perpendicularly at 90° out of the femur (Broom 1903: plate XV, fig. 17; here Fig. 59C; and Haughton & Boonstra 1930: text-fig. 34C; here Fig. 59D). The severe proximal curvature of the internal trochanter of *Bradysaurus* forms a very wide internal trochanter, different from the narrow and straight internal trochanter of *Nochelesaurus*. In *Embrithosaurus* the proximal internal trochanter is narrow in the holotype, but is thickened, wide and rugose in CGP CBT 112, BP/1/7241, and SAM-PK-9116.

Specific to *Embrithosaurus*, the distal internal trochanter has a prominent anterior (preaxial) process (Holotype, CGP CBT 112, SAM-PK-9116). Broom (1903: plate XV, fig. 17; here Fig. 58C) figured this anterior process on the holotype. The anterior process of *Bradysaurus* is very short compared to *Embrithosaurus* and it is not present in *Nochelesaurus*.

In all three species, a long, thick, and straight adductor ridge extends obliquely distally across the femur. The distal portion of the adductor ridge is very rugose in

Embrithosaurus and smoother and narrower in *Bradysaurus* and *Nochelesaurus*.

In all three species, a large nutritive foramen is present on the dorsal surface of the femur at the distal end of a long groove that shallows proximally. The distal intercondylar sulcus is a deep groove between the lateral condyle and medial condyles and is prevented from extending onto the ventral surface by a distinct ridge passing between the two condyles (Figs 60, 63, 64). On the ventral surface of the femur the large and shallow popliteal fossa is present between this ridge and another ridge at its proximal border. In cross-section, the distal articular facets of the large lateral condyle and the small medial condyle are both double-lobed and flat to slightly convex. In *Nochelesaurus* the lateral condyle of the holotype extends distally much further (70 mm) beyond the distal edge of the medial condyle than in *Embrithosaurus* (holotype 30–40 mm) and *Bradysaurus* (holotype 20–30 mm; SAM-PK-5002, 50 mm left, 40 mm right).

Tibia

Both tibiae of the holotype of *Embrithosaurus* are well preserved (Fig. 65) and the right tibia of the holotype of *Nochelesaurus* (Fig. 66) and SAM-PK-6238 (Fig. 67) are preserved. The right tibia of the holotype of *Bradysaurus baini* is virtually complete (Fig. 68), but the proximal and distal portions have been reattached with plaster at the shaft and it is anteroposteriorly crushed.

In middle Permian South African pareiasaurs, the tibia is short and stocky, anteroposteriorly flattened, and roughly oval in cross-section at the constricted shaft. The proximal and distal ends are greatly expanded, with the proximal end being mediolaterally wider. The lateral and medial sides are concave. In *Embrithosaurus* the middle of the shaft is very constricted (45 mm mediolaterally) and much narrower than *Nochelesaurus* (70–72 mm) and *Bradysaurus* (75 mm). The tibia is not very twisted since the proximal and distal expansions almost on the same plane: in the holotype of *Nochelesaurus* they are 10° apart, but 40° apart in SAM-PK-6238, indicating a wide range of twisting in this taxon; 30° apart in the holotype of *Embrithosaurus* and only 20° on the the holotype of *Bradysaurus baini*. These angles do not appear to be diagnostic.

On the posterior side of the tibia are wide depressions proximally and distally (Figs 65B, 66B, 67B, 68B), which are similar to each other, and the proximal depression is wider and deeper. A diagonal ridge extends between, and separates, these depressions. The tibia is notably rugose on the lateral border of the proximal depression suggesting that a thick cartilaginous covering was present as in *Honania* (Xu *et al.* 2015).

Anteriorly the cnemial crest of all three species is well developed, thickest proximally, and tapers distally. A deep vertical and concave lateral excavation for the reception of the fibula is positioned laterally. The cnemial crest forms a short lateral twist or overhangs the deep vertical excavation (Turner *et al.* 2015, character 126). In the holotype of *Nochelesaurus*, the cnemial crest is anteriorly poorly projected (only 33 mm high) probably due to antero-

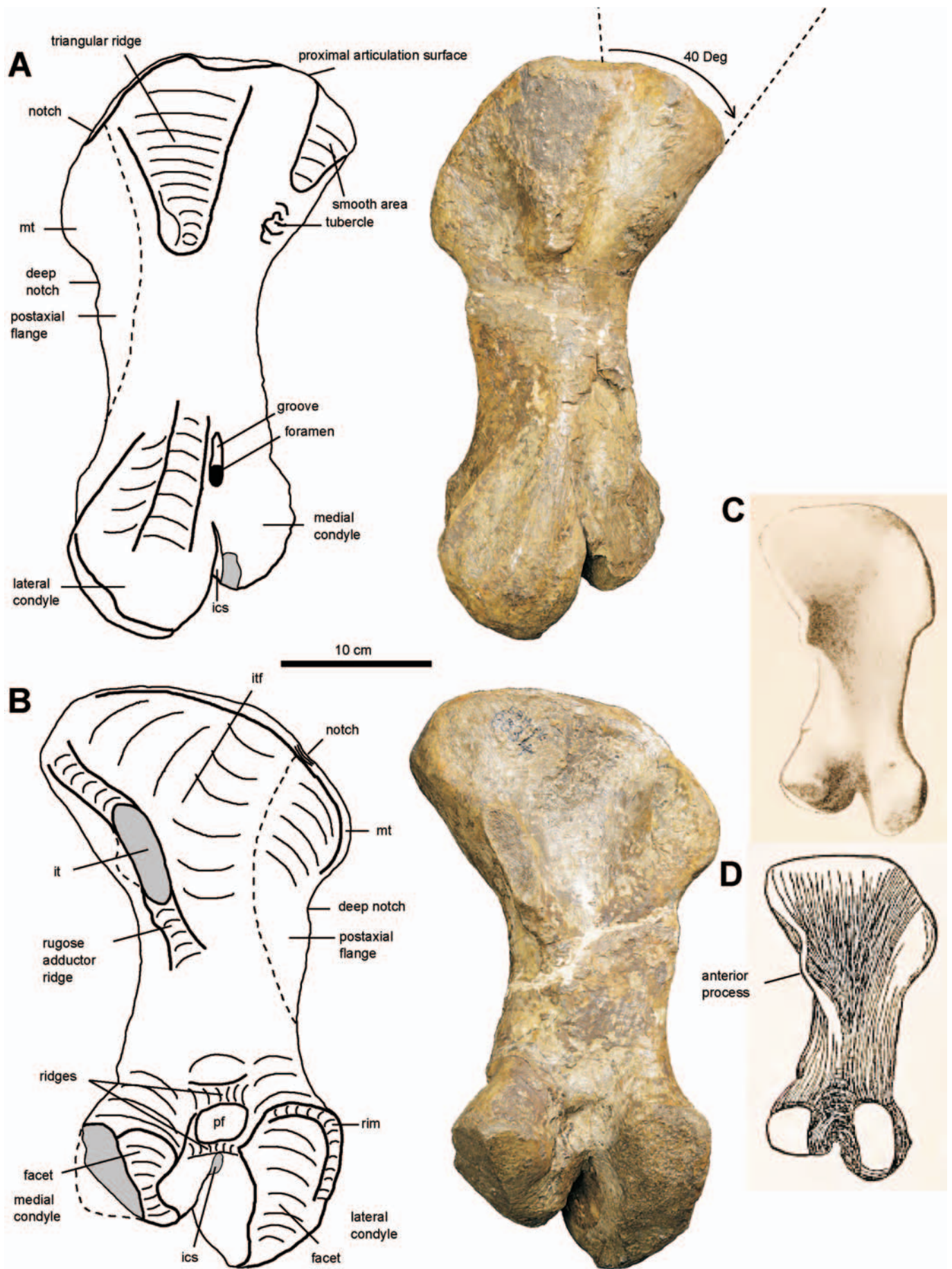


Figure 58. Photographs and interpretive drawings of the right femur of the holotype of *Embriothosaurus schwarzi* (SAM-PK-8034), (A), in dorsal view, (B), in ventral view, (C), in ventral view by Broom (1903), and (D) in ventral view by Haughton & Boonstra (1930). Proximal to the top of the page. Scale bar equals 10 cm.

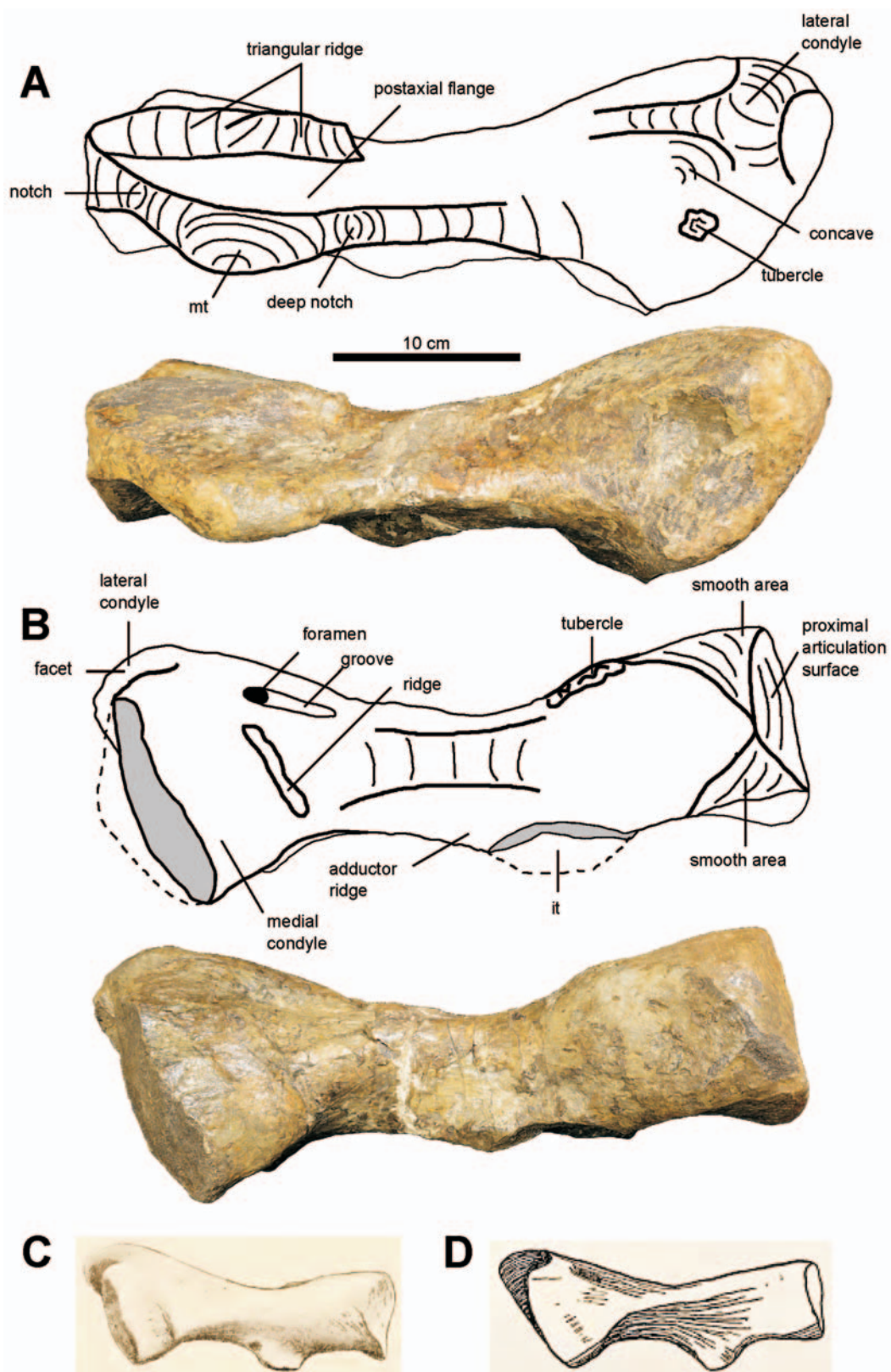


Figure 59. Photographs and interpretive drawings of the right femur of the holotype of *Embrithosaurus schwarzi* (SAM-PK-8034), (A), in posterior view, (B), in anterior view, (C) in anterior view by Broom (1903), and (D) in anterior view by Haughton & Boonstra (1930). Dorsal to the top of the page. Scale bar equals 10 cm.

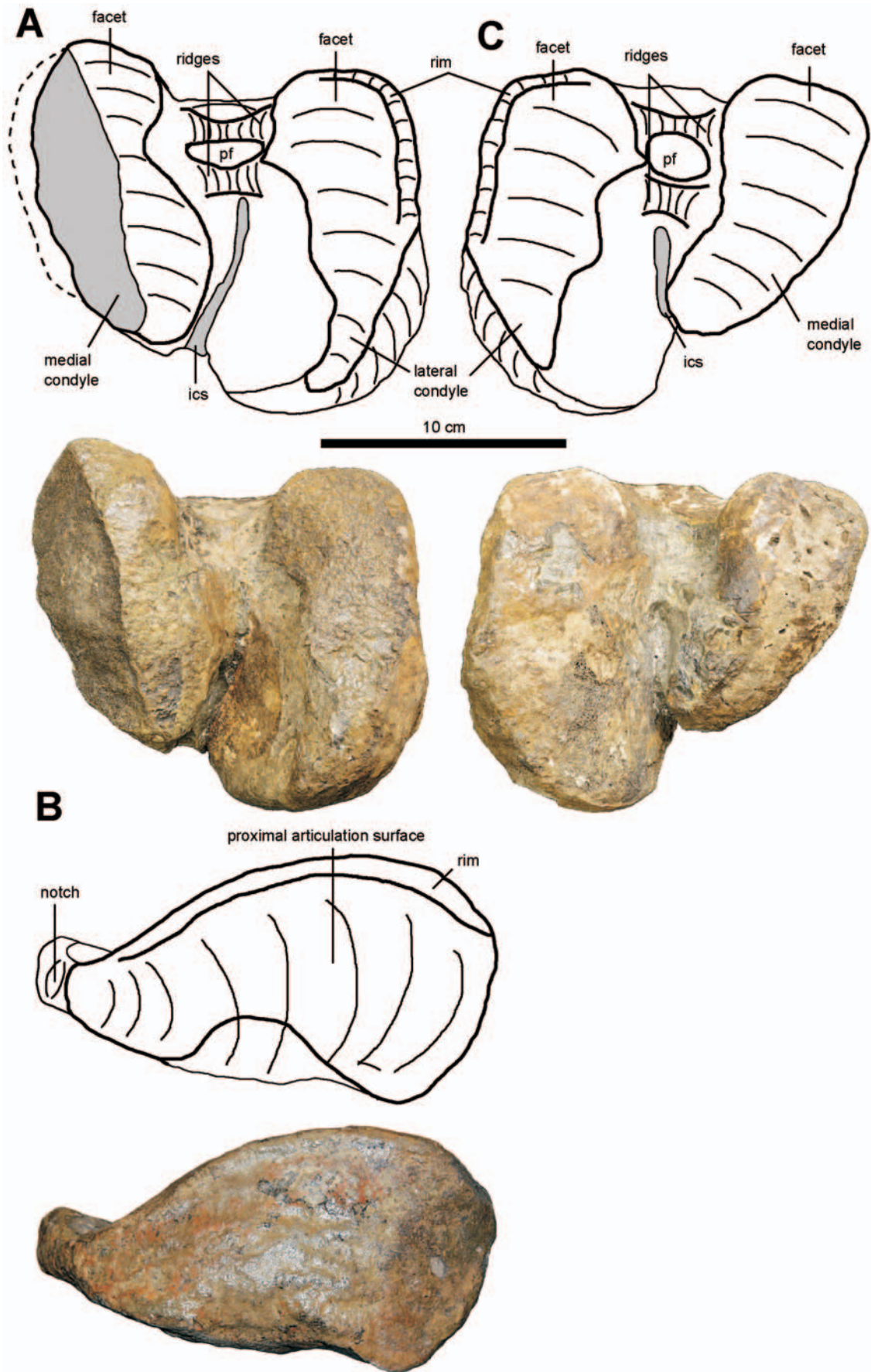


Figure 60. Photographs and interpretive drawings of the holotype of *Embrithosaurus schwarzi* (SAM-PK-8034), (A), right femur in distal view, (B), right femur in proximal view, and (C), left femur in distal view. Ventral to the top of the page. Scale bar equals 10 cm.

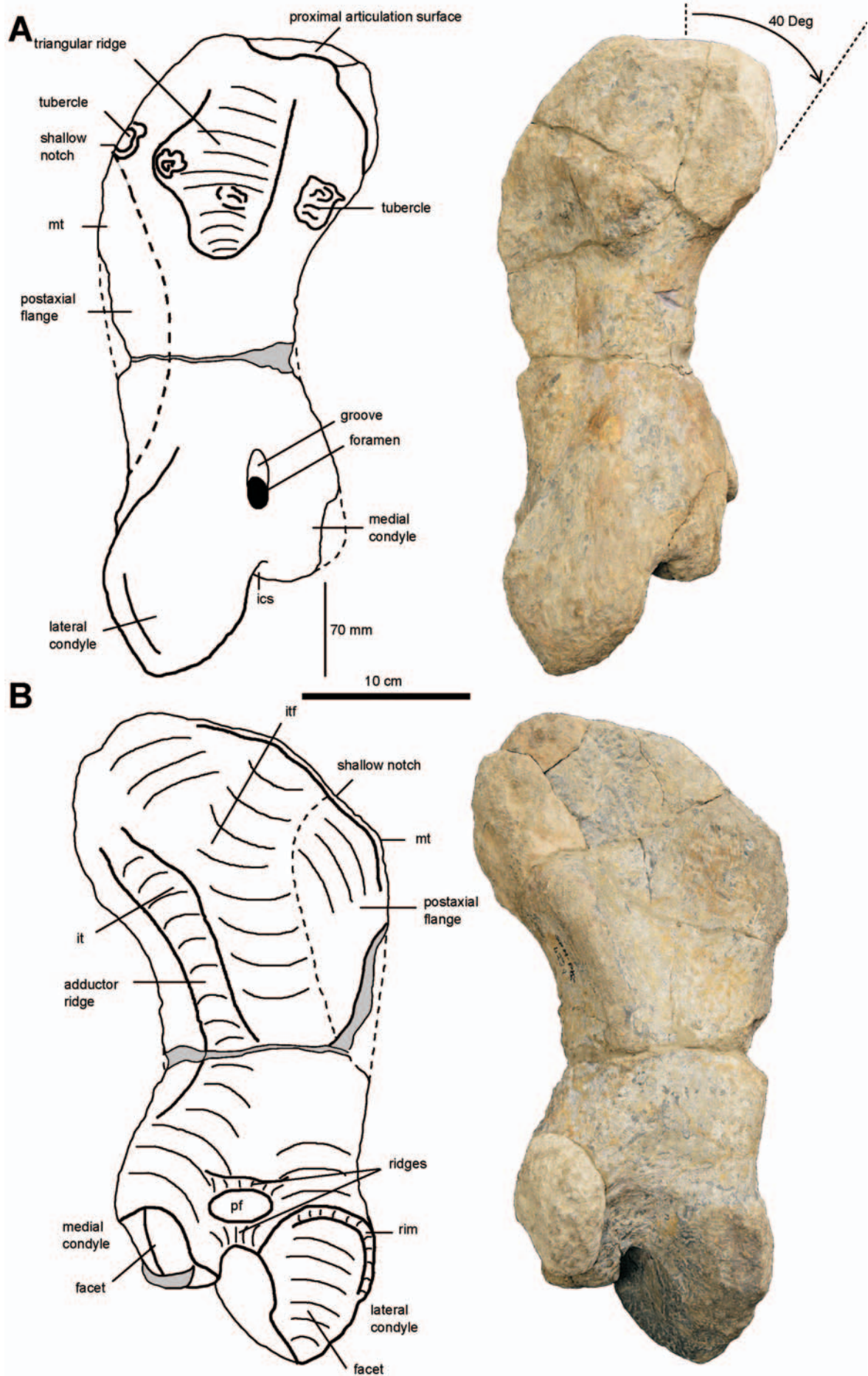


Figure 61. Photographs and interpretive drawings of the right femur of the holotype of *Nochelesaurus alexanderi* (SAM-PK-6239), (A), in dorsal view, and (B), in ventral view. Proximal to the top of the page. Scale bar equals 10 cm.

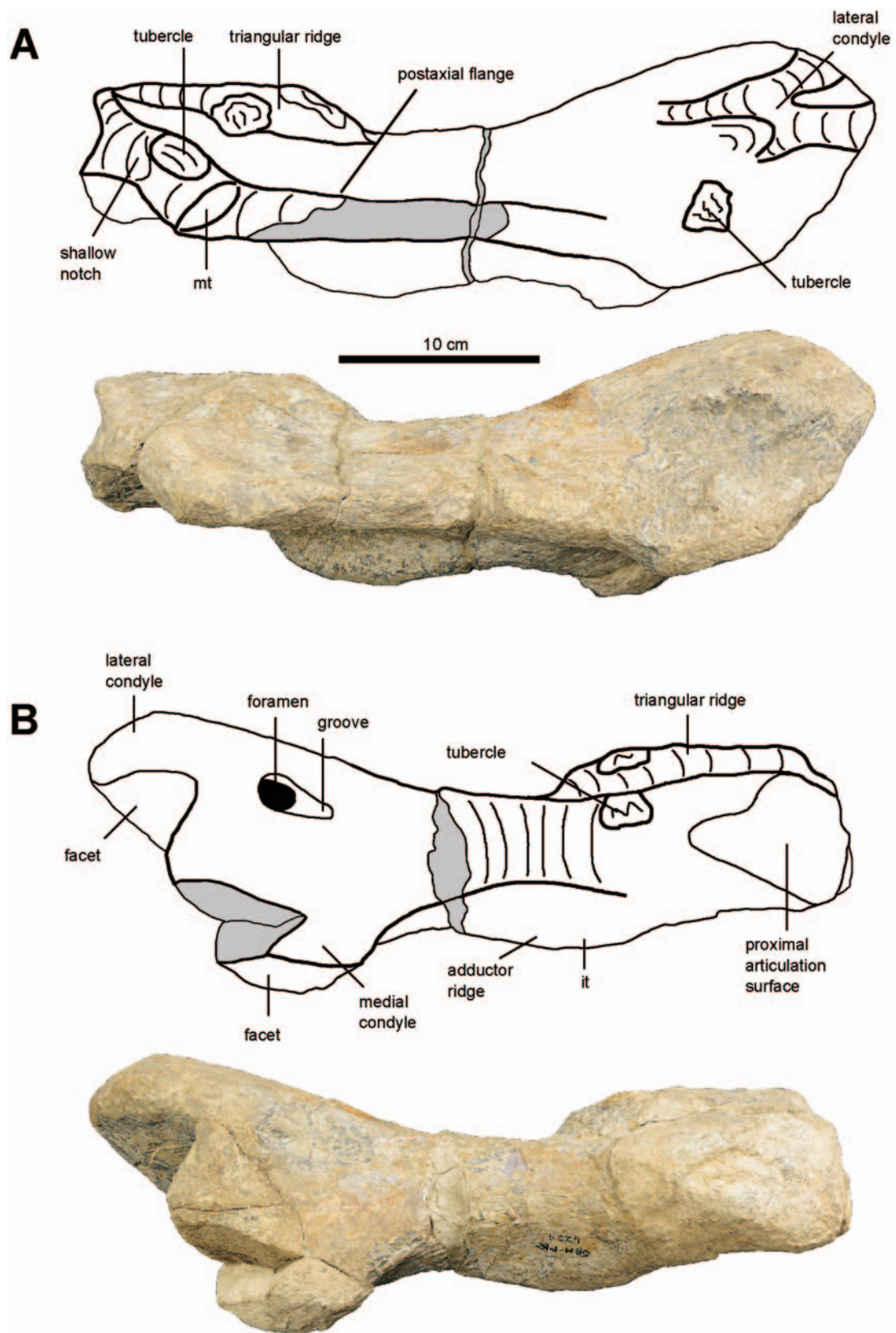


Figure 62. Photographs and interpretive drawings of the right femur of the holotype of *Nochelesaurus alexanderi* (SAM-PK-6239), (A), in posterior view, and (B), in anterior view. Dorsal to the top of the page. Scale bar equals 10 cm.

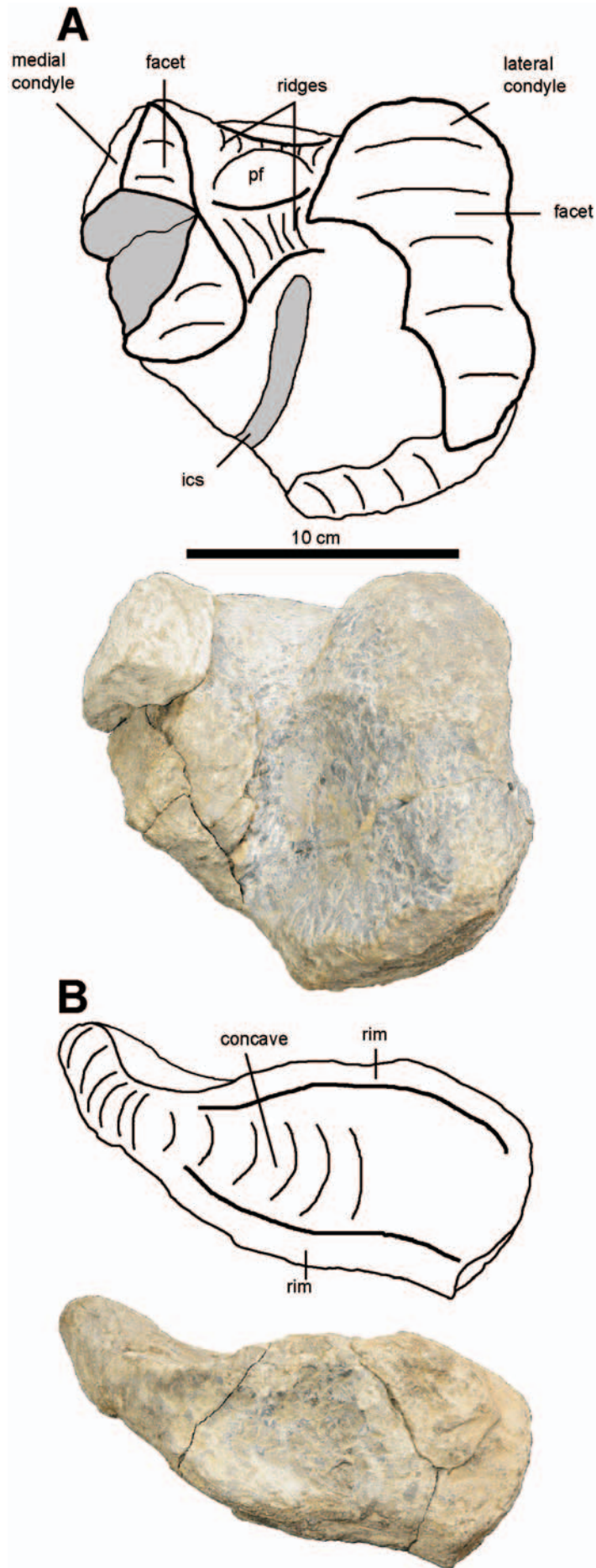


Figure 63. Photographs and interpretive drawings of the right femur of the holotype of *Nochelesaurus alexanderi* (SAM-PK-6239), (A), in distal view, and (B), in proximal view. Ventral to the top of the page. Scale bar equals 10 cm.

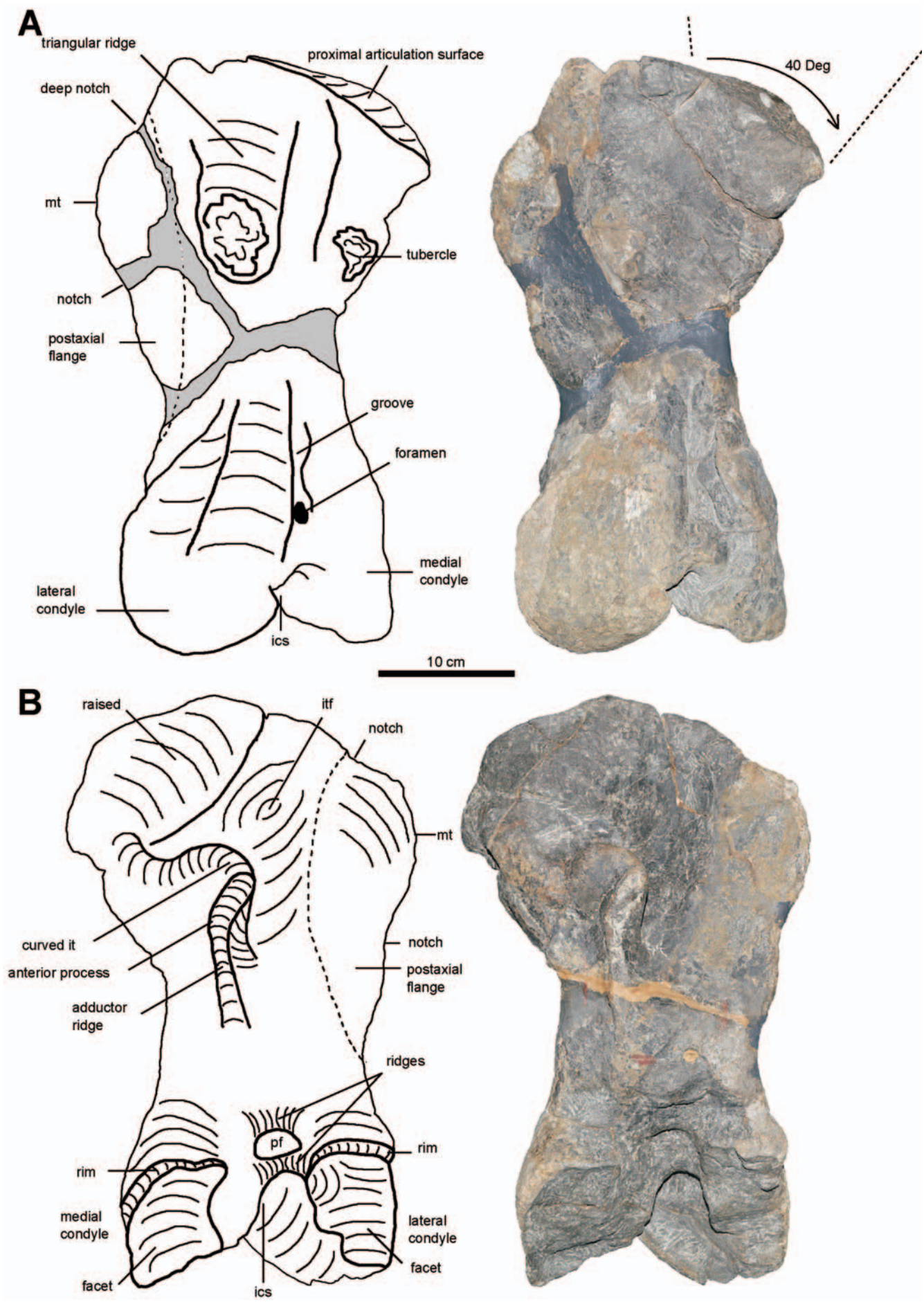


Figure 64. Photographs and interpretive drawings of the right femur of the holotype of *Bradysaurus baini* (NHMUK PV R 1971), (A), in dorsal view, and (B), in ventral view. Proximal to the top of the page. Scale bar equals 10 cm.

posterior compression, since the right tibia of SAM-PK-6238 has a very prominent cnemial crest (48 mm) which is similar to *Embrithosaurus* and *Bradysaurus* (45 mm).

The proximal articulation surface of the tibia is elongated, dominated by the anterior projection of the cnemial crest and the very deep notch for reception of the fibula (Figs 65E, 66E, 67E). This articulation surface comprises two facets that articulate with the lateral and medial condyles of the femur, and are separated by a wide, rugose obliquely curved ridge, which fits in the intercondylar sulcus groove of the femur. The medial facet is large, flat to slightly convex, and faces dorsally and slightly posteriorly, whereas the lateral facet is much smaller and significantly bent to face dorsolaterally. The planes of the lateral and medial facets of the proximal articulation are 40° apart in *Nochelesaurus* (Figs 66A, 67A) and *Bradysaurus* (Fig. 68A), but 60° apart in *Embrithosaurus* (Fig. 65A).

The distal articulation surface is oval, with a curved anterior margin and a straight posterior margin where a small, shallow notch is present (Figs 65E, 66E, 67F). About two-thirds of the surface is covered by a large convex lateral facet that articulates with the main tarsal element. There is also a small and convex medial facet. The distal ends of the tibia of *Nochelesaurus* and *Bradysaurus* are mediolaterally wider than those of *Embrithosaurus*. Their distal tibiae are ventromedially expanded with the ventrolateral side upturned (the dominant lateral facet is at an oblique angle of about 45° above the horizontal plane). This condition is absent in *Embrithosaurus*. On the lateral edge of the middle of the shaft of the tibia of *Nochelesaurus* and *Bradysaurus* is an elongated rugose ridge, dorsal to a vertical depression, whilst *Embrithosaurus* has the depression but lacks the rugose ridge.

Fibula

The right fibula of the holotype of *Embrithosaurus* is complete (Fig. 69), and only the distal half of the left one is present. *Nochelesaurus* SAM-PK-6238 preserves the complete right fibula (Fig. 70). Both fibulae of the holotype of *Bradysaurus* comprise only distal portions.

The slender fibula is slightly longer than the tibia. The shaft is narrow and triangular to cylindrical in cross-section and the ends expanded with the distal portion wider and more robust. The lateral side of the shaft is almost straight and the medial side is severely concave. Medially, the fibula has large, rugose, proximal, and distal tubercles. Laterally, the distal fibula is swollen and distinct with sharp edges. The distal articular surface is roughly diamond-shaped, with most of the surface forming a large flat facet for articulation with the main dorsal tarsal element and the rest is convexly curved. The proximal articular surface forms an elongated strongly convex arc. The planes of the distal and proximal expansions of the bone are offset by 30–45°.

The fibulae of all three genera are very similar, apart from a thin, sharp, elongated ridge or scar for muscle attachment (10 mm wide, 80 mm long) on the anterior side of the shaft of *Nochelesaurus* SAM-PK-6238, which comprises four or five small, rugose knobs. This ridge and the knobs are also present in the very large *Embrithosaurus*

CGP CBT 112, but not in the smaller, late subadult-sized holotype of *Embrithosaurus*, suggesting that the ridge develops late in ontogeny.

Tarsus

In pareiasaurs a single large and distinct tarsal element consists of a fused astragalocalcaneum (astragalus and calcaneum, Tsuji 2013, Turner *et al.* 2015, character 127). The astragalocalcaneum of *Embrithosaurus* is lost, both astragalocalcanea of the holotype of *Bradysaurus baini* are preserved and in good condition (Fig. 71) and the astragalocalcaneum of the *Nochelesaurus* holotype is in poor condition (Fig. 70G,H).

Broom (1903) briefly described and figured (plate XV: figs 23, 24; here Fig. 69G,H) a single large tarsal element in the holotype of *Embrithosaurus* (now lost), with a large foramen near the middle of the front of the bone, which Boonstra (1929b) considered as indicating the fusion of the two components of the tarsus. Boonstra (1929b: plate X) presented a labelled photograph of the tarsus of the holotype of *Embrithosaurus* in articulation with the tibia and fibula. From Broom's (1903, here Fig. 69G,H) and Boonstra's (1929b) figures, it is apparent that the bone is a flattened rectangle, with a flat ventral surface and the dorsal surface dominated by a central ridge extending the length of the bone. On either side of the apex of the ridge are the facets for articulation with the fibula and tibia respectively.

The astragalocalcanea of the holotype of *Bradysaurus baini* are five-sided and roughly rectangular. The ventral surface is flattened, slightly concave and rectangular, and the margins form a raised rim. The centre of the flat ventral surface shows a long narrow groove (65 mm long, 10 mm deep) which widens and shallows towards the centre of the bone and terminates at the opening of a large foramen. The dorsal articulation surface comprises a larger facet for articulation with the distal tibia and a smaller facet for the distal fibula, separated by a curved, 20–25 mm high, oblique, ridge. The large nutritive foramen (5 mm wide) opening is on the tibial facet. The preserved astragalocalcaneum of the holotype of *Nochelesaurus* shares all the features of the astragalocalcaneum of *Bradysaurus baini*.

Pes

Broom (1903: 124) noted that only the second and third toes of the left foot of the holotype of *Embrithosaurus* were preserved and illustrated these two digits in the full body restoration (plate XVI; here Fig. 1). Boonstra (1929b) assigned a phalangeal hind foot formula of 2, 3, 3, 4, 3 for the holotype of *Embrithosaurus* (Turner *et al.* 2015, character 128). Our research shows that the holotype of *Embrithosaurus* preserves two partial digits articulated to the ventral surface of the vertebral block containing the 14th to 16th vertebrae. One of the digits comprises three phalanges and a terminal claw, with a total of four phalanges, so possibly this is the fourth digit of one of the feet (Fig. 14). They are typical pareiasaurian pedals: robust, short, and wide and both digits end with thick, short recurved claws.



Figure 65. Photographs and interpretive drawings of the right tibia of the holotype of *Embriithosaurus schwarzii* (SAM-PK-8034), (A), in anterior view, (B), in posterior view, (C), in lateral view, (D), in medial view, (E), in dorsal view, and (F), in ventral view. Proximal to the top of the page in (A), (B), (C) and (D). Anterior to the top of the page in (E) and (F). Scale bar equals 5 cm.

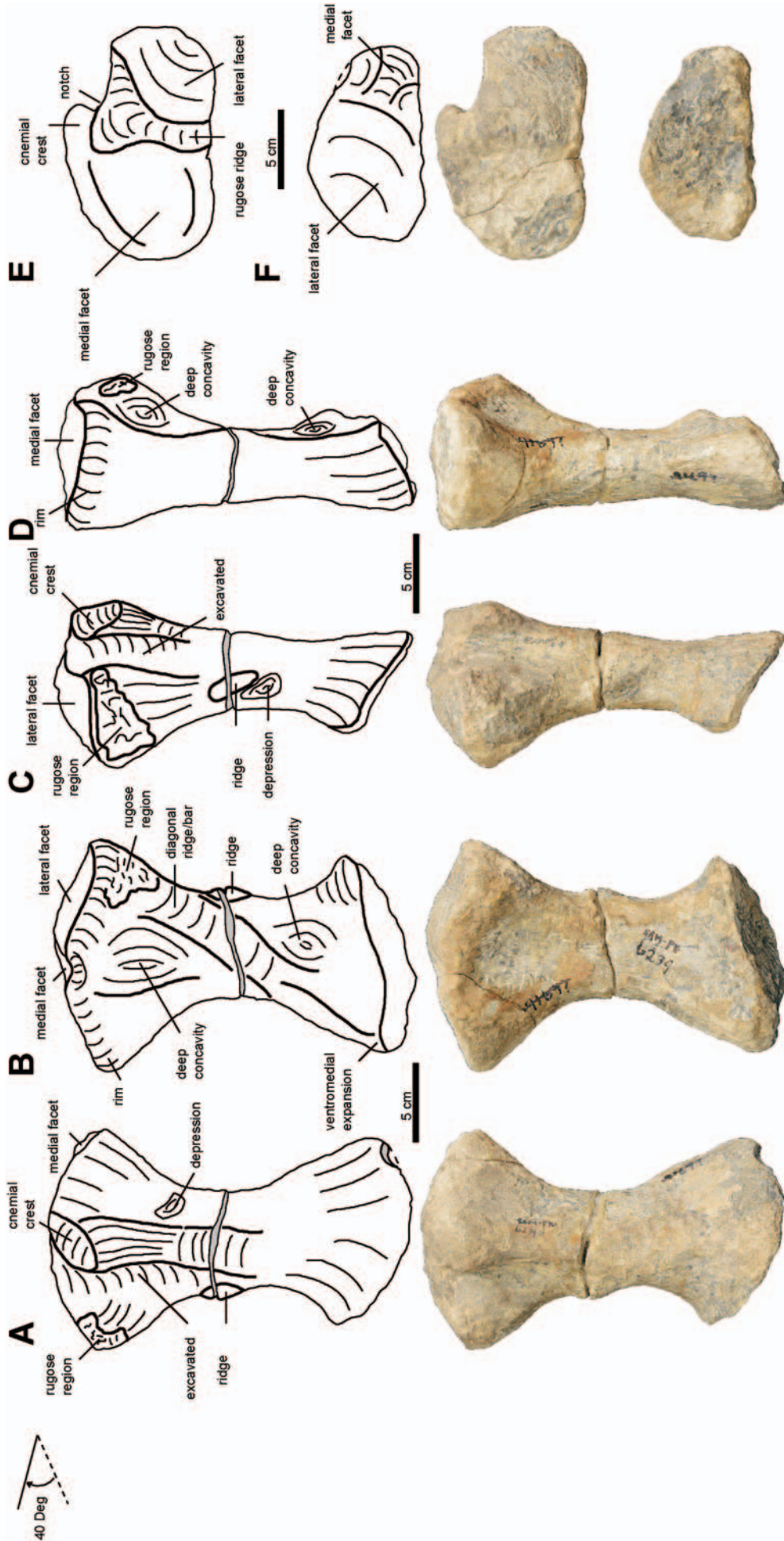


Figure 66. Photographs and interpretive drawings of the right tibia of the holotype of *Nochelesaurus alexanderi* (SAM-PK-6239) (A), in anterior view, (B), in posterior view, (C), in lateral view, (D), in medial view, (E), in dorsal view, and (F), in ventral view. Proximal to the top of the page in (A), (B), (C) and (D). Anterior to the top of the page in (E) and (F). Scale bar equals 5 cm.



Figure 67. Photographs and interpretive drawings of the right tibia of SAM-PK-6238 (*Nochelesaurus alexanderi*), (A), in anterior view, (B), in posterior view, (C), in lateral view, (D), in medial view, (E), in dorsal view, and (F), in ventral view. Proximal to the top of the page in (A), (B), (C) and (D). Anterior to the top of the page in (E) and (F). Scale bar equals 5 cm.

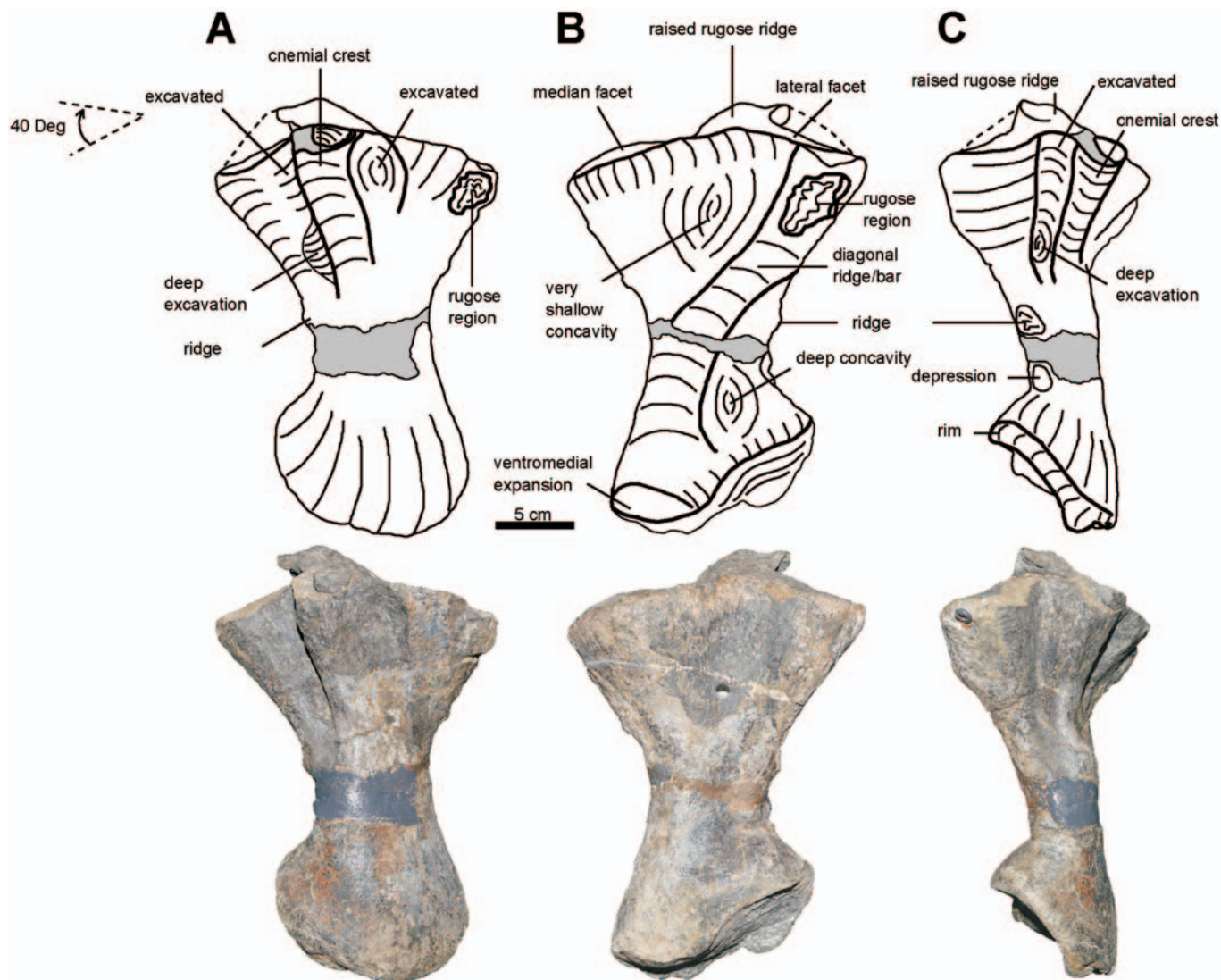


Figure 68. Photographs and interpretive drawings of the right tibia of the holotype of *Bradysaurus baini* (NHMUK PV R 1971), (A), in anterior view, (B), in posterior view, and (C), in lateral view. Proximal to the top of the page. Scale bar equals 5 cm.

The holotype of *Bradysaurus baini* preserves the right pes, arranged by Seeley (1892) from disarticulated elements, in which he assigned five digits, with short, broad flattened metatarsals and phalanges, and three phalanges per digit, including the terminal claws. Seeley noted the foot as broad and short (Turner *et al.* 2015, character 130). The preserved phalanges are nearly twice as wide as long (Turner *et al.* 2015, character 131).

Osteoderms

In the middle Permian South African pareiasaurs, the osteoderms are relatively few and cover only the dorsal part of the body above the vertebral column (Watson 1914; Boonstra 1934b; Lee 1994, 1997a).

In *Embrithosaurus*, 23 mostly complete osteoderms overlie the dorsal and lateral surfaces of several neural spines and the dorsal surfaces of several processes of the post-zygapophyses along the vertebral column (6th to 19th vertebrae). Small scute fragments are present on the 24th to 27th vertebrae. The greatest concentration of nine articulated scutes is on the block containing vertebrae 6–8 (Fig. 72, eight scutes drawn) and these were described by Boonstra (1934b). The holotype of *Nochelesaurus* preserves

a plate of bone comprising seven large roughly pentagonal osteoderms (45–55 mm wide, Fig. 73). In the holotype of *Bradysaurus baini*, osteoderms are preserved on the dorsal side of vertebrae 5–19 (Fig. 74). Seeley (1892) noted that a few osteoderms were found just behind the neck of the specimen during excavations but were not retained. Juvenile *Bradysaurus baini* CGP/1/2269 and the large CGP/1/2268 both preserve the osteoderms of the neck shield.

Boonstra (1934b), in his detailed study of South African pareiasaurian armour, provided a detailed description of the armour of *Embrithosaurus*. In terms of scute arrangement, he noted a central row of the largest scutes directly above the spinous processes, and two lateral rows of large, but slightly smaller scutes on either side resulting in five rows, extending probably along the whole length of the back (Fig. 72). Vertebrae 6–8 of *Bradysaurus baini* also has a central row of the largest scutes on the dorsal surfaces of the midline neural spines, and laterally two irregular rows of large osteoderms on the dorsal surface of the post-zygapophysis, showing an arrangement of five rows of scutes (Fig. 74A). The five longitudinal rows of osteoderms of *Bradysaurus* and *Embrithosaurus* (and probably *Nochelesaurus*) contrast strongly with the much more

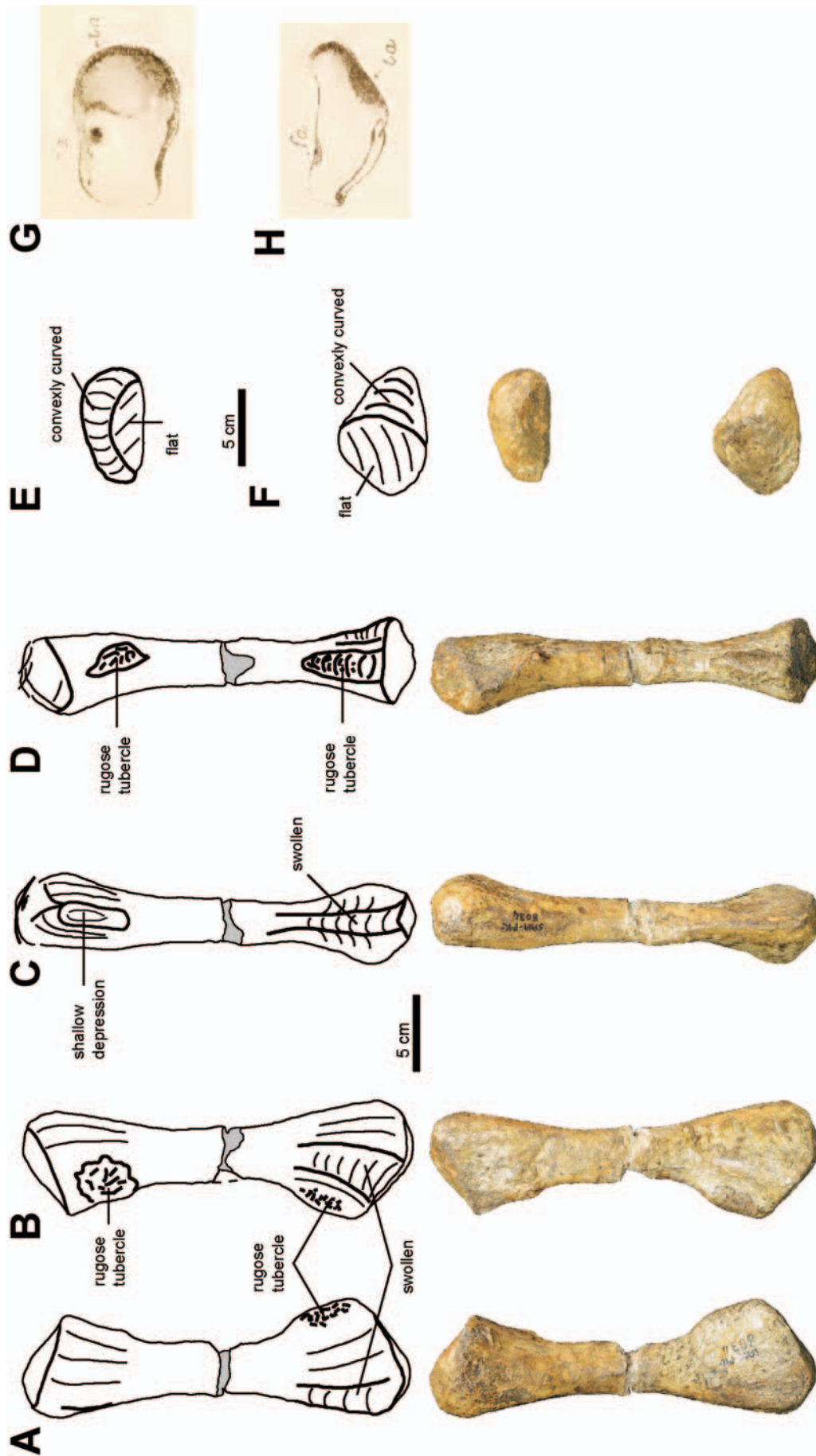


Figure 69. Photographs and interpretive drawings of the right fibula of the holotype of *Embrithosaurus schwarzii* (SAM-PK-8034), (A), in anterior view, (B), in posterior view, (C), in lateral view, (D), in medial view, (E), in dorsal view, and (F), in ventral view. Proximal to the top of the page in (A), (B), (C) and (D). Anterior to the top of the page in (E) and (F). Interpretive drawings of the astragalocalcaneum of the holotype of *Embrithosaurus schwarzii* (SAM-PK-8034) by Broom (1903), (G), in anterior view, f.a articulation for fibula, t.a articulation for tibia. Anterior to the top of the page in (G). This astragalocalcaneum is now missing. Scale bar equals 5 cm.

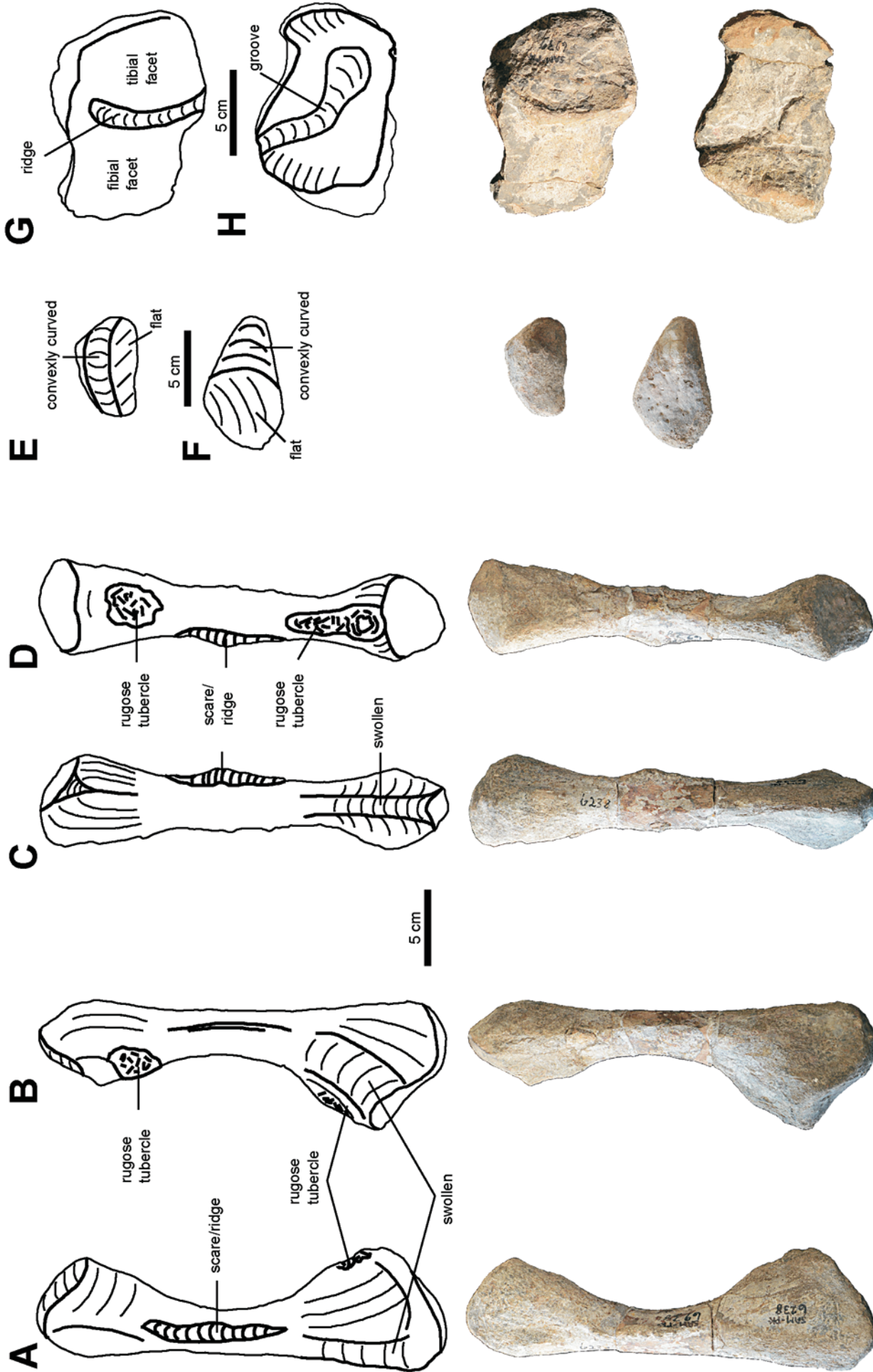


Figure 70. Photographs and interpretive drawings of the right fibula of SAM-PK-6238 (*Nochthesaurus alexanderi*). (A), in anterior view, (B), in posterior view, (C), in lateral view, (D), in medial view, (E), in dorsal view, and (F), in ventral view. Proximal to the top of the page in (A), (B), (C) and (D). Anterior to the top of the page in (E) and (F). Photographs and interpretive drawings of the proximal astragalocalcaneum of the holotype of *Nochthesaurus alexanderi* (SAM-PK-6239), (G), in dorsal view, and (H), in ventral view. Anterior to the bottom of the page in (G) and (H). Scale bar equals 5 cm.

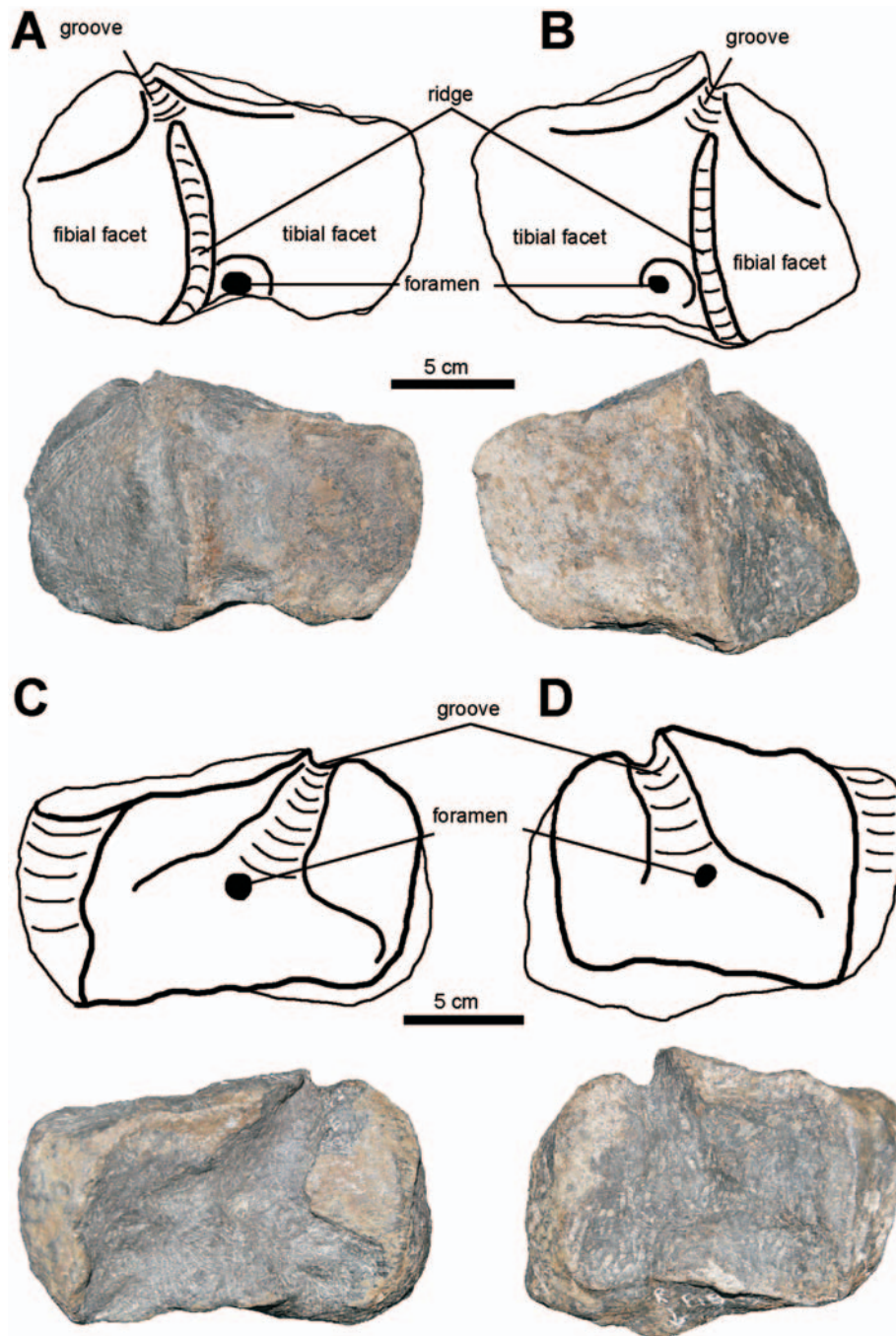


Figure 71. Photographs and interpretive drawings of both (left and right) astragalocalcanea of the holotype of *Bradysaurus baini* (NHMUK PVR 1971), (A) and (B), in dorsal views, and (C) and (D), in ventral views. Posterior to the top of the page. Scale bar equals 5 cm.

extensive coverage of the more derived South African pareiasaurs, such as *Pareiasaurus serridens* (e.g. SAM-PK-K10036).

The holotype of *Bradysaurus baini* preserves three osteoderm morphotypes: large anterior dorsal osteoderms (vertebrae 3–11), medium-sized posterior dorsal osteoderms (vertebrae 13–19) and small stud-like osteoderms. In NHMUK PVR 1971, at least seven anterior dorsal scutes are attached to vertebrae 3–8 in the neck shield region, but they are not well prepared and their dorsal surfaces are partially obscured by a thin layer of matrix (Fig. 74A). These are large, round to roughly five-sided pentagons (45 mm long, 55 mm wide), low (18–20 mm high) with a strong, evenly and smoothly convex dorsal curvature. They have a slightly raised or thickened central region

creating an incipient central boss, 25–30 mm wide, covering most of the osteoderm. Light ornamentation consists of very fine and narrow (1 mm wide), very short (2–4 mm long), straight to slightly curved radial ridges with shallow, narrow depressions between. These occur both on the incipient central boss and on the periphery, although mostly on the periphery. A few, very small, circular pits are present on a minority of scutes. Late subadult *Bradysaurus baini* specimen SAM-PK-5002 preserves four large anterior dorsal osteoderms, consistent with all these features. The 11th vertebra of the holotype has two smaller osteoderms (30 mm wide) on the postzygopophysis, with the same ornamentation style and features (Fig. 74A).

The osteoderms on vertebrae 13–19 are small, flat, thin,

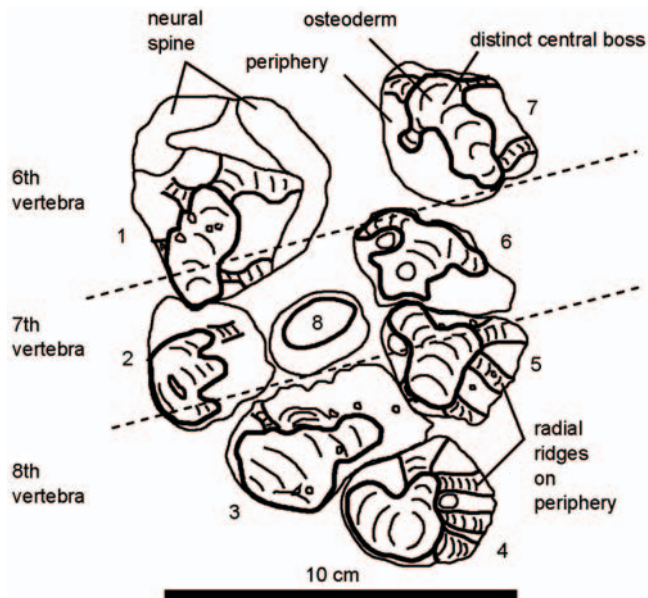


Figure 72. Photograph and interpretive drawing of the osteoderms on the 6th–8th vertebrae of the holotype of *Embrithosaurus schwarzi* (SAM-PK-8034), in dorsal view. Anterior to the top of the page. Scale bar equals 10 cm.

and disc-like (25–30 mm wide). They are gently convex and lack a central boss. Most of these osteoderms have a small, shallow, central circular hollow (6–8 mm wide). They have a very light ornamentation style as seen on the anterior dorsal osteoderms: very narrow (1 mm wide), short (2–4 mm long), straight radial ridges, with very narrow and shallow depressions between, and on a few scutes very small, shallow and circular pits. These osteoderms have the same ornamentation style as the dorsal surfaces of the neural spines making it sometimes challenging to separate osteoderms from the dorsal neural spines. A small, high, evenly smoothly convex, stud-like osteoderm is displaced and positioned lateral to the 4th vertebrae.

The holotype of *Embrithosaurus* also has three osteoderm morphotypes: large anterior dorsal osteoderms, medium-sized posterior dorsal osteoderms, and small stud-like osteoderms. On vertebrae 6–8 (Fig. 72) are seven large disc-shaped osteoderms (40–50 mm in diameter, roughly pentagonal, with straight to concave edges). These osteoderms which are 15–20 mm in total height, have very

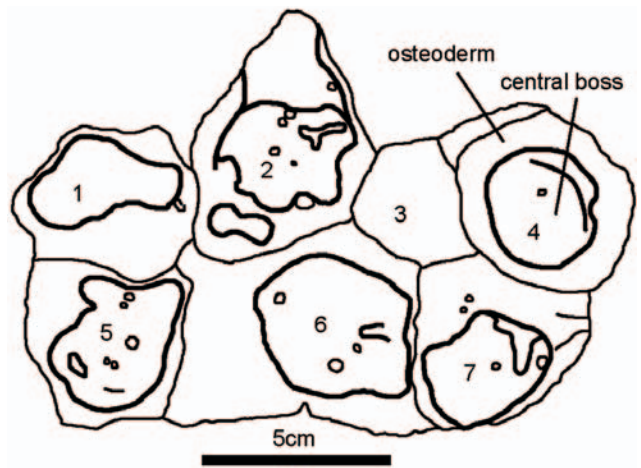


Figure 73. Photograph and interpretive drawing of the osteoderms of the holotype of *Nochelesaurus alexanderi* (SAM-PK-6239), in dorsal view. Scale bar equals 5 cm.

flat and thin disc-like peripheries (5–7 mm high) and a distinct central boss (15 mm high, 20–35 mm wide) that accounts for most of the height of the osteoderm. This central boss is irregular (L-shaped or E-shaped) comprising thickened rugose tab-like swellings or ridges. Lateral to the raised irregular central boss, the flat and thin peripheries are covered with low, straight, radiating ridges which extend toward the edges from each central boss. These very thin, flat disc-shaped osteoderms are interrupted by the distinct, irregularly raised central bosses and contrast with the smoothly or evenly convex osteoderms of *Bradysaurus baini*. In a minority of these osteoderms, the periphery is thicker, more evenly convex, and not very disc-like, but they still have a distinct raised central boss.

Posterior dorsal osteoderms are preserved near the neural spines of vertebrae 5 (Fig. 7), 10 (Fig. 10), 12 (Fig. 13), and 15 and 16 (Fig. 14) and show the same features, but are slightly smaller, only 30–40 mm wide. One smaller stud-like osteoderm (30 × 23 mm) on the neural spine of vertebra 7 (Fig. 72, boss no. 8) is very different. It is oval, high and evenly convex, and ‘stud-shaped’ as it is smoothly curved or rounded without a somewhat pointed distal tip and has no central boss. Boonstra (1934b) considered his unusual isolated, smaller scute to have been displaced from the flanks of the animal, but this is probably incorrect as, unlike late Permian pareiasaurs, these middle Permian South African forms do not have

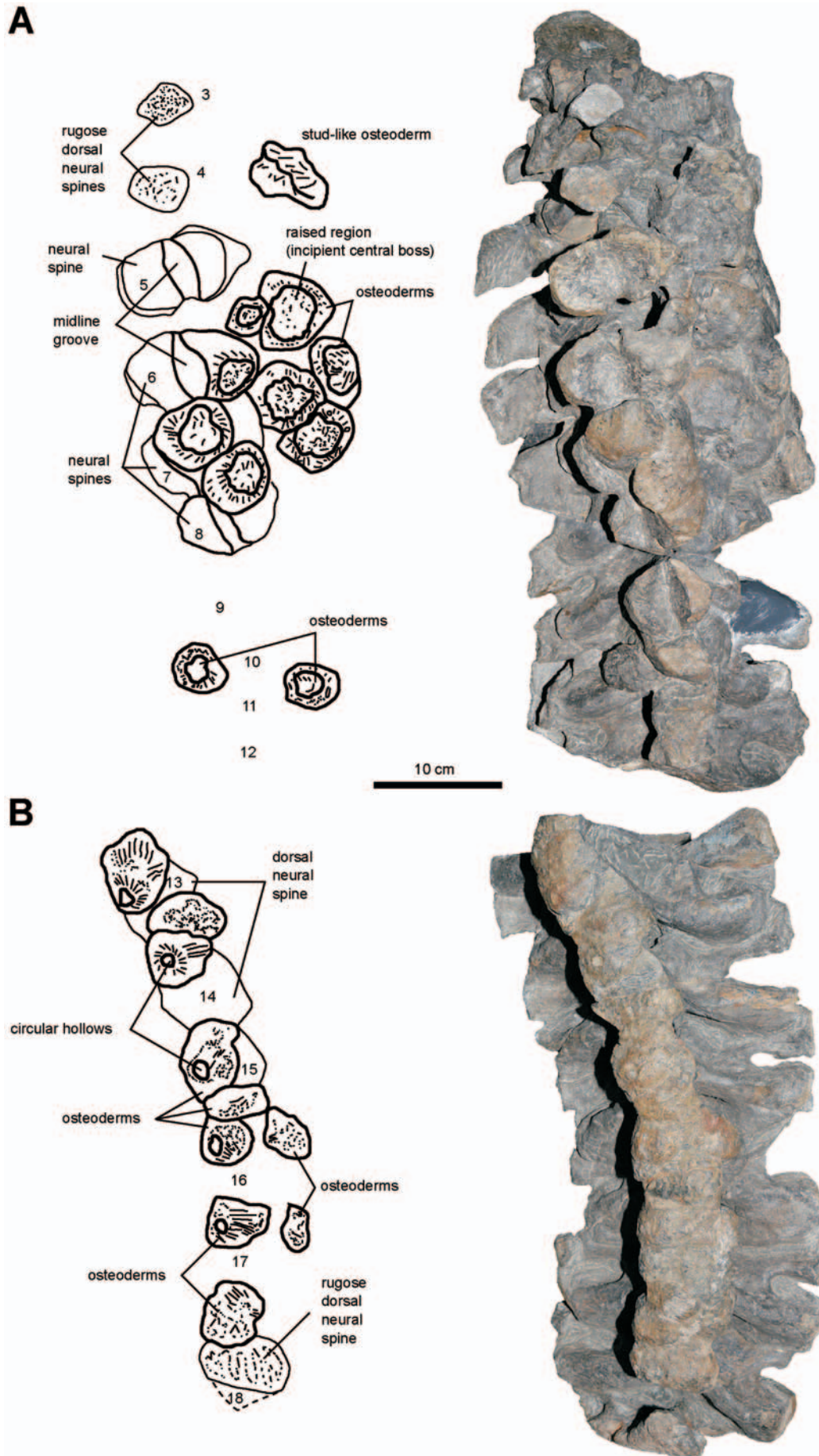


Figure 74. Photographs and interpretive drawings of the osteoderms of the holotype of *Bradysaurus baini* (NHMUK PV R 1971), (A) osteoderms preserved on the 3rd to 12th dorsal vertebrae in dorsal view, and (B), osteoderms preserved on the 13th to 19th dorsal vertebrae in dorsal view. Anterior to the top of the page. Scale bar equals 10 cm.

evidence of scutes on their ribs or sides of their bodies or limbs.

The scutes of the holotype of *Nochelesaurus* are high (30–40 mm) and strongly convex (Fig. 73). Unlike the flat, disc-like peripheries of *Embrithosaurus* osteoderms, the periphery of each scute of *Nochelesaurus* is high and thick (15–20 mm) accounting for roughly half the height of each osteoderm. Each scute has a distinct central boss, which is high (15–20 mm above the periphery) and very wide (25–40 mm) accounting for most of the width of the osteoderm. In *Embrithosaurus*, the central bosses are not as wide as in *Nochelesaurus*. In *Nochelesaurus*, some bosses are round (almost perfectly circular boss nos 4 and 7, Fig. 73) whilst others are irregularly shaped, comprising tab-like rugosities (boss nos 1, 2, 5, 6, Fig. 73). There are small, circular pits on the central bosses and some pitting, but smaller and less, on the peripheries which are smoother and which also lack the regular radial ridges of *Embrithosaurus*.

DISCUSSION

Late subadult nature of the holotype of *Embrithosaurus schwarzi*

The holotypes of *Bradysaurus baini* (NHMUK PV R 1971) and *Nochelesaurus alexanderi* (SAM-PK-6239) are large, adult specimens. The holotype of *Embrithosaurus schwarzi* (SAM-PK-8034) is slightly smaller and more gracile, and so appears to be a late subadult individual, as such the skull of *Embrithosaurus schwarzi* is shorter and smaller than those of *Bradysaurus baini* and *Nochelesaurus alexanderi*. Also, the angular boss of the *Embrithosaurus* holotype is relatively small suggesting that the skull belongs to an immature individual. This is supported by studies of Tsuji (2010) who showed that the angular boss in *Deltavjatia* undergoes a massive change during ontogeny, becoming much larger with increasing age. Postcranial late subadult features recognized in the holotype of *Embrithosaurus schwarzi* are: 1) the lack of an olecranon process on the ulna; 2) the absence of the prominent vertical scar for muscle attachment on the anterior side of the fibula; and 3) the unfused nature of the last two sacral vertebrae. Moreover, all of the postcranial elements of the holotype of *Embrithosaurus* are slightly shorter, smaller and more gracile than those of the larger holotype specimens of *Bradysaurus baini* and *Nochelesaurus alexanderi* (e.g. length of the femur: *Embrithosaurus*, 410 mm right, *Bradysaurus*, 415 mm right, *Nochelesaurus*, 420 mm right; radius: *Embrithosaurus*, 231 mm right, *Bradysaurus*, 245 mm right, *Nochelesaurus*, 250 mm right; and tibia: *Embrithosaurus*, 250 mm right, *Bradysaurus*, 275 mm right, *Nochelesaurus*, 250 mm right). We interpret the holotype of *Embrithosaurus* as close to fully grown, and term it a late subadult, since the shorter length measurements are within 5% of the large adult holotypes of *Bradysaurus baini* and *Nochelesaurus alexanderi*, and interpret the holotype specimen of *Embrithosaurus schwarzi* as mature enough to be a considered valid. This is also supported by some of the referred specimens of *Embrithosaurus* (e.g. CGP CBT 112) being appreciably larger than the holotype.

Sacral vertebrae and ribs

Historically, there has been much disagreement regarding the basic features of pareiasaurian sacral vertebrae and ribs. Seeley (1892) noted four sacral vertebrae in *Bradysaurus baini*, considering the first two ribs as massive and that all four sacral vertebrae have ribs that contact the ilium. Broom (1903) considered only two sacral vertebrae in *Embrithosaurus schwarzi* as he applied the strict definition that true sacrals must have both: 1) fused, ankylosed or coalesced centra; and 2) sacral ribs that extend to articulate with the ilium. Only the 20th and 21st vertebrae satisfied these two criteria. The centra of the first three sacral vertebrae (20th to 22nd) are clearly fused as no matrix is present between the centra (Figs 15, 17) compared to the 22nd to 23rd vertebrae where the centra are separated by matrix infill ventrally (Fig. 17A). Two large, conspicuous sacral ribs extend from the first two sacral vertebrae (20th and 21st, Fig. 16) to articulate with the ilium (Figs 54, 56). Vertebrae 22 and 23 have much smaller sacral ribs (Fig. 17) lacking lateral articulation with the ilium.

Watson (1914) considered *Embrithosaurus* and *Bradysaurus* as having four sacral vertebrae. Boonstra (1934c) compared the vertebral columns of 46 South African pareiasaurian specimens, drawing most of his conclusions from the complete vertebral column of a large *Tapinocephalus* AZ pareiasaur (SAM-PK-9168) identified at the time as *Bradysaurus seeleyi*. Boonstra considered four sacrals as the typical condition in large adult pareiasaurs, noting that the majority of specimens have four fused sacrals, but also noted exceptions such as the holotype of *Embrithosaurus* (Boonstra 1934c: 58) where the last two vertebrae are not fused. He considered that the fourth sacral rib did not reach the ilium, and was probably attached by a ligament. Lee (1997b) noted four sacral vertebrae in all basal South African pareiasaurs with the first sacral rib distally expanded and the most robust, whereas subsequent sacral ribs are more slender.

Our research shows that there are four sacral vertebrae in *Embrithosaurus* and *Bradysaurus baini*, with all four vertebrae fused in the large holotype of *Bradysaurus baini* and the centra of the last two vertebrae unfused in the smaller holotype of *Embrithosaurus schwarzi*. We consider the unfused condition in *Embrithosaurus schwarzi* to be the result of incomplete growth in this late subadult specimen. We thus consider the sacrum to comprise four vertebrae (vertebrae 20–23) in all large *Tapinocephalus* AZ pareiasaurs, with a ligamentous lateral articulation of the last two smaller sacral ribs (Boonstra 1934c).

Haughton & Boonstra (1930) were first to document that in *Embrithosaurus schwarzi* (SAM-PK-8034) the first sacral rib is the largest, whereas in the genus of *Bradysaurus* (NHMUK PV R 1971, holotype of *Bradysaurus baini*; NHMUK PV OR 49426, holotype of *Bradysaurus seeleyi*) the second sacral rib is the largest. Our observations confirm that in the holotype of *Embrithosaurus* the first sacral rib is the largest, and in several specimens of *Bradysaurus baini* (e.g. NHMUK PV R 1971, SAM-PK-5002) the second sacral rib is the largest. We propose these differences as diagnostically and taxonomically important.

The pelvis of *Embrithosaurus*

Previous authors have noted a number of differences between the pelvic girdles of *Embrithosaurus schwarzi* and *Bradysaurus baini*. Watson (1914) named and defined the genera *Bradysaurus* and *Embrithosaurus*, largely based on a few significant postcranial differences: broad, low, flat pelvis and large olecranon process in *Bradysaurus*, versus a narrow, rounded, and high pelvis and absence of an olecranon process in *Embrithosaurus*. In fact, *Embrithosaurus* and *Bradysaurus baini* are most easily distinguished by the shape and features of the pelvis.

Broom (1903) also noted the pelvis of the *Embrithosaurus* holotype as quite different from that of the holotype of *Bradysaurus baini*, which was well illustrated and described by Seeley (1892). Broom (1903) noted the anteriorly and laterally directed iliac blade of *Embrithosaurus* and also the very thick pubic symphysis, and the prominent median pubic process. Houghton & Boonstra (1930: 209, text-fig. 1) provided very detailed pelvic analyses and illustrations for several species, including *Embrithosaurus* where they noted the markedly thickened pelvic symphysis and the strong ventrally projecting carina. They noted the pelvis as very high and narrow, with a vertical ilium, producing a sharp 'v-shape' in anterior view. They reported an anteriorly diverging iliac blade, producing a wide pelvis anterodorsally; the anterior iliac blade as vertical, with no lateral bending, and a practically flat lateral side of the blade; and the symphyseal tongue of the anterior pubis as extending far forward.

Lee (1997a: 251) proposed three autapomorphies for *Embrithosaurus schwarzi*, all in the pelvis: 1) a flat, non-everted anterior iliac blade, such that this bone presents a thin edge when viewed dorsally; 2) the iliac blades diverge anteriorly, making an angle of about 40° with the sagittal plane when viewed dorsally; and 3) extremely thick pelvic symphysis, almost half as deep as long.

We support these three pelvic autapomorphies of *Embrithosaurus*. Additional distinguishing and diagnostic pelvic features compared to *Bradysaurus baini* include: high and narrow, v-shaped pelvis; pelvic shaft oriented anterodorsally 30° off the vertical plane; puboischiatic plate narrow, short and dorsally concave; thick and wide ventral keel with oblique lateral sides; median pubic process large and tongue-shaped with rounded edges, extending far anteroventrally.

Olecranon process development and ontogeny

The morphology of the proximal ulna of *Embrithosaurus schwarzi* is highly variable. Broom (1903: 132) documented the absence of an olecranon process in the holotype of *Embrithosaurus schwarzi* and highlighted its difference with the ulna of the holotype of *Bradysaurus baini*, which has a large and distinct olecranon process that forms an overhanging hook above the well-defined, socket-like articular surface. Broom added that the proximal ulna of *Embrithosaurus* is otherwise well developed and shows no sign of damage or fracture or a missing epiphysis.

Watson (1914) considered the lack of an olecranon process in the holotype of *Embrithosaurus schwarzi* as a diagnostic feature. Boonstra (1932b) also noted the

absence of an olecranon process in *Embrithosaurus* and two other middle Permian South African pareiasaurs *Bradysaurus vanderbyli* (SAM-PK-9169, SAM-PK-8941) and *Nochelesaurus alexanderi* (SAM-PK-8944) and a very weak or low process in *Dolichopareia angusta* (SAM-PK-6238).

Lee (1997b: 253) could not locate the ulnae of the holotype of *Embrithosaurus schwarzi* and suggested that the lack of an olecranon process (Boonstra 1932b; Broom 1903) was probably the result of incomplete preservation. Lee noted the complete ulnae of the large referred *Embrithosaurus* specimen CGP CBT 112 both show prominent olecranon processes. Our research shows that the ulnae of the holotype *Embrithosaurus schwarzi* are complete with the right ulna very well preserved (Figs 42, 43, 44) and the smaller and eroded left ulna corresponding with the right in terms of general shape and overall features. There is no olecranon process on either ulna, no anterodorsal limiting ridge, and so the proximal articular surface passed over smoothly from anteriorly (preaxially) to proximally (dorsally) to posteriorly (postaxially), through a groove (Figs 43, 44).

Instead of an olecranon process above the articular surface, the ulnae of the *Embrithosaurus* holotype have raised medial and lateral olecranon crests, with a groove between them. These crests have also been reported in *Bunostegos* as an autapomorphy of that taxon (Turner *et al.* 2015). In *Bunostegos*, the olecranon crests or 'folds' are described as folding towards each other, nearly touching their medial margins in the largest specimen (Turner *et al.* 2015) with the medial crest being larger than the lateral one. In the holotype of *Embrithosaurus*, the crests are lower, wider apart, extend proximally, do not fold medially, and do not touch. Turner *et al.* (2015) suggest that an extensor tendon was present in the groove between the olecranon crests of *Bunostegos*, which is probably also the case in the holotype of *Embrithosaurus*. Referred *Embrithosaurus* specimens FMNH UR 2443 and CGP CBT 112 have large and prominent olecranon processes. *Embrithosaurus*, therefore, shows marked variation of the ulna, from no olecranon process (late subadult holotype) to large olecranon processes above an enclosed articular surface (FMNH UR 2443, CGP CBT 112). An explanation is offered by Lee (1997b: 239) who maintains that the olecranon process is absent in juvenile specimens and ossifies late in ontogeny. The holotype of *Embrithosaurus* is a late subadult individual. Broom (1935: 39) also hypothesized that the lack of an olecranon in *Embrithosaurus* may be due to immature age, a hypothesis with which we concur. Specimens of *Scutosaurus karpinskii* also show great morphological differences in the proximal ulna: NHMUK PV R 4027, a cast of a very complete and large individual, has a large prominent olecranon process, whereas the mounted exhibited *Scutosaurus* skeleton at the American Museum of Natural History, New York, has no olecranon process and has high, sharp and distinct medial and lateral olecranon crests (Van den Brandt, pers. obs) as in *Bunostegos*.

It is interesting to note that *Nochelesaurus* specimen SAM-PK-6238 has an olecranon process which is of an intermediate stage of ontogenetic development. The ulna

is anterodorsally partially constricted (pinched in) and therefore there is no anterodorsal limiting ridge. There are very low (5 mm high) lateral and medial crests anteriorly only, and above which a very low (20 mm high) olecranon process exists.

The ontogenetic sequence of the development of the olecranon process appears to be thus:

- Stage 1: juveniles and subadults: short ulna, no olecranon process, no anterodorsal limiting ridge, ulna not constricted or pinched in anterodorsally, the proximal articular surface lacks a central oblique ridge and the surface passes over smoothly from anterior, to proximal, to posterior, forming a deep groove, flanked by high lateral and medial crests (e.g. subadult or late subadult holotype of *Embrithosaurus schwarzi*: SAM-PK-8034, length right ulna, 295 mm: Figs 42A, 42B, 43A, 43B, 44 and possibly the two smaller of the three described *Bunostegos* specimens: Turner *et al.* 2015);
- Stage 2: late subadults: longer ulna with a low or small convex olecranon process, ulna constricted above the proximal articular surface, no anterodorsal limiting ridge as constriction does not meet, the proximal articular surface has a central oblique ridge and the surface passes over smoothly from anterior, to proximal only (does not reach the posterior side) through a shallow groove, flanked by low lateral and medial crests (*Nochelesaurus* specimen SAM-PK-6238, length right ulna, 370 mm, Figs 45, 46, 47);
- Stage 3: large adults: long ulna, high and prominent olecranon process, ulna severely constricted above the articular surface, lateral and medial sides meet to form an anterodorsal limiting ridge that creates an enclosed socket or hook above the articular surface (*Embrithosaurus* specimens FMNH UR 2443, Figs 42C, 43C, and CGP CBT 112, length right ulna, 345 mm; holotype of *Bradysaurus baini*, length right ulna, 370 mm Figs 48, 49, 50).

As the presence and morphology of an olecranon process is highly variable in specimens of the same species at different ontogenetic stages, the use of the morphology of the olecranon processes and/or crest for species identification, such as the lack of an olecranon in the holotype of *Embrithosaurus*, is unreliable and is excluded from our diagnosis.

Humeral torsion and posture

Lee (1994, 1997a) noted the torsion between the proximal and distal expansions of the humerus as 45° for *Nochelesaurus* and *Embrithosaurus* and 60° for *Bradysaurus*. However, in the holotype of *Embrithosaurus* the left humerus is twisted by 70–80° such that the proximal and distal expansions are nearly perpendicular to each other. *Embrithosaurus* specimen FMNH UR 2443 has a torsion of about 60°. The proximal and distal ends of the right humerus of the holotype of *Embrithosaurus* were separate and were reattached for this work where the two pieces fitted (Fig. 31C), matching the 70–80° torsion of the unbroke left humerus.

The high degree of torsion in *Embrithosaurus* (60–80°) contrasts sharply with that of *Nochelesaurus* (20–40°) in

which the very flat proximal and distal expansions are almost on the same plane (Fig. 34C). Broom (1903: 131) suggested that Seeley (1892: 360) was in error when he reconstructed the separated proximal and distal expansions of both humeri of the holotype of *Bradysaurus baini* on the same plane, as it differed so markedly from the holotype of *Embrithosaurus*, with expansions nearly at right angles. Our observations of the holotype of *Bradysaurus baini* conclude that it is no longer possible to determine the original degree of torsion of the expansions in the humeri as the original bone breaks and contacts are plastered over. Other *Bradysaurus baini* specimens such as SAM-PK-5624 have torsion of 70–80° and SAM-PK-3718 torsion of 70°. Both *Bradysaurus* and *Embrithosaurus*, therefore, have high degrees of humeral torsion (60–80°) and *Nochelesaurus* is the only taxon in the group with significantly flatter expansions and less torsion (20–40°).

Turner *et al.* (2015) discussed the degree of torsion between the planes of the proximal and distal expansions of the humerus and the implications for the forelimb posture of *Bunostegos*. They suggest a more upright posture for *Bunostegos* where the humerus has proximal and distal expansions that are untwisted and are in line with each other and note that most pareiasaurs have a value around 45°, inferring a more sprawling posture. This would imply that *Nochelesaurus*, with its expansions almost in the same plane, may have had a more upright posture than *Embrithosaurus* and *Bradysaurus*, with implications for niche partitioning.

Osteoderm ornamentation

The arrangement pattern of body osteoderms of the *Tapinocephalus* AZ pareiasaurs has been known to be restricted to a narrow band above the vertebral column since Seeley's (1888, 1892) descriptions of *Bradysaurus*. These observations were used by Watson (1914) to separate genera with few osteoderms (*Bradysaurus* and *Embrithosaurus*) from those with many osteoderms (*Pareiasaurus* and *Propappus*). When preserved, the relatively few osteoderms on pareiasaurs from the *Tapinocephalus* AZ are usually found as isolated and scattered scutes, or sometimes articulated to the dorsal surfaces of vertebrae (e.g. holotypes of *Embrithosaurus schwarzi* and *Bradysaurus baini*).

Osteoderm morphology has recently been demonstrated to be of use in pareiasaurian taxonomy; for example, Maisch & Matzke (2019) demonstrated *Anthodon? haughtoni* (Huene 1944) to be a valid taxon based on autapomorphies of the osteoderms morphology and arrangement. Boyarinova *et al.* (2019) showed that in the east European pareiasaurs, *Deltavjatia* has two morphotypes and *Scutosaurus* four morphotypes.

Boonstra (1934b) described the central boss of irregular shape on the largest scutes of *Embrithosaurus* and the disc-like, very thin nature of most scutes and contrasted this with the relatively smooth convex scutes with practically no ornamentation and a thickened centre creating an incipient central boss in scutes of *Bradysaurus*. Lee (1994, 1997a) also mentioned unornamented osteoderms in *Nochelesaurus*. These descriptions are accurate with

regards to the differences between the scutes of *Embrithosaurus* and *Bradysaurus* and our research has revealed additional anatomical differences. There are three morphotypes in *Bradysaurus* and *Embrithosaurus*, found on three different areas of the body: anterior dorsal, posterior dorsal and small stud-like scutes. The stud-like scutes are not species-specific or diagnostic, but the anterior and posterior dorsal scutes are, and are the simplest and least ornamented in *Bradysaurus*, the most complex and distinct in *Embrithosaurus*, and in between these two extremes in *Nochelesaurus*.

The study of *Nochelesaurus* osteoderms has been historically neglected and our additional preparation of the scutes of the holotype reveals their ornamentation is different to that of both *Bradysaurus* and *Embrithosaurus* osteoderms. The osteoderms of *Nochelesaurus* have a wide, roughly rounded central boss (*Bradysaurus* has an incipient central boss or no boss and *Embrithosaurus* has a small, high, rugose central boss), and a periphery that is much thicker and without the radiating ridges seen in *Embrithosaurus*. We find the differences between the osteoderms of these three taxa as important distinguishing features and these have been included in our updated diagnoses.

Femoral differences

Lee (1994, 1997a) distinguished *Embrithosaurus* based on the presence of a curved, s-shaped, internal trochanter on the femur, which he contrasted with the straight internal trochanters of *Bradysaurus* and *Nochelesaurus*. Although the internal trochanter is not preserved in the holotype of *Embrithosaurus*, Broom (1903: plate XV, figs 16, 17; here Figs 58C, 59C) and Houghton & Boonstra (1930: text-fig. 34A,C; here Figs 58D, 59D) recorded it as gently curved and s-shaped. Referred *Embrithosaurus* specimens FMNH UR 244 and CGP CBT 112 also have gently curved internal trochanters. The holotype of *Bradysaurus baini* (Fig. 64) has a larger, rounder and more severely curved internal trochanter than that of *Embrithosaurus*, and although this strong curvature has been exaggerated in the crushed holotype, strong curvature is present in several other non-crushed specimens of *Bradysaurus baini*. Additionally, the proximal edge of the internal trochanter is high and perpendicular to the femur, only in these two taxa. *Embrithosaurus* alone possesses an anterior process on the distal internal trochanter (Fig. 58D). *Nochelesaurus* is the only pareiasaur in this group with a straight internal trochanter, which is very low and has an oblique proximal edge (Figs 61, 62).

Lee (1997b: 246, character 109) noted a weakly developed major trochanter as the plesiomorphic pareiasaurian condition, and proposed *Embrithosaurus* as the only middle Permian South African pareiasaur with a well-developed major trochanter. Lee argued that the weaker major trochanters of *Bradysaurus* and *Nochelesaurus* are caused by a very slight thickening of the postaxial flange. However, our measurements show that in all basal South African pareiasaur species, the dorsoventral thickness of the major trochanters are 35–40 mm, and the postaxial flange approximately 20 mm thick. Only in

specimens of *Embrithosaurus*, however, does the major trochanter protrude posteriorly 20–30 mm beyond the level of the postaxial flange (and it extends posteriorly only 5–10 mm in *Bradysaurus* and *Nochelesaurus*). We thus consider differences in the thickness of the major trochanters to be insignificant, but the posterior protrusion as diagnostic of *Embrithosaurus*.

Lee (1997a: 253, 1997b: 247, character 112) also proposed a narrower femur in *Embrithosaurus*, creating a concave postaxial edge in dorsal or ventral view. Our observations show that the femur of the holotype of *Embrithosaurus* is only 10 mm narrower than the femur of the holotype of *Nochelesaurus*, and 20–25 mm narrower than the femur of the holotype of *Bradysaurus baini*. The latter bone is severely dorsoventrally crushed and, as a result, antero-posteriorly expanded, which probably accounts for the increased anteroposterior width. The femoral width differences between these three taxa are minor and not reliable indicators for species separation. Additionally, the postaxial edge of the femur in *Embrithosaurus* is straight to slightly convex (not concave) as in all middle Permian South African pareiasaur species.

Nochelesaurus postcranial autapomorphies

In this section we discuss the three postcranial autapomorphies proposed by Lee (1994, 1997a) for *Nochelesaurus alexanderi*.

Anterior placement of the subscapular fossa

Lee (1997a: 249) stated that the subscapular fossa of *Nochelesaurus* is located 'very close to the anterior margin of the scapula blade' and that in all other pareiasaurs the groove is located more posteriorly, in the centre of the blade. Since the anterior border of the right scapulocoracoid of the holotype of *Nochelesaurus* is not preserved below the acromion processes, it is challenging to accurately determine the lateral extension of the subscapular fossa in relation to a missing anterior border. However, just above the subscapular fossa, a section of the cylindrical, convex, bar-like anterior border of the scapulocoracoid is 40 mm in anteroposterior width, suggesting that the subscapular fossa is positioned 40 mm behind the anterior border of the scapulocoracoid. In referred *Nochelesaurus* specimen SAM-PK-6238, the anterior border of the scapulocoracoid below the acromion process is also not preserved but can be estimated based on typical morphology for the group, at about 40 mm behind the anterior border. Our observations show that the subscapular fossa is positioned similarly from the anterior border in the holotypes of *Embrithosaurus* (45 mm) and the larger holotype of *Bradysaurus baini* (55 mm). Possibly Lee did not recognize that the anterior borders of the scapulocoracoids of the holotype of *Nochelesaurus* and referred *Nochelesaurus* specimen SAM-PK-6238 are not preserved, creating the misleading appearance of more anteriorly positioned subscapular fossa. Other measurements show that the subscapular fossa of the holotype of *Nochelesaurus* and SAM-PK-6238 are positioned between 90 mm (dorsally) and 130–135 mm (ventrally) from the oblique posterior border (Figs 26, 27),

which is close to the positions in the holotypes of *Embrithosaurus* (60–150 mm) and the larger holotype of *Bradysaurus* (110–175 mm). There is no convincing evidence that the subscapular fossa is positioned more anteriorly on the scapulocoracoid in *Nochelesaurus* than in *Bradysaurus* and *Embrithosaurus* specimens and it is removed from the diagnosis.

Humeral tubercle

Lee (1997a) proposed the presence of a tubercle on the centre of the dorsal surface of the entepicondyle as an autapomorphy of *Nochelesaurus*, based on the holotype of *Nochelesaurus alexanderi* and referred *Nochelesaurus* specimen SAM-PK-6238 (holotype of *Dolichopareia angusta*). A fully ossified distinct tubercle is undeniably present on the humerus of SAM-PK-6238 (Figs 35, 36). Boonstra's (1932b: 471, fig. 27) illustration of the right humerus of SAM-PK-6238 also included the tubercle. On the holotype, identification of a distinct tubercle is not as certain (Fig. 33) as the postaxial border of the intercondylar fossa of the humerus forms a swollen ridge in all large middle Permian South African pareiasaurs and could be misinterpreted as a tubercle. Referred *Nochelesaurus* specimens FMNH UR 2436 and FMNH UR 2480 both appear to show a humeral tubercle. We have also observed other *Nochelesaurus* specimens (Van den Brandt, pers. obs) that lack a humeral tubercle. When present, we ascribe a humeral tubercle to *Nochelesaurus*, and note high individual variation in the genus.

Distal femoral flange

Lee (1994, 1997a) stated that *Nochelesaurus* has an autapomorphy on the dorsal surface of the femur, which he termed a 'distal femoral flange', being a flange that projects distally beyond the postaxial tibial facet. The femur of the holotype reveals no distal flange. However, the lateral (postaxial) condyle does extend distally far (70 mm, Fig. 61A) beyond the distal edge of the medial condyle, further than the 30–40 mm extension of the holotype of *Embrithosaurus schwarzi* and the 20–30 mm estimated for the holotype of *Bradysaurus baini*. The lateral condyle extends distally further in most (but not all) specimens of *Nochelesaurus* than in specimens of *Embrithosaurus* and *Bradysaurus*, and we have observed *Nochelesaurus* specimens (Van den Brandt, pers. obs) in which the lateral condyle does not extend very far distally. We ascribe a long lateral condyle of the distal femur to *Nochelesaurus*, noting high individual variation in the genus.

CONCLUSION

After direct examination of all available material of middle Permian South African pareiasaurs, we provide, for the first time, detailed postcranial descriptions of *Bradysaurus*, *Embrithosaurus* and *Nochelesaurus*, present new diagnostic postcranial characters, and discuss previously proposed ones. We conclude that some consistent and valid morphological postcranial characters differentiate *Bradysaurus baini*, *Embrithosaurus schwarzi* and *Nochelesaurus alexanderi*. The postcranial skeleton of *Nochelesaurus* is not as well-known as that of *Embrithosaurus* and *Bradysaurus*,

as the holotype and the referred specimens listed here of *Nochelesaurus* do not preserve the pelvis.

Postcranially *Embrithosaurus schwarzi* is most easily separated from the co-occurring pareiasaur species through features of the pelvis and the unique osteoderms. The three pelvic autapomorphies of Lee (1994, 1997a) have been confirmed and retained: the iliac blades are oriented obliquely from the longitudinal midline, they stand vertically, and the midline pelvic symphysis is thick. Additionally, the pelvis of *Embrithosaurus schwarzi* is angled higher, is narrower, and is shorter than those of co-occurring taxa, with a longer median pubic process, and a concave dorsal pubioischial plate. The radius and tibia are more symmetrical than those of the co-occurring taxa, the osteoderms have the most distinct ornamentation in the group, and the major trochanter of the femur protrudes posteriorly the furthest.

The postcranial skeleton of *Bradysaurus baini* was re-described in detail, and we propose one new postcranial autapomorphy: anterior dorsal osteoderms smooth and strongly convex, with an incipient central boss, and very light ornamentation. Additional postcranial features that separate *Bradysaurus baini* from co-occurring taxa include: the wide, low, and long pelvis with iliac blades that are parasagittal posteriorly and laterally and horizontally everted or bent anteriorly; short and distally flared scapula blade; femur with a distinctive, curved, wide and high internal trochanter and lack of a large external trochanter; and the second sacral rib is the largest in the sacrum.

The postcranium of *Nochelesaurus alexanderi* has never been fully described, and we discard three postcranial autapomorphies proposed by Lee (1994, 1997a): the anterior position of the subscapular fossa; the tubercle on the humerus; and the extended distal femur. Postcranial diagnostic features of *Nochelesaurus alexanderi* compared to co-occurring taxa include: the straight internal and the small external trochanters of the femur; the longer and narrower scapula blade; the relative less twisting of the humerus; ventrolaterally expanded distal radius; and relatively rugose osteoderms with a flattened, wide, central boss.

ABBREVIATIONS

Institutional

AM	Albany Museum, Grahamstown
AMNH	American Museum of Natural History, New York
BPI	Evolutionary Studies Institute (ESI), University of the Witwatersrand, Johannesburg (formerly Bernard Price Institute for Palaeontological Research)
CGP	Council for Geosciences, Pretoria
FMNH	Field Museum of Natural History, Chicago
NHMUK	Natural History Museum of London, United Kingdom
NMQR	National Museum, Bloemfontein
PIN	Paleontological Institute, Moscow, Russia
SAM	Iziko South African Museum, Cape Town

Anatomical

ace	acetabulum
acor	anterior coracoid
acr	acromion process
ce	centrum
cla	clavicle
cle	cleithrum
cof	coracoid foramen
dcp	deltpectoral crest

dp	diapophysis
ect	ectepicondyle
ect for	ectepicondylar foramen
enf	groove for entepicondylar foramen
ent	entepicondyle
ent for	entepicondylar foramen
gl	glenoid
ib	ischial buttress
icf	intercondylar fossa
icla	interclavicle
ics	intercondylar sulcus
it	internal trochanter
itf	intertrochanteric fossa
lat.sig.p	lateral sigmoidal process
med.sig.p	medial sigmoidal process
mpp	median pubic process
mt	major trochanter
na	neural arch
nc	neural canal
nsp	neural spine
ole	olecranon process
pb	pubic buttress
pcor	posterior coracoid
pf	popliteal fossa
pof	pubic/obturator foramen
pos.pub.but	posterior pubic buttress
poz	postzygapophysis
pp	parapophysis
prox.lat.c	proximal lateral crest
prox.med.c	proximal medial crest
prz	prezygapophysis
rad fac	radial facet
sb	supra-acetabular buttress
sca	scapula blade
sgb	supraglenoid buttress
sig.n	sigmoid notch
ssf	subscapular fossa
tp	transverse process
uln fac	ulnar facet

Michael Lee, Michael Benton, Nour-Eddine Jalil, Juan Carlos Cisneros, Andrey Sennikov, Elena Boyarinova, Sean Modesto and Linda Tsuji are thanked for generously sharing their pareiasaurian knowledge and for many discussions. For access to the material studied, we thank: Ellen de Kock, Johann Neveling, and Nonhlanhla Mchunu (CGP); Bernhard Zipfel and Sifelani Jirah (ESI); William Simpson and Kenneth Angielczyk (FMNH); Sandra Chapman, Mike Day and Paul Barrett (NHMUK); V.V. Bulanov, Valeriy Golubev and Andrey Sennikov (PIN); Zaituna Skosan, Sibusiso Mtungata and Roger Smith (SAM). For additional preparation of the holotypes of *Embrithosaurus schwarzi* (SAM-PK-8034) and *Nochelesaurus alexanderi* (SAM-PK-6239), we thank Pepsop Mukanela, Gilbert Mokgethoa and Charlton Dube (ESI). The research trip to the Borissiak Paleontological Institute of the Russian Academy of Sciences, Moscow (PIN) was made possible through the support of the Bi-national Cooperation project between South Africa (NRF to Fernando Abdala) and Russia (Russian Foundation for Basic Research to Andrey Sennikov). We acknowledge the financial support provided by the Department of Science and Innovation and the National Research Foundation (DSI/NRF) Centre of Excellence in Palaeosciences (CoE-Pal), South Africa; the National Research Foundation (NRF), South Africa; the Paleontological Scientific Trust (PAST) and its Scatterlings of Africa programme, Johannesburg, South Africa; the African Origins Program (AOP) of the National Research Foundation (NRF), South Africa, under Bruce Rubidge and the University of the Witwatersrand, Johannesburg, South Africa. Fernando Abdala's research is financed by the NRF of South Africa and CONICET from Argentina. The support of the DST/NRF Centre of Excellence in Palaeosciences (CoE-Pal) towards this research is hereby acknowledged. Opinions expressed and conclusions arrived at, are those of the author and are not necessarily to be attributed to the CoE.

*ORCID iDs

M.J. Van den Brandt:  orcid.org/0000-0002-4967-7827
 J. Benoit:  orcid.org/0000-0001-5378-3940
 F. Abdala:  orcid.org/0000-0001-9838-2497
 B.S. Rubidge:  orcid.org/0000-0003-2477-1873

REFERENCES

BENTON, M.J. 2016. The Chinese pareiasaurs. *Zoological Journal of the Linnean Society* **177**, 813–853.

BOONSTRA, L.D. 1929a. Pareiasaurian studies. Part 3. On the Pareiasaurian manus. *Annals of the South African Museum* **28**, 97–112.
 BOONSTRA, L.D. 1929b. Pareiasaurian studies. Part 4. On the Pareiasaurian pes. *Annals of the South African Museum* **28**, 113–122.
 BOONSTRA, L.D. 1932a. The phylogenesis of the Pareiasauridae: a study in evolution. *South African Journal of Science* **29**, 480–486.
 BOONSTRA, L.D. 1932b. Pareiasaurian studies. Part 8. The osteology and myology of the locomotor apparatus. B – fore limb. *Annals of the South African Museum* **28**, 437–503.
 BOONSTRA, L.D. 1934a. Pareiasaurian studies. Part 9. The cranial osteology. *Annals of the South African Museum* **31**, 1–38.
 BOONSTRA, L.D. 1934b. Pareiasaurian studies. Part 10. The dermal armour. *Annals of the South African Museum* **31**, 39–48.
 BOONSTRA, L.D. 1934c. Pareiasaurian studies. Part 11. The vertebral column and ribs. *Annals of the South African Museum* **31**, 49–66.
 BOONSTRA, L.D. 1969. The fauna of the *Tapinocephalus* zone (Beaufort beds of the Karoo). *Annals of the South African Museum* **56**, 1–73.
 BOYARINOVA, E.I., BULANOV, V.V. & GOLUBEV, V.K. 2019. Significance of osteoderms for systematics of the Late Permian pareiasaurs of Eastern Europe. *Kölnener Forum für Geologie und Paläontologie* **23**, 54–55.
 Hartenfels, S., Herbig, H., Amler, M.R.W. & Aretz, M (eds). Abstracts, 19th International Congress on Carboniferous and Permian, Cologne, July 29 – August 2, 2019.
 BROOM, R. 1903. On an almost perfect skeleton of *Pareiasaurus serridens* Owen. *Annals of the South African Museum* **4**, 123–138.
 BROOM, R. 1913. On four new fossil reptiles from the Beaufort Series, South Africa. *Records of the Albany Museum* **2**, 397–401.
 BROOM, R. 1924. On some points in the structure of the pareiasaurian skull. *Proceedings of the Zoological Society of London* **1924**, 499–508.
 BROOM, R. 1935. Notes on some species of pareiasaurian reptiles. *Annals of the Transvaal Museum* **18**, 37–51.
 CANOVILLE, A. & CHINSAMY, A. 2017. Bone microstructure of pareiasaurs (Parareptilia) from the Karoo Basin, South Africa: implications for growth strategies and lifestyle habits. *The Anatomical Record* **300**, 1039–1066.
 COPE, E.D. 1896. The reptilian order Cotylosauria. *Proceedings of the American Philosophical Society* **34**, 436–456.
 DAY, M.O. 2013. *Middle Permian continental biodiversity changes as reflected in the Beaufort Group of South Africa: a bio- and lithostratigraphic review of the Eodicynodon, Tapinocephalus, and Pristerognathus Assemblage Zones*. Unpublished Ph.D. thesis, University of the Witwatersrand, Johannesburg, 387 pp.
 DAY, M.O., RAMEZANI, J., BOWRING, S.A., SADLER, P.M., ERWIN, D.H., ABDALA, F. & RUBIDGE, B.S. 2015. When and how did the terrestrial mid-Permian mass extinction occur? Evidence from the tetrapod record of the Karoo Basin, South Africa. *Proceedings of the Royal Society of London B* **282**, 20150834.
 DAY, M.O. & RUBIDGE, B.S. 2020. Biostratigraphy of the *Tapinocephalus* Assemblage Zone (Beaufort Group, Karoo Supergroup), South Africa. *South African Journal of Geology* **123**(2), 149–164. <https://doi.org/10.25131/sajg.123.0012>
 FINDLAY, G.H. 1970. Skin structure of small pareiasaurs. With comments on their taxonomy in the *Cistecephalus* zone. *Palaeontologia africana* **13**, 15–23.
 HAUGHTON, S.H. & BOONSTRA, L.D. 1929. Pareiasaurian studies. Part I. An attempt at a classification of the pareiasauria based on skull features. *Annals of the South African Museum* **28**, 79–87.
 HAUGHTON, S.H. & BOONSTRA, L.D. 1930. Pareiasaurian studies. Part 6. The osteology and myology of the locomotor apparatus. A – hind limb. *Annals of the South African Museum* **28**, 296–366.
 JALIL, N.-E. & JANVIER, P. 2005. Les pareiasaures (Amniota, Parareptilia) du Permien supérieur du Bassin d'Argana, Maroc. *Geodiversitas* **27**(1), 35–132.
 KITCHING, J.W. 1995. Biostratigraphy of the *Dicynodon* Assemblage Zone. In: Rubidge, B.S. (ed.), *Biostratigraphy of the Beaufort Group (Karoo Supergroup), Biostratigraphic Series 1*. Pretoria, South African Committee for Stratigraphy, pp. 29–34.
 KUHN, O. 1969. *Cotylosaria. Handbuch der Paläoherpetologie, Teil 6*. Stuttgart, Gustav Fischer Verlag.
 LAURENTI, J.N. 1768. *Classis Reptilium. Specimen medicum, exhibens synopsis Reptilium emendatum, cum experimentis circa venena et antidote Reptilium Austriacorum. J. Thom., Nob. et Trattneri*, Vienna.
 LEE, M.S.Y. 1993. The origin of the turtle body plan: bridging a famous morphological gap. *Science* **261**, 1716–1720.
 LEE, M.S.Y. 1994. *Evolutionary morphology of pareiasaurs*. Unpublished Ph.D. thesis, University of Cambridge, Cambridge, 392 pp.
 LEE, M.S.Y. 1997a. A taxonomic revision of pareiasaurian reptiles: implications for Permian terrestrial palaeoecology. *Modern Geology* **21**, 231–298.

- LEE, M.S.Y. 1997b. Pareiasaur phylogeny and the origin of turtles. *Zoological Journal of the Linnean Society* **120**, 197–280.
- LIU, J. & BEVER, G.S. 2018. The tetrapod fauna of the Upper Permian Naobaogou Formation of China: a new species of *Elginia* (Parareptilia, Pareiasauria). *Papers in Palaeontology* **4**(2), 197–209. <https://doi.org/10.1002/spp2.1105>
- MAISCH, M. & MATZKE, A.T. 2019. *Anthodon? haughtoni* (Huene, 1944), a pareiasaurid (Parareptilia: Pareiasauria) from the Late Permian Usili Formation of Kingori, Ruhuhu Basin, Tanzania. *Neues Jahrbuch für Geologie und Paläontologie Abhandlungen*. **291**/2, 197–204.
- NICOLAS, M.V.M. 2007. *Tetrapod biodiversity through the Permo-Triassic Beaufort Group (Karoo Supergroup) of South Africa*. Unpublished Ph.D. thesis, University of the Witwatersrand, Johannesburg, 356 pp.
- OLSON, E.C. 1947. The family Diadectidae and its bearing on the classification of reptiles. *Fieldiana Geology* **11**, 1–53.
- OWEN, R. 1876. *Descriptive and Illustrated Catalogue of the Fossil Reptilia of South Africa in the Collection of the British Museum*. London, British Museum (Natural History).
- SCHEYER, T.M. & SANDER, P.M. 2009. Bone microstructures and mode of skeletogenesis in osteoderms of three pareiasaur taxa from the Permian of South Africa. *Journal of Evolutionary Biology* **22**, 1153–1162.
- SEELEY, H.G. 1888. Researches on the structure, organisation, and classification of the fossil Reptilia. II. On *Pareiasaurus bombidens* (Owen), and the significance of its affinities to amphibians, reptiles and mammals. *Philosophical Transactions of the Royal Society of London B* **179**, 59–109.
- SEELEY, H.G. 1892. Researches on the structure, organisation, and classification of the fossil Reptilia. VII. Further observations on *Pareiasaurus*. *Philosophical Transactions of the Royal Society of London B* **183**, 311–370.
- SMITH, R.M.H. 2020. Biostratigraphy of the *Cistecephalus* Assemblage Zone (Beaufort Group, Karoo Supergroup), South Africa. *South African Journal of Geology*, **123**(2), 181–190. <https://doi.org/10.25131/sajg.123.0013>
- SMITH, R.M.H. & KEYSER, A.W. 1995a. Biostratigraphy of the *Tapinocephalus* Assemblage Zone. In: Rubidge, B.S. (ed.), *Biostratigraphy of the Beaufort Group (Karoo Supergroup)*, Biostratigraphic Series 1. Pretoria, South African Committee for Stratigraphy, pp. 8–12.
- SMITH, R.M. H. & KEYSER, A.W. 1995b. Biostratigraphy of the *Tropidostoma* Assemblage Zone. In: Rubidge, B.S. (ed.), *Biostratigraphy of the Beaufort Group (Karoo Supergroup)*, Biostratigraphic Series 1. Pretoria, South African Committee for Stratigraphy, pp. 18–22.
- SMITH, R.M.H. & KEYSER, A.W. 1995c. Biostratigraphy of the *Cistecephalus* Assemblage Zone. In: Rubidge, B.S. (ed.), *Biostratigraphy of the Beaufort Group (Karoo Supergroup)*, Biostratigraphic Series 1. Pretoria, South African Committee for Stratigraphy, pp. 23–28.
- TSUJI, L.A. 2010. *Evolution, morphology and paleobiology of the Pareiasauria and their relatives (Amniota: Parareptilia)*. Unpublished Ph.D. thesis, Humboldt-University of Berlin, Berlin, 188 pp.
- TSUJI, L.A. 2013. Anatomy, cranial ontogeny and phylogenetic relationships of the pareiasaur *Deltaojatia rossicus* from the Late Permian of central Russia. *Earth and Environmental Science Transactions of the Royal Society of Edinburgh* **104**, 1–42.
- TSUJI, L.A., SIDOR, C.A., STEYER, S.J., SMITH, R.M.H., TABOR, N.J. & IDE, O. 2013. The vertebrate fauna of the Upper Permian of Niger – VII. Cranial anatomy and relationships of *Bunostegos akokanensis* (Pareiasauria). *Journal of Vertebrate Palaeontology* **33**(4), 747–763.
- TURNER, M.L., TSUJI, L.A., IDE, O. & SIDOR, C.A. 2015. The vertebrate fauna of the Upper Permian of Niger – IX. The appendicular skeleton of *Bunostegos akokanensis* (Parareptilia: Pareiasauria). *Journal of Vertebrate Palaeontology* **35**(6), e994746.
- VAN DEN BRANDT, M.J. 2016. *Cranial morphology of Embrithosaurus schwarzi (Parareptilia, Pareiasauria) and a taxonomic and stratigraphic reassessment of the South African middle Permian pareiasaurs*. Unpublished M.Sc. thesis, University of the Witwatersrand, Johannesburg, 1–214.
- VAN DEN BRANDT, M.J., ABDALA, F. & RUBIDGE, B.S. 2020. Cranial morphology and phylogenetic relationships of the middle Permian pareiasaur *Embrithosaurus schwarzi* from the Karoo Basin of South Africa. *Zoological Journal of the Linnean Society* **188**, 202–241. <https://doi.org/10.1093/zoolinnean/zlz064>
- VAN DEN BRANDT, M., RUBIDGE, B., BENOIT, J. & ABDALA, F. 2021. Cranial morphology of the middle Permian pareiasaur *Nochelesaurus alexanderi* from the Karoo Basin of South Africa. *Earth and Environmental Science Transactions of the Royal Society of Edinburgh*, 1–21. <https://doi.org/10.1017/S1755691021000049>
- VAN DER WALT, M., DAY, M., RUBIDGE, B., COOPER, A.K. & NETTERBER, I. 2011. A new GIS-based biozone map of the Beaufort Group (Karoo Supergroup), South Africa. *Palaeontologia africana* **45**, 1–5.
- VIGLIETTI, P.A. 2020. Biostratigraphy of the *Daptocephalus* Assemblage Zone (Beaufort Group, Karoo Supergroup), South Africa. *South African Journal of Geology*, **123**(2), 191–206. <https://doi.org/10.25131/sajg.123.0014>
- VIGLIETTI, P.A., SMITH, R.M.H., ANGIELCZYK, K.D., KAMMERER, C.F., FROBISCH, J. & RUBIDGE, B.S. 2015. The *Daptocephalus* Assemblage Zone (Lopingian), South Africa: a proposed biostratigraphy based on a new compilation of stratigraphic ranges. *Journal of African Earth Sciences* **113**, 153–164. <https://doi.org/10.1016/j.jafrearsci.2015.10.011>
- WATSON, D.M.S. 1914. On the nomenclature of pareiasaurs. *Annals of the Magazine of Natural History* **14**, 98–102.
- XU, L., LI, X. W., JIA, S.H. & LIU, J. 2015. The Jiyuan tetrapod fauna of the Upper Permian of China: new pareiasaur material and the reestablishment of *Honania complicitentata*. *Acta Palaeontologica Polonica* **60**(3), 689–700.